Thermodynamics and Phase Behavior of Hydrocarbon Solvents at Capillary Conditions

by

Ilyas Hafidh Al Kindi

A thesis submitted in partial fulfillment of the requirements for the degree of

Doctor of Philosophy

in

Petroleum Engineering

Department of Civil and Environmental Engineering
University of Alberta

Abstract

Phase alteration is a physical phenomenon that constantly takes place in reservoirs, during production or injection, due to the regional change in fluids' pressures or temperatures. The transformation of phases also occurs frequently in enhanced oil recovery (cold solvent injection, CO_2 injection, etc.) or thermal enhanced oil recovery (steam injection, solvent-thermal application) at which injected fluids condense gradually throughout the matrix owing to heat loss or an increase in pressure. Achieving an accurate prediction of phase change in the porous media is important for attaining trustful forecasting of hydrocarbon recoveries, retrieval of the injected solvents, vapour-liquid equilibrium calculations, and modelling of two-phase envelopes.

Generally, the capillary effect has an impact on the properties of fluids when medium sizes are tight enough to affect the molecules and empower pore-molecule interactions. One of the fluid properties influenced by high capillary pressures is the phase-change. When pore sizes become tighter than 1000 nanometers, vaporization and condensation temperatures/pressures of confined fluids tend to shift from bulk measurements. Understanding the nature of physical state alteration (liquid-to-gas or vice versa) has attracted the attention of researchers because of its enormous importance in pressure-volume-temperature (PVT) calculations and reservoir simulation. In petroleum industries, cubic equation-of-state (EoS) models are used to predict the phase behavior of hydrocarbons in the reservoirs. One of the major limitations of the commonly used cubic EoS (Peng-Robinson EoS and Soave Redlich-Kwong EoS) is that they do not consider the confinement effect on the phase-alteration behavior of fluids. Such a drawback causes these cubic models to be inaccurate in modelling two-phase envelopes of rock fluids in extended tight reservoirs (shales, tight sands) or even in permeable rocks (sands under thermal injection).

This thesis experimentally investigates the phase-change behavior of hydrocarbons in various categories of the porous system. The experimental journey was initiated by studying the boiling behavior of single-component hydrocarbon liquids (heptane and decane) and water in silica-glass Hele-Shaw cells which is represented as simple capillary spaces with different sizes. The analysis was performed under atmospheric pressure (1 atm). Despite their simplicity, using Hele-Shaw models brought the advantage of clear vapour generation visualizations. Shifted boiling temperatures were observed in the glass cells, due to the confinement effect. The outcomes were

then used to modify the Thomson equation by suggesting alternative formulations. As a next step, the vaporization of heptane (as a pure component), heptane-decane mixture (50% mass fraction for each component), and naphtha (as a multicomponent solvent) was analyzed in homogeneous (uniform pore-throat sizes) and heterogeneous (non-uniform pore-throat sizes) silicate-glass microfluidic chips, at atmospheric pressure. Relatively, the heterogeneous micromodels had a closer representation of the rock porous media, compared to the Hele-Shaw cells. Early vaporizations of solvents were clearly observed in the micromodels, as a result of capillary effects in the porous systems.

Although microfluidic chips inherit the two-dimensional porous structure of rocks, the material properties of silicate glass are different from reservoir rock in terms of molecule adsorption effect, for example. Pore-molecule interactions, in rocks, have noticeable impact on hydrocarbon boiling temperatures, as detailed in **Chapter 5**. Therefore, the analysis was shifted forward to focus on the phase-change behavior of hydrocarbons in real reservoir rocks. The selected rocks were Berea sandstone, Indiana limestone, tight sandstone, and shale. Firstly, pore size distribution analysis was done to measure the deviation and distribution of pore diameters in each rock by quantifying nitrogen adsorption and desorption in the rock matrix. The initial set of experiments were conducted under the atmospheric pressure with water, heptane, and decane, as pure liquids. Owing to the existence of nanopores, the vaporization of tested liquids took place in the rocks at temperatures lower than the normal boiling points (at bulk conditions) and calculated boiling temperatures by the Thomson equation. Such reductions were also observed in the permeable rocks (sandstone and limestone) although the volume percentages of extended confined pores (< 100 nanometers) were less than 5%. The second set of experiments paid attention to measuring the vaporization temperature of single-component and multicomponent hydrocarbon liquids in sandstone, limestone, tight sandstone, and shale at various pressures (14.7, 64.7, 114.7 psi). The pure-component solvents (heptane and octane) were representing the injected solvents in cold solvent injection or as additives to steam, and the multicomponent solvents were representing non-complex light oil. The experimental results were, then, compared with the normal boiling points and calculated phase-change temperatures by the original version of the Peng-Robinson EoS. Noticeable deviations of measured vaporization temperatures of liquid solvents from the bulk and computed values were observed. As the medium gets smaller, interior pore surfaces begin to have influences on boiling temperatures of hydrocarbons, due to the pore-molecule interactions. The

studies also inspected the phase-change behavior of heptane and octane in Berea sandstone with different rock wettabilities (water-wet and oil-wet) and clay contents which partially control the solvent adsorption. The analysis showed that altering the wettability of sandstone could change the average nucleation temperatures of solvents, and changing the rock's liquid adsorption capability could lower the nucleation temperatures of heptane and octane by 30% from their normal boiling points.

Studying the condensation of propane in various reservoir rocks under isothermal and non-isothermal conditions was also a part of the investigation. Initially, the phase-change pressure of propane was measured in Hele-Shaw cells with various gap sizes, capillary tubes with different sizes (1 – 40 micrometers), and microfluidic chips. The capillary effect in the silica-glass models was not sufficient to alter the propane vapour and condensation pressures and they were identical to the bulk measurements or those computed by the Kelvin equation. However, as observed with the hydrocarbon liquids, vaporization of propane was taking place in sandstone, limestone, and shale at pressures which were approximately 10% lower than the bulk vapour pressure. As a further step, the vaporization of propane was inspected in sandstone, limestone, tight sandstone, and shale at various temperatures, ranging from 0℃ (273.15 K) to 40℃ (313.15 K). The experimental observations were then compared with the bulk vaporization pressures and computed saturation pressures by the Peng-Robinson EoS and Kelvin equation. The recorded vapour pressures, in the rocks, were 7% lower than the bulk values and calculated vapour pressures by the Kelvin equation. Meanwhile, the propane vapour pressures, in the rocks, were 15% (on average) lower than the pressures modelled by the Peng-Robinson EoS. Lastly, phase distribution of pure-component solvent (pentane), binary mixture (pentane-heptane), and trinary mixture (pentane-heptane-octane) was studied by comprehending the dynamical behavior of hydrocarbon phases in heterogeneous and homogeneous porous systems under capillary conditions.

Acknowledgements

Firstly, I would like to thank my supervisor, Professor Tayfun Babadagli, for his continuous support and guidance throughout my PhD journey, and I am grateful for his patience in constantly providing his assistance. I am very thankful for the unconditional support and encouragement that my parents and family provided whenever I needed it. I also thank the lab technicians, Mihaela and Lixing, for giving me the maximum help during my lab studies. Their assistance definitely had a large impact on the success of my experiments. I would like to thank Lindsey for her help in editing my papers and reports. To my amazing friends (Randy, Enoc, Fritjof, Martin, Mohammed, and Yeji), thank you very much for making the work environment encouraging, incredible, and filled with teamwork and beneficial discussions.

I am thankful to Petroleum Development Oman Co. (PDO) for providing the financial support for my graduate study at the University of Alberta. Moreover, I gratefully acknowledge the sponsorship under Professor Tayfun Babadagli's Natural Sciences and Engineering Research Council of Canada (NSERC) Industrial Research Chair in Unconventional Oil Recovery (industrial partners are Petroleum Development Oman, SUNCOR, Husky Energy, Saudi Aramco, BASF, and CNRL) and an NSERC Discovery Grant (No: RES0011227).

Contents

List of Tables

List of Figures

1 Chapter 1: Introduction

1.1 Introduction

Transformation from liquid to gaseous form or vice versa plays a critical role in controlling the dynamics of fluids and their distributions in oil and gas reservoirs. Due to continuous changes in pressure around wellbore areas, fluids tend to change their phases within the rock porous media, during production or injection periods. Hence, thoroughly understanding the nature of vaporization and condensation of reservoir and injected fluids in capillary systems is essential to achieve accurate modelling of fluid dynamics, two-phase envelopes, and enhanced oil recovery (EOR) applications. Moreover, it is important to attain precise calculations of vapour-liquid equilibrium (VLE), ultimate hydrocarbon recoveries, and liquid density.

In heavy-oil reservoirs, thermal enhanced oil recovery (EOR) processes (typically steam injection of any type), sole-solvent injection, or hybrid (thermal-solvent) applications are suggested to increase the overall oil recovery by viscosity reduction and oil mobility enhancement (Fang and Babadagli 2014). During steam-injection processes, injected steam condenses throughout the reservoir, as a result of excessive heat loss. The dynamics and propagation of steam drastically change when it transforms into water. Similarly, injecting solvents into high-pressure reservoirs can cause them to condense which considerably alters their dynamical behaviors in the rocks. Other applications, such as Solvent-Over-Steam Injection in a Fractured Reservoir (Al-Bahlani and Babadagli 2011), depend on the vaporization of trapped fluids in the matrixes as part of their recovery mechanisms. Thus, modelling such applications accurately depends on the understanding of phase-change behavior within the rock pores.

Analytical solutions have been proposed to calculate the phase transformation of fluids such as equations-of-state (Peng and Robinson 1976) and Kelvin equation (Thomson 1871). The most common thermodynamic models used in petroleum industries are the Peng-Robinson and Soave Redlich-Kwong (Soave 1972) equation-of-state. The accuracy of these cubic equations in

modeling phase-change behaviors in confined porous media is questionable since the confinement effect on vaporization and condensation temperatures/pressures is neglected.

This research aimed to experimentally study the behavior of vaporization and condensation of hydrocarbons in capillary systems. The investigation was initiated with simple confined models (Hele-Shaw cells) and ended with more complicated capillary media (reservoir rocks) which had better representations of real cases in related petroleum applications. The analytical approaches to model the fluid phase-change were also considered in this research. The Peng-Robinson equation-of-state (EoS), and the Kelvin and Thomson equations were compared to the measured values, obtained from the experiments to inspect their applicability in accurately predicting phase alterations in porous media. The analysis was done under various temperatures and pressures using specially designed equipment.

1.2 Problem Statement and Objectives

Modeling phase behavior in rocks typically assumes that the thermodynamic behavior of fluids is the same as at the bulk conditions. Reservoir rocks, however, consist of pores with wide ranges of sizes, varying from micropores (> 2 nanometers) to macropores (> 50 nanometers). Based on the conducted pore size distribution analysis (**Chapter 3**), Shale rocks are mostly occupied by pores smaller than 100 nanometers. The analyses also showed that even the permeable rocks contain minor percentages of micro and meso (2 – 50 nanometers) pores. The existence of confined channels in the reservoir rocks causes the constrained fluids to vaporize and condense at different temperatures or pressures, comparing with those existing in bulk conditions. This eventually entails testing the application conditions for any type of primary, secondary, and tertiary recovery methods.

A good example of the importance in understanding the phase-change of confined fluids occurs when modelling hybrid solvent-steam applications. Al-Bahlani and Babadagli (2011) showed that their Solvent-Over-Steam Injection in Fractured Reservoir process required estimating the optimal boiling temperature of injected solvents to obtain the maximum solvent retrieval for reducing the operational cost by eliminating the generation of unnecessary heat energy. Subsequent studies also showed that, to retrieve the solvent injection during the cyclical injection of steam and solvents,

one must apply the optimal temperature to obtain the maximum recovery of the injected solvents (Pathak et al. 2011, 2013; Cui and Babadagli 2017; Leyva and Babadagli, 2017, 2018). Also, studying the phase-change behavior in porous media can assist us to precisely predict fluid dynamics in the reservoir or model the condensation of injected steam in near-wellbore areas, due to the heat sink. Other examples of pressure and temperature sensitive recovery applications include production from gas-condensate reservoirs and gas injection into unconventional (shale and, tight sand reservoirs) to enhance oil recovery.

The widely used cubic equations-of-state (Peng-Robinson and Soave Redlich-Kwong) do not take capillary effect and pore-molecule interactions into account; as a consequence, such cubic equations might result in overestimated or underestimated vapour-liquid equilibrium (VLE) calculations when used to model phase behavior of constrained fluids. This is highly critical as the above summarized application types require critical pressure and temperature to prevent any phase change for a technically effective and economically efficient process.

The main objective of this research was to measure vaporization temperatures and condensation pressures of several hydrocarbon fluids in several porous systems (Hele-Shaw cells, microfluidic chips, and reservoir rock samples). Using different types of porous media assisted us in understanding how the inner capillary structure could influence the generation temperature/pressure of vapour phase. In rock experiments, one of our targets was to inspect the boiling and condensation of hydrocarbons under various pressures (14.7 – 114.7 psi) and temperatures (0 – 40°C). The calculated outcomes from the Peng-Robinson equation-of-state, and the Kelvin and Thomson equations were considered and compared with the experimental values to analyze the deviations. As a part of the investigation, the phase distribution of liquid hydrocarbons during vaporization stages was studied using microfluidic chips.

1.3 Solution Methodology

Figure 1-1 illustrates an overall structure of the research. Basically, the experimentation was divided into three main categories: (a) measurement of vaporization temperatures of several hydrocarbons at the ambient pressure (1 atm) and other higher surrounding pressures (64.7 and 114.7 psi); (b) measurement of condensation pressures of propane at the ambient temperature

(21°C) and other temperatures (0, 10, 30, and 40°C); (c) investigation of hydrocarbon phase distributions and dynamics in microfluidic chips at the atmospheric temperature (21°C). In the measurement of boiling temperature and vapour pressure, the experiments were always initiated with simple capillary silica-glass models (Hele-Shaw cells). Then, systems with more complicated porous structures (microfluidic chips and reservoir rocks) were utilized to study the hydrocarbon phase behavior in capillary media. In non-isobaric and non-isothermal conditions, all the experiments were conducted with only rock samples. During the analysis of phase distribution in porous media, homogeneous and heterogeneous micromodels were utilized to perform the investigation.

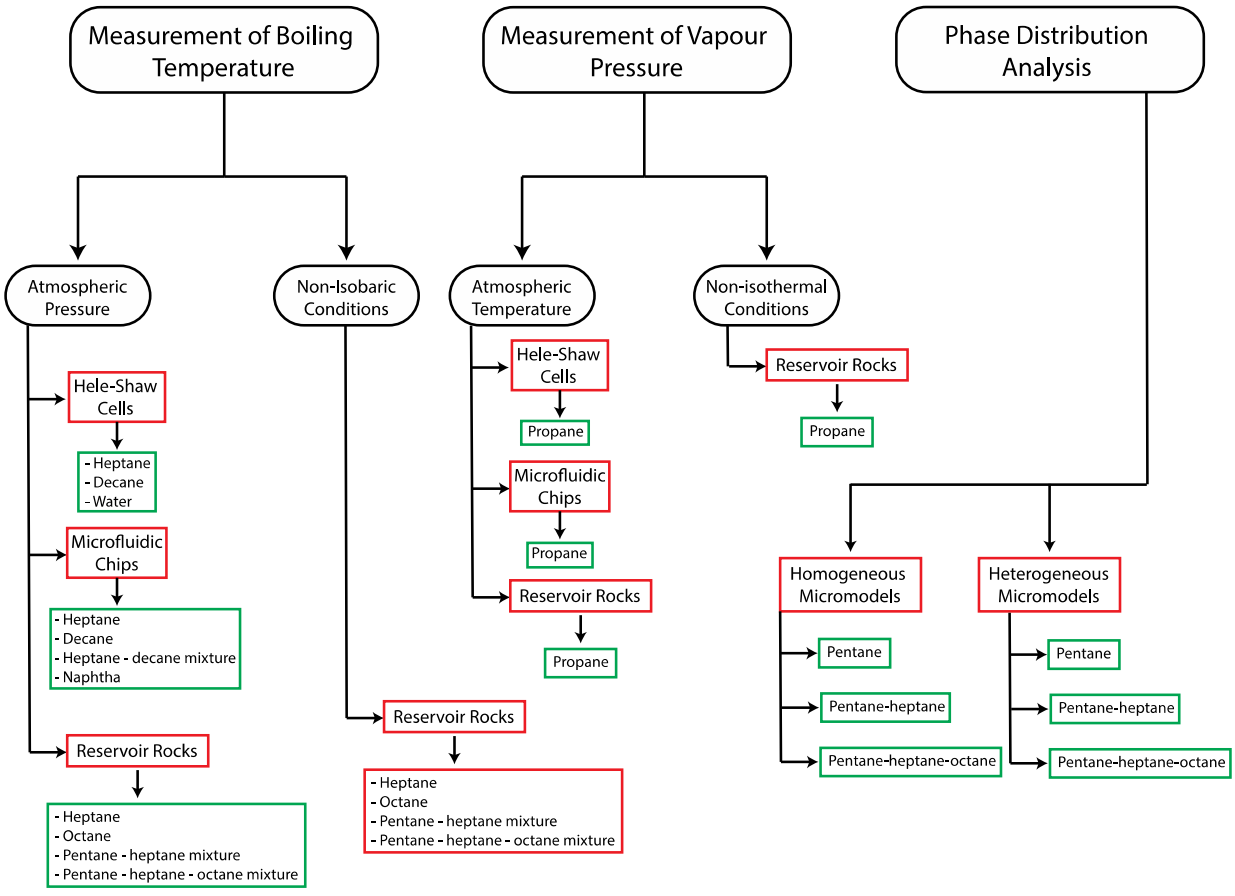

Figure 1-1: Proposed Research Methodology.

1.4 Thesis Structure

This paper-based thesis consists of eight papers that cover eight chapters in this thesis. Each chapter covers detailed information about each paper, including the preface, introduction, and conclusion. **Chapter 1** gives introductory information about the importance of achieving accurate modeling of fluid phase alteration in petroleum applications and numerical reservoir simulations. This chapter also defines the problem and the methodology used to thoroughly understand the phenomenon of phase change in porous media.

Chapter 2 covers our initial experiments conducted to visualize the vaporization of pure liquids (water, heptane, and decane) in Hele-Shaw glass cells. A comparison between measured vaporization temperatures and computed boiling temperatures by the Thomson equation is also shown in this chapter. Several modifications of Thomson equation are presented which were suggested using a regression analysis.

Chapter 3 presents experimental outcomes of boiling temperature measurement of single-component (heptane and decane) and multicomponent (heptane-decane mixture and naphtha) solvents in homogeneous, heterogeneous, and capillary-tube microfluidic chips to study the effect of medium size on their phase-change behavior.

Chapter 4 shows detailed results of vaporization temperature measurements in Berea sandstone, Indiana limestone, tight sandstone, and shale. In the analysis, single-component (heptane and octane) and multicomponent (binary and trinary mixtures) hydrocarbons were used, and all the experiments were conducted at the atmospheric pressure.

Chapter 5 covers the measurement of phase-change temperatures of single-component (heptane and octane) and multicomponent (binary and trinary mixtures) hydrocarbons in the reservoir rocks at various pressures. The experimental outcomes are compared with the computed two-phase envelopes, obtained by the Peng-Robinson equation-of-state.

In **Chapter 6**, detailed analysis of the effect of rock wettability and adsorption on the vaporization of single-component hydrocarbons (heptane and octane) is explained, including the theoretical explanation of pore-molecule interactions with respect to pore sizes.

Chapter 7 shows the initial experimental observation of propane condensation in Hele-Shaw cells, micromodels, and reservoir rocks under ambient temperature. A comparison between measured vapour pressures and computed phase-change pressures by the Kelvin equation is shown in this chapter which was conducted with various medium sizes of silicate glass models.

Chapter 8 presents the measurement of propane phase-change pressure in Hele-Shaw cells and micromodels under the ambient temperature. The investigation of propane's vapour pressure in several reservoir rocks, at different temperatures, and a comparison between measured vapour pressures and computed phase-change pressures by the Kelvin equation and Peng-Robinson equation-of-state are shown and explained.

In **Chapter 9**, an investigation of displacement characteristics of gas-liquid systems, phase distribution, and vapour phase dynamics is shown and described. The analysis was conducted using microfluidic chips, and several pure and mixed hydrocarbons were studied accordingly.

Chapter 10 provides a summarization of all the included papers, research contributions, and suggested future works for further improvements. Also, a reference list for each chapter is presented.

2 Chapter 2: Revisiting Thomson Equation for Accurate Modeling of Pore Scale Thermodynamics of Hydrocarbon Solvents

A version of this chapter was presented and published as a conference paper at the SPE Annual Technical Conference and Exhibition held in San Antonio, Texas, USA, 9-11 October 2017 (SPE-187384-MS). Additionally, an updated version was published in Physics of Fluids, 2019, **31**(12): 122004.

2.1 Abstract

As stated by the classical Thomson equation, the pore scale thermodynamics of solvent is different from bulk conditions being critically controlled by capillary characteristics. This equation shows that the boiling point temperatures decrease remarkably as the pore size becomes smaller, after a threshold value. This paper investigates this phenomenon for hydrocarbon solvents experimentally and compares the results with the values, obtained from the Thomson equation, to test its applicability in modelling heavy-oil recovery by solvents under non-isothermal conditions. As an initial step, the boiling point temperatures of two single-component solvents (heptane and decane) were measured by saturating Hele-Shaw type cells with variable apertures (ranging from 0.04 mm to 5 mm) and monitoring the boiling process. One experiment was run with a thickness of 12 mm to represent the bulk case. As the aperture (pore size) became smaller, the boiling point temperature decreased. For example, the measured boiling temperatures of heptane and decane were approximately 58°C and 107°C for the aperture values less than 0.15 mm, which were considerably lower than the "bulk" values (around 40%). In the next step, the same experiments were repeated using micromodels, representing porous media. Using the Thomson equation, the boiling points of the selected liquids were mathematically computed and compared with the experimental results from Hele-Shaw and micromodel experiments. Finally, modifications to the Thomson equation and alternative formulations were suggested.

2.2 Introduction

Heavy-oil recovery can be achieved by reducing the viscosity of oil using thermal and solvent injection methods. Although steam injection is the most common heavy-oil recovery technique in practice, it has limitations owing to the high cost and environmental problems. Due to excessive cost and high risk of solvent retainment, the sole injection of solvents is economically unfeasible. Therefore, hybrid applications have been suggested as solvent addition to steam (ES-SAGD-expanded solvent steam assisted gravity drainage-and LASER-liquid addition to steam to enhance recovery), thermally aided (steam or electromagnetic heating) solvent (SOS-FR-steam-over-solvent injection in fracture reservoir), or hot solvent injection.

Solvents can be introduced as a co-injected fluid with steam to improve the process efficiency (Ali and Abad 1976; Redford and McKay 1980; Shu and Hartman 1988; Nasr and Ayodele 2005). The other option is to inject heated solvent. The effect of a superheated paraffinic solvent injection on heavy-oil recovery was investigated by Allen et al. (1984). The superheated solvent (pentane) was injected at an elevated and sufficient pressure to cause a solvent diffusion into the viscous oil and increase the reservoir pressure. A number of thermal recovery processes with solvent injection were proposed and experimentally tested to minimize the operational cost of steam injection (Mohammed and Babadagli 2013; Naderi and Babadagli 2016).

Steam Alternating Solvents process (SAS) was experimentally and numerically investigated by Zhao et al. (2004, 2005). The main idea of SAS process is to inject steam and solvent alternately with similar well configurations to the Steam Assisted Gravity Drainage process (SAGD). The SAS process has the capability of combining the advantages of SAGD and VAPEX processes (Zhao et al. 2004, 2005). The impact of temperature on the performance of solvent injection in terms of recovery improvement was investigated by Pathak and Babadagli (2010). They concluded that rising temperature could improve the recovery up to a certain temperature, which is slightly above the saturation point for a given pressure.

One of the disadvantages of steam-solvent recovery processes is high cost of hydrocarbon solvents. Recycling a great percentage of injected solvents can have an impact on reducing the overall cost of these technologies (Cui and Babadagli 2016). Solvent retrieval is a process of recovering solvents after heavy-oil production. Gupta et al. (2004) reported a study on the Solvent Aided Process (SAP), which aimed to enhance the SAGD performance by adding hydrocarbon solvents to the steam, after analysing the performance of SAP by simulation and laboratory experiments. They also discussed the importance of solvent retention in a porous medium and its impact on the economics.

Steam-Over-Solvent in Fractured Reservoir (SOS-FR) was introduced by Al-Bahlani and Babadagli (2009) to efficiently recover heavy-oil from fractured reservoirs. The main idea of the process is to inject steam and solvents in three stages: (a) inject steam to recover the oil thermally; (b) injected solvent to recover the remaining oil by diffusion process; (c) injected steam to retrieve the trapped solvent and recover additional volumes of oil. To visualize the effect of temperature, wettability, and solvent type on solvent retrieval process at pore scale, Marciales and Babadagli

(2016) investigated the retrieval process of heptane and naphtha solvents using micromodels. The retrieval of the two solvents was achieved up to 90% by increasing the temperature up to the boiling point of the solvent. This research was then continued by Cui and Babadagli (2017) considering the oil viscosity as well. Solvent vaporization and mobilization were visualized under different temperatures. Using carbon dioxide (CO_2) as an alternative solvent in SOS-FR was studied by Naderi and Babadagli (2014). Experiments were performed by injection steam first and then CO_2 as a second stage. Lastly, steam was injected to recover more volumes of oil in the reservoir. It was concluded that CO_2 could be a reasonable option for replacing hydrocarbon solvents in terms of lowering operational cost.

To apply the solvent retrieval process effectively, it is important to understand solvents' behaviour in tight media under various temperatures, including boiling points. Boiling point is a stage at which vapour pressure is equal to surrounding pressure. In other words, when phase change starts to take place in the liquid, gradually converting to vapour. Boiling temperature of liquids can be affected by several factors such surface tension, surrounding pressure, and heat of vaporization.

According to the Thomson equation, pore size also has an impact on boiling temperature of any pure-component liquid; meaning the boiling point of a certain liquid in a bulk medium is not equal to the boiling point of the same liquid in a tight medium. Hence, boiling temperature is expected to decline as the pore size reduces (Berg 2010). Bao et al., 2017 investigated n-propane bubble nucleation and phase transition in sub-100 nanometre capillary channels under pressure drawdown process. The measured pressures were then compared with calculated vapour pressures from the Kelvin equation, nucleation theory equation, and Spinodal limit equation. The results showed that n-propane remained in liquid phase in nano pores under pressure much lower than the saturation pressure at bulk conditions owing to the cavitation effect. Similarly, Zhong et al., 2018 investigated the phase-change behaviour of n-propane to validate the Kelvin equation in an eight nanometres channel. The phase behaviour was observed simultaneously under various temperatures, ranging between 286.15 and 339.15 K. It was found that the condensation initiation of n-propane in 8 nm channel nearly matched with the results obtained by Kelvin equation. Tsukahara et al., 2012 studied the water saturated vapour pressure in nano spaces (10 – 100 nm). It was proved that the saturated vapour pressure of water declines as the channel size decreases, and the Kelvin equation is valid even in extremely confined media (<100 nm).

In solvent retrieval process, the trapped solvent is heated by injecting hot fluids such as hot water or steam (Al-Bahlani and Babadagli 2008). Understanding liquids' behaviour in tight media at different temperatures is an essential point in solvent retrieval process. Thus, identifying the boiling point of the trapped solvent in reservoir is a critical task in the process. Thomson equation is a mathematical approach that can be used to compute boiling temperatures of pure solvents in tight porous media. Nonetheless, the equation is only effective when the pore size is less than 1000 nm (Berg 2010). The purpose of this paper is to evaluate the applicability of Thomson equation by comparing it with experimental observations. We initiated boiling point measurements by using Hele-Shaw glass samples that represented a thin and hollow tight medium. Then, to obtain a more realistic understanding of the solvent behaviour at pore scale under different temperatures, micromodels were used.

Investigating the phase-change behaviour in different types of media (Hele-Shaw cells and microfluidic chips) was one of the unique features of this study. Heat transfer analysis was considered to minimize the temperature measuring errors, inspect the temperature difference between the heating plate and outer glass surface, and provide an accurate estimation of fluid average temperature during the experiments. The phase transformation of water was also studied experimentally under various heating rates and conditions.

Temperature measurement in micromodel visual experiments is highly critical especially in studies focusing on phase alteration or fluid heat transfer along microfluidic glass chips. In prior works, different measuring methods were used to detect the outer surface temperatures of micromodels at various points. Syed et al. (2016) studied the performance of SAGD process with various alkaline additive concentrations at pore scale by using a glass micromodel. The process was evaluated by using optical and thermal approaches. An infrared thermal sensor was utilized to measure the steam temperature along the microfluidic chip and at steam chamber interface. The recovery mechanisms of Solvent-Aided SAGD process with chemical additives (n-pentane and n-hexane) was investigated by Mohammadzadeh et al. (2015). The study was performed by using glass micromodels, continuously measuring steam temperature along the model by recording the glass surface temperature at 15 positions using thermocouples. In the present paper, outer surface temperatures of Hele-Shaw and microfluidic glass chips were measured by using thermocouples

similar to their approach. Errors due to temperature measurement were minimized by performing heat transfer analysis along the glass model thickness.

2.3 Statement of the Problem and Objectives

Solvent retrieval is highly critical in hybrid thermal-solvent application as it controls the economics of the process critically. This becomes more difficult in heterogeneous systems such as fractured carbonates, layered sandstones, or unconsolidated sands after cold production with sands. In these systems, solvent cannot be easily retrieved by viscous displacement after diffusing into lower permeability matrix. However, it is possible by vaporizing the solvent to be relieved from lower permeability (matrix) to the higher permeability medium. The dynamics and thermodynamics of this process are different in the bulk condition and capillary media. The Kelvin and Thomson equations define the relationship between the pressure and temperature for bulk and capillary conditions, respectively. This, however, is to be tested experimentally for different capillary conditions and solvent type to properly design the applications at the field conditions.

According to the Thomson equation, lower boiling points are needed as the pore size gets smaller and interfacial properties change. The boiling temperatures of different liquids were measured using Hele-Shaw approach and micromodels, then compared with the Thomson equation. By doing so, a clear understanding of the applicability of Thomson equation for oil recovery applications is achieved, and its variations/deviations from the experimental data is also clarified.

2.4 Background

Laplace equation (also known as Young-Laplace equation) reflects the mechanical equilibrium condition of a curved interface by considering its work of expansion of a single bubble in a liquid and its surface tension (Firoozabadi 2016). The work of expansion can be expressed as the following:

$$dW = \Delta P \, dV = \sigma \, dA \tag{1}$$

where dW is change of work done, ΔP is change of pressure between bubble and liquid, dV is change of bubble volume, σ is surface tension of bubble, and dA is change of bubble area. The Laplace equation takes the following form:

$$\Delta P = \sigma \left[\frac{1}{R1} + \frac{1}{R2}\right] \tag{2}$$

where ΔP is change of pressure, σ is surface tension of bubble, $R1$ is radius of first curvature, and $R2$ is radius of second curvature. While dealing with a single spherical bubble, the Laplace equation can be expressed as the following:

$$\Delta P = \frac{2\,\sigma}{R} \tag{3}$$

where ΔP is change of pressure between bubble and liquid, σ is surface tension of bubble, and R is radius of the spherical bubble. Kelvin equation considers the effect of curvature on the equilibrium properties of bulk liquids (Berg 2010). The effect is also named as the Kelvin effect. The main ideology of the Kelvin effect is that when a liquid is fully or partially constrained by a curved interface and is in contact with another fluid, the phase equilibrium properties of the system are different compared with a situation where both phases or fluids are separated by a flat interface.

In order for the curved interface to exist, a pressure difference must take place between the two fluids unlike in the case with a flat interface where both fluids have equal pressures. Hence, the Kelvin effect states that vapor pressure of a small liquid drop is higher than the vapor pressure of the same liquid involved with a flat surface. Likewise, in porous media, the vapor pressures of liquids in tight pores are not the same as when they are located in bulk media or linked with flat surfaces. The Kelvin equation is illustrated as following:

$$P_r = P_\infty exp\left[\frac{-2\,\sigma\,v^L}{r\,R\,T}\right] \tag{4}$$

where P_r is vapor pressure at curved interface, P_∞ is vapor pressure at flat surface, σ is surface tension, v^L is molar volume of the liquid, r is droplet (or capillary) radius, R is universal gas constant, and T is temperature. From this equation, it can be observed that vapor pressure at curved interface P_r had an inverse relationship with droplet radius *r*. The Thomson equation considers the

effect of curvature on droplet temperature (boiling point) at a constant pressure. The equation was derived by assuming that molar volume of liquid v^L and heat of vaporization ΔH_{vap} are constant parameters (Berg 2010). The Thomson equation then takes the form:

$$T_r = T_\infty \, exp\left[-\frac{2\,\sigma\,v^L}{r\,\Delta H_{vap}}\right] \tag{5}$$

where T_r is temperature at porous medium, T_∞ is temperature at bulk medium, σ is liquid surface tension, v^L is molar volume of liquid, r is droplet (or pore radius), and ΔH_{vap} is heat of vaporization of liquid. The equation states that boiling temperature declines as the radius of liquid droplet or pore reduced.

Similarly, the boiling temperatures of liquids in tight media (such as porous media) were lower than those in bulk media. **Figure 2-1** shows the change of water, heptane, and decane boiling point T_r with the change of droplet or pore radius *r*.

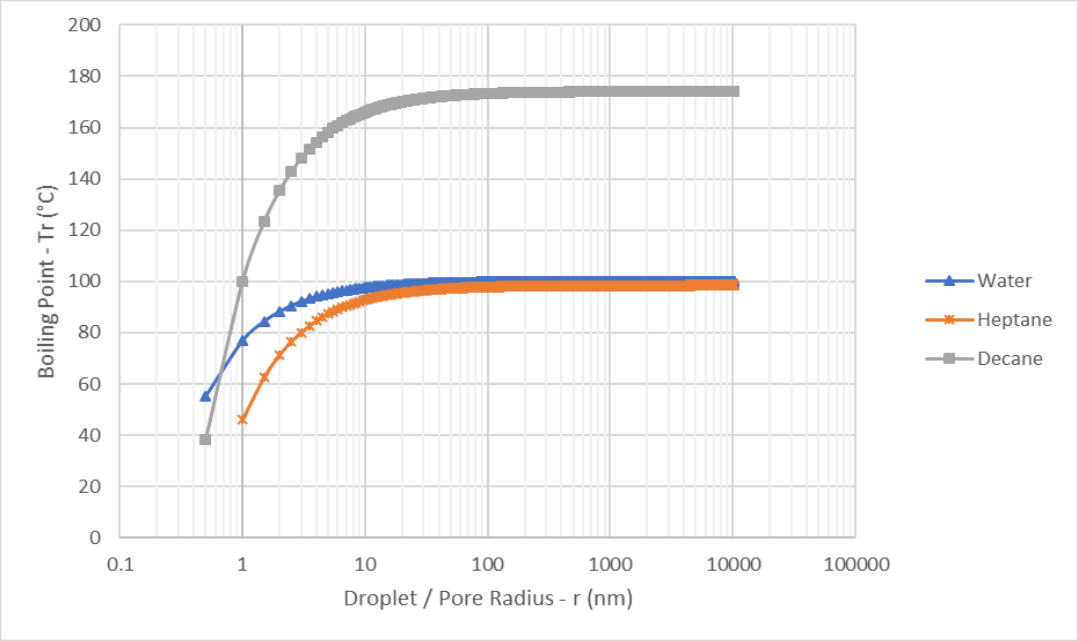

Figure 2-1: Boiling Point behavior with droplet/pore radius variation.

As seen in **Figure 2-1**, before reaching a critical value (300 nm) an exponential decline in temperature was obtained and boiling point could be reduced by approximately 50% by decreasing the pore size two orders of magnitude.

2.5 Experimental Work

The boiling points of different liquid solvents were experimentally measured by using Hele-Shaw glass chips and homogeneous/heterogeneous micromodels representing porous media. Various thicknesses of Hele-Shaw glass samples were used to investigate the effect of medium thickness on liquid boiling temperature. As a further step, homogeneous and heterogeneous micromodels were used to obtain more realistic observations of the impact of pore structure on boiling point.

2.5.1 Hele-Shaw Approach

The Thomson equation is derived by considering that the surface or pore is completely wetting ($cos\ \theta\ = 1$). For the Hele-Shaw glass samples used in our experiments, all used liquids fully spread on the surfaces representing a strongly liquid-wet system. This glass property brought an advantage of having surface property close to the assumption considered in the Thomson equation. By using metal spacers, the glass samples were made with different gap thicknesses, ranging from 0.04 to 5 mm. To represent a case of bulk medium, a glass sample with 1.2 cm was prepared, as well. Three liquids were selected to be tested in the experiments: deionized water (H_2O), heptane (C_7H_{16}), and decane ($C_{10}H_{22}$). Deionized water was used as a reference or benchmark. Heptane and decane (as pure components) were used to compare their experimental boiling points with the calculated boiling points by the Thomson equation. All liquids were evacuated for a few hours to remove the trapped air from the liquids and avoid any bubble generation due to dissolved gases in the liquid solvents.

Experiment setup. Figure 2-2 illustrates the experimental system, which contained a DSLR camera to capture various stages of the liquid, heating plate, UV light, temperature controller, and Hele-Shaw glass chip. All three liquids were dyed by IFWB-C7 Fluorescent Red (for deionized water) and DFSB-K175 Fluorescent Orange (for organic solvents). Thus, the UV light was used to glow the liquid and clearly visualize the bubbles.

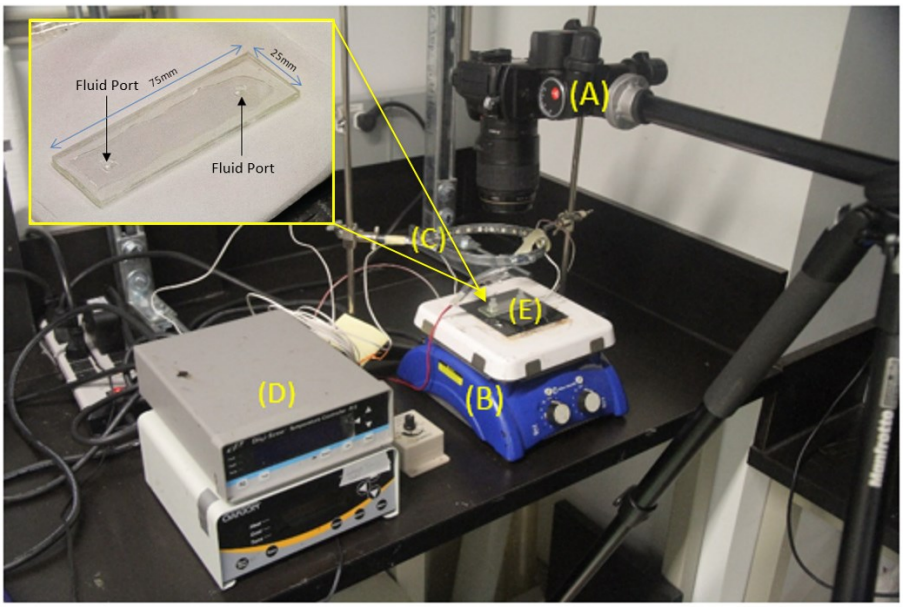

Figure 2-2: Experimental system: (A) DSLR camera, (B) heating plate, (C) UV light, (D) temperature controller and (E) Hele-Shaw glass sample.

Procedure. To initiate the experiments, liquids were injected into the glass samples with the help of plastic syringes. After that, the samples were placed horizontally on the heating plate to be heated gradually until boiling point was reached. The thermocouple was attached to the outer surface of Hele-Shaw glass cells to measure the outer surface temperature during the experiment. During the experiment, the DSLR camera took photos of different liquid stages while the liquid was heated.

At the same time, the temperature at each stage was recorded by using a temperature controller. All Hele-Shaw experiments were conducted under atmospheric pressure and the ports in the glass samples were open to the atmosphere to avoid any pressure build-up inside the samples during the heating process.

Results and discussions. Initially, deionized water was used to observe its behaviour at different temperatures in capillary media with various thicknesses as a benchmark and calibration. Five glass samples having different gap thicknesses ranging from 0.2 mm to 1.2 cm were used. While heating the glass samples gradually, attention was paid to three main stages: (a) first bubble

appearance, (b) increase of bubbles number to a certain size, and (c) rapid and continuous formation of bubbles. Based on the kinetic molecular theory, increasing temperature or pressure in any system leads the energy of molecules to change, which results into quicker or slower movements of molecules (Tro 2012). Mainly, in certain circumstances, this phenomenon causes the fluids to change from physical state to another. One of the major challenges is that these molecular movements are extremely random in direction and hard to predict. As a result, the initial stages of phase change might take place unpredictably, especially in cases where we have medium sizes that are close to each other. Basically, the appearance of the first bubbles highly depends on how the molecules move and collide with each other. In our analysis, the major phase change (boiling stage) of the liquid was taken under consideration since it normally happens at specific temperatures and does not take place randomly.

In the Hele-Shaw experiments, we considered that stage C (rapid and continuous formation of bubbles) was an identification that boiling point was reached. **Figure 3a** shows deionized water in a 0.3 mm gap thickness glass sample at room temperature (25°C). At a temperature of 45°C, the first bubbles appeared in the liquid (**Figure 3b**). The number of bubbles started to increase at a temperature of 55°C (**Figure 3c**). At 66°C, bubbles begin to form continuously and rapidly as shown in **Figure 3d**. At this stage, it was believed that deionized water had reached its boiling temperature at which the vapor pressure was equal to the surrounding pressure ($\approx 1\ atm$). We expected that the boiling point of deionized water would be less than 98°C as the aperture of the Hele-Shaw glass chip decreased. The same experiment was repeated using glass chips with 0.2 mm, 3 mm, 5 mm, and 1.2 cm gap thicknesses. Table 2-1 presents deionized water temperatures at various stages and gap thicknesses.

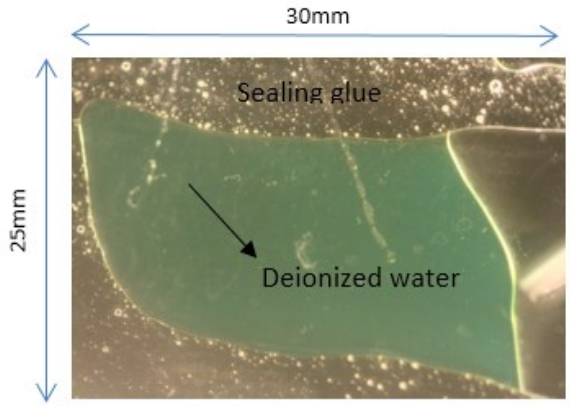

Figure 3a

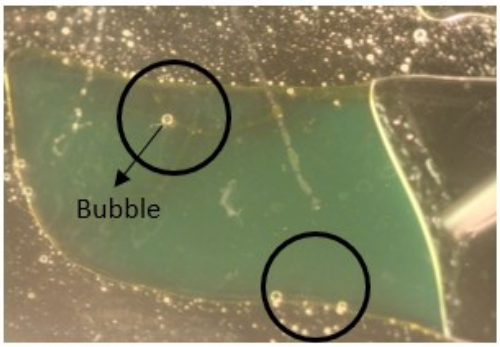

Figure 3b

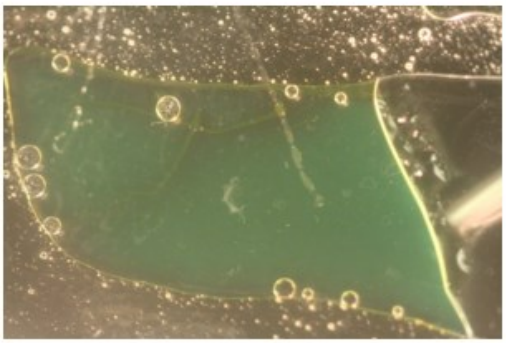

Figure 3c

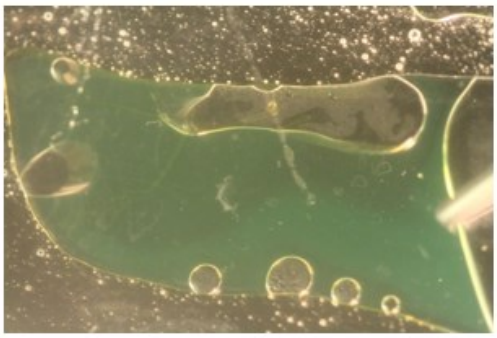

Figure 3d

Figure 2-3: (a): 0.3 mm gap thickness glass sample with deionized water at 25°C; (b): 0.3mm gap thickness glass sample with deionized water at 45°C; (c): 0.3mm gap thickness glass sample with deionized water at 55°C; (d): 0.3mm gap thickness glass sample with deionized water at 66℃.

Table 2-1: Deionized water temperatures at various stages and gap thicknesses.

Deionized water – 0.2mm gap spacing

Stage	Temperature (℃)
First bubble appearance	40
Increase of bubbles number	61
A rapid and continues formation of bubbles	64

Deionized water – 3mm gap spacing

Stage	Temperature (℃)
First bubble appearance	56
Increase of bubbles number	65
A rapid and continues formation of bubbles	69

Deionized water – 5mm gap spacing

Stage	Temperature (℃)
First bubble appearance	54
Increase of bubbles number	66
A rapid and continues formation of bubbles	71

Deionized water – 1.2cm gap spacing

Stage	Temperature (℃)
First bubble appearance	68
Increase of bubbles number	84
A rapid and continues formation of bubbles	98

The heating plate ensures a uniform heat distribution along the Hele-Shaw glass cells. To validate the previous results with water, a set of experiments were redone by measuring the temperature at three points on the outer surface of the glass cells, as illustrated in Figure 19. Accordingly, the average temperature over the three points was considered for each chip. Table 2-2 shows the boiling temperatures of water in various gap sizes.

Table 2-2: Water boiling temperatures in different gap sizes.

Gap size (mm)	Water – Boiling Point (℃)
0.04	60
0.2	62
0.5	63

As a further step, heptane (C_7H_{16}) and decane ($C_{10}H_{22}$) were used to measure their boiling points using Hele-Shaw cells with different apertures. For heptane and decane, five glass samples with 0.15 mm, 0.45 mm, 0.75 mm, 1.02 mm, and 1.2 cm gap thicknesses were selected. With all glass chips, both liquids went through the same stages as observed previously with deionized water. Table 2-3 presents heptane and decane boiling point temperatures at various stages and gap thicknesses.

Table 2-3: Heptane and decane temperatures at various stages and gap thicknesses.

Heptane (C7H16) – 0.15mm gap spacing	
Stage	Temperature (℃)
First bubble appearance	39
Increase of bubbles number	44
A rapid and continues formation of bubbles	58
Heptane (C7H16) – 0.45mm gap spacing	
Stage	Temperature (℃)
First bubble appearance	43
Increase of bubbles number	48
A rapid and continues formation of bubbles	61

Heptane (C7H16) – 0.75mm gap spacing

Stage	Temperature (℃)
First bubble appearance	45
Increase of bubbles number	60
A rapid and continues formation of bubbles	64

Heptane (C7H16) – 1.2cm gap spacing

Stage	Temperature (℃)
First bubble appearance	50
Increase of bubbles number	55
A rapid and continues formation of bubbles	93

Decane (C10H22) – 0.15mm gap spacing

Stage	Temperature (℃)
First bubble appearance	80
Increase of bubbles number	91
A rapid and continues formation of bubbles	107

Decane (C10H22) – 0.45mm gap spacing

Stage	Temperature (℃)
First bubble appearance	72
Increase of bubbles number	82
A rapid and continues formation of bubbles	109

Decane (C10H22) – 1.02mm gap spacing

Stage	Temperature (℃)
First bubble appearance	73
Increase of bubbles number	104
A rapid and continues formation of bubbles	109

Decane ($C_{10}H_{22}$) – 1.2cm	
Stage	Temperature (℃)
First bubble appearance	94
Increase of bubbles number	100
A rapid and continues formation of bubbles	170

For the sake of verification, experiments with heptane and decane were repeated using a wider variety of gap thicknesses, ranging from 0.04 to 1.15 mm. Table 2-4 illustrates the measured heptane and decane boiling points from repeated experiments. **Figures 2-4a** and **2-4b** show the variation of measured boiling point temperatures obtained from the Hele-Shaw experiments. The experiments were repeated several times to inspect the reoccurrence of the phenomena and to check for possible error involved under the same previous conditions. Heat transfer analysis was performed to understand the heat loss that took place during the heating process and eliminate the measurement errors as much as possible while measuring temperatures. The experimental setup was prepared under similar thermodynamic conditions as the bulk case. Additionally, temperature measurement was done in a comparable method as it was done in bulk condition. This is another verification of experimental accuracy as the boiling points of liquids used (water, heptane, and decane) are known at the atmospheric pressure. As seen in **Figures**. **2-4a** and **2-4b**, experimental measurement error involved is typically less than +/- 1% and even 0% in certain gap thickness cases.

Table 2-4: Heptane and decane boiling temperatures at various gap thicknesses.

Gap thickness (mm)	Heptane (C7H16) – Boiling Point (℃)	Decane (C10H22) – Boiling Point (℃)
0.04	56	104
0.05	59	106
0.15	60	107
0.45	61	109
1.02	63	110
1.15	64	111

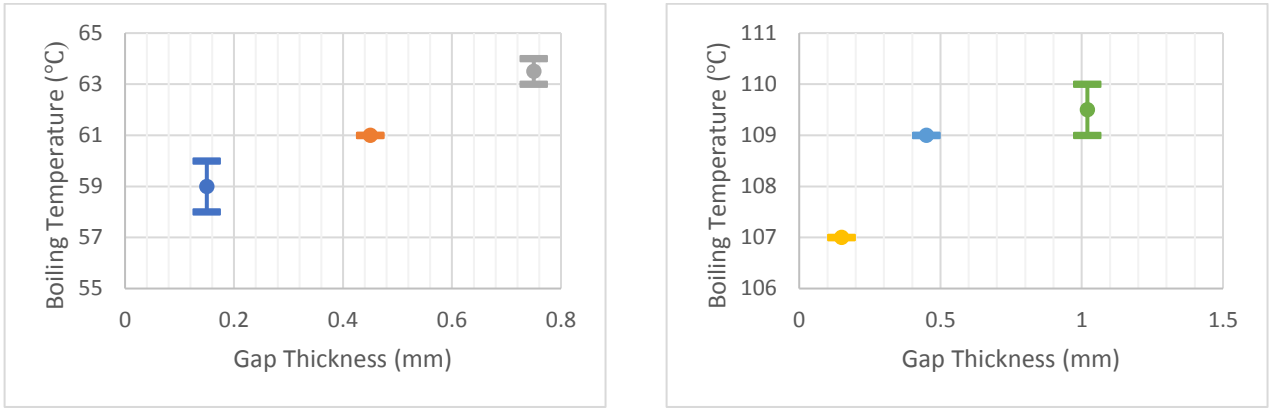

(a) **(b)**

Figure 2-4: (a): Errors of measured boiling point temperatures obtained from the heptane experiments; (b): errors of measured boiling point temperatures obtained from the decane experiments.

2.5.2 Micromodel Analysis

Microfluidics have become one of the well-known technologies in medical and engineering applications owing to the extended tight volumes that these microchips could consist with. The main advantage of glass microfluidic models is the chemical resistance, which is highly beneficial in applications that involve the usage of reactive or acidic fluids. Featuring a high optical detection

is a major benefit that allows a clear visualization of fluid's behaviour in micro (< 20 nm), meso (2 - 50 nm), or macro (> 50 nm) channels. The fabrication of glass microfluidic chips consists of three main processes, where are DC sputtering, photolithography, and wet etching. Firstly, a thin film of chromium (Cr) and gold (Au) is deposited on the surface of a substrate to act as a masking layer for the glass. Then, in photolithography stage, the photomask design is transferred onto the masking layer by exposing it to radiation and UV light, after coating the layer with photoresist (light-sensitive material). The formed photoresist image on the masking layer is converted to an underlying layer by the wet etching process.

Using micromodels provides a more representative observation of porous conditions, comparing with Hele-Shaw glass chips. In this paper, three categories of micromodels were used: (a) uniform grain diameter and pore throat size, (b) non-uniform grain diameter and pore throat size, and (c) capillary tubes with different sizes. For the uniform property micromodel, two models with different grain diameters and pore throat sizes were utilized. In the capillary tube micromodels, tube sizes ranged from 5 to 40 micrometers. The purpose of using various micromodel types is to inspect the influence of system structure on boiling point of solvents. In micromodel experiments, vacuumed water, pure heptane, a heptane-decane mixture, and naphtha were used. In the heptane-decane mixture, each component had a mass fraction of 50%. Naphtha combines around 115 hydrocarbon components starting from pentane (C_5). Components from C_5 to C_{12} have the highest mass fraction comparing with the remaining components in naphtha.

Experimental setup. The setup consists of Zeiss Stemi 2000C microscope, 7D canon DSLR camera, LED light, temperature measurement device (National Instruments), thermocouple, and electric heating plate.

Procedure. Firstly, micromodels were saturated with solvents using a syringe pump. Solvents were injected through the micromodels at a constant flowrate of 1.5 microliter per minute for around 10 h. After saturation process was completed, the saturated micromodels were placed horizontally on the electrical heating plate to be heated gradually. Images and temperature readings were taken continuously every 2 sec with the help of a DSLR camera and temperature measurement device. As with the Hele-Shaw experiments, all of the micromodel experiments were conducted under ambient pressure (14.7 psia) with open ports to the surrounding pressure;

therefore, there was no pressure build-up inside the micromodel when fluid temperature was raised.

Results and discussions. The experiments were started with uniform properties micromodels and pure heptane as a solvent. Using a microscope assisted with clearly visualising the phase change within the pores when the boiling point of the solvent was reached. With the uniform properties micromodel (0.11 mm grain diameter and 0.01 mm pore throat), the pure heptane started to boil and convert to vapor at a temperature of 72℃ (**Figure 2-5a**). At 79℃, most of the heptane had changed into vapour (**Figure 2-5b**). A large volume of heptane in the micromodel boiled and transformed into gas at a temperature of 82℃ (**Figure 2-5c).**

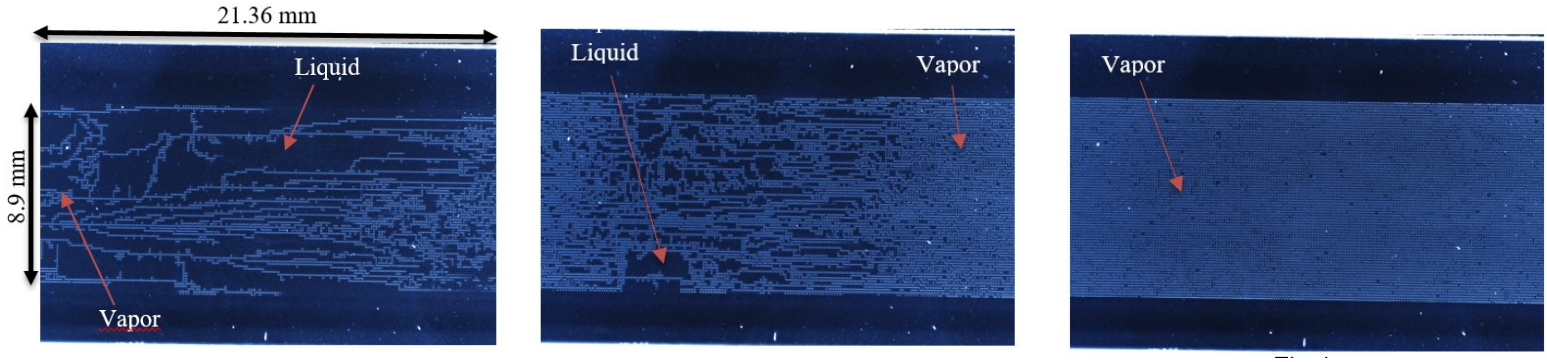

Figure 2-5 - (a): Homogeneous micromodel at 72℃; (b): Homogeneous micromodel at 79℃; (c): Homogeneous micromodel at 82℃.

Using a micromodel with larger grain diameter resulted in a higher boiling temperature of heptane. In a micromodel with 0.22 mm grain diameter and 0.01 mm pore throat, heptane began to boil at a temperature of 83℃ (**Figure 2-6a**). Most of the heptane in the micromodel converted into gas at 86℃ (**Figure 2-6b**); however, the trapped heptane (**Figure 2-7**) remained in the pore throats even when the temperature went up to 111℃. The residual liquids in porous media require more heat or energy to boil due to the pores wettability of the system.

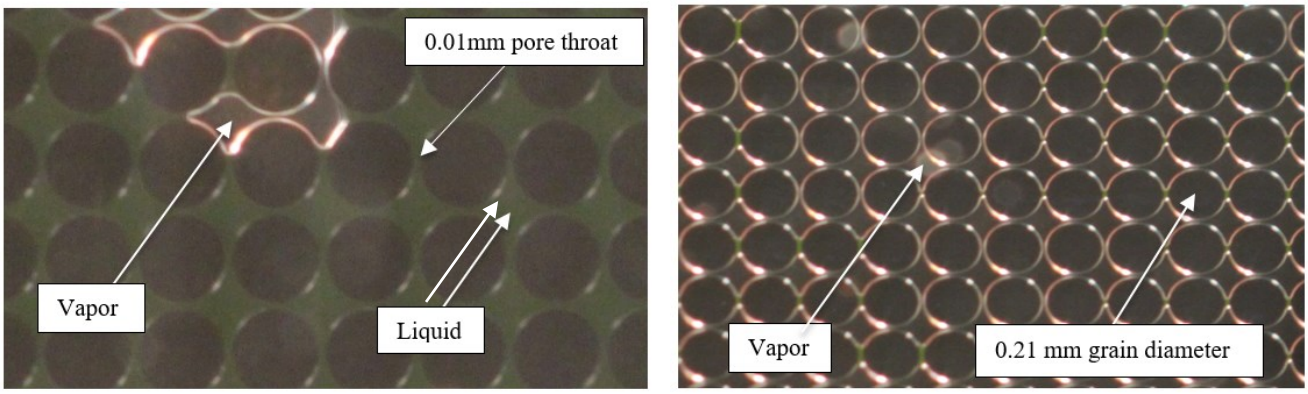

(a) (b)

Figure 2-6 - (a): Homogeneous micromodel at 83℃; (b): Homogeneous micromodel at 86℃.

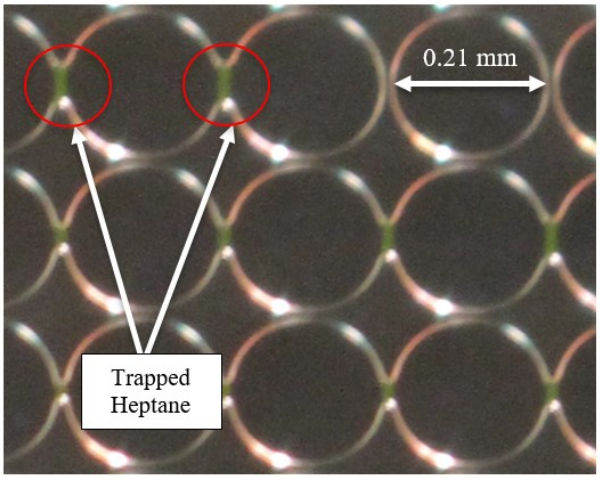

Figure 2-7: Trapped heptane in pore throats.

A mixture of heptane and decane was injected into homogeneous micromodels to observe its behavior in porous media under different temperatures. Boiling stage of the mixture in a homogenous micromodel (0.21 mm grain diameter and 0.01 mm pore throat) initiated at 79℃. At 111℃, most of liquid mixture had converted to gas. Naphtha was also observed in homogeneous micromodels under various temperatures. In a 0.11 mm grain diameter and 0.01 mm pore throat micromodel, naphtha started to boil at 58℃. Heterogeneous micromodels were used in the experiments to observe the solvents behavior in media where grain and pore throat sizes were distributed non-uniformly. The pore throat in the heterogeneous micromodel ranged between 0.05 and 0.3 mm; moreover, the average grain size was 1 mm. In one of the models, heptane started to

change in phase at 90℃ as shown in **Figure 2-8**. **Table 2-5** displays the boiling point of different liquids in heterogeneous micromodels.

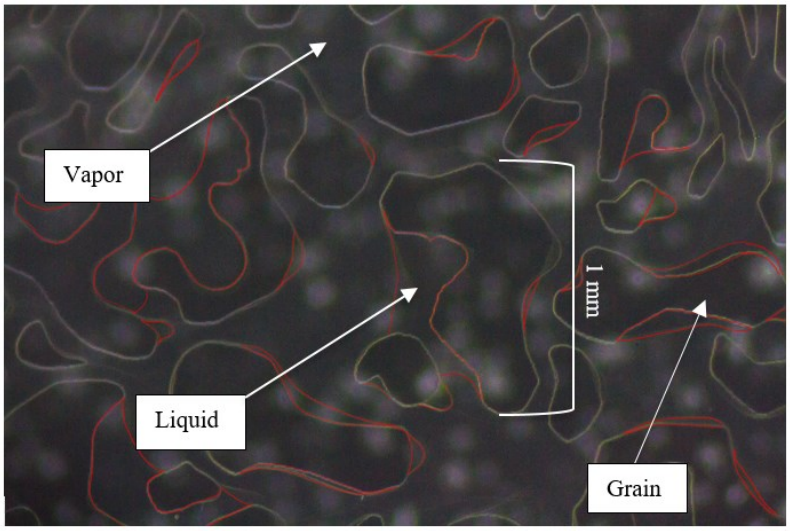

Figure 2-8: Heterogeneous micromodel at 90℃.

Table 2-5: Boiling points of heptane, heptane-decane mixture, and naphtha in heterogeneous micromodel.

	Boiling Point (℃)
Heptane	90
Heptane-Decane Mixture	80
Naphtha	103

Capillary tube micromodels were used as a continuation of previous investigations with Hele-Shaw cells and micromodels. Using such model provided an advantage of getting a clear visualization of phase interface between liquid and vapor during the boiling stage. All the models used in our experiments, including capillary tube microfluidic chips, had a liquid-wet behavior towards water, heptane and decane. Hence, it is expected for the boiling point temperatures to decline with the reduction of pore sizes due to the concave behavior. Initially, the tubes were saturated with vacuumed water to observe its phase change behavior under various temperatures. At a temperature of 80℃, phase change took place in water as shown in **Figure 2-9**. Pure heptane

was also used to inspect its phase change behavior in confined media. At a temperature of 75℃, heptane started to change in phase. Table 2-6 presents the boiling points of vacuumed water, heptane, and decane in capillary tube micromodels with various tube sizes. **Figures 10a** and **10b** show the errors of water and heptane measured boiling point temperatures, obtained from the capillary tube experiments. Error involved in the measurements (up to 5-6% in certain cases) is somewhat higher than the Hele-Shaw cases due to the nature of the experiments. As it is not possible to observe the whole capillary tube, unlike the Hele-Shaw case, and the minimum depth of focus should be kept at a certain value to be able to capture the boundary between the liquid and vapour phase, as the time the vapour phase takes to reach the focused area might be slightly different for each case, thus causing this measurement error.

Table 2-6: Vacuumed water, heptane and decane boiling temperatures at different capillary tube sizes.

	5μm	**10**μm	**20**μm	**30**μm	**40**μm
Water boiling point (℃)	84	81	76	-	80
Heptane boiling point (℃)	77	74	76	-	75
Decane boiling point (℃)	136	-	122	130	127

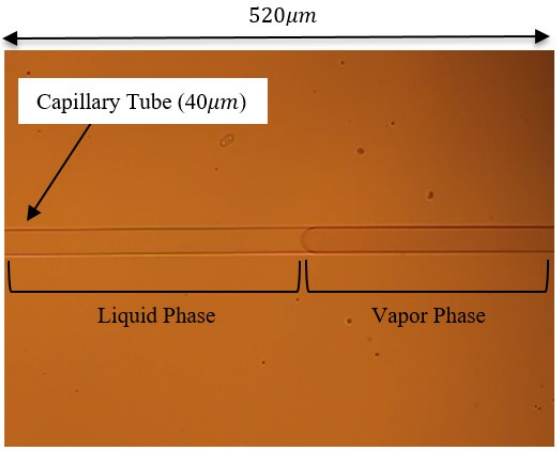

Figure 2-9: 40 micrometers capillary tube at 80℃.

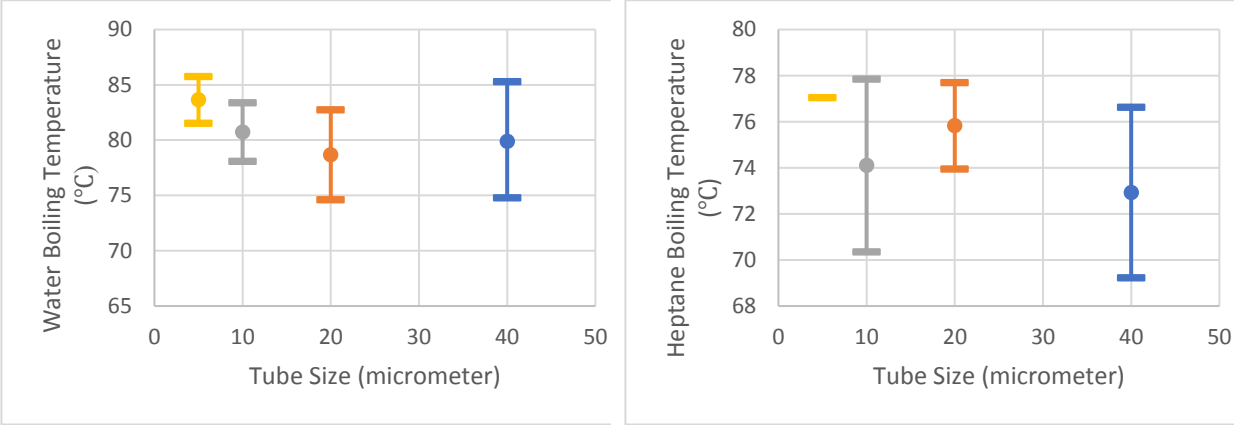

(a) **(b)**

Figure 2-10: (a): Errors of measured boiling point temperatures obtained from the water experiments; (b): errors of measured boiling point temperatures obtained from the heptane experiments.

2.6 Heat Transfer Analysis

In all conducted Hele-Shaw and micromodel experiments, temperatures were measured at the outer surface of the upper glass assuming that injected liquids in the glass chips would share the same temperature as the outer glass surface and the whole system would have a uniform and homogeneous heat and temperature distribution (**Figure 2-11**). To validate the assumption, the temperatures of both the heating plate and outer glass surface were measured to calculate the

temperature difference; therefore, an insight into heat loss along the glass cell thickness could be gained. Based on that, the average fluid temperature in glass chips was estimated accordingly. Details of the heat transfer calculations are presented in the Appendix.

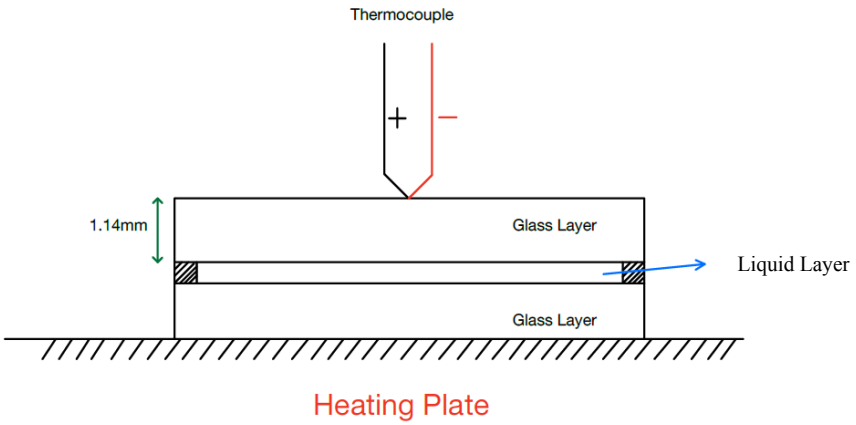

Figure 2-11: Schematic of a Hele-Shaw glass cell on a heating plate.

2.7 Sensitivity Study

In such an investigation, it is critical to examine various factors, of which might have an impact on phase-change behaviour in capillary media. In this paper, three main factors were considered: (A) heating conditions, (B) heating rate, and (C) medium type.

2.7.1 Heating Condition

Heating condition is the method that is used to rise the model temperature. During the experiments, temperature was increased by using either an oven or a heating plate. The heating direction towards the model normally changes according to the heating method that is utilized. Using a heating plate as a source of heat results in a single-directional heat flow, transferring towards the model. Another way of heating is using an oven where the heat flow is equally distributed around the glass chip.

Changing the heat-flowing nature caused noticeable alteration in liquids' boiling points. For instance, in the 0.2 and 3mm gap thickness cells, water started to boil at temperatures of 64℃ and 70℃, respectively. However, heating a 0.35mm gap thickness cell in an oven led the water to boil at a temperature of 80℃ (**Figure 2-12**). The heating regime has an effect on liquids' reaction when heat migrates into the glass models. Raising the temperature of the Hele-Shaw cell with a heating plate usually results in an aggressive and one-directional transfer of heat to the model. Nonetheless, heating the cell in an oven causes a uniform heat distribution around the cell. Also, the heat transfer to the glass model is slower which results in a relatively low heating rate.

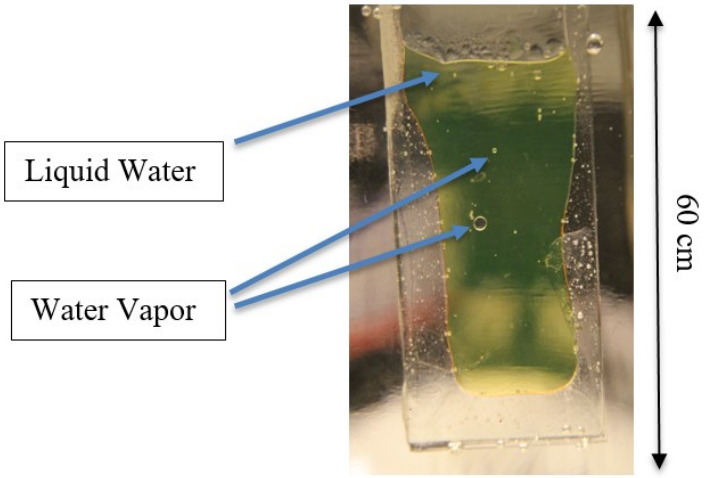

Figure 2-12: 0.35mm gap thickness Hele-Shaw cell at 80℃.

2.7.2 Heating Rate

To inspect the effect of heating rate on phase-change behaviour, the rate was changed by using the temperature controller. The investigation was done on a 20μm capillary tube saturated with water. The micromodel was heated at two rates, which were 0.16 and 0.25 ℃/sec. With a heating rate of 0.16 ℃/sec, phase-change of water initiated in the tube at 83℃. Meanwhile, using a heating rate of 0.25 ℃/sec, boiling stage was achieved at a temperature of 75℃.

2.7.3 Medium Type

As a validation, boiling point of solvents was investigated by using several models with different medium characteristics. Hele-Shaw models have hollow inner volumes with various thicknesses. Micromodels represent porous media that are characterized by different pore volumes, permeabilities, porosities and grain distributions.

Due to the change in contact angle and confinement, these media have non-identical impact on the phase behaviour of liquids as suggested by the Laplace and Kelvin equations. In the Hele-Shaw experiments, solvents tended to boil at temperatures that were nearly 30% lower than their normal boiling points depending on the cell thickness. Whereas, in micromodels, same solvents boiled at temperatures that were approximately 20% less than their normal boiling points depending on the micromodel confinement. **Figure 2-13** illustrates a summary of the measured boiling temperatures of heptane obtained in Hele-Shaw, micromodel, and capillary tube experiments at different pore sizes.

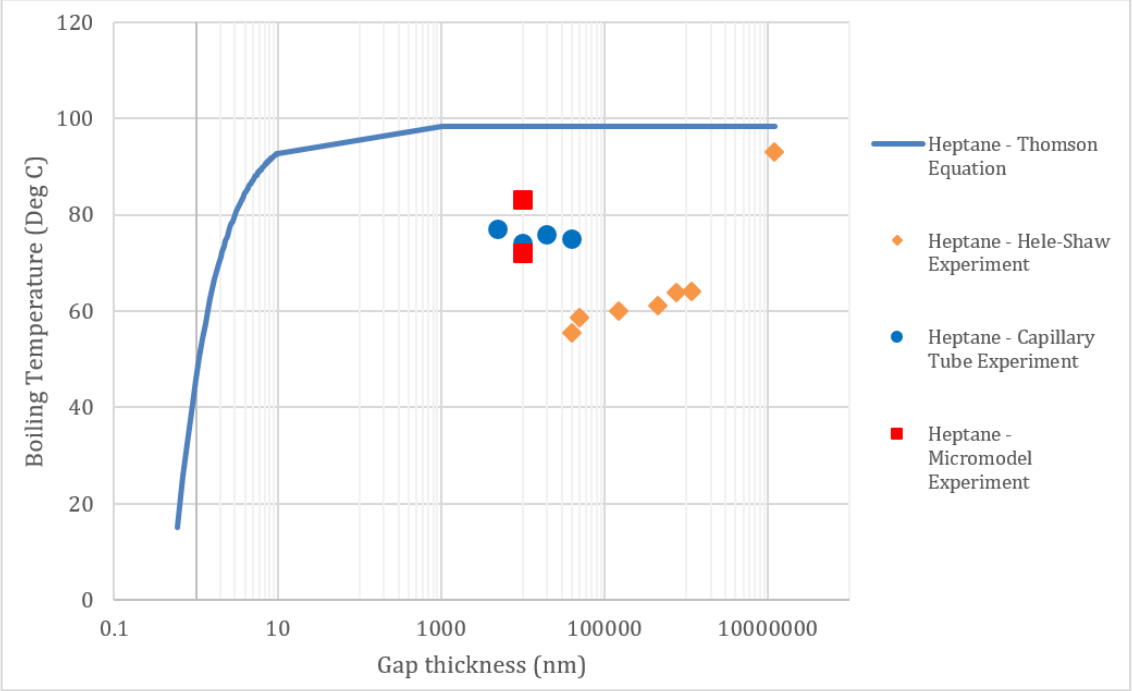

Figure 2-13: Boiling point of heptane at various pore sizes.

2.8 Quantitative analysis

The overall aim was to revisit the Thomson equation by comparing its computed boiling points with experimentally measured boiling temperatures. In the Thomson equation, any medium size larger than 1000 nm is considered a bulk medium; therefore, the calculated boiling point of a certain liquid would be simply a boiling temperature of that liquid in a bulk volume. Nevertheless, this consideration might contradict the results observed in Hele-Shaw and micromodel experiments.

Figure 2-14a to 2-14c show comparative results between measured and computed boiling points of deionized water, heptane, and decane. The experimental results shown in **Figure 2-14a to 2-14c** were from the Hele-Shaw experiments. **Figure 2-14d** presents comparative results between calculated and measured boiling points of vacuumed water, heptane, and decane in capillary tube micromodel experiments. We can clearly observe the difference between experimental and calculated outcomes, which indicate the limitation of the Thomson equation. Boiling points of liquids are affected by medium thickness even if the gap space is larger than 1000 nm as proved from previous experiments.

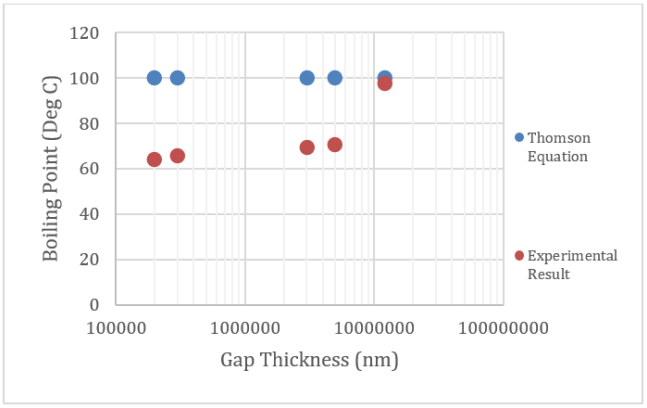

(a)

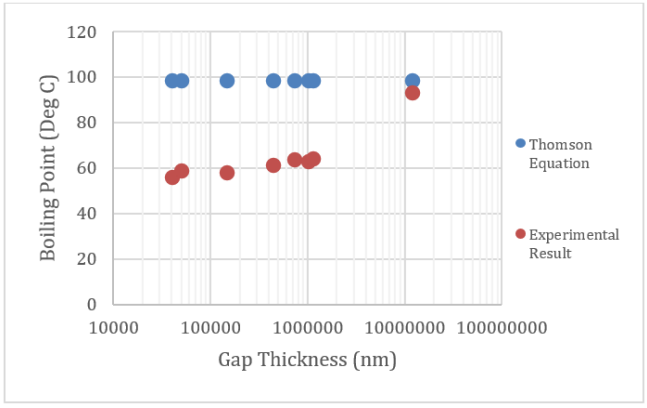

(b)

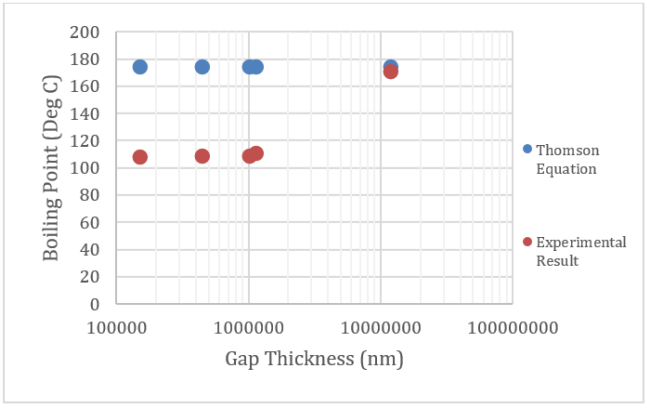

(c)

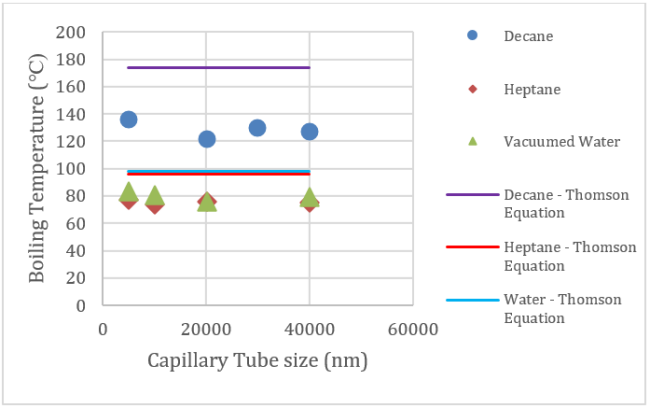

(d)

Figure 2-14: (a): Deionized water boiling points at various gap thicknesses; (b): heptane boiling points at various gap thicknesses; (c) decane boiling points at various gap thicknesses; (d): measured and calculated boiling points of water, heptane and decane at different capillary tube sizes.

As mentioned, the Thomson equation was effective when the pore size was less than $1000\ nm$ ($1\mu m$). Having experimentally measured boiling points at pore sizes ranging from 0.04 mm to 1.2 cm, modification of the equation is possible through curve-fitting approach (regression analysis) to make it applicable with pore sizes larger than $1000\ nm$.

The regression analysis was done through two main trials and each one was categorized according to the data and coefficients used in the equation. For comparison, the analysis was performed with and without bulk boiling points (observed at 12 mm gap thickness of the Hele Shaw models). Thus, both trials were divided into two groups: (a) with bulk values and (b) without bulk values. Initially, only heptane experimental data was considered (trials 1a and 2a). Then, the resulted equation was applied to compute boiling points of heptane, decane, and deionized water. In the other trials, all the experimental data from heptane, decane, and deionized water were used to modify the equation through regression and to calculate boiling temperatures of the liquids (trials 1b and 2b). Different modifications to Thomson equation were implemented to observe the best fitting model. **Table 2-7** presents the modified Thomson equations.

Modified equations from trials 1a and 2a (Table 7) provided better fit to experimental boiling points comparing with trials 1b and 2b (Table 7). The regression analysis was performed based on outcomes obtained from Hele-Shaw experiments. As a result, the modified equations might be limited to applications where the media have the same medium characteristics as Hele-Shaw glass cells. Although these modified equations are not universal and cannot be used for a wide range of pore sizes without further experimental (or analytical) supports, they can be useful in terms of presenting the deviation ⌊ ɔint for the boiling curve (Figure 2) above 1000 nm pore radius.

The applicability of modified equations from trials 1a and 2a was only limited with pore sizes less than 0.00115 m (1.15 mm) and larger than 0.00003 m (0.03 mm). **Figures 2-15a** and **2-15b** show the deviation of computed boiling temperatures from the experimental boiling points of heptane, decane, and deionized water in both trials.

Table 2-7: Modified equations for each trial.

	Modified Equation
Trial 1 – (a) Bulk value (1.2 cm) was considered. Only heptane is used as data.	$Tr = T_{\infty}^{0.98}\left(e^{-\frac{2\sigma V_L}{r H_{vap}}}\right)^{11794.87}$
Trial 1 – (b) Bulk value (1.2 cm) was considered. Heptane, decane and water are used as data.	$Tr = T_{\infty}^{0.98}\left(e^{-\frac{2\sigma V_L}{r H_{vap}}}\right)^{5593.71}$
Trial 2 – (a) Bulk value (1.2 cm) was not considered. Only heptane is used as data.	$Tr = T_{\infty}^{0.98}\left(e^{-\frac{2\sigma V_L}{r H_{vap}}}\right)^{16990.21}$
Trial 2 – (b) Bulk value (1.2 cm) was not considered. Heptane, decane and water are used as data.	$Tr = T_{\infty}^{0.98}\left(e^{-\frac{2\sigma V_L}{r H_{vap}}}\right)^{8753.82}$

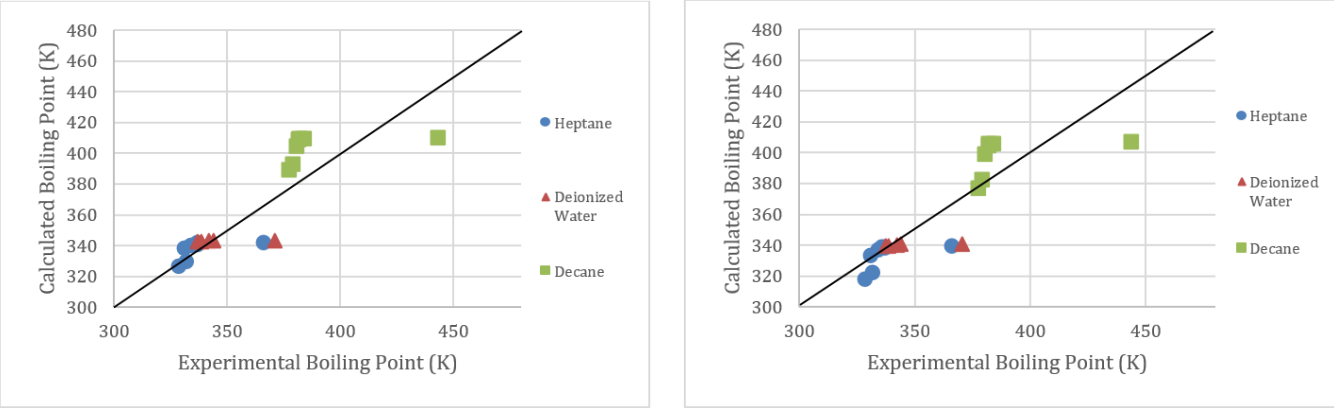

Figure 2-15 - (a): Variation of calculated boiling points from experimental data (Trial 1 – a); (b): variation of calculated boiling points from experimental data (Trial 2 – a).

Figure 2-16 presents the variation of heptane boiling point with different pore sizes by using the Thomson equation and modified equations from trials 1a and 2a with the experimental data. As the bulk value was not considered in the regression analysis, the fit to higher values of aperture was not good while the fit to the experimental data (circled area in Figure 16) was reasonably well. But the extrapolation to the lower values of aperture (lower than the experimental values) can be used to interpret the boiling conditions at smaller pore sizes (nano scale). Although our analysis was based on Hele Shaw type models rather than circular capillaries, the trends and qualitative observations indicate that the boiling points of single component solvents in capillary media was much lower than the ones obtained from the purely theoretical Thomson equation.

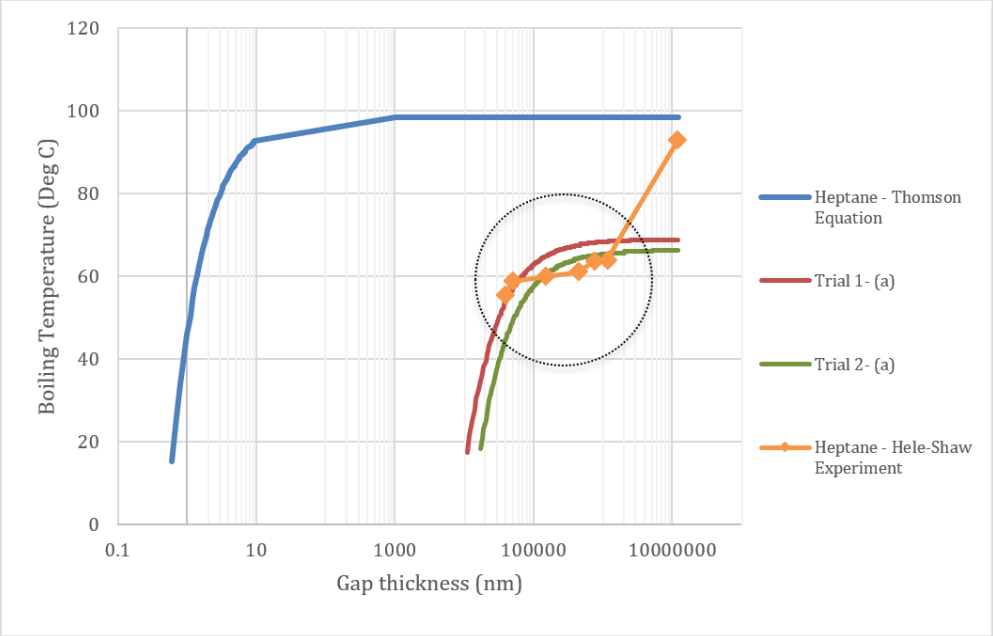

Figure 2-16: Heptane boiling point variation with the change of pore radius.

When the whole data was considered (the whole range of apertures including the bulk size) in the regression analysis, the fit to the Thomson equation did not yield a high correlation coefficient. Therefore, the above analysis suggests that a single equation (at least in the form of the Thomson equation) may not define the boiling behaviour of the whole range of capillary sizes, from the bulk size (order of cm) to nano pores (order of nanometre). Then, the following analysis was performed to propose a stronger correlation and the Thomson equation was modified with respect of the general exponential equation used in the curve fitting analysis.

As a first attempt to achieve this, the boiling points between 1.15mm and 12mm were forecasted by using a polynomial equation since there is a significant gap between these two thicknesses in the experimental data. The general exponential model used in the curve fitting process is as follows:

$$a * exp\ exp\ (b * x)\ + c * exp\ (d * x) \tag{6}$$

where **a**, **b**, **c**, and **d** are coefficients and **x** is the independent variable. By fitting the equation with the experimental data of heptane, the coefficients were estimated, and the Thomson equation was

modified accordingly. The coefficient **c** is usually close to bulk boiling point of the liquid; thus, it can be considered as following:

$$c = T_{\infty} - 38 \tag{7}$$

where T_{∞} is boiling temperature of the liquid. In Eq. 8.1, the first exponential function with coefficient **a** describes the deviation from the original Thomson equation. In other words, when coefficient **a** is equal to zero, the equation returns to its original form (Thomson equation) and coefficient **c** becomes simply the bulk boiling temperature of the liquid. **Table 2-8** presents the modified Thomson equation.

Table 2-8: Modified equation using the function given in Eq 6.

	Modified Equation
Trial 3 – Bulk value (1.2 cm) was considered. Only heptane is used as data.	$T_r = 38.87 \cdot \exp\left(\frac{-2 \cdot \sigma \cdot V_L}{r \cdot H_{vap}} \cdot 1.793 \cdot 10^7\right) + \left((T_{\infty} - 38) \cdot \exp\left(\frac{-2 \cdot \sigma \cdot V_L}{r \cdot H_{vap}} \cdot 2883\right)\right)$

Figure 2-17 shows the deviation between the computed and the experimental boiling points of heptane, decane, and deionized water when the equation given in Table 8 (Trial 3) is used. **Figure 2-18** illustrates the variation of heptane boiling point with different pore sizes obtained from the Thomson equation and modified equations (Trials 1a, 2a and 3), including the experimental data. Trial 3 (Eq. given in Table 8) captures the behaviour at the bulk conditions unlike the other two trials. When this equation is used to estimate the boiling point at lower apertures (pore sizes), we observe that boiling temperature tends to stabilize at a certain pore size (~0.001m) and minimal change in temperature with the pore size is observed. This trend is different from the other three models (Thomson equation and Trials 1a and 2a). Trial 3 shows a good match to a wide range of experimental data obtained for the pore's size range of three orders of magnitude.

This suggests that experimental observations do not agree with the Thomson equation, and its derivatives tested in this paper and a totally different behaviour of the change of boiling points with pore sizes should be considered in modelling studies.

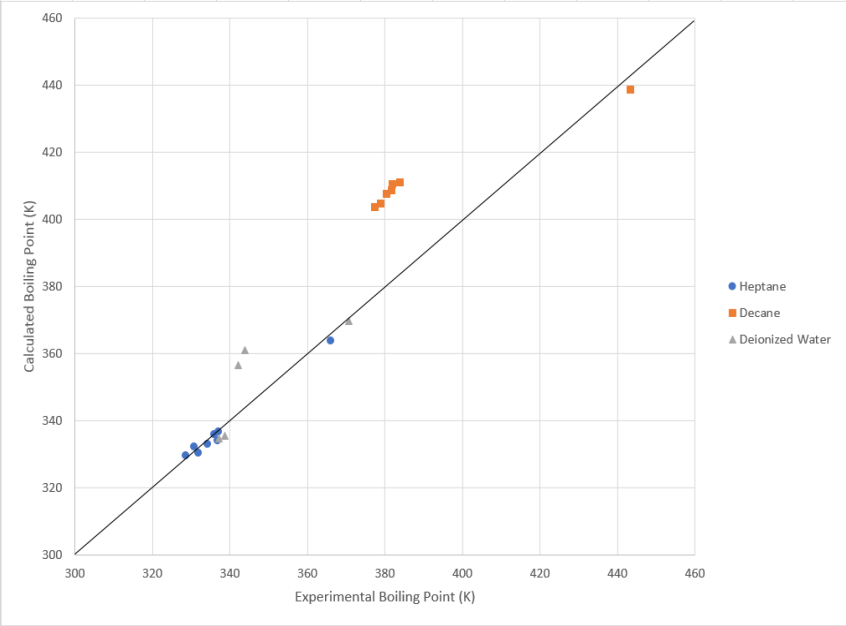

Figure 2-17: Variation of calculated boiling points from experimental data (Trial 3).

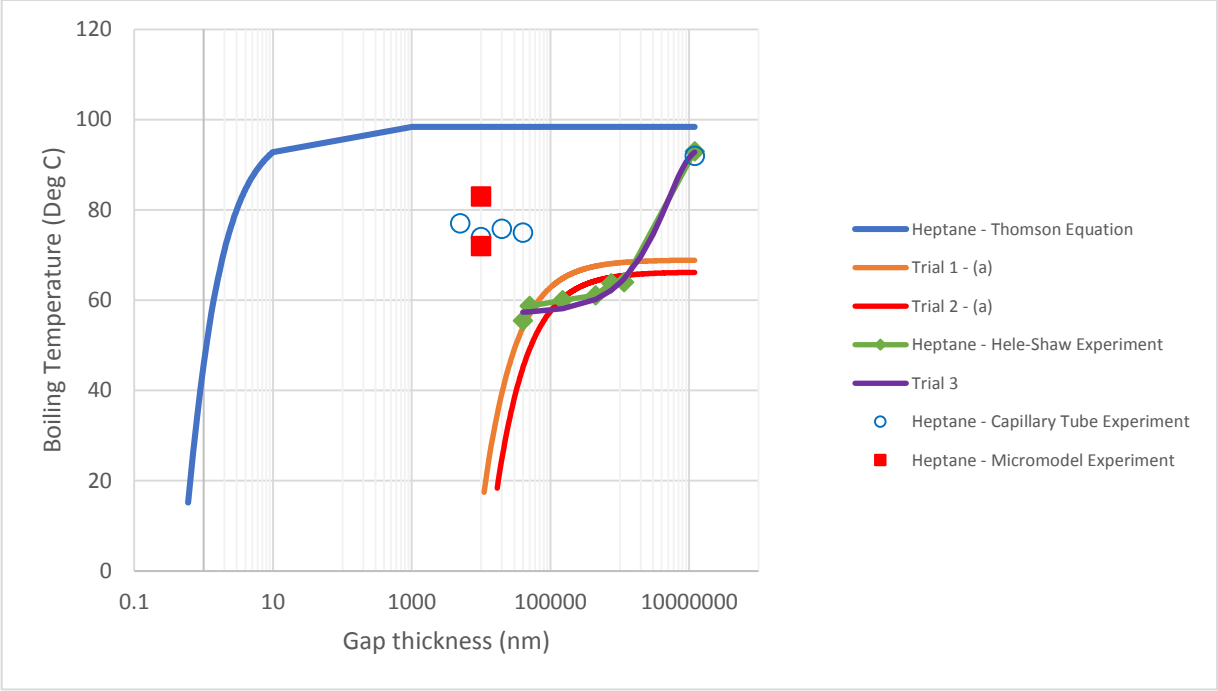

Figure 2-18: Heptane boiling point variation with the change of medium size.

2.9 Conclusions and Remarks

The applicability of the Thomson equation in calculating liquids boiling points was visually analysed and evaluated experimentally. This was performed using two experimental approaches: (1) Hele-Shaw model and (2) micromodel analysis. In Hele-Shaw experiments, the effect of medium thickness on boiling point was investigated using various gap thicknesses of glass samples, varying from 0.04 mm to 1.2 cm. With the assistance of micromodels, a more realistic representation of porous media was achieved. The main conclusions can be summarized as follows:

1. Per the Thomson equation, the boiling points of liquids at capillary conditions can significantly differ from those at bulk volumes. But, the Thomson equation is only limited with pore sizes under 1000 nm (Berg 2010); otherwise, computed boiling points become overestimated and higher than the real boiling temperatures as observed in Figure 2-2. We observed through Hele-Shaw and micromodel experiments that, unlike the Thomson

equation, the boiling points of liquids can be less than their normal boiling points (at bulk volumes) if they are placed in pores or channels larger than $1000\ nm$.

2. Three different approaches (equation types) were used to propose modifications to the Thomson equation. Although the applicability of modified equations may be limited to a specific range of pore size and medium, they can be sufficient to roughly represent the change in the boiling point when the pore radius is above 1000 nm.
3. One may qualitatively state that the boiling points of single component solvents in capillary media are lower than the ones obtained from the purely theoretical Thomson equation.
4. The analysis of experimentally and computationally obtained data suggests that experimental observations do not agree with the Thomson equation and its derivatives tested in this paper (Table 2-7). A different behaviour of the change of boiling points with pore sizes should be considered in modelling studies.

2.10 Nomenclature and abbreviations

dW: change of work done

ΔP: change of pressure $[Pa]$

dV: change of bubble volume $[m^3]$

σ: surface tension $[N/m]$

dA: change of bubble area $[m^2]$

$R1$: radius of first curvature $[m]$

$R2$: radius of second curvature $[m]$

v^L: liquid molar volume $[m^3/mol]$

r: droplet radius $[m]$

R: universal gas constant $\left[\frac{J}{K\ mol}\right]$

T: temperature $[K]$

P_∞: vapor pressure at flat surface $[Pa]$

P_r: vapor pressure at curved interface $[Pa]$

T_r: temperature at porous medium $[K]$

T_∞: temperature at bulk medium $[K]$

ΔH_{vap}: heat of vaporization $[J/mol]$

2.11 Appendix: Heat Transfer Analysis

A heat transfer analysis was done by using linear heat equations to obtain the temperature difference between the glass layer and heating plate mathematically, and the fluid temperature was computed accordingly. The temperature was measured at three points on the top surface of the Hele-Shaw cell to observe the heat distribution along the glass chip, as shown in Figure 19. In the following analysis, the heat, producing by the heating plate, was assumed to be constant along the Hele-Shaw cell thickness. With a gap size of 0.04mm ($40\ \mu m$), it was observed that water vaporized at nearly 60℃; meanwhile, the heating plate was heated at 64.91℃ ($337.9\ K$). The average heat rate, at the boiling stage, was calculated as 4.017 $\frac{Joules}{second}$ ($Watts$). By using the Fourier's law of heat conduction, the temperature difference (ΔT), in glass plate A, was computed, as shown in the calculations below:

$$Heat\ rate\ (\dot{Q}) = \frac{Glass\ thermal\ conductivity\ (-K)\ \times\ Area\ (A)\ \times\ Temperature\ difference\ (\Delta T)}{Thickness\ (L)}$$

$$\Delta T = \frac{\dot{Q} \times L}{-K \times A} = \frac{4.017 \times 1.14 \times 10^{-3}}{-1.38 \times 1.875 \times 10^{-3}} = -1.77\ Kelvin$$

By knowing the temperature difference in plate A, the temperature at the top surface (T_2) was calculated as the following:

$$-\Delta T = T_2 - T_1 \xrightarrow{Rearranging} T_2 = T_1 - \Delta T = 337.9 - 1.77 = 336.13\ Kelvin\ (63.13\ ℃)$$

The water layer was treated as a thin film with a thermal conductivity of 0.6 $\frac{W}{m\ .\ K}$. Estimating the surface temperature (T_2), below the water film, allowed us to compute the temperature above the liquid layer (T_3), which also presented the temperature of the water film.

$$\Delta T = \frac{\dot{Q} \times L}{-K \times A} = \frac{4.017 \times 0.04 \times 10^{-3}}{-0.6 \times 1.875 \times 10^{-3}} = -0.142\ Kelvin$$

$$-\Delta T = T_3 - T_2 \xrightarrow{Rearranging} T_3 = T_2 - \Delta T = 336.13 - 0.142$$
$$= 335.98\ Kelvin\ (62.97\ ℃)$$

Then, by finding the fluid temperature (T_3), the temperature of the outer surface (T_4) could be found as illustrated below:

$$\Delta T = \frac{\dot{Q} \times L}{-K \times A} = \frac{4.017 \times 1.14 \times 10^{-3}}{-1.38 \times 1.875 \times 10^{-3}} = -1.77\ Kelvin$$

$$-\Delta T = T_4 - T_3 \xrightarrow{Rearranging} T_4 = T_3 - \Delta T = 335.98 - 1.77$$
$$= 334.21\ Kelvin\ (61.21\ ℃)$$

It was expected that the outer surface temperature (T_4) would be close to what was measured experimentally, during the boiling stage. The upper surface temperature of the glass cell was measured as nearly 60℃; whereas, the top plate surface (attached with the thermocouples) temperature was 61.21℃. The error percentage, between the recorded and calculated temperature,

was 2.01; the error is partially caused by the assumption of constant heat rate along the sample thickness.

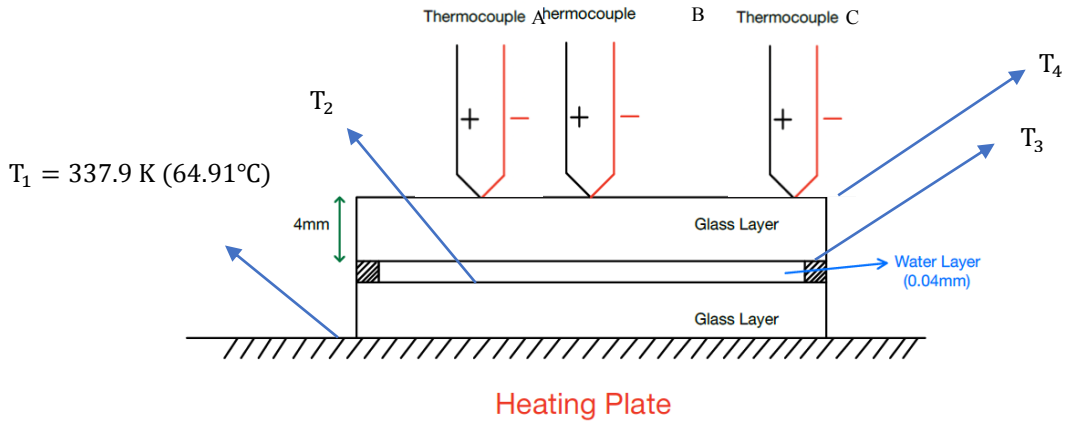

Figure 2-19: Schematic of a Hele-Shaw glass cell on a heating plate.

3 Chapter 3: Thermodynamics of Hydrocarbon Solvents at the Pore Scale during Hybrid Solvent-Thermal Application for Heavy-Oil Recovery

A version of this chapter was presented and published as a conference paper at the SPE EOR Conference at Oil & Gas West Asia held in Muscat, Oman, 26-28 March 2018 (SPE-190469-MS).

3.1 Abstract

Phase behavior of fluids at capillary conditions differs from that in bulk media. Therefore, understanding the thermodynamics of solvents in confined media is essential for modeling thermal EOR applications. The Thomson equation states that pore sizes have a control on boiling points of liquids in capillary channels. As pore spaces become smaller, boiling points become lower than normal boiling temperatures of the same liquids. The target of this paper is to inspect this phenomenon by physically measuring the boiling points of several solvents and compare them with the calculated boiling temperatures for different capillary structures. Furthermore, the feasibility and accuracy of the Thomson equation is investigated to check its applicability in heavy-oil recovery modelling. To do so, Hele-Shaw cells with several gap thicknesses (0.04, 0.45, 1.02, and 12 mm) are used to measure the boiling points of heptane, heptane-decane mixture, and naphtha. Experiments are repeated for the same solvents on homogeneous and heterogeneous micromodels to observe the phase behavior in a more realistic porous medium. Finally, the effect of surface wettability on boiling temperatures is examined in Hele-Shaw and micromodel experiments.

3.2 Introduction

Additional methods are usually needed in heavy-oil recovery. The most common technologies to achieve an economic recovery in heavy-oil reservoirs are (1) thermal enhanced oil recovery (EOR) processes, (2) sole injection of solvents, and (3) hybrid thermal-solvent applications that aim to reduce oil viscosity with the assistance of both heat transfer and solvent dilution (Fang and Babadagli 2014). The concept of using solvents as steam aids was highly focused on throughout the last decades due to their potential effects on the improvement of the process efficiency by reducing oil viscosity with reduced steam use. In a pioneering study, an experimental investigation of Athabasca bitumen recovery using a vertical tar sand pack and solvents, as additives to steam, was performed by Farouq and Abad (1976). They concluded that solvent volume, placement, and type have a major influence on bitumen recovery. Higher recovery was achieved when steam and

solvent were injected into separate wells. In spite of the quick breakthrough and asphaltene precipitation, using naphtha as a steam aid resulted in a considerably improved recovery.

Nasr et al. (2003) studied the effect of different solvents in oil drainage rate enhancement. They stated that injecting non-condensable hydrocarbon solvents (C_1 and C_2) had no improvement on the rate of oil drainage. In comparison, combining steam with condensable hydrocarbon (C_3 to C_8) gave better results in terms of oil drainage rate. The recovery raised as the solvent carbon number increased. Additionally, solvents with vaporization temperatures near to steam temperature had more participation in improving oil drainage rate. Solvent (mainly pentane) in addition to steam aided to improving the overall performance of cyclic steam stimulation (CSS) in a recent study by Léauté and Carey (2007). The concept was experimented in the Cold Lake field through a pilot cycle test. Zhao et al. (2004, 2005) examined the performance of Steam Alternating Solvents (SAS) method through experimental and numerical work. The SAS process was advantaged by the performance combination of Steam Assisted Gravity Drainage (SAGD) and VAPEX processes. Temperatures of injected solvents could influence the dilution rate of solvents in oil. More recently, Pathak et al. (2010, 2011, 2012) reported a series of studies on the impact of solvent's temperature on the overall recovery from sands and carbonates (2013).

Sole injection of hydrocarbon or non-hydrocarbon solvents might be an alternative to thermal EOR processes. In a pioneer work, Das and Butler (1997) reported initial experimental observations of vapor extraction method (VAPEX) using pure vaporized propane for bitumen recovery. By using a Hele-Shaw glass cell, they found that driving force for gravity drainage became higher when a vaporized solvent (propane) was injected. The experimental goal was to visualize the VAPEX process in a vertical Hele-Shaw cell, which represented a thin (2-D) section of a reservoir. Injecting non-hydrocarbon solvents, such as CO_2, has a considerable impact on heavy oil recovery (Naderi and Babadagli 2014a–c, 2016). Generally, although solvent injection demands less energy comparing with steam injection, implementing it in oil fields could be expensive and uneconomical since huge volumes of solvents are required to achieve desired recoveries in addition to their high cost.

Al-Bahlani and Babadagli (2009) investigated a steam-solvent injection process to enhance viscous oil recovery from fractured reservoirs, which brought the idea of joining oil recovery, through steam and solvents, with solvent retrieval. Basically, Steam-Over-Solvents in Fractured Reservoir (SOS-FR) method grouped three mechanisms in one process: (1) recovering oil thermally by injecting steam; (2) diluting the remained oil by injecting solvent; (3) retrieving the trapped solvent through steam injection. In a subsequent work, Marciales and Babadagli (2016) reported that 90% of used solvents (heptane and naphtha) could be retrieved when the temperature was close to their boiling points. Micromodels were utilized to visually observe the impact of wettability and temperature on heptane and naphtha retrieval process (Cui and Babadagli 2017a–b). As a continuation of Al-Bahlani and Babadagli work, Naderi and Babadagli (2014c) studied the usage of CO_2 as a solvent to recover the oil chemically and reported the optimal condition to achieve 80-90% retrieval of injected CO_2.

Considering the importance of the retrieval of the used hydrocarbon solvents in hybrid applications in the reduction of the overall operational cost, one has to optimize the process giving the lowest temperature that maximized the oil recovery and solvent retrieval. To achieve this, understanding the thermodynamics of solvents at porous media conditions becomes an essential task to apply thermal-solvent hybrid processes. Boiling is a bulk related phenomenon, strongly depending on the surrounding pressure. Unlike the boiling point, evaporation phenomenon is more related to the phase change of molecules on liquid's surface and it might occur at any temperature below the normal boiling temperature. Boiling points of liquids could alter when the medium size changes. William Thomson (Lord Kelvin) mathematically described the effect of pore radius and interface curvature (droplet surface) on vapor pressure through the Kelvin equation. Similarly, the Thomson equation defined the alteration of boiling points with the variation of porous medium size. This paper deals with the latter, variance of temperature in the boiling process in different capillary conditions, and investigates the effect of capillary properties experimentally using visual (Hele-Shaw cells and micromodels) systems. Furthermore, it observes the suitability and accuracy of the Thomson equation in estimating mathematically the boiling points of solvents in capillary media.

3.3 Statement of the Problem and Objectives

Phase change is a physical transformation that takes place in most of thermal EOR processes. Likewise, injecting hydrocarbon solvents into high temperature reservoirs could cause phase transformation of solvents under non-isothermal conditions. Consequently, comprehending the thermodynamic behavior of solvents in tight pores is essential in predicting the phase alteration, based on existing temperature and average pore size. This is needed in the determination of optimal temperature and pressure condition to maximize the oil recovery and solvent retrieval.

Implementing hybrid processes is one of the most efficient methods to effectively recover heavy oil owing to the use of heat energy and chemical diffusion simultaneously. Large consumption of solvents in solvent-thermal applications is accounted as a drawdown because of high solvent cost. Hence, retrieving trapped solvents after injection helps decrease the overall expenses of such EOR applications. In order to do so, one option is to thermally convert the trapped solvents to vapor to release them from low permeable matrixes. This technique has an advantage in fractured or high heterogeneous reservoirs. Liquids in capillary conditions might behave differently from those in bulk media with regard to vapor pressure and boiling point. Generally, the Thomson equation represents the curvature effect on boiling temperatures. The impact on liquid's boiling point gets larger with higher curvature. As the pore radius decreases, the boiling point of liquid decreases, as well. This paper investigating this phenomenon and is a continuation of a previous work by Al-Kindi and Babadagli (2017), which aimed to measure boiling points of various liquids using Hele-Shaw cells and to test the validity of the Thomson equation.

The major target of this paper is to compare the experimentally measured boiling temperatures of different hydrocarbon solvents with boiling points computed by the Thomson equation. The experiments are started using Hele-Shaw cells with various gap thicknesses (0.04, 0.45, 1.02 and 12 mm). To obtain more realistic observations, micromodels with uniform and non-uniform properties (grain size and pore throat) are utilized. Conducting these experiments will provide a clear study on the solvents' behaviors in porous conditions under different temperatures and the equation's feasibility in the application design of solvent-thermal and solvent retrieval processes.

3.4 Background

The formation of a vapor bubble in a liquid requires an additional energy, depending on the interface curvature. Vapor pressures along curved interfaces differ from those across place surfaces. At equilibrium state, the pressure of vapor (in contact with a liquid) is higher when the interface between two phases is convex (Thomson 1871). Based on this theory, the Kelvin equation (**Eq. 1**) is derived to describe the relation of vapor pressure with pore radius and interfacial tension:

$$P_r = P_\infty exp\left[\frac{-2\,\sigma\,v^L}{r\,R\,T}\right] \quad (1)$$

where P_r is vapor pressure at a convex interface or inside a capillary channel, P_∞ is vapor pressure at place interface, σ is surface tension, v^L is liquid molar volume, T is medium temperature, R is universal gas constant, and r is pore or channel radius. Eq. 1 indicates the inverse relationship between vapor pressure and pore size.

With a similar concept, Thomson equation (**Eq. 2**) is linked to the variation of boiling temperatures of liquids under confined media and constant pressures. The equation takes the form:

$$T_r = T_\infty \exp\left[-\frac{2\,\sigma\,v^L}{r\,\Delta H_{vap}}\right] \quad (2)$$

where T_r is liquid boiling point under capillary condition, T_∞ is liquid boiling point in bulk conditions, σ is surface tension, v^L is liquid molar volume, ΔH_{vap} is liquid vaporization heat, and r is pore or channel radius. The Thomson equation determines the non-inverse (direct) relationship of boiling points with pore sizes; meaning boiling temperatures are expected to decline as the pore sizes get tighter.

3.5 Experimental Work

Experiments shown in this paper are progressive experiments from our previous work (Al-Kindi and Babadagli 2017). The main objective is to detect boiling points of solvents under porous conditions close to those in real reservoir conditions and their boiling temperature deviations with pore space variations. To achieve this, micromodels with different properties (uniform and non-uniform) were used. As done in the prior work, the experiments were initiated with Hele-Shaw glass cells for two reasons: (a) To determine a clear visualization of vapor bubbles formation, which could be difficult to observe in micromodels; (b) to examine the influence of glass surface wettability on boiling point.

3.5.1 Hele-Shaw Cells

A Hele-Shaw cell is a pair of flat glasses or plastic plates, separated by a tight space. In general, it is useful in getting a rough approximation of certain applications such as fluid flow and dynamics through confined spaces. Moreover, it provides an advantage of achieving a clear visualization of fluid propagation either in viscous liquids (steam fingering in heavy oil) or porous media. In our case, Hele-Shaw cells are used to image the bubbles' creation in solvents under various temperatures, starting from room condition (20℃) to normal boiling point of the solvent. Four gap thicknesses were used in the experiments: (1) 0.04 mm, (2) 0.45 mm, (3) 1.02 mm, and (4) 12 mm. With each Hele-Shaw cell, the experiment is repeated twice. One is conducted with pure heptane (C_7H_{16}) and other with a mixture of heptane (C_7H_{16}) and decane ($C_{10}H_{22}$). Each component covers 50% of total mixture mass fraction. **Figure 3-1** illustrates the Hele-Shaw cell used in the experiments.

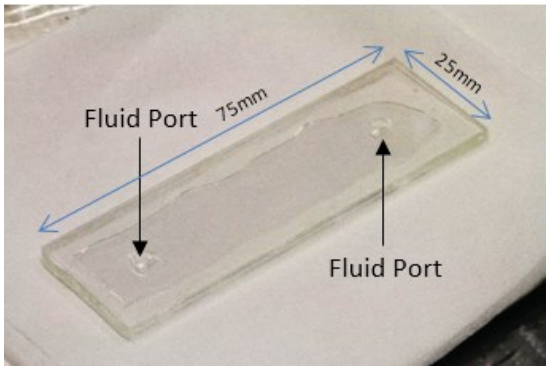

Figure 3-1: Hele-Shaw glass cell (0.15 mm gap thickness).

The effect of surface wettability on the boiling points is firstly observed with Hele-Shaw samples. The glass plates are initially water-wet. The surface property is changed using dichlorodimethylisilane, which alters the glass wettability from water-wet to oil-wet. **Figure 3-2** shows a water drop behavior on a glass piece in air and toluene before and after surface wettability change.

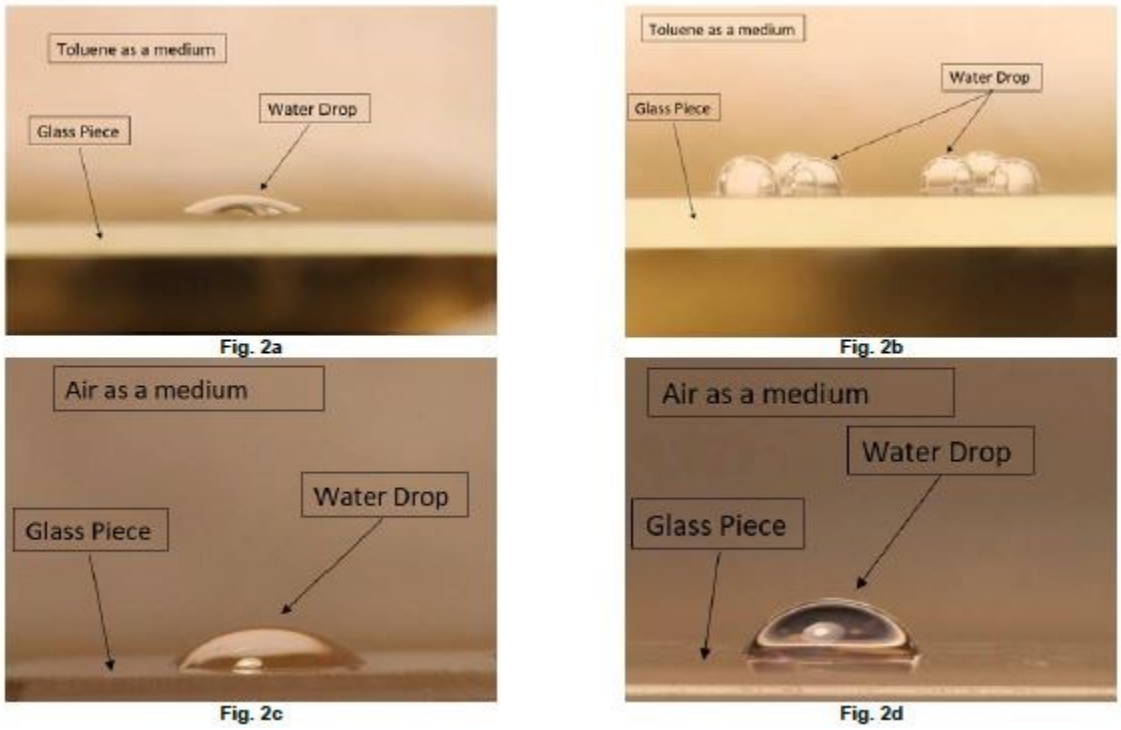

Figure 3-2: (a) – Before wettability change; (b) – After wettability change; (c) – Before wettability change; (d) – After wettability change.

Experimental setup. Figure 3-3 presents the utilized equipment in Hele-Shae experiments. The setup contains Canon 7D DSLR camera, electrical heating plate, temperature measurement device (National Instruments), thermocouple, and light source (lamp).

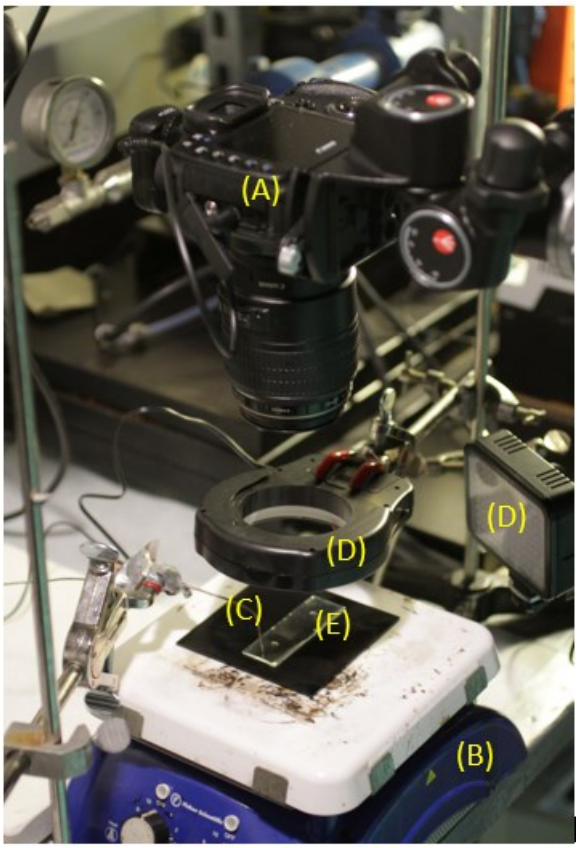

Figure 3-3: Experimental system: (A) 7D canon DSLR camera, (B) electrical heating plate, (C) thermocouple, (E) Hele-Shaw glass cell and (D) LED lights.

Procedure. To obtain a clear visualization of phase change in solvents, DFSB-K175 Fluorescent is used to dye the hydrocarbon solvents to a green colour. The experiments are performed in ambient pressure (14.7 psia) with open ports to the atmosphere to prevent pressure increase in the cell.

After saturating the Hele-Shaw sample with the solvent, it is placed on the electrical heating plate horizontally. The DSLR camera and temperature measurement device are programmed to take images and record temperatures every 2 sec while the cell is heated gradually.

Results and discussion. Experiments are initiated using pure heptane in order to perceive its behavior under various temperatures and gap spaces as a benchmark. Unlike vaporization point,

boiling stage is related to the liquid bulk at which it starts to change in phase, forming continuous and rapid vapor bubbles. In the Hele-Shaw experiments, we considered that boiling point is reached when a continuous and fast bubble formation takes place in the solvent. It is expected that boiling temperatures of solvents will deviate from their normal boiling points as the cell's gap thickness becomes tighter. To represent a bulk condition, a glass cell of 12 mm gap thickness is used. To inspect the glass surface property impact on boiling point, experiments are repeated two times: (1) before wettability alteration to oil wet and (2) after wettability to oil wet.

Figure 3-4a shows a 0.04 mm gap thickness cell (before wettability alteration) saturated by pure heptane at ambient temperature (20℃). At 30.62℃, the first vapor bubble takes place in heptane (**Figure 3-4b**). A continuous and quick creation of bubbles starts to form in heptane at 57.68℃ as shown in **Figure 3-4c**. The last stage indicates that boiling point of pure heptane in the glass cell is reached, which is less than the normal boiling temperature of heptane (98.42℃) at bulk media and atmospheric pressure. **Table 3-1** displays the temperature of heptane with different Hele-Shaw cell gap thicknesses at main two stages: (a) first bubble appearance and (b) continuous and quick formation of vapor bubbles.

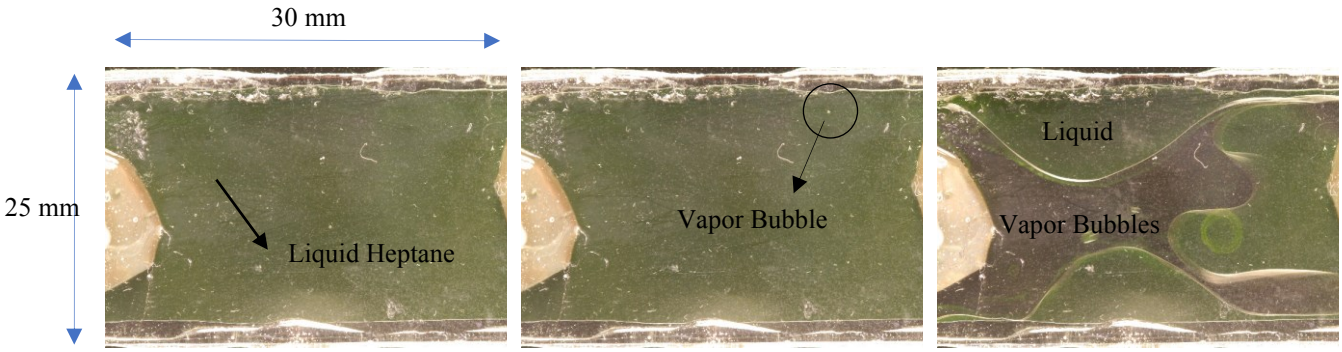

Figure 3-4: (a) – 0.04 mm Hele-Shaw cell at 20℃; (b) – 0.04 mm Hele-Shaw cell at 30.62℃; (c) – 0.04 mm Hele-Shaw cell at 57.68℃.

Table 3-1: Heptane temperature at various fluid stages and Hele-Shaw cell gap spaces.

Heptane (C7H16) – 0.04 mm gap spacing

Stage	Temperature (℃)
First bubbles appearance	30.62
Continuous formation of bubbles	57.68

Heptane (C7H16) – 0.45 mm gap spacing

Stage	Temperature (℃)
First bubble appearance	30.7
A rapid and continues formation of bubbles	59.7

Heptane (C7H16) – 1.02 mm gap spacing

Stage	Temperature (℃)
First bubble appearance	23.25
A rapid and continues formation of bubbles	60.18

Heptane (C7H16) – 12 mm gap spacing

Stage	Temperature (℃)
First bubble appearance	50.83
A rapid and continues formation of bubbles	94.33

As a continuation, a mixture of heptane (50% mass fraction) and decane (50% mass fraction) is injected into the Hele-Shaw samples to examine the effect of medium size variation on boiling points of solvents' mixtures. In a sense, this represents oil-solvent mixture, represented by decane and heptane respectively, injected and mixed for recovery improvement. Then, additional temperature is applied to retrieve solvent and recover more oil. Normally, while having a mixture of components with different boiling points, lower boiling temperature components tend to boil first when heat is applied to the liquid mixture. In our case, focus is given to the temperature of the first bubble appearance and continuous bubbles formation as a liquid overall. Similar gap

thicknesses (0.04, 0.45, 1.02 and 12 mm) of the glass cells are used with heptane and decane mixture. **Figure 3-5a** illustrates a 0.04 mm gap space cell saturated with heptane and decane mixture at 25℃. The first vapor bubble appears in the liquid at 58.83℃ (**Figure 3-5b**). A continuous and rapid creation of vapor bubbles takes place in the liquid mixture at 84.12℃ as shown in **Figure 3-5c. Table 3-2** presents the temperature of the mixture with different Hele-Shaw cell gap thicknesses at two stages: (a) first bubble appearance and (b) constant and rapid formation of bubbles.

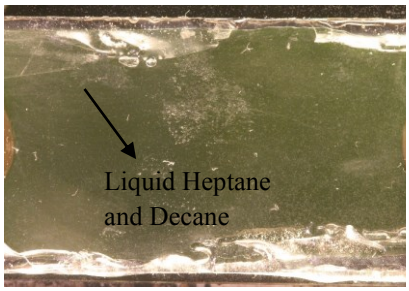

Figure 5a

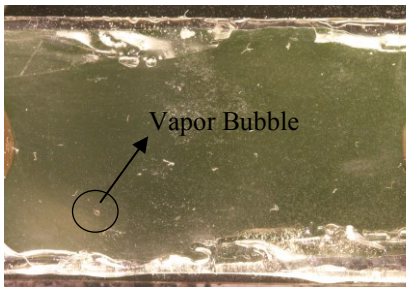

Figure 5b

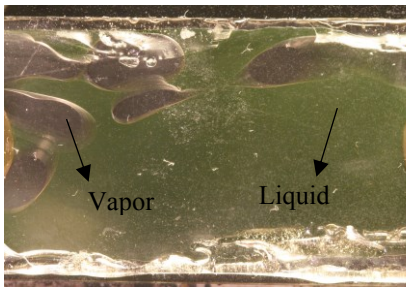

Figure 5c

Figure 3-5:(a) – 0.04 mm Hele-Shaw cell at 25℃; (b) – 0.04 mm Hele-Shaw cell at 58.83℃; (c) – 0.04 mm Hele-Shaw cell at 84.12℃.

Table 3-2: Heptane-decane mixture temperature at various fluid stages and Hele-Shaw cell gap spaces.

Heptane (C7H16) and Decane (C10H22) – 0.04 mm gap spacing

Stage	Temperature (℃)
First bubbles appearance	58.83
Continuous formation of bubbles	84.12

Heptane (C7H16) and Decane (C10H22) – 0.45 mm gap spacing

Stage	Temperature (℃)
First bubbles appearance	38.35
Continuous formation of bubbles	84.22

Heptane (C7H16) and Decane (C10H22) – 1.02 mm gap spacing

Stage	Temperature (℃)
First bubbles appearance	35.41
Continuous formation of bubbles	85.23

Heptane (C7H16) and Decane (C10H22) – 12 mm gap spacing

Stage	Temperature (℃)
First bubbles appearance	65.76
Continuous formation of bubbles	107.32

Surface wettability of Hele-Shaw glass samples is changed from water-wet to oil-wet to observe how solvent-glass contact behavior will affect the boiling point. As Eq. 2 points out, the boiling temperature is related not only to the capillary size but also to the interfacial properties (interfacial tension is included in this equation, not wettability directly). Therefore, it is expected that wettability alteration of the glass surface will have a degree of effect on the boiling temperature of liquids since the inner surface of Hele-Shaw cells have a flat contact with liquids. With similar liquids and medium spaces, all experiments were repeated after altering the glass surface wettability to oil-wet. **Table 3-3** represents the boiling points (continuous and quick formation of bubbles) of heptane and heptane-decane mixture after surface wettability change. **Figure 3-6** gives a summery of all measured boiling points of liquids used in Hele-Shaw experiments before and after modifying the glass wettability.

Table 3-3: Heptane and heptane-decane mixture temperatures at various fluid stages and Hele-Shaw cell gap spaces.

Heptane (C7H16) – 0.04 mm gap spacing

Stage	Temperature (℃)
First bubbles appearance	51.94
Continuous formation of bubbles	61.62

Heptane (C7H16) – 0.45 mm gap spacing

Stage	Temperature (℃)
First bubble appearance	24.73
A rapid and continues formation of bubbles	59.15

Heptane (C7H16) – 1.02 mm gap spacing

Stage	Temperature (℃)
First bubble appearance	26.71
A rapid and continues formation of bubbles	62.86

Heptane (C7H16) and Decane (C10H22) – 0.04 mm gap spacing

Stage	Temperature (℃)
First bubble appearance	48.46
A rapid and continues formation of bubbles	80.53

Heptane (C7H16) and Decane (C10H22) – 0.45 mm gap spacing

Stage	Temperature (℃)
First bubbles appearance	38.97
Continuous formation of bubbles	86.28

Heptane (C7H16) and Decane (C10H22) – 1.02 mm gap spacing

Stage	Temperature (℃)
First bubble appearance	22.58
A rapid and continues formation of bubbles	84.22

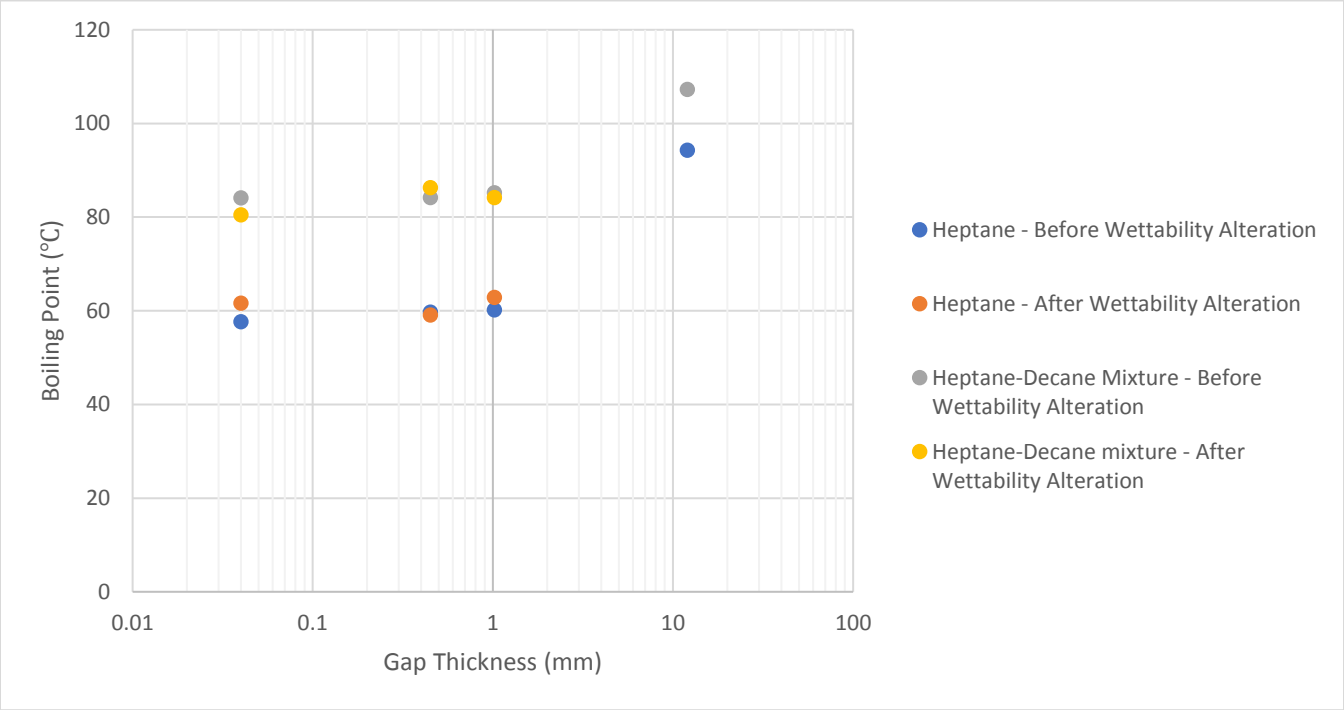

Figure 3-6: Measured boiling temperatures at different Hele-Shaw cell gap thicknesses before and after glass surface wettability change.

3.5.2 Micromodel Analysis

Using micromodels provides a more representative observation of porous conditions, comparing with Hele-Shaw glass chips. In this paper, two categories of micromodels were used: (a) uniform grain diameter and pore throat size (**Figure 3-7a and** 3-**7b**) and (b) non-uniform grain diameter and pore throat size (**Figure 3-8**). For the uniform property micromodel, two models with different grain diameters and pore throat sizes are utilized. The purpose of using various micromodel types is to inspect the influence of system structure on boiling point of solvents. In micromodel experiments, pure heptane, heptane-decane mixture, and naphtha are used. In heptane-decane mixture, each component has a mass fraction of 50%.

Naphtha combines around 115 hydrocarbon components starting from pentane (C_5). Components from C_5 to C_{12} have the highest mass fraction comparing with the remaining components in

naphtha. Similar to Hele-Shaw experiments, the effect of micromodel wettability on boiling points is observed as well. The micromodels are originally water-wet and changing their wettability properties can be done by injecting dichlorodimethylisilane into the micromodels.

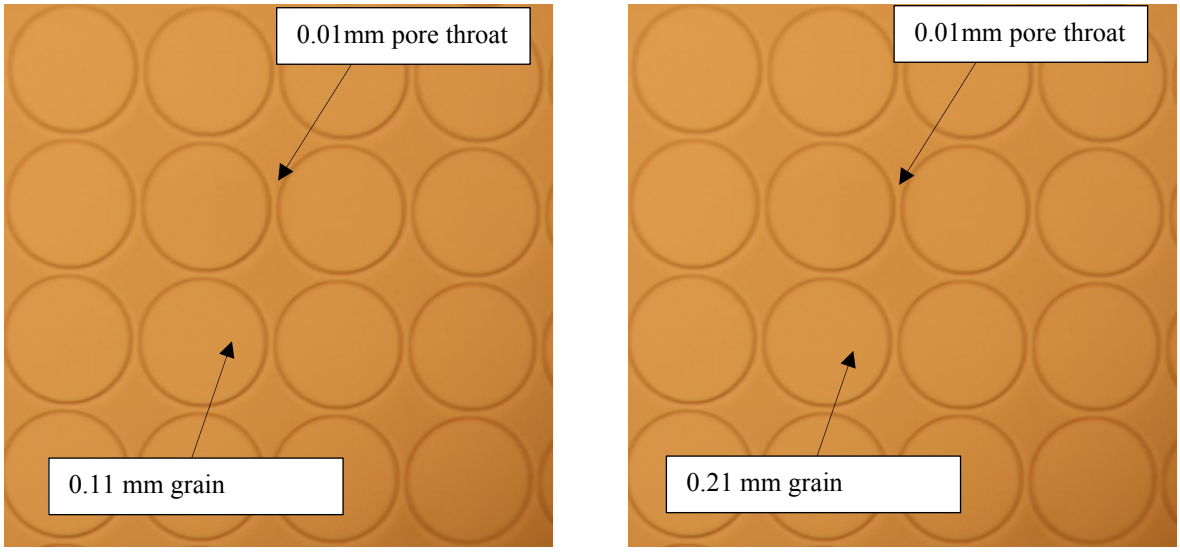

Figure 3-7: (a) – Micromodel with uniform properties (0.11 mm pore diameter and 0.01 mm pore throat); (b) – Micromodel with uniform properties (0.21 mm pore diameter and 0.01 mm pore throat).

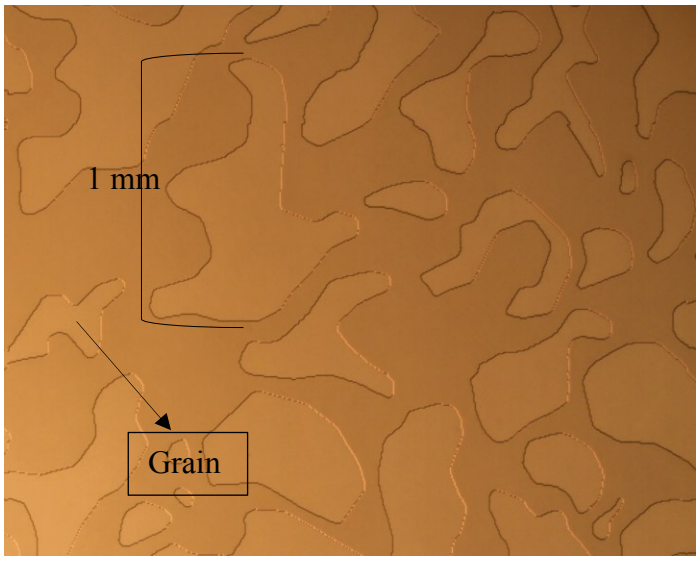

Figure 3-8: Micromodel with non-uniform properties (grain diameter and pore throat size).

Experimental setup. The setup consists of Zeiss Stemi 2000C microscope, 7D canon DSLR camera, LED light, temperature measurement device (National Instruments), thermocouple, and electric heating plate. **Figure 3-9** shows the tools used in the micromodel experiments.

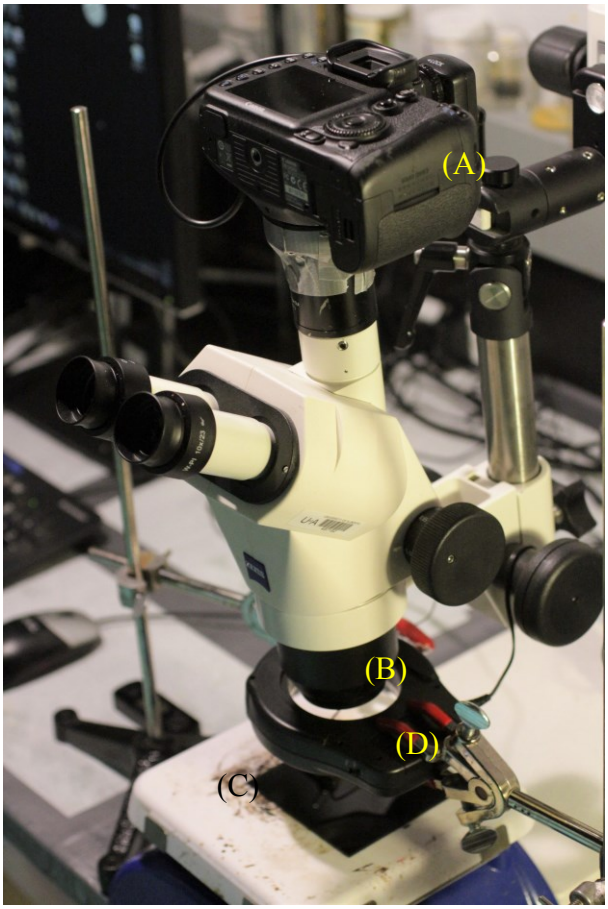

Figure 3-9: Experimental system: (A) 7D canon DSLR camera, (B) Zeiss Stemi 2000C microscope, (C) electrical heating plate and (D) LED light.

Procedure. Firstly, micromodels are saturated with solvents using a syringe pump. Solvents are injected through the micromodels at a constant flowrate of 1.5 microliter per minute for around 10 h. After saturation process is completed, the saturated micromodels are placed horizontally on the electrical heating plate to be heated gradually. Images and temperature readings are taken continuously every 2 sec with the help of a DSLR camera and temperature measurement device. As with the Hele-Shaw experiments, all of the micromodel experiments are conducted under

ambient pressure (14.7 psia) with open ports to the surrounding pressure; therefore, there is no pressure build-up inside the micromodel when fluid temperature is raised. As a second step, the wettability is altered by injecting dichlorodimethylisilane constantly into the micromodels for 24 h until fully saturated by the chemical. Then, heptane is injected into the models to flash out the entire remaining chemical.

Results and discussions. The experiments are started with uniform properties micromodels and pure heptane, as a solvent. Using a microscope assists with clearly visualising the phase change within the pores when boiling point of the solvent is reached. With the uniform micromodel (0.11 mm grain diameter and 0.01 mm pore throat), the pure heptane started to boil and convert to vapor at a temperature of 72℃ (**Figure 3-10a**). At 79.1℃, most of the heptane has changed into vapor (**Figure 3-10b**). A large volume of heptane in the micromodel boiled and transformed into gas at a temperature of 81.7℃ (**Figure 3-10c).**

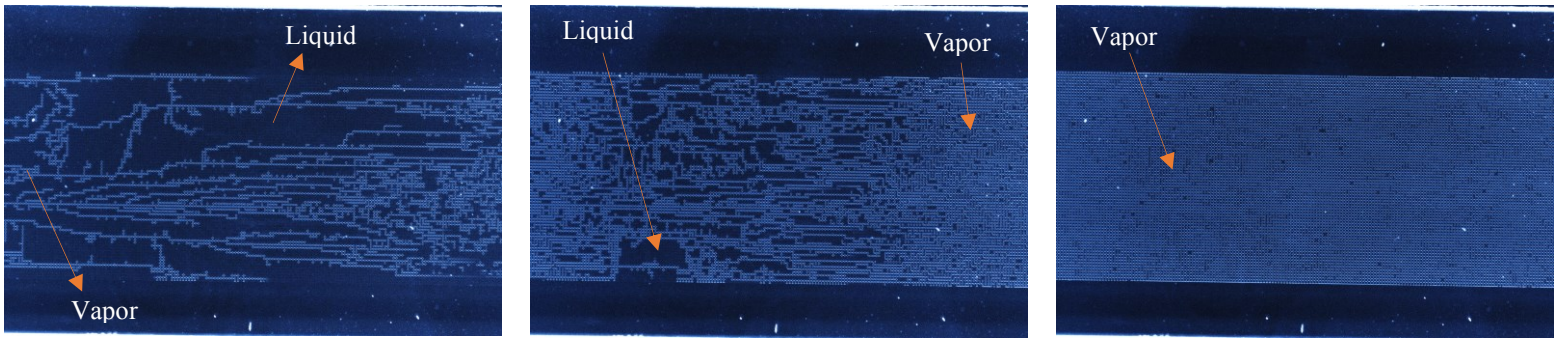

(a) **(b)** **(c)**

Figure 3-10: (a) – Homogeneous micromodel at 72℃; (b) - Homogeneous micromodel at 79.1℃; (c) - Homogeneous micromodel at 81.7℃.

Using a micromodel with larger grain diameter results into a higher boiling temperature of heptane. In a micromodel with 0.22 mm grain diameter and 0.01 mm pore throat, heptane begins to boil at a temperature of 83℃ (**Figure 3-11a**). Most of heptane in the micromodel converted into gas at 85.6℃ (**Figure 3-11b**). However, the trapped heptane (**Figure 3-12**) remains in the pore throats

even when the temperature goes up to 110.7℃. The residual liquids in porous media require more heat or energy to boil due to the pores wettability of the system.

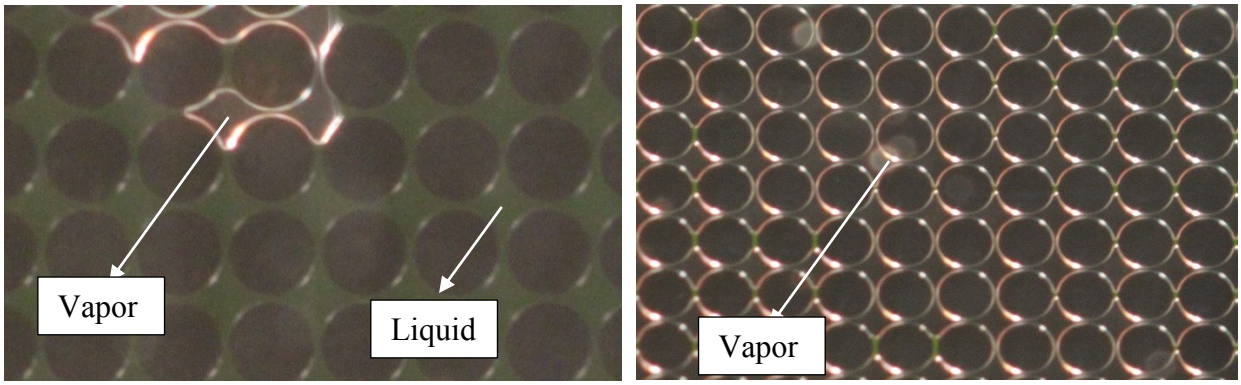

(a) (b)

Figure 3-11: (a) – Homogeneous micromodel at 83℃; (b) Homogeneous micromodel at 85.6℃.

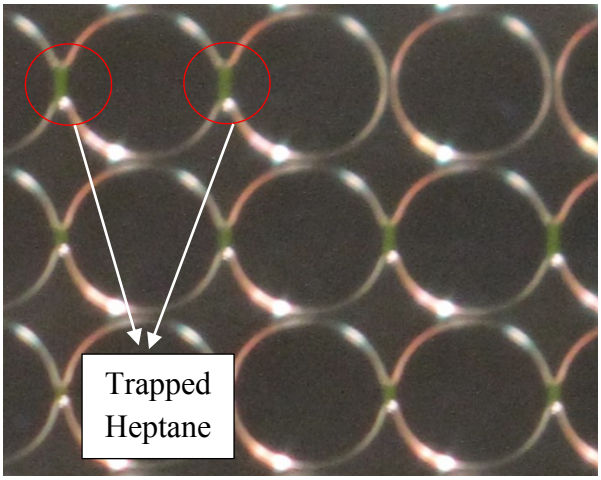

Figure 3-12: Trapped heptane in pore throats.

Because of the curved contact between liquids and pores in micromodels, the inner surface wettability can have a remarkable influence on the boiling points. Therefore, this effect is inspected by changing the wettability of homogeneous micromodels. In a 0.11 mm grain diameter and 0.01 mm pore throat micromodel, changing the surface property to oil-wet causes the heptane to boil at 80.99℃. With a 0.21 mm grain diameter and 0.01 mm pore throat micromodel, altering the

wettability to oil-wet results in the heptane to boil at 98.32℃. **Table 3-4** demonstrates the boiling points of heptane in both micromodels before and after wettability alteration.

Table 3-4: Heptane boiling points before and after wettability alteration.

	0.11 mm grain diameter and 0.01 mm pore throat micromodel	0.21mm grain diameter and 0.01 mm pore throat micromodel
Boiling point before wettability alteration (℃)	72	83
Boiling point after wettability alteration (℃)	80.99	98.32

A mixture of heptane and decane is injected into homogeneous micromodels to observe its behavior in porous media under different temperatures. **Figure 3-13a** illustrates the beginning of boiling stage of the mixture in a homogenous micromodel (0.21 mm grain diameter and 0.01 mm pore throat) at 79.37℃. At 111.39℃, most of liquid mixture has converted to gas (**Figure 3-13b**).

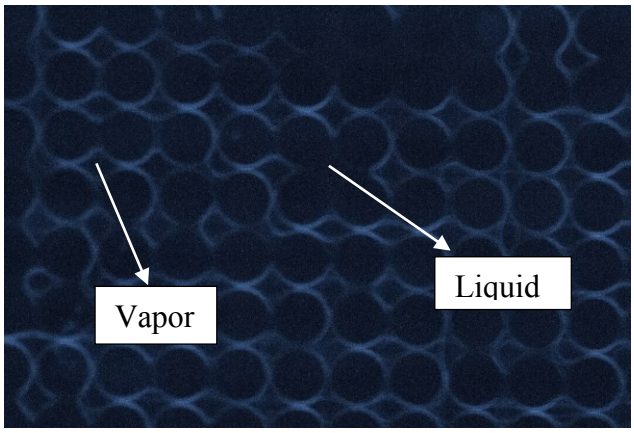

Figure 14a

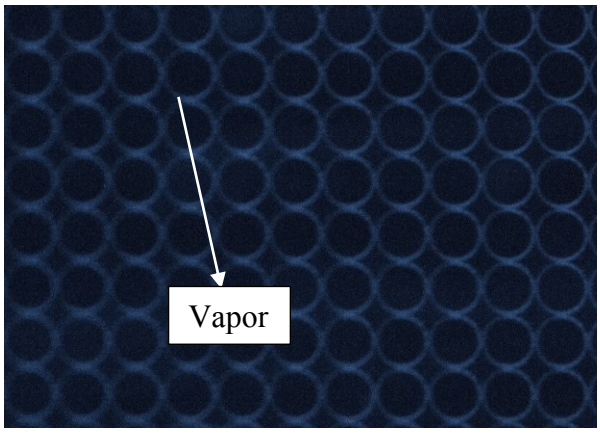

Figure 14b

Figure 3-13: (a) – Homogeneous micromodel at 79.37℃; (b) – Homogeneous micromodel at 111.39℃.

Naphtha is also observed in homogeneous micromodels under various temperatures. In a 0.11 mm grain diameter and 0.01 mm pore throat micromodel, naphtha starts to boil at 57.93℃. Heterogeneous micromodels are used in the experiments to observe the solvents behavior in media where grain and pore throat sizes are distributed non-uniformly. The pore throat in the heterogeneous micromodel ranges between 0.05 and 0.3 mm; moreover, the average grain size is 1 mm. In one of the models, heptane starts to change in phase at 90.25℃ as shown in **Figure 3-14**. **Table 3-5** displays the boiling point of different liquids in heterogeneous micromodels.

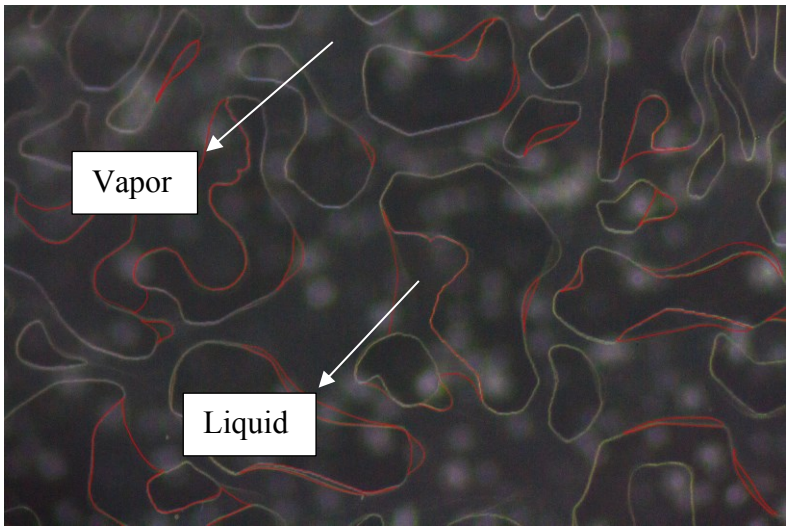

Figure 3-14: Heterogeneous micromodel at 90.25℃.

Table 3-5: Boiling points of heptane, heptane-decane mixture, and naphtha in heterogeneous micromodel.

	Boiling Point (℃)
Heptane	90.25
Heptane-Decane Mixture	80.48
Naphtha	103.48

Quantitative analysis. According to the Thomson equation, medium-size capillary has an impact on boiling points of liquids when pore radius is less than 1000 nanometer (**Figure 3-15**). The Hele-Shaw and micromodel experimental results show that pore size has an influence on boiling temperatures even if it is higher than 1000 nm. The comparative results between calculated and measured boiling points of heptane are shown in **Figure 3-16**. In this graph, the gap between the computed and measured boiling temperatures can demonstrate the limitation and applicability of the Thomson equation in computing boiling points in capillary conditions.

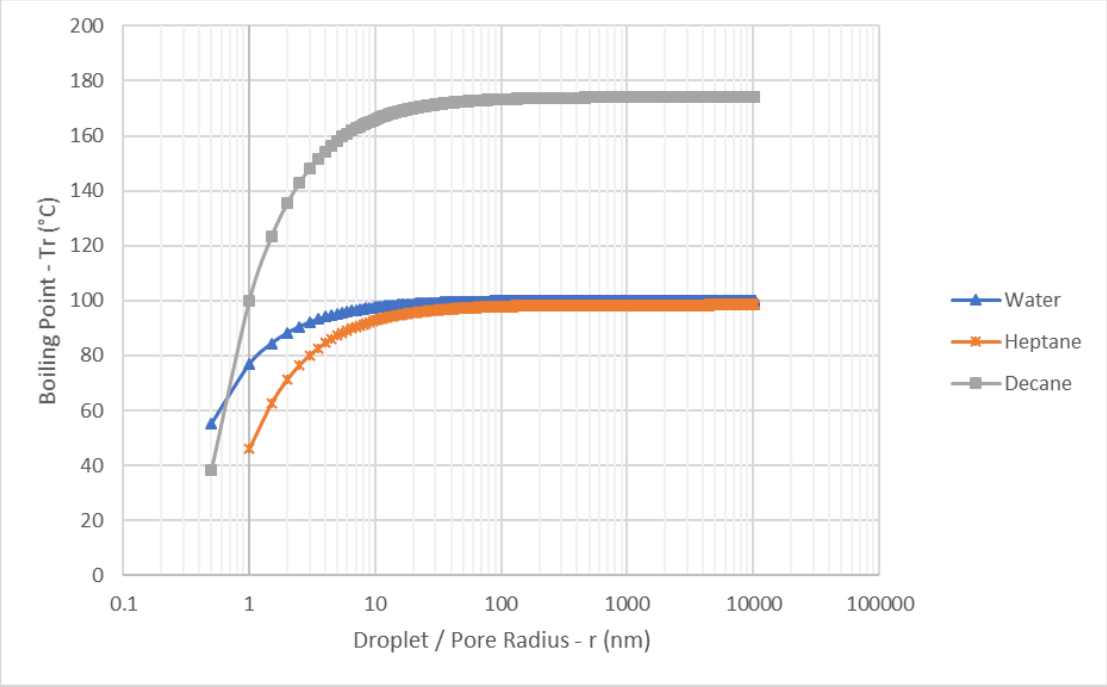

Figure 3-15: Calculated boiling points of water, heptane, and decane at different pore radiuses.

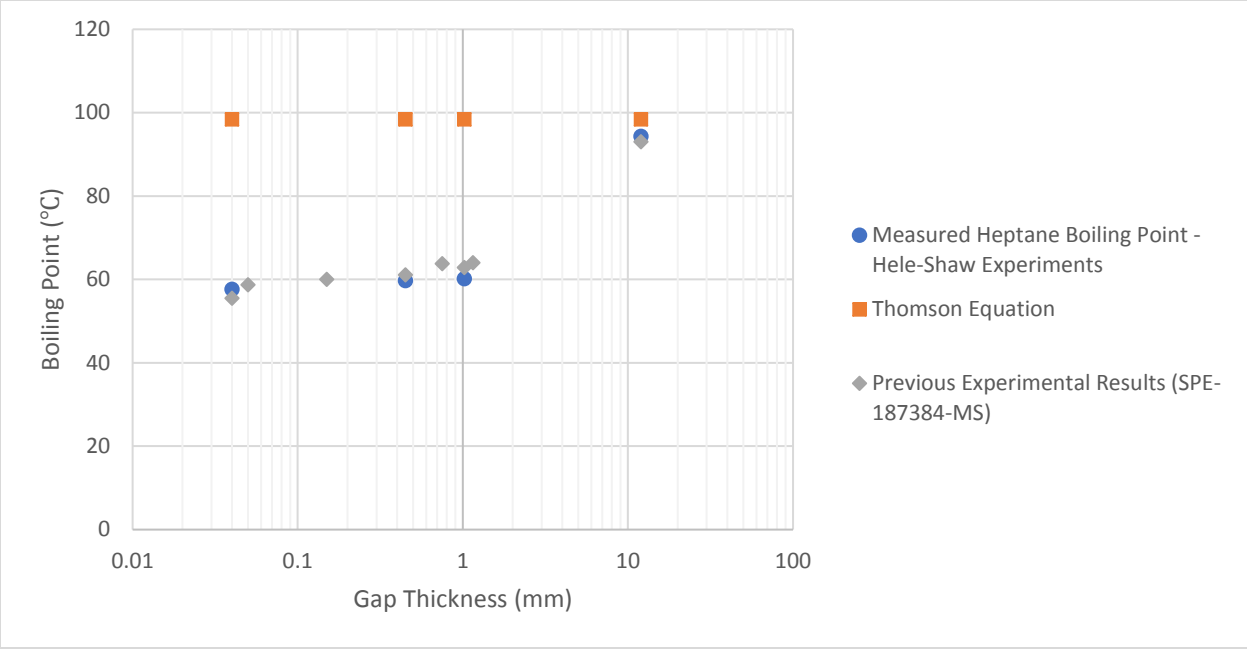

Figure 3-16: Measured and calculated boiling points of heptane at different Hele-Shaw gap thicknesses.

3.6 Conclusion and Remarks

By performing Hele-Shaw and micromodel experiments, boiling points of several liquids are investigated in confined capillary/porous media. Then, the results were matched to the values obtained from the Thomson equation by comparing computed boiling points with measured boiling temperatures. The conclusions can be listed as follows:

1. The Hele-Shaw experiments showed that the boiling temperatures of pure heptane and heptane-decane mixture decline with the reduction of medium size although it is more than 1000 nm.
2. Surface wettability does not remarkably influence boiling points of liquids when there is a flat contact between liquids and solid surfaces, as observed in Hele-Shaw experiments.
3. Surface wettability has a significant effect on boiling points when this is a curved contact between liquids and pores in porous media, as noticed in micromodel experiments.

4. Trapped solvents in pore throats need more heat to be converted to vapor because of the effect of surface wettability.
5. In homogeneous and heterogeneous micromodels, solvents tend to boil before their normal boiling temperatures due to the confined space.
6. The experimental results do not match or agree with the boiling points measured by the Thomson equation. In the equation, the boiling point is only affected by pore radius when it is smaller than 1000nm.

3.7 Nomenclature

EOR: Enhanced Oil Recovery

GCOS: Great Canadian Oil Sands

C_1: Methane

C_2: Ethane

C_3: Propane

C_8: Octane

CSS: Cyclic Steam Stimulation

SAS: Steam Alternating Solvents

SAGD: Steam Assisted Gravity Drainage

CO_2: Carbon Dioxide

SOS-FR: Steam-Over-Solvents in Fractured Reservoir

v^L: Liquid molar volume $[m^3/mol]$

r: Droplet radius $[m]$

R: Universal gas constant $\left[\frac{J}{K\ mol}\right]$

T: Temperature $[K]$

P_∞: Vapor pressure at flat surface $[Pa]$

P_r: Vapor pressure at curved interface $[Pa]$

T_r: Temperature at porous medium $[K]$

T_∞: Temperature at bulk medium $[K]$

ΔH_{vap}: Heat of vaporization $[J/mol]$

4 Chapter 4: Thermodynamics of Liquids in Capillary Medium

A version of this chapter was published in Journal of Fluid Mechanics, 2020, **905**: A32-23.

4.1 Abstract

Phase behavior of fluids at capillary conditions differs from that in bulk media. Therefore, understanding the thermodynamics of solvents in confined media is essential for modeling non-isothermal and non-isobaric engineering applications in porous media—including enhanced oil and heavy-oil recovery. The Thomson equation states that pore sizes have control over the boiling points of liquids in capillary channels. As pore spaces get smaller, boiling temperatures become lower than the normal boiling temperatures of the same liquids. The objective of this paper is to inspect this phenomenon by physically measuring the boiling points of different liquids at capillary conditions and comparing them with the values at bulk conditions and boiling temperatures obtained from the Thomson equation. Several types of microfluidic chips were used as capillary media to observe the phase-change behavior of heptane, heptane-decane mixture, and naphtha. Additionally, vaporization of water, heptane, and decane was investigated in Berea sandstone, Indiana limestone, tight sandstone, and shale. Pore size distribution analysis was performed to identify the pore diameter variations in each rock sample, and how the existence of extended nanopores in the rocks could impact the phase alteration.

4.2 Introduction

The thermodynamics and phase behavior in capillary media are different from the bulk condition (Al-Kindi and Babadagli 2019a-b). This was first formulated by Lord Kelvin (Thomson 1872) indicating that the saturation pressure and temperature are inversely proportional to the capillary size. This yields lower temperatures for boiling (Al-Kindi and Babadagli 2018, 2019b) or lower pressures for condensation (Tsukahara et al. 2012; Bao et al. 2017; Zhong et al. 2018; Al-Kindi and Babadagli 2019a) than those in bulk media. Thome (2004) studied the evaporation behaviour and two-phase flow in microchannels and provided experiments and theory related to the evaporation in confined channels. It was stated by the author that the change of physical properties of fluids in microchannels has to be considered in order to develop more accurate general methods to predict the flow and evaporation in micro media.

From a practical point of view, this phenomenon is commonly encountered in energy production from underground reservoirs including heavy-oil recovery by hybrid injection of heat and solvent, oil or gas production from unconventional reservoirs (tight sand or shale), or geothermal fluid production. These highly pressure and temperature sensitive applications require accurate estimation of saturation pressure and temperatures (boiling and condensation points) for optimal design of the processes.

Especially, highly costly solvent injection applications entail to minimize the temperatures and pressures for economically viable applications (Nasr et al. 2003; Al-Bahlani and Babadagli 2011; Pathak et al. 2012; Leyva and Babadagli 2018). Although using solvents as co-injectors with steam improves viscous oil recovery, implementing such applications in heavy-oil fields could be uneconomical since huge volumes of solvents are required to achieve desired recoveries, in addition to their high cost. Al-Bahlani and Babadagli (2009, 2011) proposed a new hybrid method (SOS-FR -steam over solvent injection in fractured reservoirs) to improve heavy-oil recovery from fractured reservoirs with efficient solvent retrieval. Subsequently, it was reported that a critical temperature exists to maximize the solvent retrieval (80 to 90% of injected solvents), which was close to the saturation (boiling) temperatures (Al-Bahlani and Babadagli 2011; Pathak et al. 2012; Leyva-Gomez and Babadagli 2016; Marciales and Babadagli 2016).

On the basis of these observations, understanding the thermodynamics of hydrocarbons (in the oil and gas industry) or other types of liquids (in other energy production industries such as geothermal fluids) in porous media becomes an essential task. The main argument is that the boiling temperature of liquids could alter in the capillary medium in which the pore size and other capillary characteristics, such as wettability and interfacial tension, play a critical role in this phenomenon. William Thomson (Lord Kelvin) described the impact of confinement and interface curvature on the saturation pressure (Thomson 1872), and the Thomson equation defined the shift of boiling temperatures in confined spaces. This paper investigates the influence of capillary properties on phase-transition temperature using different capillary models (visual microfluidic chips) having different capillary characteristics. To achieve an observation closer to the reservoir conditions, rock samples were also utilized to investigate the phase behavior of solvents in naturally occurring porous structures. Finally, the paper compares computed phase-change

temperatures (obtained by the Thomson equation) of water, heptane, and decane to the experimental observations.

4.3 Statement of the Problem and Solution Methodology

Liquids in capillary conditions might behave differently from those in bulk media with regards to vapor pressure and boiling point. Generally, the Thomson equation represents the curvature effect on boiling temperatures, stating that the impact on liquids' boiling points gets lower with higher curvatures. As the pore radius decreases, the boiling point of liquids declines as well. In this study, we selected water, as a base case, and hydrocarbon solvents due to their common use in industrial applications as liquid samples and tested their phase behaviors in capillary media under non-isothermal conditions.

When hydrocarbon solvents are injected into the reservoir to enhance oil and gas recoveries in different types of energy production systems (oil, heavy-oil, unconventional reservoirs such as shale and tight sands), a phase transformation takes place under non-isothermal conditions; therefore, understanding the thermodynamics and phase behavior of solvents in porous (capillary) media is essential in accurate modeling of such processes. The determination of optimal temperature and pressure conditions to maximize the oil recovery and solvent retrieval is essential for economically viable processes.

The economics of these kinds of processes is mainly controlled by the retrieval of the solvent at the end of the project. This can be achieved by transforming the solvent into vapor phase, especially in heterogeneous (fractured) reservoirs in which any other displacement methods are not practically effective. A large consumption of solvents in solvent-thermal (mainly steam injection) applications is accounted as a drawdown because of the high solvent cost. Hence, retrieving trapped solvents after injection helps decrease the overall expenses of such enhanced oil recovery applications. To do so, one option is to thermally convert the trapped solvents to vapor in order to release them from the low permeable rock matrix (Al-Bahlani and Babadagli 2011).

The main objective of this paper is to measure the boiling temperatures of water (as a base case), heptane (C_7H_{16}), and decane ($C_{10}H_{22}$), which are representative of hydrocarbon solvents to be used in practical applications. To obtain more representative observations, microfluidic chips with uniform and non-uniform grain size / pore throat were used. Phase-transition temperature in rock samples (limestone, sandstone, tight sandstone, and shale) was studied correspondingly. The experimental observations provided a clear understanding of the solvents nucleation in porous (capillary) media at different temperatures and valuable data were presented to compare with the bulk conditions and the theoretical model (Thomson equation).

4.4 Theoretical Background

The Young-Laplace equation quantifies the pressure difference between a liquid phase and a vapor phase at the curved interface. Mainly, the pressure difference (ΔP) increases, as the interface curvature becomes larger, which is represented by the curvature radius (r). Based on this phenomenon, the Kelvin equation describes the relationship between the saturation pressure and curvature of liquid-gas contact surface, including other parameters, such as interfacial tension (Thomson 1872). The general form of the Kelvin equation can be expressed as follows (Berg 2009):

$$RTlog\left(\frac{P_v}{P_\infty}\right) = -\frac{2\,\sigma^{LV}\,v^L}{r} + 2v^L(P_v - P_\infty) \quad (1)$$

where P_v represents the vapor pressure at a curved interface, P_∞ is the vapor pressure at the bulk condition, σ^{LV} is the interfacial tension at the vapour-liquid interface, v^L is the liquid molar volume, T is the fluid temperature, R is the universal gas constant, and r is the curvature radius. Several assumptions were considered to approximate the equation and use it as a comparison with our experimentally measured phase-change temperatures. First, the relationship between pressure and temperature is expressed by ideal gas law ($P\bar{V} = RT$). Second, the liquid is fully wetting the

solid surface which results in a contact angle of zero ($\cos\theta = 1$). Lastly, the interfacial tension (σ^{LV}) does not change with temperature or pressure. The last term ($P_v - P_\infty$) is negligible due to its extremely small value. The approximated expression of the Kelvin equation can be expressed as follows:

$$P_r = P_\infty exp\left[\frac{-2\,\sigma^{LV} v^L}{r\,R\,T}\right] \tag{2}$$

The confinement of any medium can have an effect on the vaporization temperature of liquids, as explained by the Thomson equation. By using the reductions of ordinary partial derivation with the addition of the Clausius-Clapeyron equation and Kelvin equation (Eq. 2), the general Thomson equation can be obtained as following (Berg 2009):

$$\left(\frac{\partial T_r}{\partial r}\right)_{P_r} = \frac{-\left(\frac{\partial P_r}{\partial r}\right)_{T_r}}{\left(\frac{\partial P_r}{\partial T_r}\right)_r} = \frac{2\,\sigma^{LV}\,v^L T_r}{r^2\,\Delta H_{vap}} \tag{3}$$

in the final step, by assuming that liquid molar volume (v^L) and heat of vaporization (ΔH_{vap}) are constant, the Thomson equation can be found by integrating Eq. 3 (Berg 2009):

$$T_r = T_\infty \exp\left[-\frac{2\,\sigma^{LV}\,v^L}{r\,\Delta H_{vap}}\right] \tag{4}$$

where T_r is the liquid vaporization temperature in the confined space, T_∞ is the liquid boiling point in the bulk condition, σ^{LV} is the interfacial tension at the liquid-vapour interface, v^L is the liquid molar volume, ΔH_{vap} is the heat of vaporization, and r is the pore radius. According to the equation (Eq. 4), in convex situations, the boiling temperatures tend to decline with the reduction of pore sizes.

4.5 Experimental Background - Microfluidic Analysis

To test the theory presented in the previous section and detect the boiling points of solvents at pore scale (capillaries from nano to macro scale), experiments were performed on microfluidic chips. In a series of works, the investigation was initiated by using Hele-Shaw glass cells to visualize the

nucleation (Al-Kindi and Babadagli 2018, 2019b), and vaporization (Al-Kindi and Babadagli 2019a) of several liquids in confined spaces with capillary sizes ranging between 0.04 mm and 12 mm. All the experiments with Hele-Shaw cells and microfluidic chips were conducted under atmospheric pressure (1 atm). To avoid any pressure buildup in the glass models, the injection ports were kept open to the atmosphere. The Hele-Shaw cells consist of two parallel silica-glass plates separated by a thin gap. Metal spacers were utilized to control the gap size down to a minimum thickness of 40 μm. The glass plates were attached together with a high-temperature adhesive.

Thomson equation considers the assumption of an ideal condition at which liquids are completely wetting the inner pore surface. Using clean silica-glass chips allowed us to create media practically close to the idealistic environment that the Thomson equation takes into account. Due to the smoothed glass surface, all used polar and non-polar liquids entirely spread on the material surface indicating a strongly liquid-wet medium. Hydrocarbon solvents were injected into the cells using a syringe pump and then heated gradually using a heating plate with an average heating rate of 0.25 $℃/sec$. **Figure 4-1** presents the experimental setup, which consisted of a camera, syringe pump, data acquisition system, and heating plate. Using a contact thermocouple, the temperature of the exterior Hele-Shaw surface was measured constantly as the cell was heated. Reduction of boiling temperatures was observed when the gap sizes were less than 1.15 mm. For verification purposes, the Hele-Shaw experiments were repeated with identical gap sizes to study the repeatability of the phenomenon under similar thermal conditions.

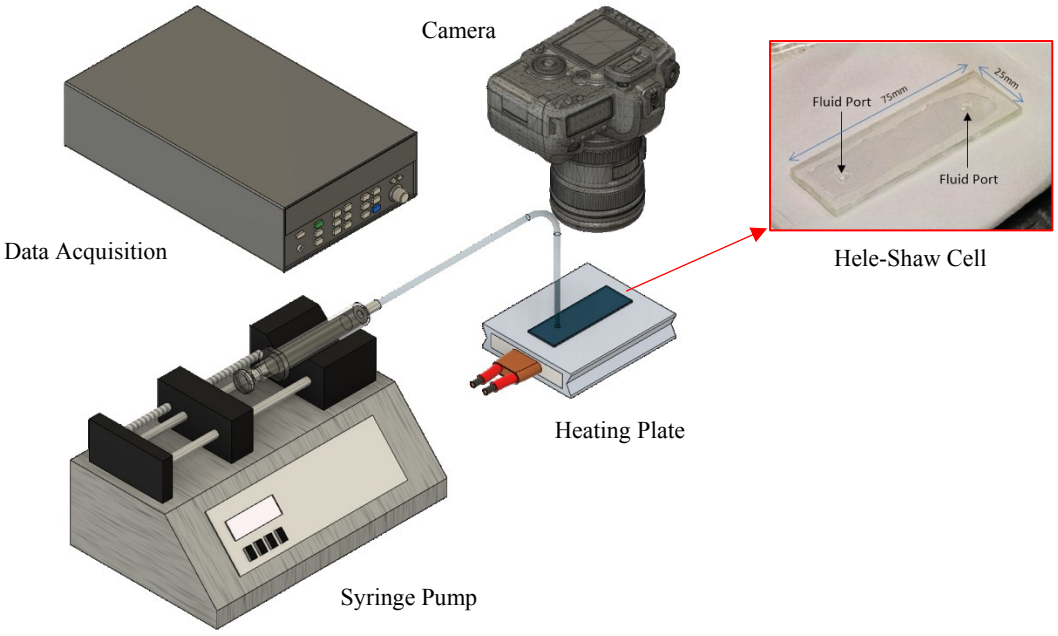

Figure 4-1: Illustration of the setup used in Hele-Shaw experiments.

To achieve precise measurements, a heat transfer study was implemented using the Fourier's law of heat conduction (Al-Kindi and Babadagli 2019b). In the microfluidic and Hele-Shaw experiments, the temperature was sensed on the exterior surface of the chips. Such method of temperature measurement can result into slight measurement errors, since the liquid temperature, within the chip, is higher than what is normally on the outer surface, due to the heat loss along the thickness of the glass cell. Thereby, the analysis assisted us in computing temperature differences between the liquid and exterior outer chip surface; thus, the fluid temperatures could be estimated accordingly. To perform the heat transfer analysis, the temperature at three different locations was measured on the top surface of the Hele-Shaw and microfluidic cells to observe the heat distribution along the silica-glass models, as illustrated in **Figure 4-2**. In the analysis, the heat was assumed to be constant along the thickness of glass models. With a gap thickness of 40 μm, water started to vaporize at a temperature of 60℃ (top surface temperature); whereas, the recorded temperature of heating plate was 64.91℃. In this case, the computed heat rate was 4.017 Joules per second (J/s). The temperatures at points 1, 2, 3, and 4 was calculated using Fourier's law of heat conduction, as shown in Figure 2. The calculations were validated by comparing them with the real measured temperatures. The computed top surface temperature (T_4) was close to the

measured temperature during the boiling stage, which was 60℃ in this case. The error percentage between the calculated and measured temperatures was 2%, and it was mainly a result of the assumption of constant heat rate along the model thickness and neglecting the heat loss on the sides of the glass cell. Such analysis was repeated with every experiment to calculate the actual fluid temperature within the Hele-Shaw and microfluidic models.

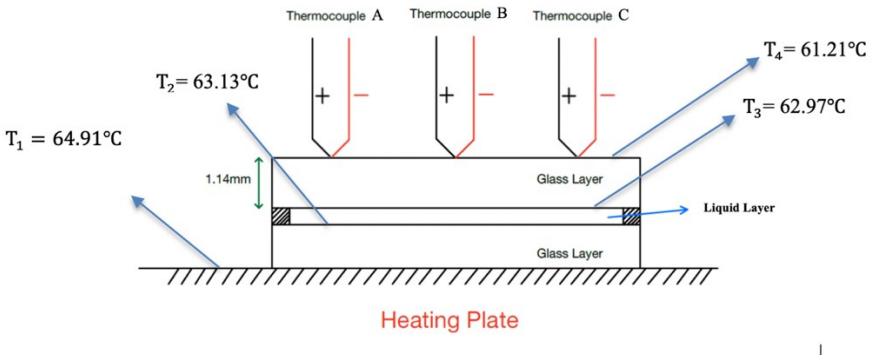

Figure 4-2: Schematic of a Hele-Shaw/microfluidic chip placed on a heating plate (Al-Kindi and Babadagli 2019b).

Three categories of micromodels were used: (a) uniform grain diameter and pore throat size (homogeneous micro model), (b) non-uniform grain diameter and pore-throat size (heterogeneous micro model), and (c) capillary channels with different widths. The grain diameter is the diameter of the silica-glass substrate material within the microfluidic chip. Microfluidic chips have become one of the advanced technologies in engineering and medical fields to study the behavior and dynamics of confined fluids. Using the silica-glass micro models provides several remarkable advantages that make these models one of the best tools to observe flow and phase behavior in nanoscale channels. Since the silica-glass microfluidic chips are chemical resistant, such characteristic provides the possibility of studying the phase behavior of reactive hydrocarbons or acidic fluids inside the glass chips. The high transparency of glass gives a benefit of clear visualization of phase alteration within the pore throats. Three main procedures are normally involved to fabricate glass microfluidic models:
(1) DC sputtering, (2) photolithography, and (3) wet etching. Firstly, a chromium (Cr) and gold (Au) ultra-thin layer is deposited on the substrate surface as a masking layer for the glass (**Figure 4-3a**). Next, after coating the masking layer with photoresist (light-sensitive material), the photomask design is adopted to the layer by exposing it to UV light and radiation (**Figure 4-3b**).

Lastly, the created photoresist image on the masking film is altered to an underlying layer by masking the layer etching process, then the glass layer is etched accordingly by the wet-etching process (**Figure 4-3c**). Like the Hele-Shaw experiments, a heating plate was used to gradually heat the micro models with a heating rate of 0.25 $℃/sec$ in average. **Figure 4-4** shows the experimental setup used to investigate the vaporization of water and hydrocarbon liquids in the silica-glass porous media.

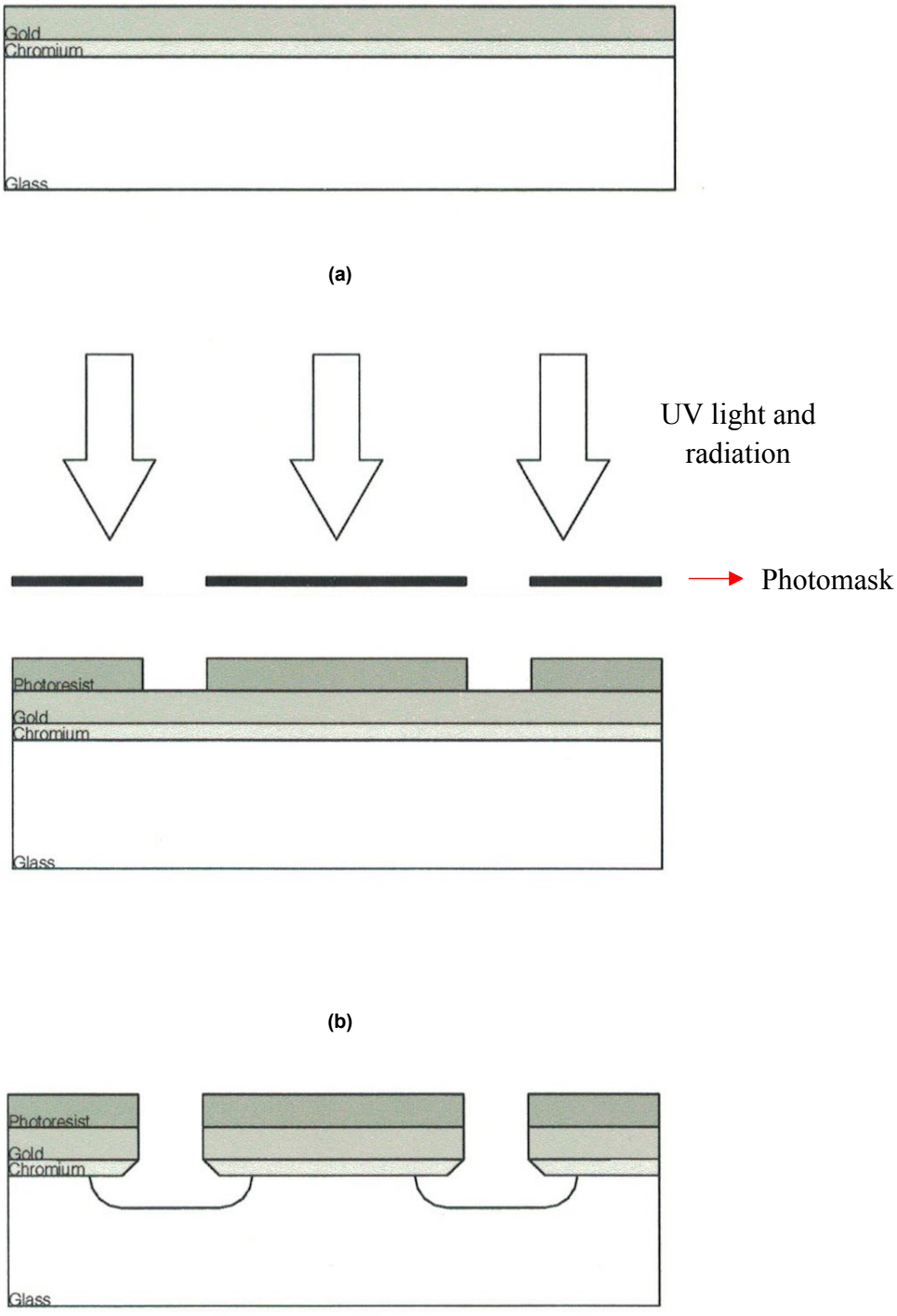

Figure 4-3: Process flow of glass microfluidic device fabrication: (a) deposition of the masking layer; (b) masking film photolithography (expose and develop photoresist); (c) masking layer and glass etching (Tai 2005).

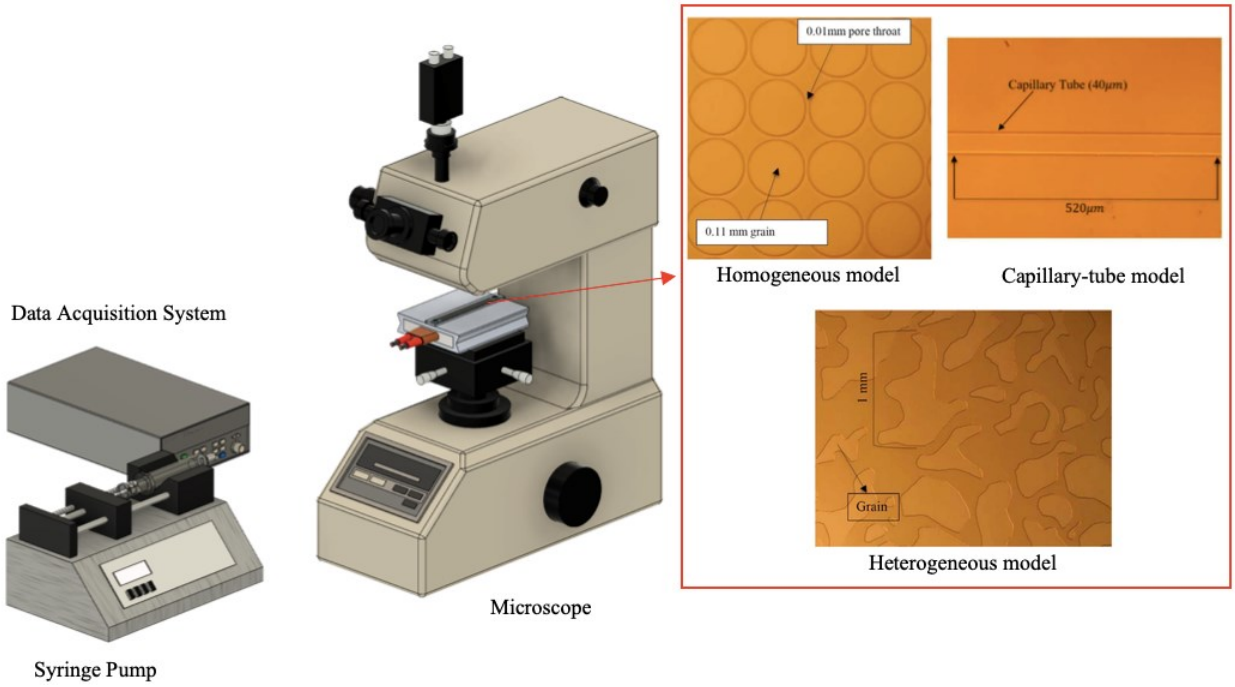

Figure 4-4: Illustration of the setup used in microfluidic experiments.

For the homogeneous micromodel, two models with different grain diameters and pore throat sizes were used. In the case of capillary-channel micromodels, the channels' widths ranged from 5 to 40 micrometers. The purpose of using various micromodel types was to inspect the influence of system configuration on the boiling point of water and hydrocarbon solvents.

The experiments were initiated with the homogeneous micromodels saturated with heptane. Using a microscope assisted in providing a clear visualization of the phase change within the pores when the boiling point of the solvent was reached. In Hele-Shaw and microfluidic experiments, on average, achieving the vaporization temperature could take 8-10 minutes. With the homogeneous micromodel (0.11 mm grain diameter and 0.01 mm pore throat), heptane started to boil at a temperature of 72℃, as shown in **Figure 5-5a**. At 79.1℃, most of the heptane vaporized (**Figure 5-5b**). A considerable volume of heptane changed into gas at a temperature of 81.7℃ (**Figure 5-5c**). Higher boiling temperatures of heptane were observed in the micromodel with a larger grain diameter.

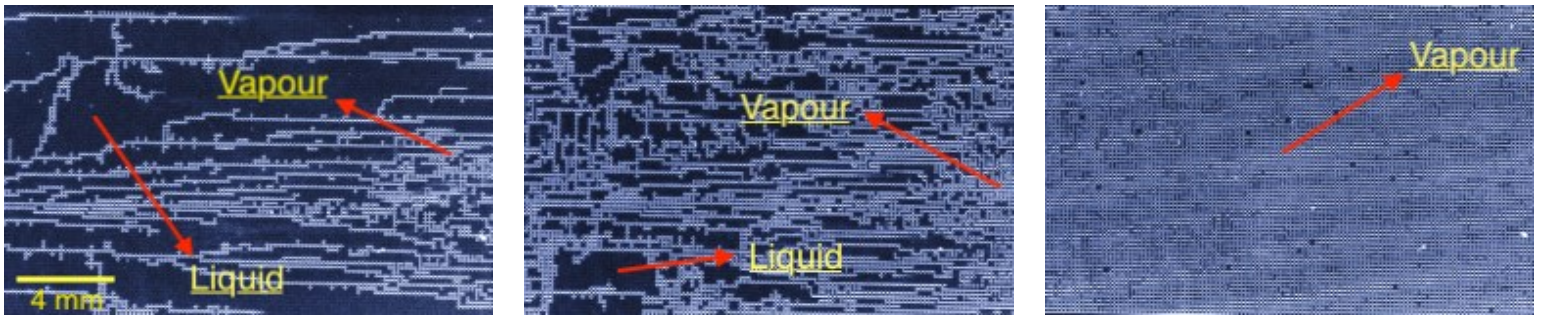

(a) (b) (c)

Figure 4-5 – (a) Initiation of heptane vaporization in the microfluidic chip at 72℃; (b) heptane vaporization in the porous media at 79.1℃; (c) the denomination of heptane vapor in the homogeneous micromodel at 81.7℃ (Al-Kindi and Babadagli 2018). White and black areas represent vapor and liquid phases of heptane.

In a homogeneous microfluidic chip with 0.22 mm grain diameter and 0.01 mm pore throat, heptane vaporized at 83℃. The majority of heptane transformed into gas at 85.6℃. The phase-change temperature of the heptane-decane mixture was investigated in a homogeneous micromodel with 0.21 mm grain diameter and 0.01 mm pore. The vaporization of the mixture initiated at a temperature of 79.37℃. Most of the liquid mixture vaporized at 111.39℃. The phase-change behavior of Naphtha was observed in a homogeneous micromodel with 0.11 mm grain diameter and 0.01 mm pore throat. Naphtha started to vaporize at a temperature of 57.93℃ (Al-Kindi and Babadagli 2018).

Heterogeneous micromodels were used to inspect the phase-alteration behavior of the solvents in media, where the grain and pore throat sizes were non-uniform. The pore throat size ranged between 0.05 and 0.1 mm; moreover, the average grain size was 0.2 mm. In such micromodel, heptane began to vaporize at 90.25℃, as shown in **Figure 6**.

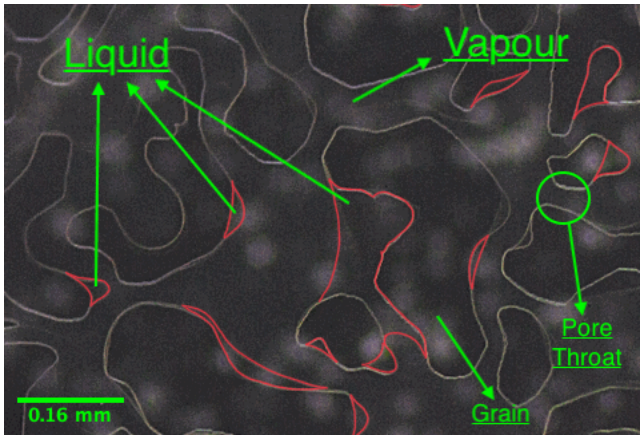

Figure 4-6:Vaporization of heptane in the heterogeneous micromodel at 90.25℃ (Al-Kindi and Babadagli 2018).

The investigation of phase-transformation behavior in microfluidic chips was continued by using capillary tube micromodels. The tubes were featured with various sizes, varying between 5 and 40 μm. The observation was initiated by inspecting the vaporization of water in such tubes. **Figure 4-7** shows the phase change of water in a capillary tube with a diameter of 40 μm. **Figure 4-8** summarizes the outcomes, obtained from the repeated Hele-Shaw experiments, and measurements on microfluidic models and capillary tubes. In the Hele-Shaw cells, a flat contact takes place between the liquid and inner glass surface. Conversely, the occurrence of curved solid-liquid contacts in the microfluidic chips and capillary tubes causes a different vaporization behavior of liquid than in the Hele-Shaw chips. Owing to the curved-contact effect in the micromodels, the phase-change temperatures of heptane in the Hele-Shaw models were lower than the boiling temperatures of the same solvent in the capillary tube, homogeneous, and heterogeneous micromodels as observed in Figure 8. The curved-contact effect becomes weaker as the medium size becomes larger, since the curvature of the solid-fluid interface becomes smaller as the tube diameter increases. Due to this phenomenon, the vaporization of heptane at bulk condition occurred in both capillary tubes and Hele-Shaw cells at identical temperatures (an average value of 93℃). The boiling point measurement at bulk conditions was conducted at the reference pressure of 1 atm (atmospheric pressure).

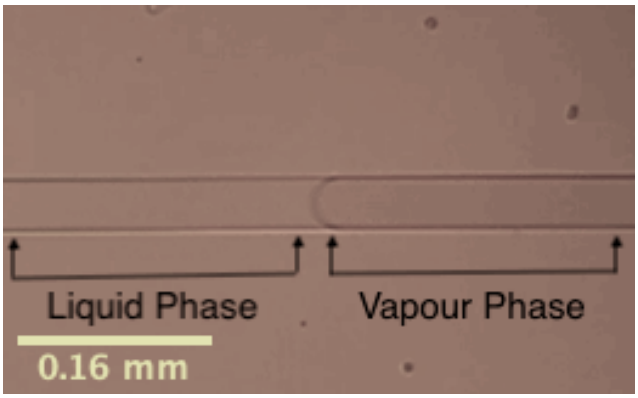

Figure 4-7: Phase change of heptane in the 40 micrometers capillary tube at 80℃ (Al-Kindi and Babadagli 2018).

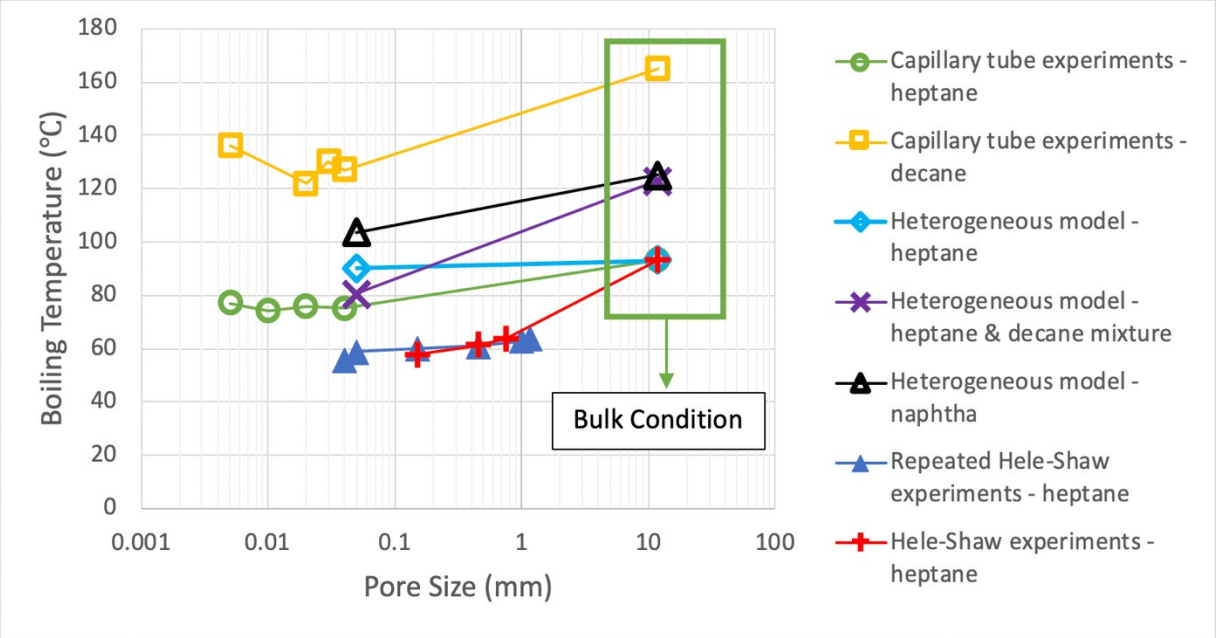

Figure 4-8: Vaporization temperatures of several hydrocarbon liquids in a variety of silica-glass porous media (data obtained from Al-Kindi and Babadagli 2018, 2019b).

The vaporization temperature of the heptane-decane mixture (80.5℃) in the heterogeneous micromodel (average pore-throat of 0.05mm) was slightly higher than the phase-alteration of heptane in the 40μm tube (75℃) and lower than the phase-change temperature of naphtha (103℃) in the heterogeneous microfluidic chip (average pore-throat of 0.05mm). In hydrocarbon mixtures, lighter components tend to vaporize first when their temperatures are raised. The mass fraction of heptane in the mixture was 0.5, and reaching the boiling temperature of heptane caused the mixture

to partially vaporize. Because of this, the vaporization took place in the mixture at a temperature close to the boiling temperature of heptane in the $40\mu m$ capillary tube. However, a complete vaporization of the mixture required higher temperatures, due to the existence of decane.

4.6 Experimental Work: Rock Experiments

With inspiration from the synthetic porous media models, we moved forward and tested the vaporization process on naturally developed porous media. Investigating the vaporization behavior of hydrocarbon solvents and water in various rock types delivers the advantage of studying the influence of pore size effect, also including its variability, on the nucleation and boiling temperatures. Unlike the microfluidic chips, reservoir rocks can contain micro (less than 2 nm) and meso (between 2 and 50 nm) pores, even in some permeable rocks such as sandstone and limestone. The existence of such channels in the rocks results in a vaporization of pre-existing rock fluids at temperatures different from those located at bulk condition, depending on the surface properties and wettability. The inspection was performed with Berea sandstone, Indiana limestone, tight sandstone, and shale samples representing different pore size distribution and petrophysical properties. The results were, then, compared with the bulk condition to obtain a clear understanding of how the boiling temperatures would alter with the reduction of the pore sizes. To do so, a bulk model (**Figure 4-9**), which consisted of a number of capillary tubes, was prepared. Because the size of the tubes was not tight enough to cause a confinement effect on the vaporization temperature, it was expected that any liquid in such model would vaporize at its normal boiling temperature.

The rock permeability, generally, reflects the interconnectivity of pores and flow capability of fluids within a specific rock. Also, the permeability relates to the size of pores within the rock. In some rocks, such as sandstone and limestone, their high permeabilities indicate a higher pore interconnectivity and larger pore sizes, comparing with tight rocks like shale and tight sandstone, featured with permeabilities lower than 0.1 millidarcies. **Table 4-1** presents the permeability ranges of the rocks used in this study.

Table 4-1: Permeability range of different rock types in millidarcys.

Rock Type	Permeability Range (millidarcy)	Density (kg/m^3)
Berea sandstone	274	2129
Indiana limestone	30	2246
Tight sandstone	0.1	2400
Shale	< 0.01	2200

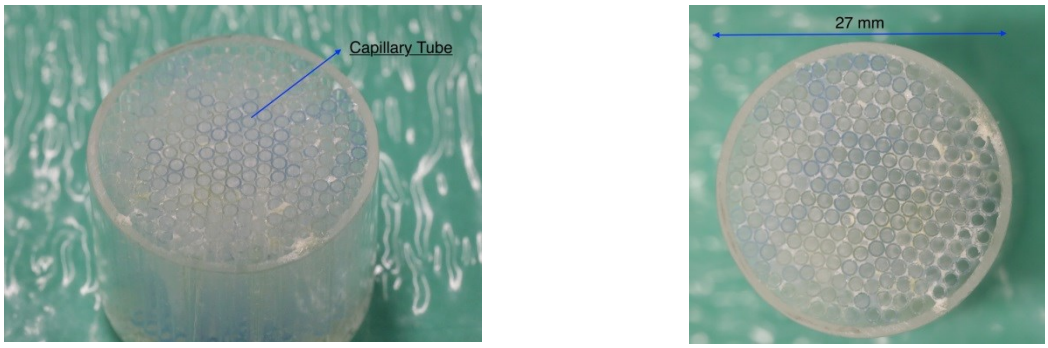

(a) **(b)**

Figure 4-9 – (a) Bulk model (consisting of a bundle of capillary tubes) from the side view; (b) bulk model from the top view.

4.7 Pore Size Distribution Analysis

Reservoir rocks are heterogeneous and complex matrixes, consisted of pores with uneven sizes and geometries. One method to estimate the distribution of pore sizes and shapes, in such systems, is to quantify the gas-solid interactions through the gas sorption generation and nitrogen adsorption and desorption on the rock surface. Alternatively, an average pore-throat radius can be estimated analytically by using the Pittman's or Winland equation. The Winland equation was introduced by Kolodizie (1980), and it is widely used in petroleum applications (Lucia 2007):

$$k = 49.5\ \emptyset^{1.470}\ r_{35}^{1.701} \quad (5)$$

where k is the rock permeability in millidarcys, $\emptyset$ is the porosity, as a fraction, and r_{35} is the average radius of the pore-throats at 35% mercury saturation.

According to the International Union of Pure and Applied Chemistry (IUPAC), micro pores are the extended tight channels at which their diameters are 2 nanometres (nm) or less. Meso pores represent media with sizes ranging between 2 and 5 nm. Pores with diameters larger than 50 nm are named as macro pores. Although high-permeable rocks, such as sandstone and limestone, consist mostly of macro pores, they can contain micro and meso pores in small fractions, compared with the overall pore volumes of the rocks. Due to the presence of extended tight pores in high-permeable rocks, it is expected to observe early vaporizations in the reservoir rocks. In pores, with less than 100 nm in diameter, the phase change of fluids behaves differently, owing to the effect of interface confinement, surface-fluid interaction, and intermolecular forces (Barsotti et al. 2016).

Initially, the average pore-throat sizes of Berea sandstone, Indiana limestone, tight sandstone, and shale were computed using the Winland equation. Since the calculated pore sizes by the equation were approximated, the pore size distribution analysis was specifically performed, as a second approach, to find precisely the size distribution of the pores that are smaller than 1000 nm in each rock type. Then, weighted average (median) pore diameters, below 1000 nm, were estimated for every rock.

Table 4-2 presents the average pore-throat sizes, calculated by the Winland equation in sandstone, limestone, tight sandstone, and shale. Additionally, the table shows the median pore sizes for channels that are below 1000 nm and their volume percentages in the rock samples.

Table 4-2: Average pore size analysis and pore volume percentages in sandstone, limestone, tight sandstone, and shale.

Rock Type	Average Pore-Throat Sizes Winland Equation (nm)	Median Pore Size of Channels below 1000 nm (nm)	Volume Percentage of pores smaller than 1000 nm (%)
Berea sandstone	22800	350	4.4
Carbonate limestone	7680	470	4.6
Tight sandstone	800	300	38.2
Shale	52	125	94.3

Although the sandstones and limestones consist of pores tighter than 500 nm, such confined pores cover minor percentages of the overall pore volumes of the rocks, as observed in Table 2. **Figure 4-10** illustrates the variation of pore volumes of different pore sizes in each rock type. In shale and tight sandstone, the pore volumes of pores, with a size range of 3–10 nm, are relatively higher than what is observed with sandstone and limestone. Furthermore, larger pore volumes in mesopores (2–50 nm) are detected in shale and tight sandstone, comparing with Berea sandstone and Indiana limestone. As a part of the analysis, desorption of nitrogen from pores with different sizes, ranged between 1 and 100 nm, was measured in each rock type (**Figure 4-11**). Based on the pore volume investigation (Figure 10), it was expected to observe higher nitrogen desorption from micropores and mesopores in shale and tight sandstone, compared to sandstone and limestone, which justified the high pore volume percentages of such confined channels in both tight rocks.

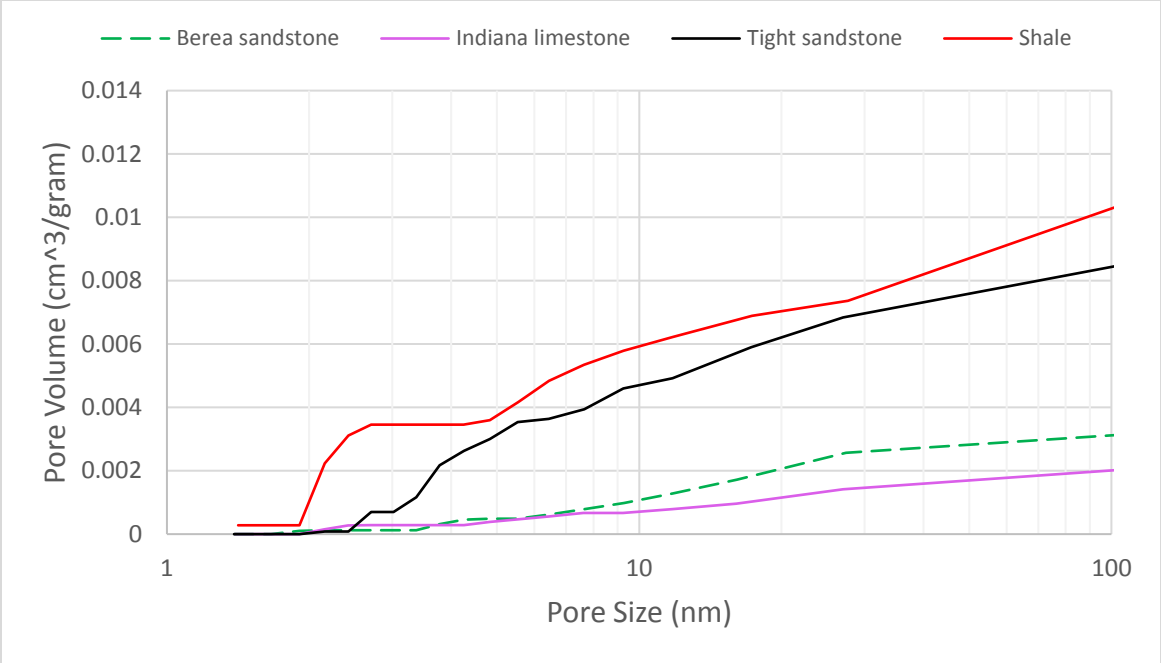

Figure 4-10: Change of pore volumes of various pore diameters, ranging between 1 and 100 nm, based on nitrogen desorption.

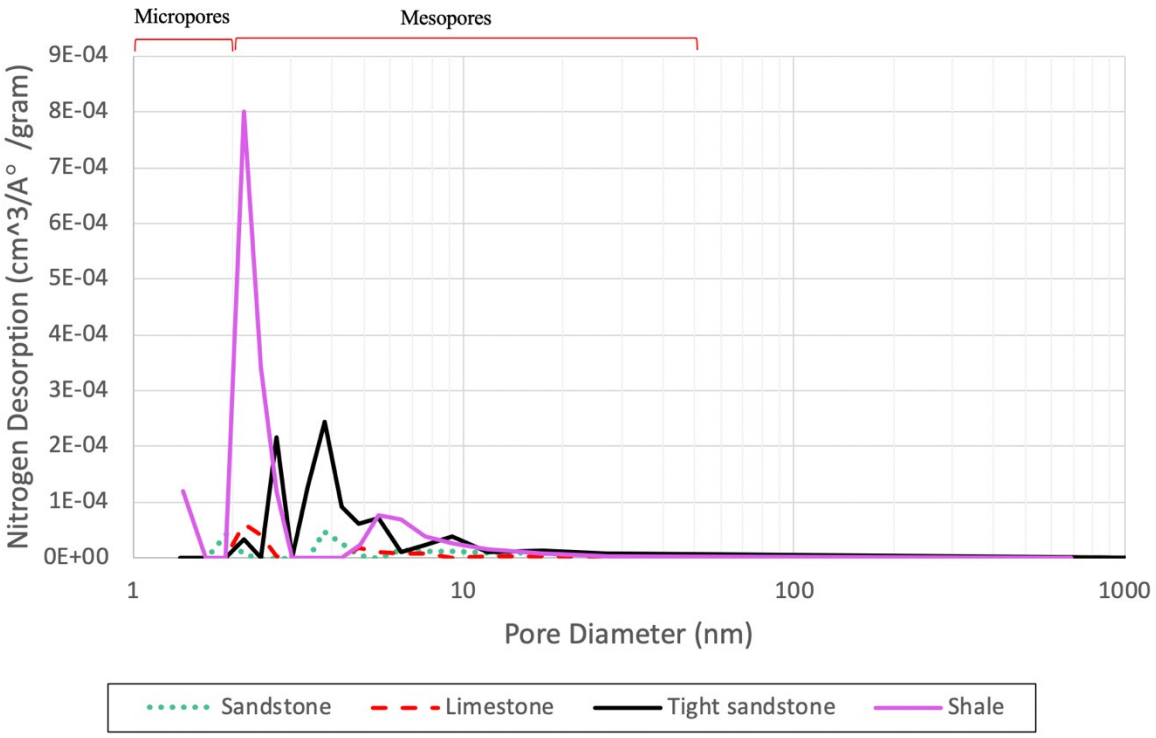

Figure 4-11: Pore size distribution of Berea sandstone, limestone, tight sandstone, and shale, based on nitrogen desorption.

4.8 Experimental setup

The setup consisted of a DSLR camera, temperature controller, thermocouple, glass container, glycerol or mineral oil as heating liquids, and electrical oven. **Figure 4-12** shows the external and internal experimental setup.

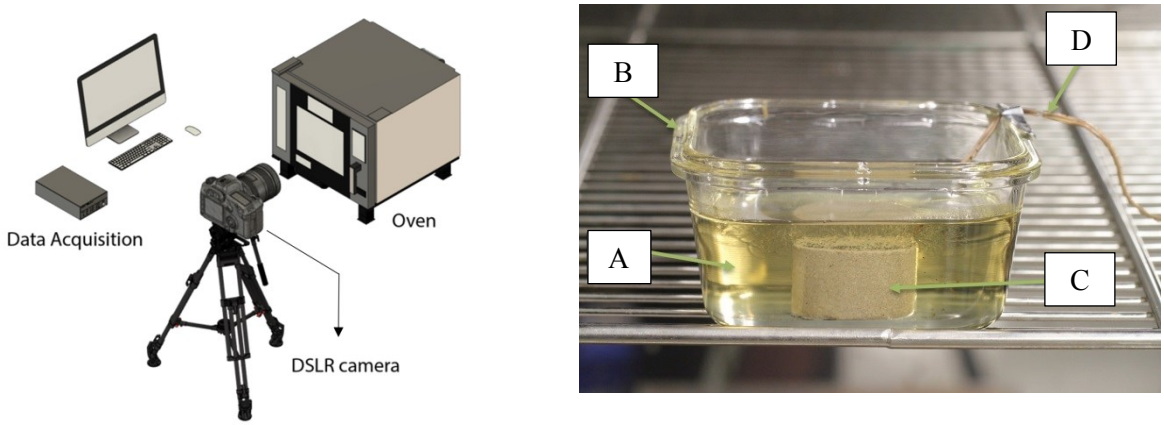

(a)

(b)

Figure 4-12 – (a) External experimental system (Al-Kindi and Babadagli 2020); (b) internal experimental system: (A) glycerol / mineral oil, (B) glass container, (C) rock sample, and (D) thermocouple.

4.9 Procedure

Initially, the core samples were heated in the oven at a temperature of 80℃ for 48 hours to fully dry the samples and make sure there was no residual water within the rocks. Then, the samples were vacuumed for 48 hours to completely remove all the trapped air in the rocks. The rocks were saturated with liquid (water or solvent) under a vacuum pressure of 93 KPa (below atmospheric pressure) for almost 48 hours. In rock experiments, using a heating plate would not ensure a uniform heat distribution around the rock volume. Hence, to ensure a uniform heat distribution around the cores, rock samples were immersed in a glycerol bath, and the system was heated gradually by the oven with a constant heating rate of $1.5℃/min$. By increasing the temperature of inner environment inside the oven, the heat transfers uniformly to the liquid bath which provides a homogeneous heat migration around the rock sample. **Figure 4-13** shows an illustration of heat transfer from the oven to the sample. Mineral oil was used as a heating liquid for the rocks that were saturated with water to prevent the liquid bath from mixing with water during the heating process. All the experiments were performed at ambient pressure (1 atm).

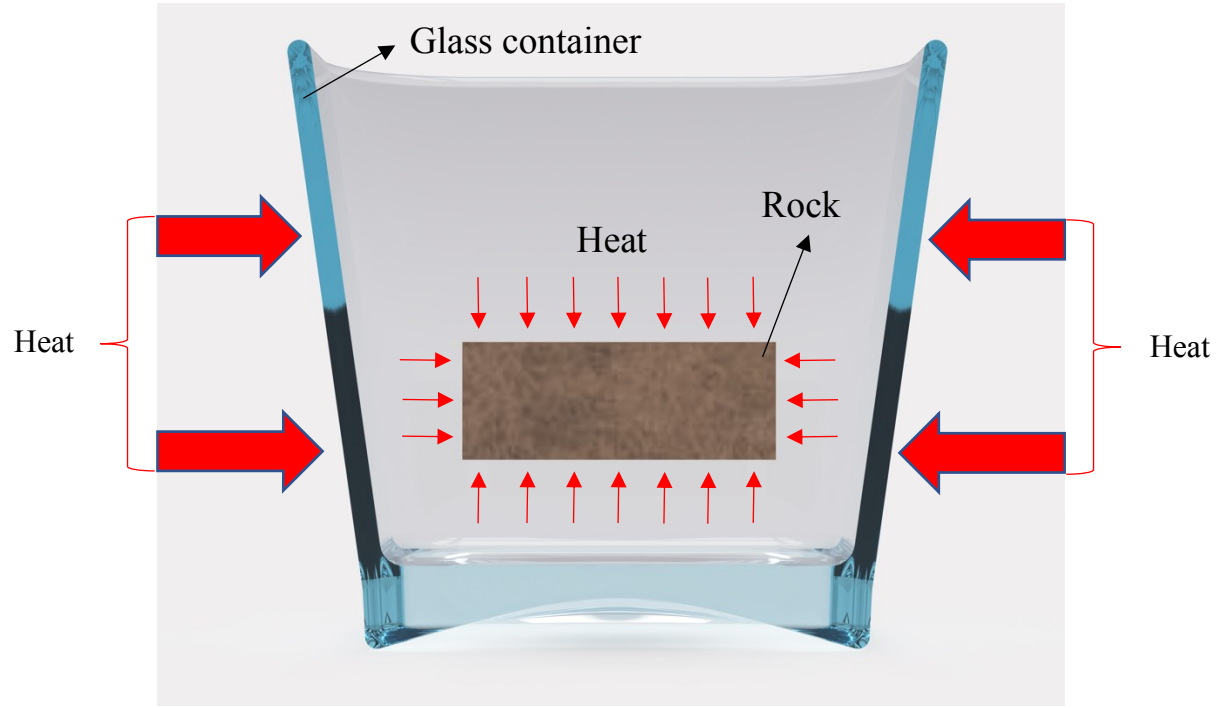

Figure 4-13: Schematics representation of heat transfer from the surrounding medium inside the oven to the liquid bath and rock sample.

4.10 Results and Discussions

As a first step, boiling temperatures of water and heptane were measured in the bulk models. Both liquids began to vaporize at temperatures close to their normal boiling temperatures. Then, the phase transformation behavior of water, heptane, and decane was visually studied in different types of rocks. In rock experiments, reaching the temperature at which vapour started to come out from the sample took from 40 minutes to 1 hour, depending on the initial temperature of the oven, liquid bath, and rock sample. While heating the rock samples, three main stages were focused on in the determination of boiling point: (1) initial bubbles creation, (2) slow and continuous formation of bubbles, and (3) rapid and continuous formation of bubbles. The results, shown in **Figures 4-14 to 4-16**, are for the bulk and two selected rock samples, showing the extreme permeability and pore sizes (Berea sandstone and shale). As seen, the sizes of the bubbles discharged are comparable

to the average pore sizes (as given in Table 4-2 and **Figure 4-9** for the rock samples and the bulk model, respectively).

In the bulk model, initial water bubble formation occurred at 87℃ (360.15 K) as shown in **Figure 4-14a**. An increase of vapor bubbles was noticed at a temperature of 90℃ (363.15 K) (**Figure 4-14b**). At a temperature of 96℃ (369.15 K), fast formation of bubbles took place, which was considered as the normal boiling point of water (the third stage shown in **Figure 4-14c**). This value was taken as a benchmark (boiling in the bulk condition) and compared with the experiments done on the rock samples. Because of the presence of micro and meso pores, early vaporization of heptane, decane, and water was clearly noticed in all the used rocks. With the Berea sandstone sample, for example, heptane vapor bubbles started to appear on the rock surface at 71℃ (344.15 K) (**Figure 4-15a**). At a temperature of 76℃ (349.15 K), slow formation of bubbles took place in the core, as shown in **Figure 4-15b**. A quick and continuous creation of gas bubbles of heptane took place at 81℃ (354.15 K) (**Figure 4-15c**).

Another example of an early vaporization was the water phase change in shale. At a temperature of 76℃ (349.15 K), the first water gas bubble appeared on the surface (**Figure 4-16a**). Slow formation of bubbles took place at 82℃ (355.15 K), as presented in **Figure 4-16b**. A rapid and continuous formation of gas bubbles of water occurred at 84℃ (357.15 K) (**Figure 4-16c**). **Figure 4-17** presents the temperatures of the three stages of water, heptane, and decane in Berea sandstone, Indiana limestone, tight sandstone, and shale, including their normal boiling temperatures in the bulk models. The occurrence of phase alteration in fluids highly depends on the random motion of molecules due to the change of their energies. As a result, the actual boiling stage might happen at any temperature between the first and third stage. In all the cases, the third stage was treated as the boiling temperature of the liquid. Although considering the third stage as the boiling phase of the liquid could result in overestimated boiling temperatures, taking such consideration brought pessimistic outcomes. In other words, the highest possible temperature value was taken as the bubbling point to avoid any errors caused by experimental error. Even in these circumstances, the values obtained were much lower than those in the bulk conditions as will be discussed in the next sections.

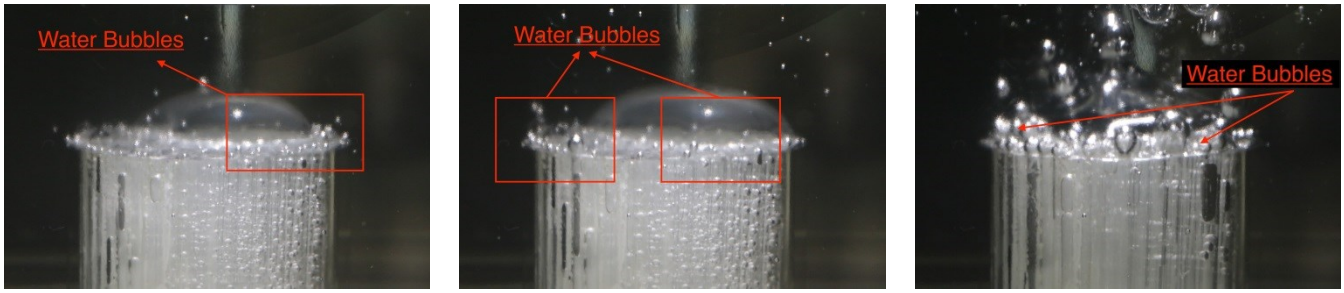

(a) (b) (c)

Figure 4-14 – (a) First water bubbles formation (stage No. 1) at 87℃ (360.15 K) in the bulk model; (b) slow water bubbles creation (stage No. 2) at 90℃ (363.15 K)in the bulk model; (c) rapid water bubbles formation (stage No. 3) at 96℃ (369.15 K) in the bulk model.

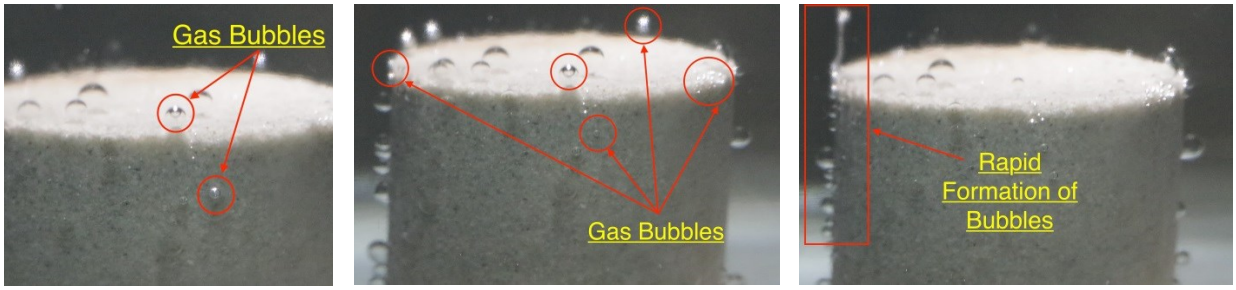

(a) (b) (c)

Figure 4-15 – (a) Initial heptane bubbles creation (stage No. 1) at 65℃ (338.15 K) in sandstone; (b) slow and continuous heptane bubbles formation (stage No. 2) at 80.3℃ (353.45 K) in sandstone; (c) rapid and continuous heptane bubbles formation (stage No. 3) at 88℃ (361.65 K) in sandstone.

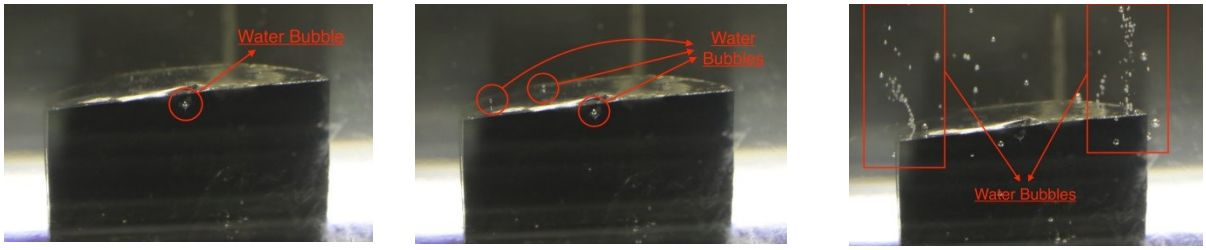

(a) (b) (c)

Figure 4-16 – (a) Initial water bubbles creation (stage No. 1) at 76℃ (349.15 K) in shale; (b) slow and continuous water bubbles formation (stage No. 2) at 82℃ (355.15 K) in shale; (c) rapid and continuous water bubbles formation (stage No. 3) at 84℃ (357.15 K) in shale.

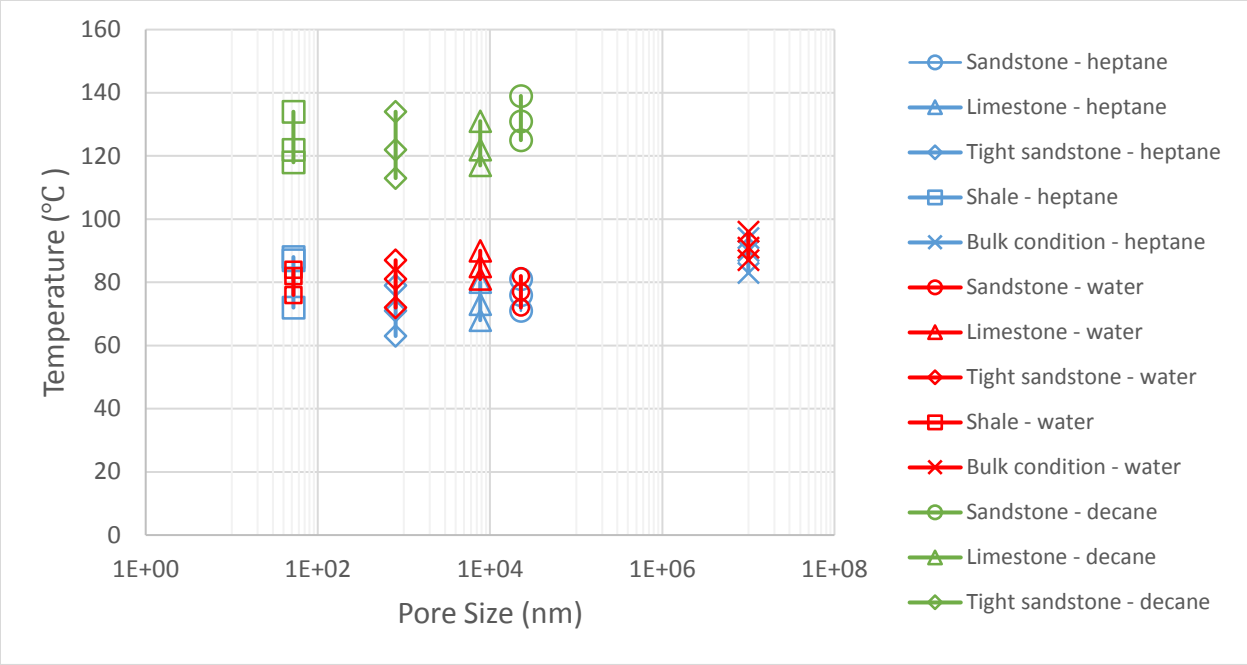

Figure 4-17: Temperatures of the three main stages of water, heptane, and decane in Berea sandstone, Indiana limestone, tight sandstone, shale, and bulk model.

4.11 Comparison of experimental results with theory (Thomson equation)

According to the Thomson equation (Eq. 2), porous media (capillary condition) can have a significant impact on the boiling points of liquids when the pore radius is less than 1000 nm. Since extended tight pores (smaller than 100 nm) do exist in the permeable rocks, liquids tend to boil in such matrixes at lower temperatures than their normal boiling point temperatures. **Figs. 4-18** and **4-19** illustrate the average vaporization temperatures and temperatures of the two reading points (first and third stage) of water, heptane, and decane in Indiana limestone, Berea sandstone, tight sandstone, shale, and bulk condition. Moreover, the experimental results were compared with computed vaporization temperatures, obtained from the Thomson equation. For the rock samples, average pore-throat sizes, in Figure 18, were estimated using the Winland equation and considered to compare the outcomes with the computed vaporization temperatures.

Meanwhile, median pore sizes (given in Table 4-2) were considered as another way to represent a single pore size value. These values were calculated by measuring areas under the curves in pore

size distribution graphs assuming that the pore sizes smaller than 1000nm dictate the "early" boiling process. This assumption is based on the theoretical observations and the Thomson equation, implying that the 1000nm is the threshold above which the porous structures behave like bulk (see solid lines in Figure 4-18). The results for the median pore size are shown in Figure 4-19. In both average (obtained by the Winland equation) and median pore size cases, the observed vaporization of water, heptane, and decane in the rocks took place at temperatures lower than the bulk cases, as shown in Figs. 4-18 and 4-19.

Figure 4-20 summarizes the results, obtained from the Hele-Shaw and microfluidic experiments with heptane, and compares them with the observed outcomes from the rock experiments and computed heptane vaporization temperatures by the Thomson equation. Since the nature of the curved interface is not identified in the silica-glass models and rock porous media, the interfacial tension at the vapour-liquid interface (σ^{LV}) was assumed to be unaffected by the curvature. Furthermore, it was assumed that the rock molecules were not interfering with the vapour-liquid interface. According to the microfluidic experiments, on average, the reduction of heptane vaporization temperatures, from the bulk condition and computed vaporization point, was 22% (4.8% in kelvin unit) in an average pore throat of 15000 nm (0.015 mm). As a result of the non-curved solid-liquid contact in the Hele-Shaw glass cells, the recorded phase-change temperatures of heptane were nearly 20% (4.3% in kelvin unit) lower than what were found in the micromodel observations. Generally, the vaporization of heptane in the rocks took place at temperatures lower than the bulk condition by almost 22% (4.8% in kelvin unit). The average boiling temperature of heptane (73℃, 346.15 K) in sandstone, limestone, and tight sandstone was 24% (5.4% in kelvin unit) below the calculated phase-transition temperature (98℃, 371.15 K), estimated by the Thomson equation. In shale, the measured heptane boiling point (83℃, 356.15 K) was noticed to be lower than the computed temperature (93℃, 366.15 K) by 15% (3.2% in kelvin unit). Overall, the outcomes, obtained from the rock experiments, were consistent with the microfluidic observations, as shown in Figure 4-20.

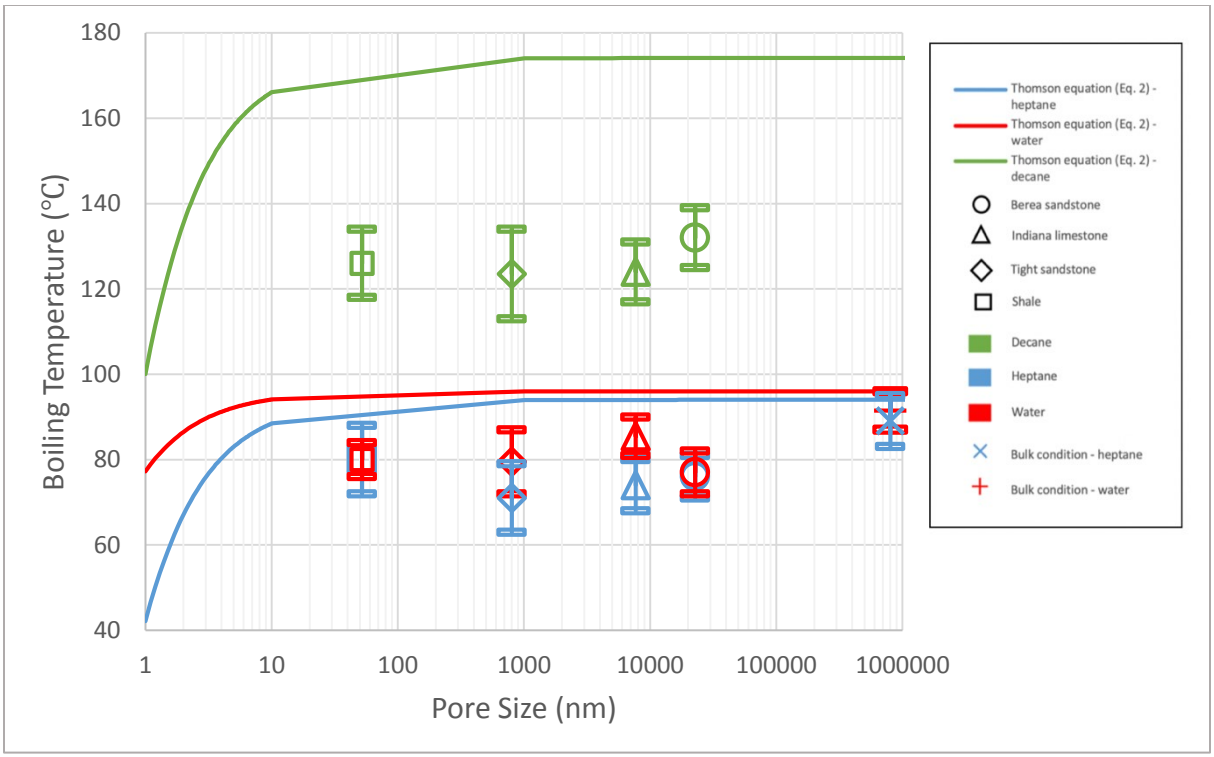

Figure 4-18: Calculated vaporization temperatures and measured boiling points of heptane, water, and decane in bulk case and different rock samples; the average pore size of each rock was computed by the Winland equation. The boiling temperatures were measured under atmospheric pressure (1 atm).

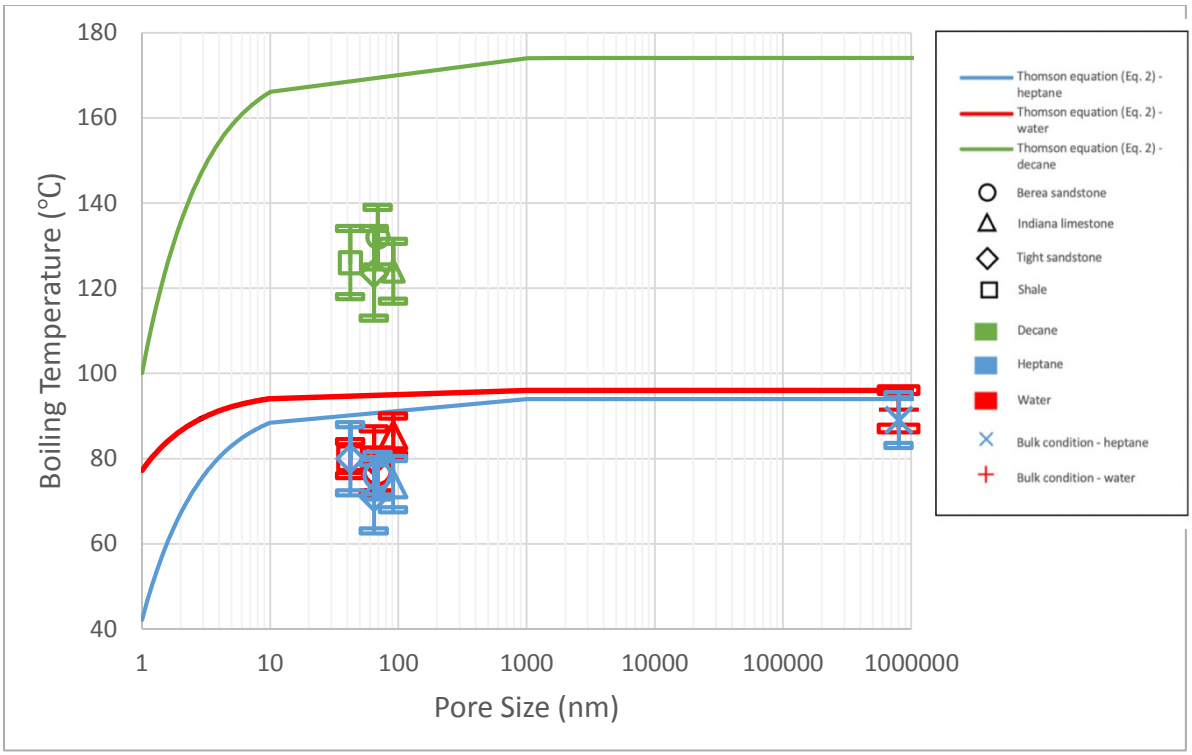

Figure 4-19: Calculated vaporization temperature and measured boiling points of heptane, water, and decane in bulk case and different rock samples; median pore diameters were considered. The boiling temperatures were measured under atmospheric pressure (1 atm).

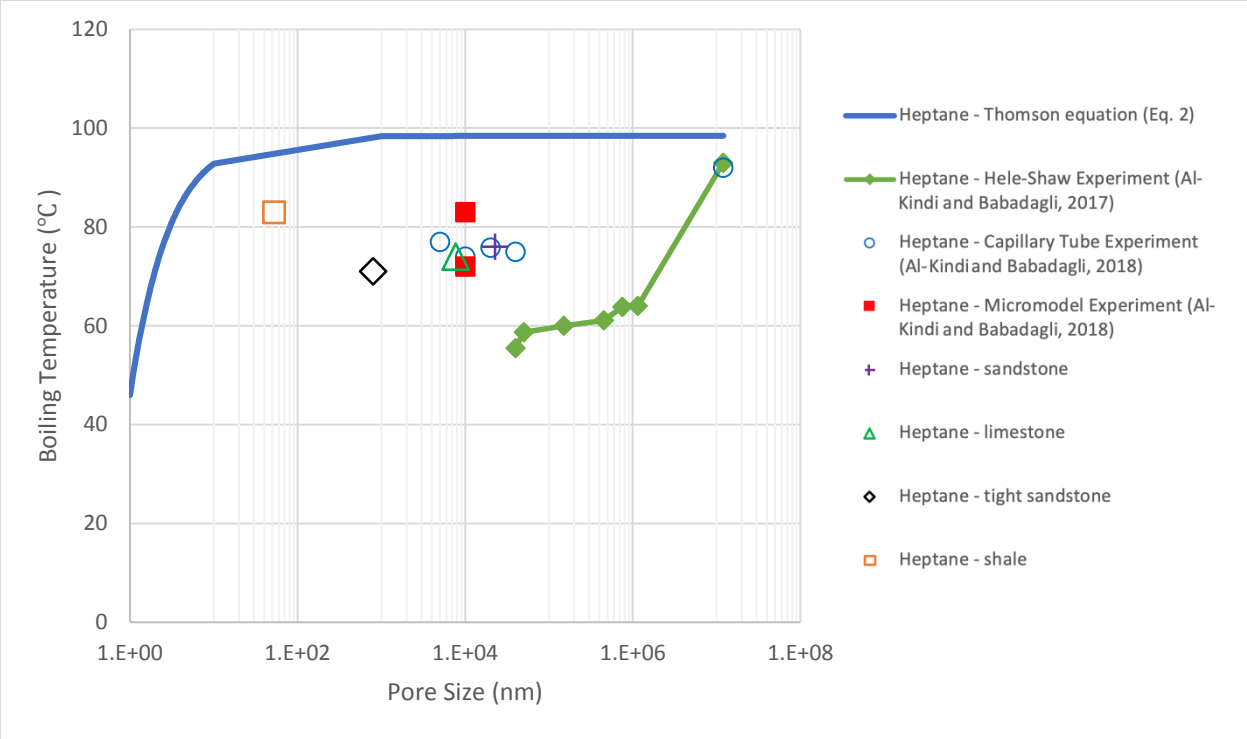

Figure 4-20: Measured boiling temperatures of heptane from Hele-Shaw, micromodel, and rock experiments and calculated phase-transition temperatures, obtained from the Thomson equation.

4.12 Sensitivity of Bubble Point Detection

The temperatures of the first, second, and third stages were measured based on the appearance of gas bubbles on the rock surface (Figure 4-14). With the same liquid, the first stage (formation of initial bubbles) was noticed to take place in the rocks at different temperatures. For instance, **Figure 4-21** presents the temperatures of the three stages of heptane in the used rock samples. During the first stage, the existence of the first bubbles depends partially on the size of pores. Nonetheless, initial heptane gas bubbles started to appear on the shale's surface at a temperature (72℃, 345.15 K) that was higher than what was observed in sandstone, limestone, and tight sandstone, although the pores in shale are tighter than the inner channels of the other rocks. The reason behind such a phenomenon was the low permeability of shale, which restricted the movement of gas bubbles within the rock. Similarly, the second and third stage, in shale, occurred

at temperatures higher than what were measured in other rocks, due to its tight nature (much lower permeability than other samples).

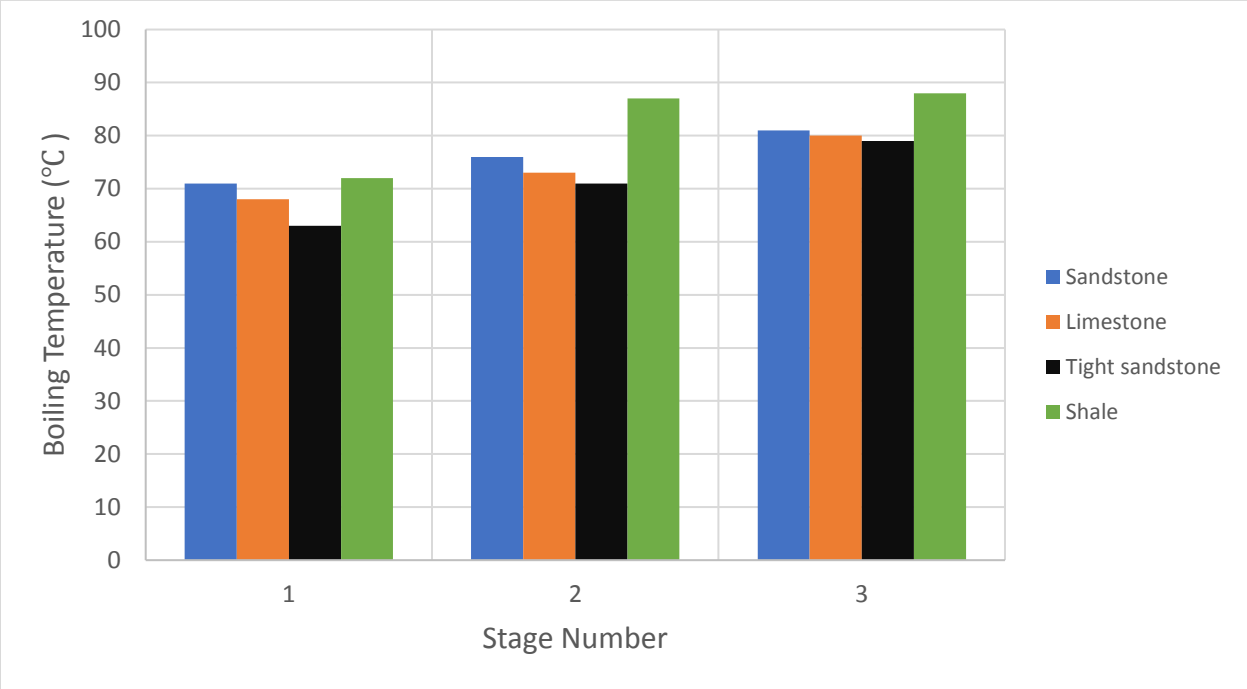

Figure 4-21: Temperatures of the three stages of heptane in Berea sandstone, Indiana limestone, tight sandstone, and shale.

4.13 Detailed Analysis of Bubble Point Detection in Rocks

Bubble generation and nucleation in microfluidic glass models can be visualized promptly due to the transparent nature of the micromodels. The vaporization inside the rock pores, nonetheless, cannot be observed unless the bubbles appear on the rock surface. The migration of the bubble from a point of generation to the surface may take a while if the permeability (or pore size) is small. This delay can be attributed to wettability and clay content as well. Hence, further analysis was performed to detect a possible margin of error caused by those factors, and the temperature values at which bubbling starting for each rock types were compared.

Figures 4-22 to 4-24 show the temperatures values at which the first bubble and continuous bubbling developed in the sandstone, limestone, tight sandstone, shale, and bulk model. Characteristically, the first bubble appeared on the tight sandstone compared to other rock types. This makes sense as its permeability (Table 4-1) and median pore size is smaller than 100nm as well as the volume content in the whole system (Table 4-2) is much smaller than that of the Berea sandstone and Indiana limestone samples.

On the other hand, one would expect that liquids should vaporize in shales at a lower temperature than the tight sandstone as almost all pores are smaller than 1000nm (Table 4-2 and Figure 4-11) and the average/median pore size of the shale sample is considerably lower than that of the tight sandstone. This might be due to the fact that the ultra-low permeability of shale slowed the motion of the bubbles upward in the rock, leading the vapour bubbles to appear on the rock surface at higher temperatures than what were observed with the other rocks. In other words, in the tight sandstone, water, heptane, and decane bubbles appeared on the rock surfaces at lower temperatures than what were measured in shale—even though both rocks contained a comparable amount of pore sizes smaller than 1000nm (Figure 4-10). Due to the higher permeability of tight sandstone, the mobility of vapour bubbles in the rock was more than the case in shale, which explains the appearance of water, heptane, and decane bubbles on the outer surface of the tight sandstone sample at lower temperatures than what was observed in shale at the same conditions.

Also note that the temperature values at which the first bubble was detected for Berea sandstone and Indiana limestone is lower than that of the shale sample for heptane (Figure 4-22) and decane (Figure 4-24) even though both samples are extremely low in pore sizes smaller than 1000nm (Table 4-2 and Figure 4-11). This can be attributed to the permeability effect, which caused a delay in discharging the bubble out of the rock in the case of the shale sample.

The above observations are valid for the hydrocarbon solvents (heptane and decane). In the case of water, one may see the effect of permeability on bubble discharge mechanism but Berea sandstone and Indiana limestone showed a different behavior compared to the solvent cases. The lowest temperature at which the first bubble appeared was measured for Berea sandstone (Figure 4-23). Indiana limestone showed the highest temperature value among all four samples for the detection of the first bubble. These observations could be attributed to another characteristic of capillary medium, wettability, which is controlled by the rock mineralogy and thereby clay

content. As a result of the rock wettability, certain liquids are held by the inner pore surface, which could be the case of limestone, of which shows less water wet nature. The clay content also plays a role due to higher adsorption capacity, especially for solvents. The solvents have a higher tendency to be adsorbed onto clays, and Berea sandstone shows high clay content. The effect leads to stronger surface-molecule forces, which require more thermal energy or higher temperatures to break them. In the case with heptane (Figure 4-22), however, the formation of the first bubbles on the sandstone's surface was noticed at the identical temperature as tight sandstone. Despite the low volume percentages of pores below 1000 nm in sandstone and limestone (Table 4-2), their existence could result into early vaporizations at temperatures similar to what could be observed with tight sandstone.

The results with the bulk model were used as benchmarks and comparisons with the temperature values obtained with the rocks and, despite all the uncertainties described above, one may observe that the lowest and highest temperatures taken as the indicator of boiling (first bubble appeared and continuous boiling, respectively) are still considerably lower than that of the bulk case as could be observed in Figures 4-22 to 4-24. In other words, the nucleation temperatures in sandstone, limestone, tight sandstone, and shale were lower than what were detected in the bulk model, owing to the confinement effect in the rocks.

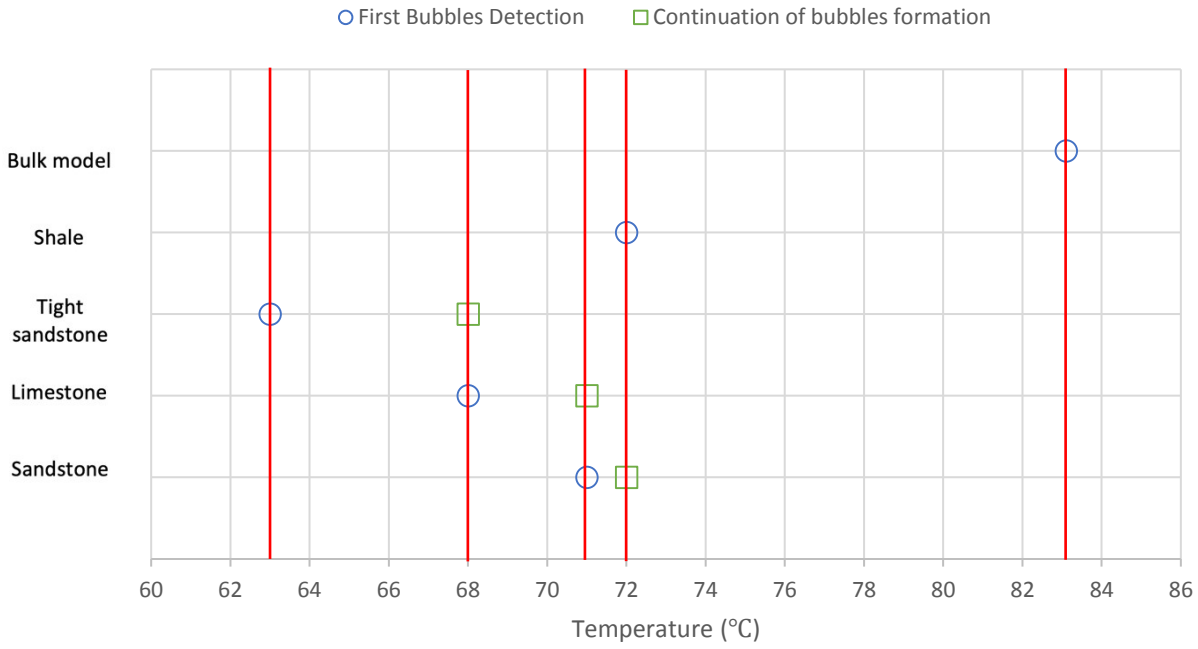

Figure 4-22: Bubble point detection temperatures for heptane in sandstone, limestone, tight sandstone, shale, and bulk model.

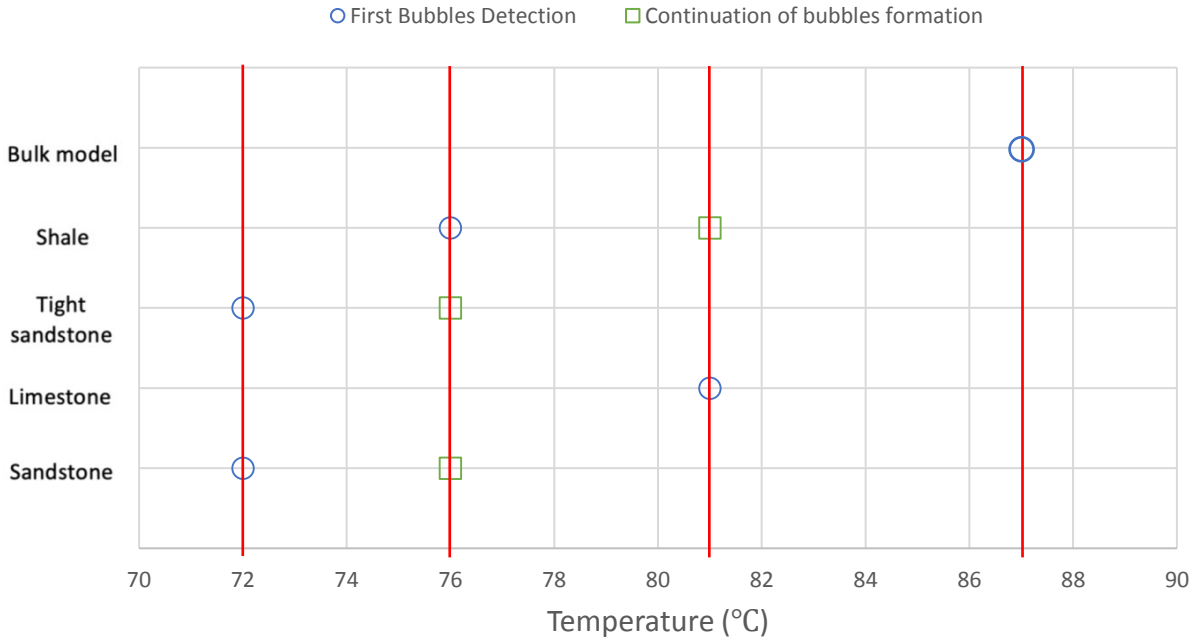

Figure 4-23: Bubble point detection temperatures for water in sandstone, limestone, tight sandstone, shale, and bulk model.

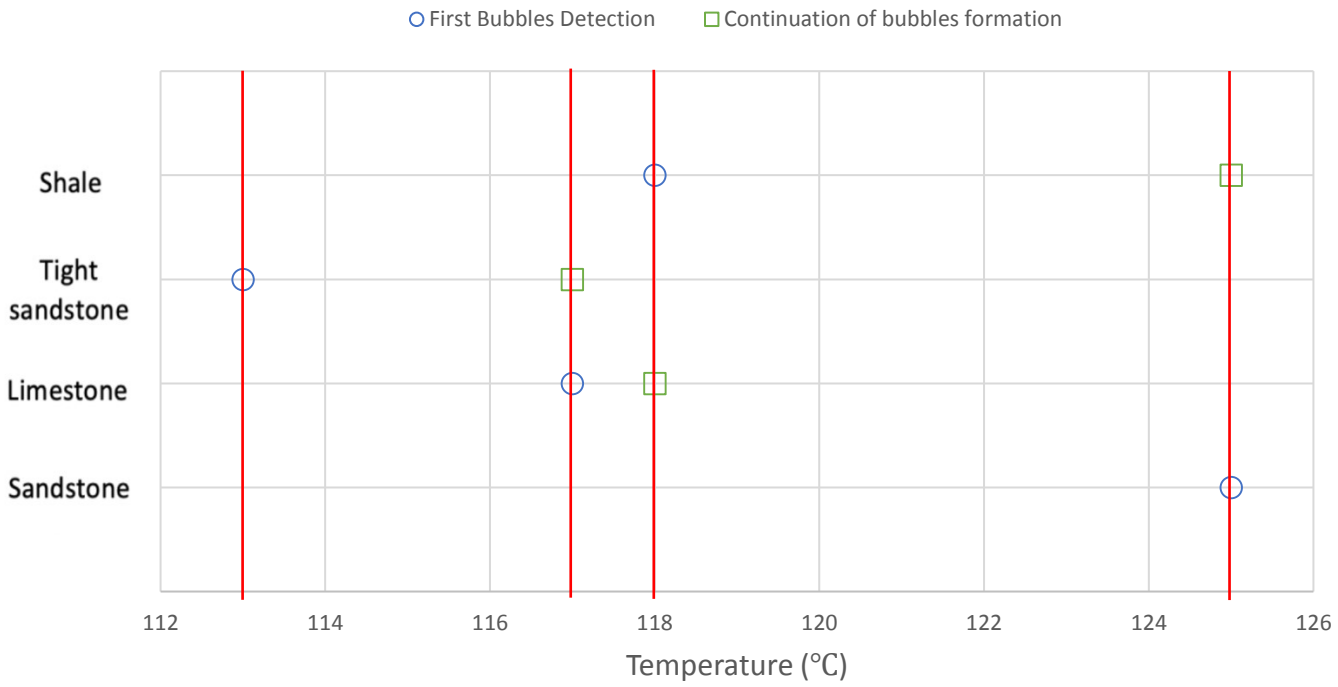

Figure 4-24: Bubble point detection temperatures for decane in sandstone, limestone, tight sandstone, and shale.

4.14 Conclusion and Remarks

By performing the microfluidic and rock sample experiments, boiling temperatures of water and several hydrocarbon solvents were investigated in confined capillary / porous media. Then, the experimental observations were compared with the calculated vaporization temperatures, obtained from the Thomson equation. The conclusions can be listed as follows:

- The microfluidic experiments showed that the boiling temperatures of heptane, heptane-decane mixture, and naphtha decline by 20% (4.3% in kelvin unit) approximately with the reduction of medium size.
- Although the volume percentages of micro ($\leq$ 2 nm) and meso (2 – 50 nm) pores were less than 5% in Berea sandstones and Indiana limestones, the presence of such pores

resulted in early vaporizations of water, heptane, and decane, as observed in Figure 17.

- Due to the considerable volume percentages of extended nanopores ($\leq$ 100 nm) in shale and tight sandstone, noticeable reductions of water, heptane, and decane vaporization temperatures by nearly 18% (3.8% in kelvin unit) were observed.
- At reservoir scale, such reductions of boiling temperature could have a considerable impact on history matching and performance forecasting for oil, gas, and geothermal production, especially in tight reservoirs.

5 Chapter 5: Phase Behavior of Single and Multi-Component Hydrocarbons at Nano-Capillary Scale

A version of this chapter was submitted to a journal for publication.

5.1 Abstract

Phase-alteration phenomenon has a considerable influence on the dynamics and distribution of fluids in porous media. One of the major factors affecting the phase behaviour of fluids in reservoirs is the capillarity effect, which becomes unavoidably significant as the media becomes tighter and contains more pores at nano sizes. Comprehending the nature of vaporization and condensation of hydrocarbon in such confined media is important for accurate modelling of two-phase envelopes and thereby the performance of energy production from hydrocarbon reservoirs. This paper studies the vaporization of single- and multicomponent hydrocarbons in different types of rocks (namely sandstones, limestones, tight sandstones, and shales). The vaporization temperatures were measured experimentally in each rock type and compared with boiling points measured at bulk conditions to investigate the deviation between the phase-change temperatures in capillary media and bulk values. The vaporization temperatures, obtained from the experiments, were also compared with the computed two-phase envelopes, calculated by the classical Peng-Robinson Equation of State.

5.2 Introduction

One of the highly common physical phenomena in hydrocarbon reservoirs, during production or injection stages, is the fluid phase alteration due to the change of regional pressure or temperature. Throughout the production periods, the gradual pressure declines in near-wellbore areas resulting in a vaporization of lighter components over time. Injecting foreign gases in enhanced oil recovery (EOR) applications, for example, leads to a considerable phase alteration of introduced gases in the reservoir, owing to the non-isobaric conditions in the porous media. Such a phenomenon can take place frequently in high-pressure reservoirs.

One common practice in heavy-oil applications is injecting steam into the matrix to reduce oil viscosity thermally and, therefore, enhance its mobility within the capillary system. Because of the massive heat loss, steam tends to lose its heat energy and condense after injection which makes it

higher in density. Generally, the occurrence of vaporization and condensation in the reservoirs is of primary importance since it impacts the dynamical behaviour of fluids, i.e., the distribution and propagation rate of fluids. Another common practice in oil reservoirs is to use liquid or gas solvents with or without thermal assistance. Change in the temperature and pressure during this type of application critically affects the hydrocarbon recovery and retrieval of expensive solvent.

Under such circumstances, it is extremely critical to accurately predict the phase change in the porous matrixes since having a desired phase can have a significant improvement on both the oil recovery and cost. A propane-injection project in tight Bakken reservoirs is a suitable example for cases which the phase of injected fluid plays a major role in achieving an ultimate oil recovery. One of the main objectives of injecting hydrocarbon solvents is reducing the heavy-oil viscosity as soon as the solvents contact the oil. Injecting the solvents in their gaseous forms is restricted by the high capillary resistance within the pores which limits the propagation of gases and contact with the oil. In Bakken reservoirs, propane was selected because of its suitable phase-change pressure that allowed it to be in liquid phase at the reservoir condition as well as it having efficient contact with the oil (Nagarajan et al. 2020).

In simulation studies of the said applications, accurate data entry for the phase behavior of hydrocarbons is critical since it has a considerable impact on the dynamics of the processes and, therefore, oil recovery prediction. Peng and Robinson (1976) developed an equation of state (EoS) model to predict the phase behaviour of pure-component and multicomponent fluids, including other physical properties, such as densities and volumetric behaviours. Earlier, Redlich and Kwong (1948) proposed an equation which linked the variation of pressure with volume and temperature. The equation was, then, modified by Soave (1972) to enhance the accuracy of the previous EOS model (Redlich and Kwong 1948). One of the limitations of the classic Peng Robinson (PR) and Redlich Kwong (RK) cubic EoS is that they do not take the capillary pressure and adsorption effect into account. However, it has recently been showed that neglecting these factors may cause the PR-EoS and RK-EoS to yield inaccurate estimation of phase behavior in confined porous media, especially when consisting of a larger percentage of nanopores (Al-Kindi and Babadagli 2019, 2020a, 2021a).

Several studies were conducted to apply the notion of capillary effect in the original cubic EoS. Travalloni et al. (2013) developed an extended version of PR-EoS which considered the capillarity and pore-molecule effects on the phase behaviour of confined fluids. Nojabaei et al. (2012) included the capillary pressure in vapour-liquid equilibrium (VLE) calculations and then, adopted to PR-EoS to compute the pressure-temperature phase envelopes for a number of binary mixtures. Considering the capillarity effect in the VLE equations led to a reduction in the bubble point pressure and an increase/decrease in the dew point pressure. As the medium becomes tighter, constrained fluids start to get highly affected by the pore wall (molecule-pore interaction), owing to the limited number of molecules (Cui et al. 2018) which results in a heterogeneous fluid distribution (Jin and Firoozabadi 2016). Cui et al. (2018) introduced a modified version of PR-EoS by adjusting the molar volume term based on the fluid reduced mole number, of which is resulted by the adsorption phenomenon.

Comprehending the phase-change behaviour of fluids in porous media is an important aspect to accurately predict fluids' dynamics, phase distribution, and oil/gas recoveries. The issue becomes more critical in tight reservoirs (shale, tight sandstone, etc.) since such rocks are mainly governed by nanopores (Alharthy et al. 2013; Al-Kindi and Babadagli 2020). Shifted phase-alteration temperatures and pressures of fluids become observable once the medium sizes go below 1000 nanometers (nm) as stated by the classical Kelvin equation (Thomson 1872) or 100 nm as reported by Cui et al. (2018).

In previous studies (Al-Kindi and Babadagli 2020a, 2020b), pore size distribution analysis was performed to identify the deviation of pore sizes in shale, tight sandstone, Indiana limestone, and Berea sandstone. The analysis showed that around 4% of the channels in the permeable rocks (sandstone and limestone) were smaller than 100 nm. As a result, shifted vaporization pressures of propane, heptane, and octane were noticed in the permeable rocks, including the tight rocks (shale and tight sandstone) at which a high percentage of their pore diameters are in nanoscale (< 100 nm). This paper is a continuation of our previous works and it investigates the vaporization temperature of pure-component hydrocarbon solvents, binary mixtures, and ternary mixtures in different reservoir rocks and under various pressures. The experimental outcomes are then compared with computed vaporization temperatures obtained by the classical PR-EoS.

5.3 Theoretical Background and Hypothesis

Confined fluids inherit distinctive physical properties different from those existing in bulk conditions (Tsukahara et al. 2012); consequently, the confinement effects tend to alter the phase-change behaviour of constrained fluids (Barsotti et al. 2016; Bao et al. 2017; and Zhong et al. 2018). In bulk conditions, the behaviour of phase transition is mainly governed by molecule-molecule interactions (intermolecular bonds), and the majority of the fluid molecules are not impacted by the adhesion forces, due to the solid-molecule interaction. The ratio of molecule number over the space volume reduces as the medium size tightens. As a consequence, the influence of adhesion forces (pore-molecule interaction) on a large portion of molecules begins to take place and introduces molecule adsorption on the pore wall. This phenomenon contributes in altering the phase-change temperature/pressure of constrained fluids (Travalloni et al. 2013). Moreover, the molecule adsorption in nanopores results in a heterogeneity of fluid density distribution that could be the cause of shifted phase behaviours (Liu et al. 2017). **Figure 5-1** illustrates a schematic representation of molecules' interactions with the pore wall in the bulk and capillary conditions.

The Soave-Redlich-Kwong (SRK) cubic EoS (Soave 1972) was commonly used to model phase behaviour of hydrocarbons, due to simplicity and its ability to perform VLE calculations with practical accuracy. One of the drawbacks of SRK was the lack of precision to predict hydrocarbon liquid densities, which were 7% higher than the experimental values (at reduced temperatures lower than 0.65) and about a 27% error at critical points (Peng and Robinson 1976). Peng and Robinson (1976) introduced alternative cubic EoS which provided more precise values of liquid densities, vapour pressures, and equilibrium ratios. The equation for pure-component fluids is formed as the following:

$$P = \frac{RT}{V_m - b} - \frac{a\,(T)}{V_m(V_m + b) + b(V_m - b)} \tag{1}$$

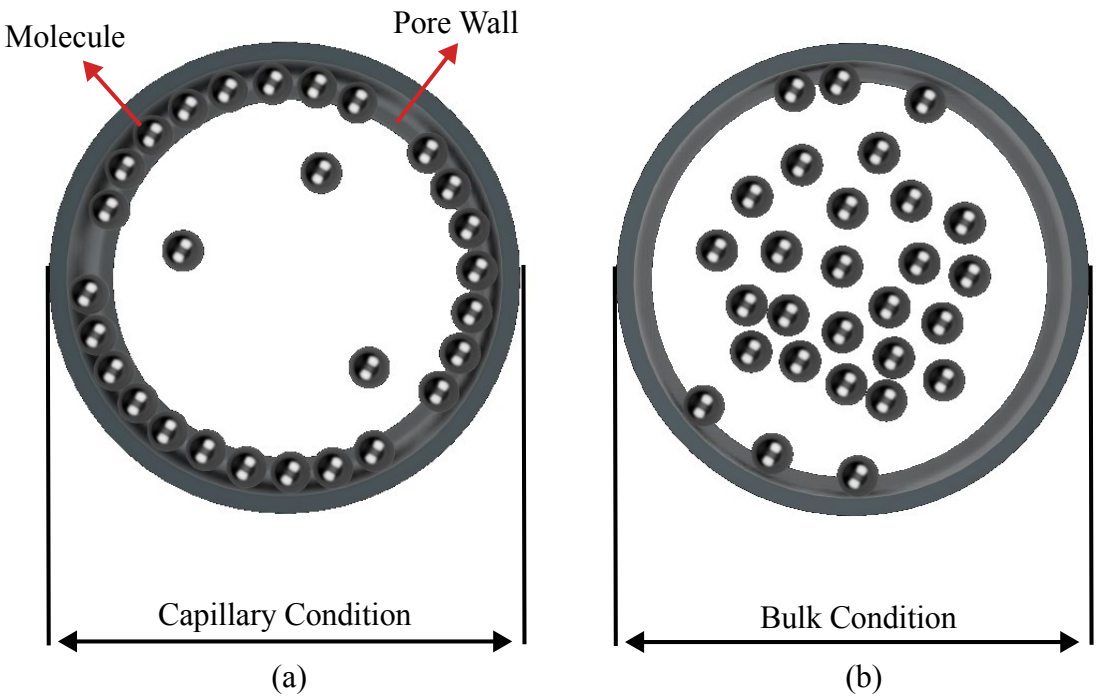

Figure 5-1–(a) Distribution of fluid molecules in a tight pore. Due to the confinement effect, most of the molecules are adsorbed by the inner pore surface; (b) distribution of fluid molecules in a bulk medium with no capillary effect. The minority of the molecules are adsorbed by the solid surface since the cohesion forces (intermolecular forces) are the dominant.

5.4 Problem Statement and Solution Methodology

Phase change of the fluids in the reservoir has a significant control on fluid dynamics in porous media and, therefore, influences the distribution of phases in the reservoir, propagation of reservoir gases and injected solvents, and overall hydrocarbon recoveries. Injecting high-temperature fluids (i.e., steam, hot water), injecting solvents as an additive to steam (Gupta et al. 2004; Al-Bahlani and Babadagli 2011), or during reservoir pressure depletion, vaporization or condensation of contacted reservoir and injected fluids continuously occurs throughout the production or injection stages. Tight reservoir rocks are mainly characterized with extended tightness, introducing a significant capillary effect on the phase behaviour. Hence, understanding thoroughly the impact of capillarity on the nature of phase transformation is essential to achieve accurate modeling of fluid

properties and conduct precise VLE calculations for confined fluids in tight reservoirs. Standard cubic EoS's do not consider the effect of confinement on the phase change which leads them not to be suitable candidates for achieving precise VLE calculations for confined fluids in tight media. Besides the improved accuracy of phase dynamic predications, modelling the phase behaviour precisely in reservoir rocks is critical in high-temperature EOR applications (i.e., steam injection) to estimate the right temperatures for attaining optimum hydrocarbon recoveries. For instance, knowing the right temperature of the injected steam/hot water in Solvent-Over-Steam Injection in a Fractured Reservoir (SOS-FR) is important to reach the optimal recovery of injected solvents (Al-Bahlani and Babadagli 2011). The correct estimation of temperature is beneficial in reducing the operational cost by eliminating the need for excessive heat energy. Pore size distribution analysis (PSDA) was conducted previously in our prior works (Al-Kindi and Babadagli 2020a and 2020b) to experimentally measure the deviation of pore sizes in several reservoir rocks. The studies showed around 4.5% of the pore volume in permeable rocks (Berea sandstone and Indiana limestone), despite their relatively high permeabilities. The existence of nanopores could result in shifted vapour pressures or boiling temperatures in the permeable rocks, although the volume percentage of confined pores (< 1000 nm) is considerably minor.

This paper investigates the influence of confinement on vaporization temperatures of hydrocarbon pure liquids, binary mixtures, and ternary mixtures in tight reservoir rocks (shale and tight sandstone) and permeable reservoir rocks (Berea sandstone and Indiana limestone). The single-component solvents (heptane and octane) represented the injected hydrocarbon solvents in cold solvent injection or thermal EOR application at which solvents are used as additives to steam. The binary mixture (pentane-heptane) represented a non-complex light oil; meanwhile, the ternary mixture acted as a heavier oil with a slightly more complexity in terms of components, comparing with the binary mixture. The shifted boiling temperatures were measured under three main pressures: (a) atmospheric pressure (1 atm, 14.7 psi); (b) 64.7 psi; (c) 114.7 psi. A special high-pressure-high-temperature (HPHT) windowed cell was used to perform the analysis and kept in a constant-temperature oven to control the temperature of the windowed cell and, specifically, the rocks in the cell. At vaporization temperatures, the generated vapour bubbles were detected using a video camera, featured with a magnification system which provided a clear visualization of the micro vapour bubbles on the outer rock sample. The shifted boiling temperatures were compared

with computed vaporization temperatures by PR-EoS, and deviation percentages were calculated between the measured values from the experiments and computed values from the cubic EoS.

5.5 Experimental Design and Methodology

The HPHT cell shown in **Figure 5-2** was pressurized at constant pressures by an inert gas. Nitrogen was selected as the pressurizing gas since it is chemically inactive with the fluids inside the cell at the condition of our experiments, and it is generally one of the major pre-existing gases in oil and gas reservoirs. The applicable pressure range was 14.7–114.7 psi based on the maximum design temperature of the windowed cell, which was 260℃ (533.15 K). Going beyond 114.7 psi would require us to exceed the maximum design temperature in order to approach the bulk phase-change temperatures of the used solvents.

The pressure of the system was controlled by a syringe pump, featured with a standard pressure accuracy of 99.5%. The overall cell temperature was raised gradually from the room temperature (21℃) to the bulk boiling temperature of the tested solvent, either a pure-component liquid or mixture, by using the constant-temperature oven. In all the experiments, temperatures were increased with a heating rate of 0.05℃/sec. Before initiating the trials, selected rocks were vacuumed at 12 psi (below atmospheric pressure) to thoroughly remove the trapped air. Then, they were saturated with the hydrocarbon solvents for at least 24 hours to insure a complete saturation in each rock sample. One of the critical points in the investigation is to guarantee a uniform distribution of heat around the rock. To do so, the rock samples were immersed in a glycerol bath which acted as a heating liquid. Glycerol, as a water-soluble liquid, is not soluble in non-polar hydrocarbon solvents; hence, such a chemical property would prevent the tested solvents to mix with glycerol, forming a solution.

Figure 5-2 illustrates schematically the experimental setup used to study the phase behaviour of hydrocarbon solvents in reservoir rocks. By using a data acquisition system, the pressure and temperature of HPHT cell, including the rocks, were recorded every second with the assistance of an immersion thermocouple and a pressure transducer. The low heating rate (0.05℃/sec) was

chosen to prevent any temperature difference between the heating liquid (glycerol) and rock sample during the heating process. Thus, the temperature of glycerol was recorded continuously along with the pressure. At vaporization stages, the formed vapour phase was detected by a video camera to capture the formation of gas bubbles on the rock surface.

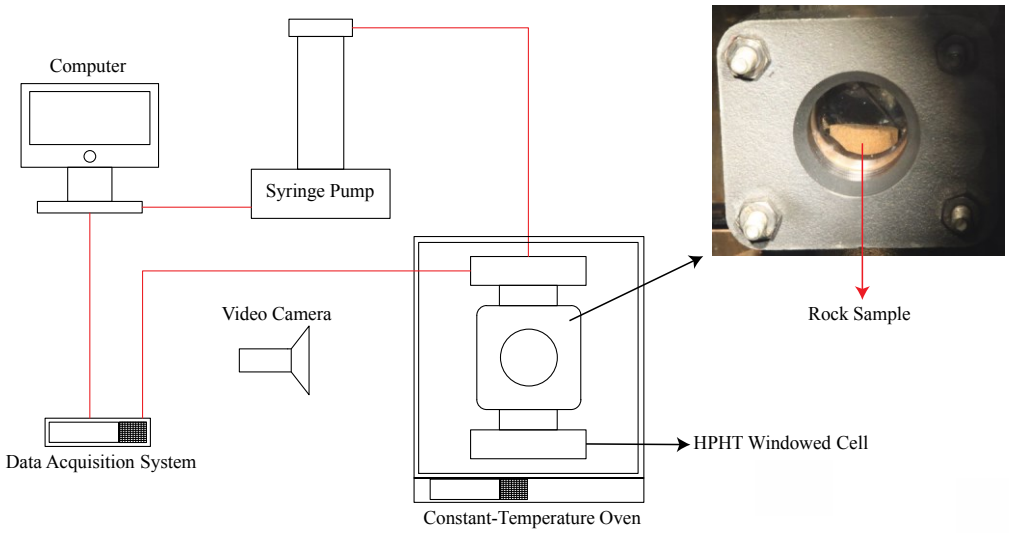

Figure 5-2: A schematic of the experimental system utilized for solvent vaporization temperature measurement. The rock sample was immersed in glycerol which acted as a heating liquid. The thermocouple was also immersed in glycerol to measure its temperature continuously.

5.6 Pore Size Distribution Analysis (PSDA)

In our previous studies (Al-Kindi and Babadagli 2020a and 2020b), PSDA was performed to measure deviation of pore sizes in Berea sandstone, Indiana limestone, tight sandstone, and shale. The study showed several measured parameters including occupation percentage of pores tighter than 1000 nm in each rock. The analysis of pore size distribution was done by quantifying the nitrogen desorption and adsorption on the rock surface. **Table 5-1** presents volume percentages of nanopores (< 1000 nm), permeability, density in sandstone, limestone, tight sandstone, and shale.

Table 5-1: Permeability, density, and pore volume percentages in various tested reservoir rocks (Al-Kindi and Babadagli 2020a).

Rock type	Permeability (md)	Density (kg m^{-3})	Volume percentage of pores tighter than 1000 nm (%)
Berea sandstone	274	2129	4.4
Indiana limestone	30	2246	4.6
Tight sandstone	0.1	2400	38.2
Shale	< 0.01	2200	94.3

The high-permeability rocks (sandstone and limestone) mainly consist of macropores and nearly 95.5% of the pores are larger than 1000 nm, according to the PSDA. Based on the literature, the phase behaviour of fluids inside the majority of the pores in the permeable rocks could be possibly predicted by the classical PR-EoS since the capillary effect would not be sufficient to cause any alteration to boiling temperatures. Nonetheless, fluids in confined pores, which act as minority in sandstone and limestone, would behave differently in terms of phase alteration due to high capillary pressures and adsorption effects. Also, the shifted boiling temperatures would not be modelled accurately by conventional cubic EoS, such as PR-EoS and RK-EoS. In tight matrixes (shale and tight sandstone), modelling the phase-change behaviour of hydrocarbons is extremely critical since confined pores (< 1000 nm) occupy the tight rocks at considerable percentages.

5.7 Experimental Results

Owing to the heterogeneous nature of reservoir rocks, the motion of vapour phase inside the rock porous medium would slightly change in every trial, meaning that the temperature at which the generated bubble would appear on the rock surface could marginally vary. Therefore, experiments were repeated more than once to obtain representative values by averaging the measured boiling

temperatures. The experimental values of phase-change temperatures at various pressures in bulk conditions were considered in the analysis as shown in **Figures 5-4**, **5-5**, **5-6**, and **5-7**. The values for bulk conditions were obtained from literature or other sources (catalogs etx.) and highly comparable values were observed between the PR-EoS and bulk measurement of vaporization temperatures as seen in these plots. The measured phase-change temperatures of solvents in the reservoir rocks were different from the bulk measurement and calculated values from PR-EoS.

The investigation was initiated by studying the vaporization behaviour of single-component solvents (heptane and octane). Then, the study focused on more complicated mixtures with binary and ternary hydrocarbon components. The mass fraction of the binary mixture was 50% for each component. For the ternary mixture, the mass fraction was $\frac{100}{3}$% for each component. **Figure 5-3** shows the generation of vapour phase of pure-component solvents and hydrocarbon mixtures in different reservoir rock types and pressures. **Table 5-2** presents the measured solvent boiling temperature in each rock, at each selected pressure, and the deviation percentage (ΔT_B%) between the temperatures obtained from the experiments and those measured in bulk conditions, given as follows:

$$\Delta T_B\% = \left|\frac{T_B - T_{exp}}{T_B}\right| \times 100 \qquad (2)$$

where T_B is the boiling point of solvent at bulk condition, and T_{exp} is the experimental vaporization temperature in the rock. With pure hydrocarbon solvents (heptane and octane), the deviation percentages were observed to be varying from 4.4 (1.6% in Kelvin unit) to 19.7% (5.2% in Kelvin unit), due to the existence of confined pores in the reservoir rocks. Meanwhile, with hydrocarbon mixtures, the deviation percentages were observed to be varying from 1.4 (0.4% in Kelvin unit) to 27.6% (5.3% in Kelvin unit).

Table 5-2: Shifted vaporization temperatures of several hydrocarbon liquids in different reservoir rocks and at various surrounding pressures (14.7, 64.7, and 114.7 psi). The bulk vaporization temperatures were obtained from a phase-change experimental analysis at bulk conditions.

Heptane (C_7H_{16}) – 14.7 psi			
Rock Type	Experimental Vaporization Temperature (°C)	Bulk Vaporization Temperature (°C)	Deviation Percentage (%)
Berea sandstone	83	98.4	15.6
Indiana Limestone	81	98.4	17.6
Tight sandstone	79	98.4	19.7
Heptane (C_7H_{16}) – 64.7 psi			
Berea sandstone	137	158	13.2
Indiana Limestone	135	158	14.5
Tight sandstone	151	158	4.4
Shale	133	158	15.8
Heptane (C_7H_{16}) – 114.7 psi			
Berea sandstone	172	189	8.9
Indiana Limestone	171	189	9.5
Tight sandstone	170	189	10
Shale	179	189	5.2
Octane (C_8H_{18}) – 14.7 psi			
Berea sandstone	103	125.6	17.9

Indiana Limestone	108	125.6	14
Tight sandstone	108	125.6	14
Octane (C_8H_{18}) – 64.7 psi			
Berea sandstone	176	192	8.3
Indiana Limestone	163	192	15.1
Tight sandstone	174	192	9.3
Shale	181	192	5.7
Pentane-heptane mixture – 14.7 psi			
Berea sandstone	59	55	7.2
Indiana Limestone	62	55	12.7
Tight sandstone	65	55	18.1
Shale	47	55	14.5
Pentane-heptane mixture – 64.7 psi			
Berea sandstone	103	113	8.8
Indiana Limestone	104	113	7.9
Tight sandstone	108	113	4.4
Shale	101	113	10.6
Pentane-heptane mixture – 114.7 psi			
Berea sandstone	132	140	5.7
Indiana Limestone	116	140	17.1

Tight sandstone	134	140	4.2
Shale	138	140	1.4
Pentane-heptane-octane mixture – 14.7 psi			
Berea sandstone	61	65	6.1
Indiana Limestone	74	65	13.8
Tight sandstone	83	65	27.6
Shale	72	65	10.7
Pentane-heptane-octane mixture – 64.7 psi			
Berea sandstone	140	132	6
Indiana Limestone	118	132	10.6
Tight sandstone	121	132	8.3
Shale	127	132	3.7

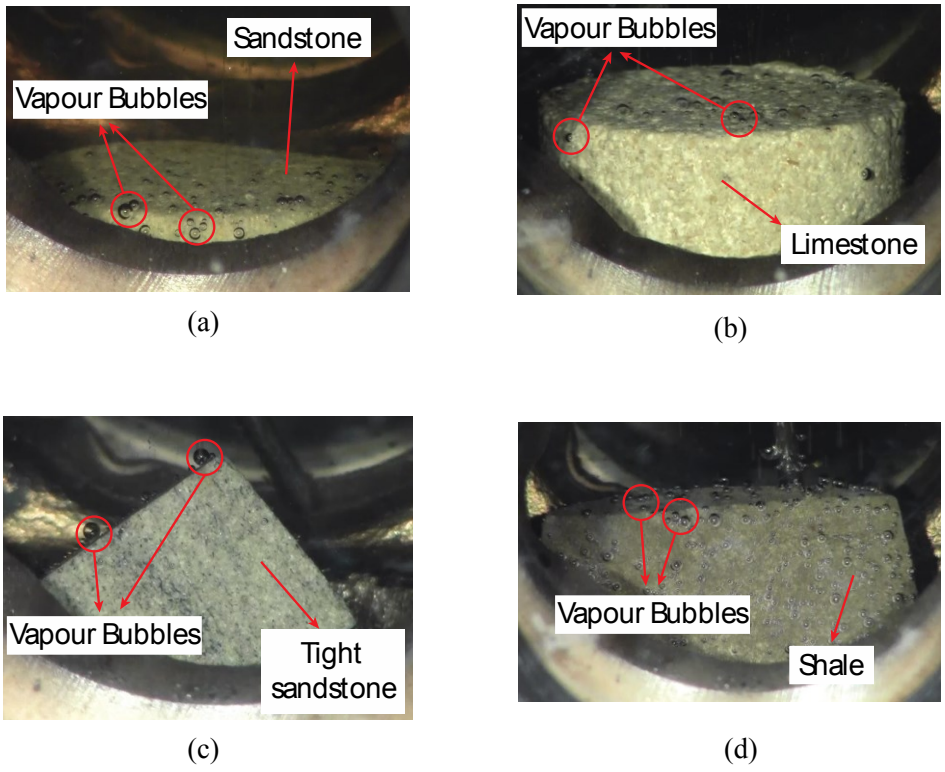

Figure 5-3–(a) Vaporization of pure heptane in sandstone at 137 ℃ and 64.7 psi; (b) vaporization of pure octane in limestone at 163℃ and 64.7 psi; (c) vaporization of pentane-heptane mixture in tight sandstone at 134℃ and 114.7 psi; (d) vaporization of pentane-heptane-octane mixture in shale at 127℃ and 64.7 psi.

5.8 Quantitative Analysis

The PR-EoS was used to model two-phase envelopes for the single-component and multicomponent hydrocarbon solvents. The two-phase envelopes were generated by the assistant of Computer Modelling Group (CMG) software. The selected ranges of temperature and pressure for the phase envelope calculations were 0℃ (273.15 K) - 250℃ (523.15 K) and 0 psi (0 bar) - 200 psi (13.7 bar). The measured phase-change temperatures in the rocks were then compared with those computed by the cubic EoS. For mixtures, the measured temperatures were compared with the bubble point temperatures calculated by the PR-EoS. For each trial, the deviation percentage

($\Delta T_v\%$) between the shifted temperature values and calculated values from the PR-EoS was obtained, and it was expressed as following:

$$\Delta T_v\% = \left|\frac{T_v - T_{exp}}{T_v}\right| \times 100 \quad (3)$$

in which T_v is the computed bubble point temperature by the PR-EoS at the given pressure, and T_{exp} is the measured vaporization temperature in the rock. **Table 5-3** presents the measured solvent boiling temperature in each rock, at various surrounding pressures, and the deviation percentage ($\Delta T_v\%$) between the temperatures obtained from the experiments and those modelled by the PR-EoS.

Figure 5-4 and **5-5** show the measured vaporization temperatures of heptane and octane, respectively, as pure-component solvents in sandstone, limestone, tight sandstone, and shale. Figs. 6 and 7 display the measured vaporization temperatures of pentane-heptane mixture and pentane-heptane-octane mixture in sandstone, limestone, tight sandstone, and shale, respectively. Furthermore, they present the computed two-phase envelopes of the tested solvents using the classical PR-EoS, including the bulk boiling temperatures of each solvent which were measured experimentally at bulk conditions with no capillary effects. Owing to the capillary effect in the rocks, the deviation percentages between the measured and calculated phase-change temperatures were ranging from 4.4 (1.6% in Kelvin unit) to 19.3% (5.1% in Kelvin unit) with pure solvents (heptane and octane). Whereas, with multicomponent solvents, the deviation percentages were ranging from 2.1 (0.7% in Kelvin unit) to 25.7% (5% in Kelvin unit).

Table 5-3: Shifted vaporization temperatures of several hydrocarbon liquids in different reservoir rocks and at various surrounding pressures (14.7, 64.7, and 114.7 psi). The calculated vaporization/bubble point temperatures were obtained from the PR-EoS.

Heptane (C_7H_{16}) – 14.7 psi			
Rock Type	Experimental Vaporization Temperature (°C)	Computed Vaporization\Bubble Point Temperature (°C)	Deviation Percentage (%)
Berea sandstone	83	98	15.3
Indiana Limestone	81	98	17.3
Tight sandstone	79	98	19.3
Heptane (C_7H_{16}) – 64.7 psi			
Berea sandstone	137	158	13.2
Indiana Limestone	135	158	14.5
Tight sandstone	151	158	4.4
Shale	133	158	15.8
Heptane (C_7H_{16}) – 114.7 psi			

Berea sandstone	172	188	8.5
Indiana Limestone	171	188	9
Tight sandstone	170	188	9.5
Shale	179	188	4.7
Octane (C_8H_{18}) – 14.7 psi			
Berea sandstone	103	126	18.2
Indiana Limestone	108	126	14.2
Tight sandstone	108	126	14.2
Octane (C_8H_{18}) – 64.7 psi			
Berea sandstone	176	188	6.3
Indiana Limestone	163	188	13.2
Tight sandstone	174	188	7.4
Shale	181	188	3.7
Pentane-heptane mixture – 14.7 psi			

Berea sandstone	59	56	5.3
Indiana Limestone	62	56	10.7
Tight sandstone	65	56	16
Shale	47	56	16
Pentane-heptane mixture – 64.7 psi			
Berea sandstone	103	114	9.6
Indiana Limestone	104	114	8.7
Tight sandstone	108	114	5.2
Shale	101	114	11.4
Pentane-heptane mixture – 114.7 psi			
Berea sandstone	132	141	6.3
Indiana Limestone	116	141	17.7
Tight sandstone	134	141	4.9
Shale	138	141	2.1
Pentane-heptane-octane mixture – 14.7 psi			

Berea sandstone	61	66	7.5
Indiana Limestone	74	66	12.1
Tight sandstone	83	66	25.7
Shale	72	66	9
Pentane-heptane-octane mixture – 64.7 psi			
Berea sandstone	140	130	7.6
Indiana Limestone	118	130	9.2
Tight sandstone	121	130	6.9
Shale	127	130	2.3

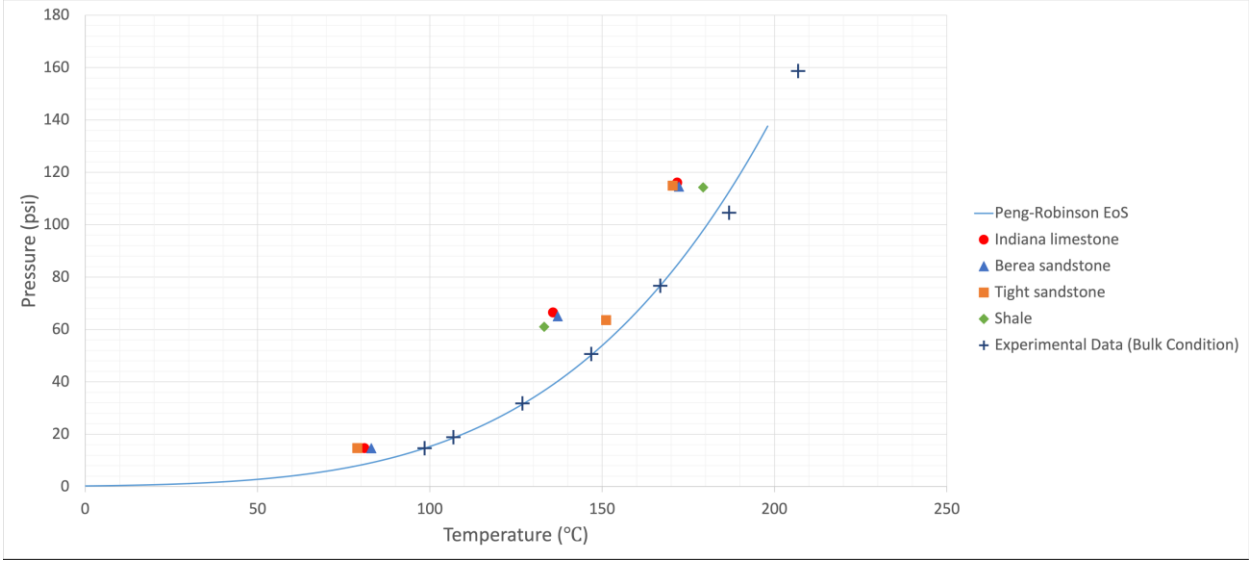

Figure 5-4: Measured vaporization temperatures of heptane in various rocks and computed phase-change temperatures obtained from the PR-EoS at different pressures. The experimental data were obtained from the phase-change measurement at bulk conditions.

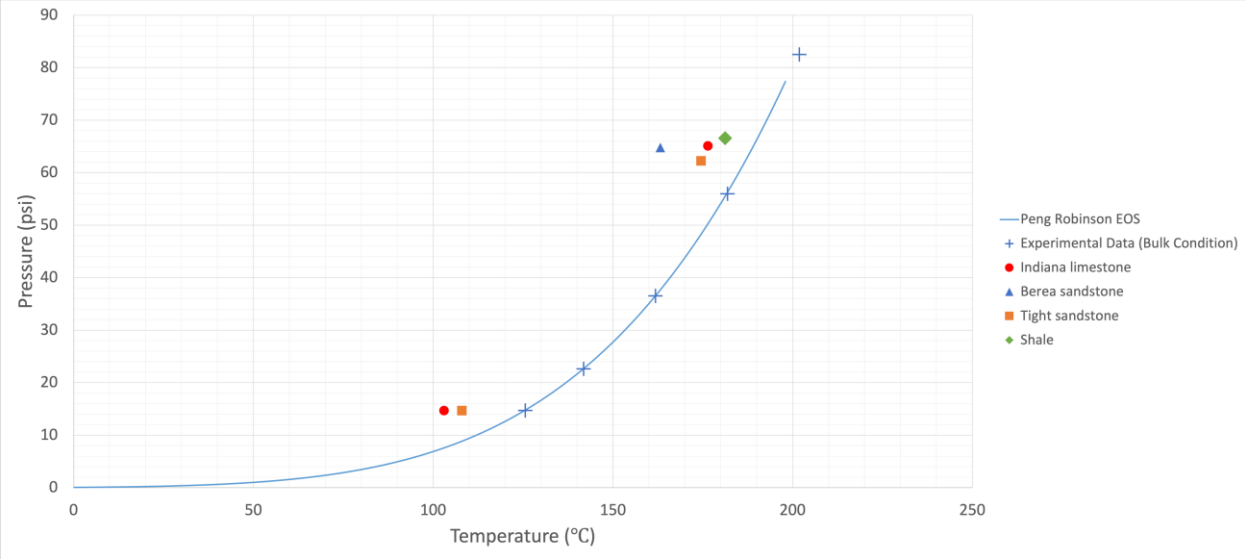

Figure 5-5: Measured vaporization temperatures of octane in various rocks and computed phase-change temperatures obtained from the PR-EoS at different pressures. The experimental data were obtained from the phase-change measurement at bulk conditions.

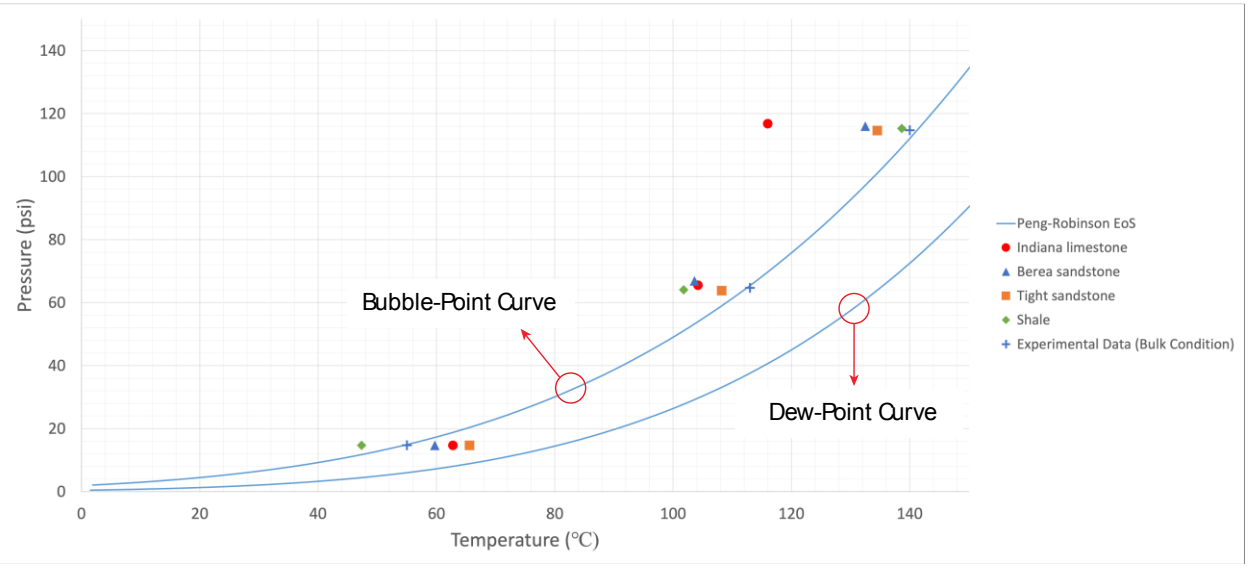

Figure 5-6: Measured vaporization temperatures of pentane-heptane mixture in various rocks and computed bubble-point/dew-point temperatures obtained from the PR-EoS at different pressures. The experimental data were obtained from the phase-change measurement at bulk conditions.

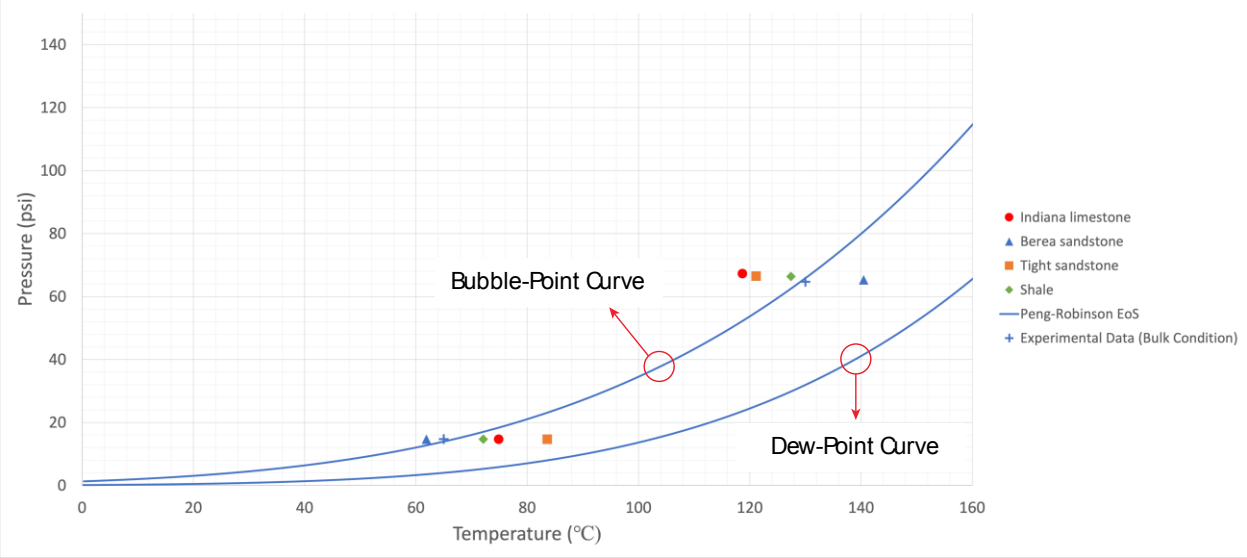

Figure 5-7: Measured vaporization temperatures of pentane-heptane-octane mixture in various rocks and computed bubble-point/dew-point temperatures obtained from the PR-EoS at different pressures. The experimental data were obtained from the phase-change measurement at bulk conditions.

5.9 Discussion

Figure 5-8, **5-9**, **5-10**, and **5-11** illustrate the deviation of experimentally measured vaporization temperatures in the rocks from the bulk measurements of heptane, octane, binary mixture (pentane-heptane), and ternary mixture (pentane-heptane-octane). With pure-component solvents (Figure 8 and 9), the shift of measured vaporization temperatures from the bulk measurements was observed at all selected pressures and rock types. Systematically, the temperature required for a given pressure to start the boiling is lower than that of bulk conditions with no exception. Meanwhile, with binary and ternary mixtures, relatively minor deviations were detected at the atmospheric pressure (Figure 10 and 11). As the pressure increased, the difference between the measured and bulk values increased. The temperatures required for boiling was observed to be lower than the bulk condition at higher pressures (Figure 10 and 11) as similar to the single component cases (Figure 8 and 9).

The capillary characteristics of the rocks such as permeability, pore texture, wettability, and clay content may also play a role in the boiling process. All these parameters affect the phase distribution and entrapment of generated gas, which eventually results in different phase behavior in multi-component systems. In situations where a single-component solvent exists, at the phase-change stage, a large percentage of the vapour phase does not get interrupted or trapped by the liquid phase from the same fluid (Al-Kindi and Babadagli 2021b). This phenomenon explains the cause of noticeable temperature deviations of pure solvents from their normal boiling points (Figure 8 and 9). On the other hand, with multicomponent solvents, the liquid phase of heavier components with higher boiling temperatures restricts the movement of the vapour phase of lighter components as observed in our previous study (Al-Kindi and Babadagli 2021b) in silicate glass microfluidic chips. The delay of vapour bubbles to appear on the rock surface results in reduction of the temperature deviations specifically at the atmospheric pressure. Hence, the impact of rock -interfacial- properties is more pronounced in case of multi-component systems, and this requires further research.

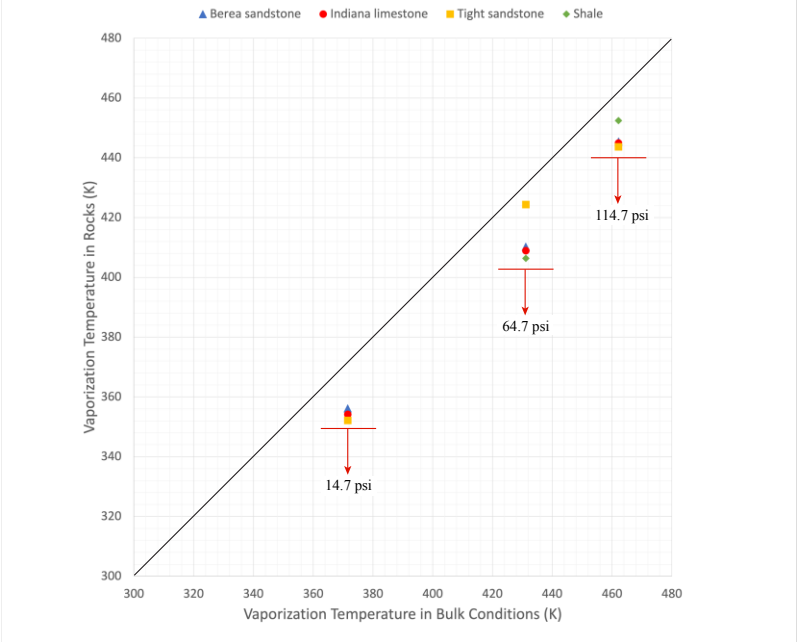

Figure 5-8: Deviation of measured vaporization temperatures of heptane from bulk measurements.

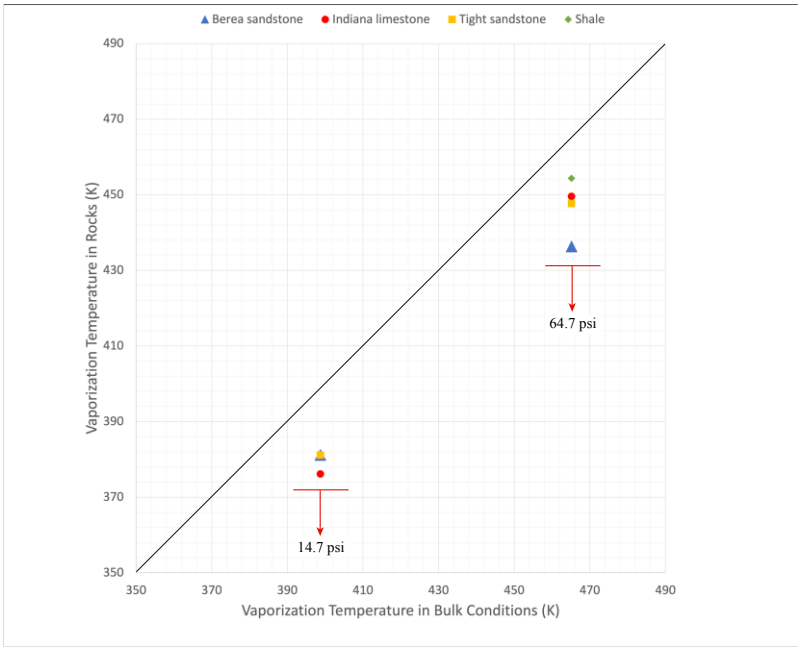

Figure 5-9: Deviation of measured vaporization temperatures of octane from bulk measurements.

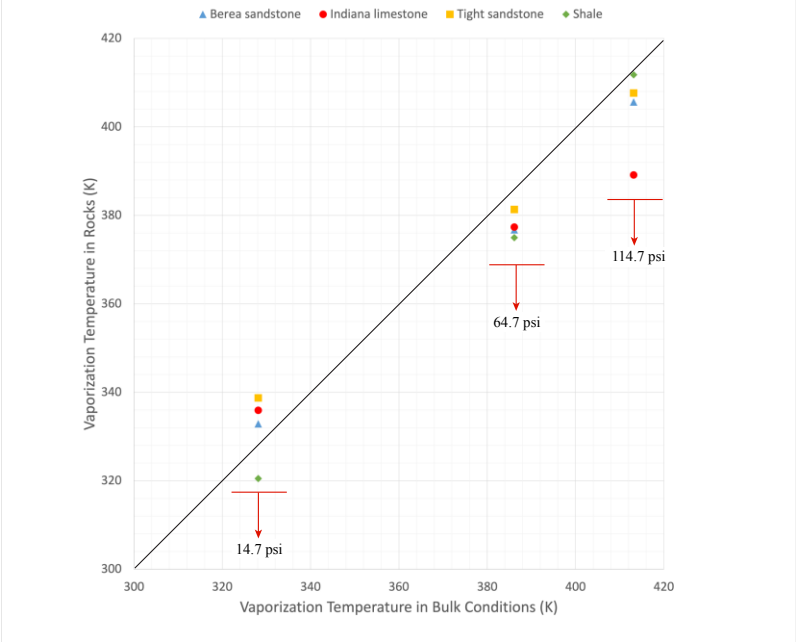

Figure 5-10: Deviation of measured vaporization temperatures of pentane-heptane mixture from bulk measurements.

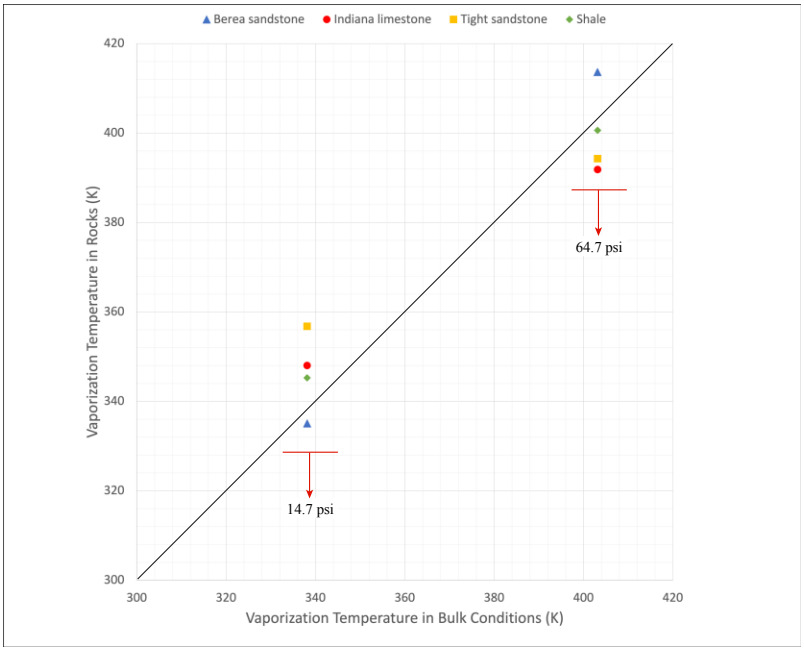

Figure 5-11: Deviation of measured vaporization temperatures of pentane-heptane-octane mixture from bulk measurements.

5.10 Conclusions

Understanding the phase behaviour in reservoir rocks is essential to achieve precise predictions of fluids' dynamics and distributions in the porous media. The impact of confinement effect on vaporization and condensation behaviors becomes more pronounced in tight reservoirs, such as shale and tight sandstone matrixes. The existence of nanopores in permeable rocks (Berea sandstone and Indiana limestone) could also result in shifted phase-change temperatures, as observed in Table 5-2 and Figure 5-4, 5-5, 5-6, and 5-7. The deviation percentages of measured vaporization temperatures in all the rock samples from the bulk measurements ranged from 4.4% (1.6% in Kelvin unit) to 19.7% (5.2% in Kelvin unit) with single-component solvents and 1.4% (0.4% in Kelvin unit) to 27.6% (5.3% in Kelvin unit) with the hydrocarbon mixtures. The shifted phase-change temperatures were also compared with the modelled two-phase envelopes by the original version of PR-EoS, as observed in Table 5-3 and Figure 4, 5, 6 and 7. The deviation percentages of measured vaporization temperatures from the computed values were at least 4.4% (1.6% in Kelvin unit) with single-component solvents and 2.1% (0.7% in Kelvin unit) with the hydrocarbon mixtures.

The aim of this paper was to show how the phase behavior of hydrocarbon mixtures in real reservoir rocks (capillary -confined- media) deviate from the bulk conditions. This was achieved through an experimental study. Our future study will focus on the modification of the original version PR-EoS to make it more applicable in modelling the phase-change behaviour in confined porous media. The experimental data provided in this work would be useful in the validation of such analytical/computational models.

5.11 Nomenclature

PR-EoS: Peng Robinson Equation-of-State

EOR: Enhanced Oil Recovery

PR: Peng Robinson

RK: Redlich Kwong

VLE: Vapour-Liquid Equilibrium

R: universal gas constant

T: temperature

$a\ (T)$: attraction parameter

V_m: molar volume

b: van der Waals co-volume

Z: compressibility factor

A, B: constants

P: pressure

PSDA: Pore Size Distribution Analysis

HPHT: High-Pressure-High-Temperature

K: Kelvin

℃: Degree Celsius

Sec: second

Psi: pound per square inch

$\Delta T_B\%$ and $\Delta T_v\%$: deviation percentages

T_B: boiling point of solvent at bulk condition

T_{exp}: experimental vaporization temperature in the rock

T_v: computed bubble point temperature by the PR-EoS

%: percentage

C: carbon atom

H: hydrogen atom

C_7H_{16}: heptane

C_8H_{18}: octane

SOS-FR: Solvent-Over-Steam Injection in Fractured Reservoirs

6 Chapter 6: Effect of Wettability on Vaporization of Hydrocarbon Solvents in Nano Capillaries

A version of this chapter was presented and published as a conference paper at the SPE Annual Technical Conference and Exhibition held in Denver, Colorado, 5-7 October 2020 (SPE-201258-MS). Additionally, an updated version was submitted to a journal for publication.

6.1 Abstract

Tight rock reservoirs have gained popularity and become a subject of great interest due to their huge recovery potential. A substantial portion of the potential hydrocarbon could be removed from the reservoir by injecting solvent gases (hydrocarbon or CO_2) as an Enhanced Oil Recovery (EOR) application. Achieving a precise modeling of these processes and an accurate description of hydrocarbon dynamics requires a clear understanding of phase-change behaviour in a confined (capillary) medium. It was previously shown that early vaporization of liquids could occur in channels that were larger than 1000 nanometers. The surface wettability plays a critical role in influencing the vaporization and condensation nature in confined systems. This paper studies the influence of the medium wettability on phase-transition temperatures of liquid hydrocarbons in macro (> 1000 nm) and nano (< 500 nm) channels by using different types of rock samples. The boiling temperature of hydrocarbon solvents was measured in two extreme wetting conditions: (1) strongly water wet, and (2) strongly oil wet. Boiling temperatures of heptane and octane in sandstone, limestone, and tight sandstone were observed to be lower than their bulk boiling points by closely 13% (4% in Kelvin unit), on average. Altering rock wettability characteristically changes the average hydrocarbon nucleation temperatures being as critical as the pore size. The experimental outcomes also showed that reducing the solvent adsorption on clays in Berea sandstone lowers the nucleation temperature of heptane and octane from their normal phase-change temperatures by 30% (6.5% in Kelvin unit).

6.2 Introduction

Phase changes of the injected fluid, reservoir oil/gas, and their mixture inevitably occur during conventional and unconventional EOR processes. One particular example is gas injection in which phase interaction (or behavior) occurs under non-isobaric conditions (Firoozabadi 1999; Yortsos and Stubos 2001). Phase change is observed in heavy-oil applications due to the non-isothermal nature of the process when steam is used. When solvent is included as part of the thermal applications (Al-Bahlani and Babadagli 2011; Pathak et al. 2012; Naderi and Babadagli 2014; Leyva-Gomez and Babadagli 2016) the phase behavior of reservoir fluids become more pronounced.

The phase behavior is more complex during unconventional EOR as the capillarity effects start playing a critical role due to the smaller pore sizes (at the nano-scale) of the tight rock matrices (Alharthy et al. 2013a; Barsotti et al. 2016; Wang et al. 2016; Luo et al. 2018). Recently, Al-Kindi and Babadagli (2017, 2018, 2019a, 2019b) showed through experiments on both the visual and rock models the effect of capillarity on the phase behavior of hydrocarbon solvents at larger pores (>1000nm). Then, theoretically proposed a modification for the Thomson equation to compute boiling points in pores larger than 1000nm. Factors other than the pore size potentially controlling the phase behavior in a confined (capillary) medium are the interfacial characteristics such as interfacial tension and wettability (Thomson 1872; Hamada et al. 2007).

Typically, injecting foreign fluids into reservoirs with higher pressures leads the injected gases to condense, depending on their saturation pressures. The phenomenon has a significant effect in sole-solvent injection, since the existence of solvents in liquid phases slows the solvent diffusion into the heavy oil (Mohammed and Babadagli 2020). Similarly, in Thermal Enhanced Oil Recovery (TEOR) applications, the injected steam condenses in the rock matrix with time, because of the heat loss caused by the temperature difference between steam and reservoir rocks. Moreover, introducing steam into the reservoir results in vaporizations of light hydrocarbon components which alters their flow dynamics within the porous media. Along with pressure-volume-temperature (PVT) laboratory studies, equation-of-state (EOS) conventional models are used to mathematically model the phase-change behaviour of fluids in reservoir, based on pressure and temperature variations.

Ideal gas equation, van der Waals EOS, Soave-Redlich-Kwong EOS, and Peng-Robinson EOSs are some of the well-known models to predict the phase behaviour of vapor and liquid in the reservoirs (Fanchi 2020). Confined matrices affect thermodynamically the physical properties of existing fluids in the porous media, which alter their vaporization and condensation behaviors. The phenomenon was firstly explained by William Thomson (1872), done by quantifying the effect of a curved liquid surface on the vapor pressure of the same liquid. Thomson's equation has described the relationship between capillary tube size and vapor pressure; the change of saturated vapor pressure decreases or increases, depending on the vapor/liquid contact surface behaviour if the contact is concave or convex (Thomson 1872).

The vaporization and condensation behaviour of confined fluids in extended tight spaces have caught a great deal of attention recently due to their importance in PVT and phase-change modelling. Zhong et al. (2017, 2018) studied experimentally the condensation of propane in nanochannels smaller than 100 nanometers. Pathak et al. (2017) inspected the saturation pressure of a hydrocarbon mixture (decane and methane) in mesopores (< 50 nm). Alfi et al. (2017) investigated the bubble point temperature of hydrocarbon solvents (pentane, hexane, and heptane) in 10, 50, and 100 nm pores.

Several theoretical studies were done to model the phase behaviour of confined hydrocarbons. Jin (2018) used engineering density functional theory and canonical Monte Carlo to analyse bubble and dew points of hydrocarbons in nanopores. The conventional EOS models do not consider the confinement effect on fluids' phase behaviors (Cui et al. 2018; Al-Kindi and Babadagli 2021a). Additionally, they do not account for the high pressure differences at vapor-liquid interfaces in micro (< 2 nm) and meso (2 – 50 nm) pores. Adsorption has a noticeable influence on phase transformation of fluids in capillary conditions especially in porous media tighter than 100 nm. In this work, we have studied the vaporization behaviour of heptane and octane in Berea sandstone, Indiana limestone, and tight sandstone. To inspect the impact of pore wettability on phase-transition temperatures, the wettability of Berea sandstone was chemically altered from water-wet to oil-wet using a siliconizing fluid. Due to the existence of kaolinite, illite, and chlorite, water and hydrocarbon-solvent adsorptions naturally take place in Berea sandstone, which affect the phase-transition behaviour of liquids in nanopores. Such phenomenon was analysed by measuring nucleation temperatures of heptane and octane in fired Berea sandstone with inactive clay content. Nitrogen adsorption tests were performed to quantify the adsorbed volume of nitrogen in Berea sandstone with and without active clay content. Similar tests were also done to observe the effect of wettability alteration on the nitrogen adsorption in sandstone.

6.3 Statement of the Problem and Objectives

Achieving an accurate modeling of phase behaviour in nano-porous media is critical in simulating the performance of steam flooding and miscible gas (CO_2, gas hydrocarbons) injection. Furthermore, considering the confinement effect in the phase-change modeling leads to a more precise modeling of fluid dynamics in the reservoir since vaporization and condensation have a

significant influence on flow behaviour of the reservoir and injected fluids. This is of particular importance in unconventional reservoirs composed largely of nano-size pores as well as at the conditions of both non-isobaric and non-isothermal type applications.

Considering the properties of confined fluids is similarly important in designing steam-over-solvent injection in fractured reservoirs (SOS-FR), as proposed by Al-Bahlani and Babadagli (2009). One of the main ideas of this method is retrieving the injected solvent by vaporizing it with steam or hot water. Identifying accurately the phase-transition temperature of injected solvents is essential, as it helps in determining the sufficient temperature of steam/hot water needed to vaporize the injected solvent. Due to considerable shifts of phase envelopes in micro and meso pores (Alharthy et al. 2013), simulating hydrocarbon recovery factors and future reserves by using conventional EOS models could lead to overestimation or underestimation issues. Paying attention thoroughly to the phase-change behaviour of confined fluids in capillary media is prime, especially in modelling EOR methods where their performances are partially affected by the phase alteration of injected fluids in the reservoir. For instance, in Steam Enhanced Oil Recovery (SEOR) applications, the steam propagation in the matrix highly depends on the vapor condensation which alters its flow dynamics because of the change of physical properties, such as density and viscosity. Micro and meso pores are dominant in extended tight rocks, like shale. Nevertheless, based on a recent pore size distribution analysis, confined pores (smaller than 100 nm) do exist in permeable rocks, such as Berea sandstone and Indiana limestone (Al-Kindi and Babadagli 2020). Although pore volumes of nanopores in permeable rocks are minor, the confinement effect on phase alterations could take place in such matrices which, in a reservoir scale, could impact the simulated oil recovery and reserves.

This investigation is a continuation of our prior work (Al-Kindi and Babadagli 2017, 2018, 2019b) that focused on the effect of confinement on the vaporization of hydrocarbon solvents by using various silica-glass porous media, such as Hele-Shaw cells and microfluidic chips. We particularly inspect the effect of wettability on the nucleation temperature of heptane (C_7H_{16}) and octane (C_8H_{18}) in permeable rocks (Berea sandstone, Indiana limestone, and a tight sandstone). Pore size distribution analysis was performed to estimate the pore volumes of nanopores (< 100nm) in each rock sample, based on its total pore volume. Furthermore, we studied the influence of wettability on the vaporization behaviour in Berea sandstone with different clay contents (fired and unfired

sandstone), various pore structures (with and without clay presence), and dissimilar rock wettability (water-wet and oil-wet).

6.4 Theoretical Background and Hypothesis

Young-Laplace equation quantifies the pressure difference (ΔP) at the interface between two motionless fluids. The capillary pressure difference is impacted by the surface tension (γ) and shape of surface or interface curvature:

$$\Delta P = -\gamma \left(\frac{1}{R1} + \frac{1}{R2}\right) \tag{1}$$

where ΔP is the pressure difference, γ is the surface tension, and $R1$ and $R2$ are the radii of curvature. In cases with a circular and slim tube, the vapor-liquid interface forms a spherical surface at which the pressure difference is a function of surface tension and sphere radius. The radius of the spherical surface is affected by the contacting behaviour of the liquid interfacing with the solid material. As shown in **Figure 6-1**, the sphere radius is a function of contact angle (θ) and tube radius (r). In this case, the Young-Laplace equation can be expressed as following:

$$\Delta P = \frac{2\,\gamma\,\cos\theta}{r} \tag{2}$$

where θ is the contact angle and r is the tube radius. By using the Young-Laplace concept, William Thomson derived the Kelvin equation, which described the shift of vapor pressure in tight tubes affected by capillary pressure:

$$P_r = P_{Bulk}\, exp\left(\frac{-2\,\gamma\,V_m}{r\,R\,T}\right) \tag{3}$$

where P_r is the vapor pressure of confined fluid, P_{Bulk} is the bulk vapor pressure of the fluid, γ is the surface tension, V_m is the fluid molar volume, r is the tube radius, R is the gas constant, and T is the vapor/liquid temperature. In capillary conditions, the pressure of vapor alters based on the curvature of vapor-liquid interface (concave or convex). Thomson equation described the alteration of boiling points with respect to the pore size by quantifying the inverse relationship between the two parameters:

$$T_r = T_\infty \exp\left[-\frac{2\,\sigma\,v^L}{r\,\Delta H_{vap}}\right] \tag{4}$$

where T_r is the boiling temperature of confined liquid, T_∞ is the bulk boiling temperature, σ is the liquid surface tension, v^L is the liquid molar volume, r is droplet or pore radius, and ΔH_{vap} is the heat of vaporization of liquid. The Thomson equation inherited the notion of both the Clausius-Clapeyron and Kelvin equation to describe the influence of interface curvature on the vaporization temperature in isobaric environments (Berg 2009). As the droplet size becomes smaller, boiling temperatures reduce; therefore, fluids in nanopores would vaporize at temperatures lower than their bulk boiling points. Kelvin and Thomson equations have several limitations that cause a reduction in their accuracies. In confined pores, surface adsorption has a considerable effect on phase-transition behaviour due to the limited numbers of molecules in such conditions. Both equations do not take surface-fluid interactions into account. Moreover, due to the confinement effect, interfacial tensions can have values that are dissimilar with handbook values (Jin 2018). The two approaches are not compatible with multicomponent fluids; as a result, using them with complex fluid systems (reservoir hydrocarbons) becomes very challenging.

Cubic EOS models are widely used to simulate the phase behaviour of hydrocarbon mixtures under various pressures and temperatures. The usage of such equations become very handy when the laboratory PVT data is limited or not available (Fanchi 2020). Ideal gas equation ($P\overline{V} = RT$) was the earliest EOS to model the PVT behaviour of gases; however, its accuracy reduces in high-pressure and low-temperature conditions. The cubic EOS models were developed to overcome the limitation of the ideal gas equation. In fluids, phase-alteration behaviours are governed by intermolecular/attraction and repulsive forces. The main key to predict the phase behaviour of fluids is to model the attractions and repulsions between molecules; accordingly, the cubic EOS models empirically simulate these forces. Since the modeling is performed empirically, EOS

models calculate the overall reaction of molecules. Such approach can impact the accuracy of cubic EOS in conditions at which intermolecular forces are strong—such as the case in water (Fanchi 2020).

One of the drawbacks of cubic EOS models is that they do not consider the confinement and capillary pressure effect on the phase behaviour of fluids. Several modifications on the Peng-Robinson EOS, for instance, were made to include the capillary impact on predicted phase envelopes. Cui et al. (2018) considered the impact of molecule adsorption on the molar volume of fluids; correspondingly, the molar volume term in Peng-Robinson EOS was modified to be a function of adsorption and pore size. Alharthy et al. (2013) reformed the critical pressure and temperature terms in Peng-Robinson EOS with correlated relative shift of critical pressure and temperature to model the phase envelope of dry gas condensate in confined media.

As the medium size gets smaller, the ratio of molecule number over volume decreases thus impacting the molecule dynamics in the medium and provides them less freedom of motion (**Figure 6-2**). In the bulk conditions, the majority of molecules are governed by the cohesion forces (intermolecular bonds), whereas a small percentage of them get adsorbed on the solid surface by the adhesion forces. In such cases, for vaporization to take place, a sufficient heat energy is needed to break the intermolecular bonds, and the adhesion forces almost have no influence on the cause of a major liquid boiling. In confined volumes, as most of the molecules get closer to the solid surface with a much lower molecule numbers, the adhesion forces will have higher control on the molecules which will impact the phase transition of restrained fluids. As a result of the increased effect of adhesion forces in capillary conditions, solid surface wettability could noticeably alter the phase-change behaviour of fluids. As illustrated in **Figure 6-3**, owing to the limited number of molecules in nanopores and water-wet pores, most of the water molecules get adsorbed by the well. Meanwhile in an oil-wet nanopore, the water molecules tend to stick with each other. Such a phenomenon causes the boiling points to shift from their normal vaporization temperatures.

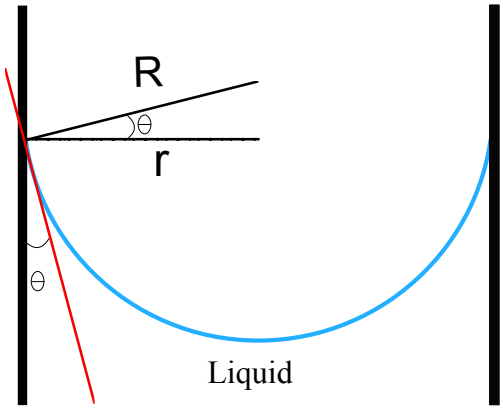

Figure 6-1: Illustration of a concave interface in a wetting media.

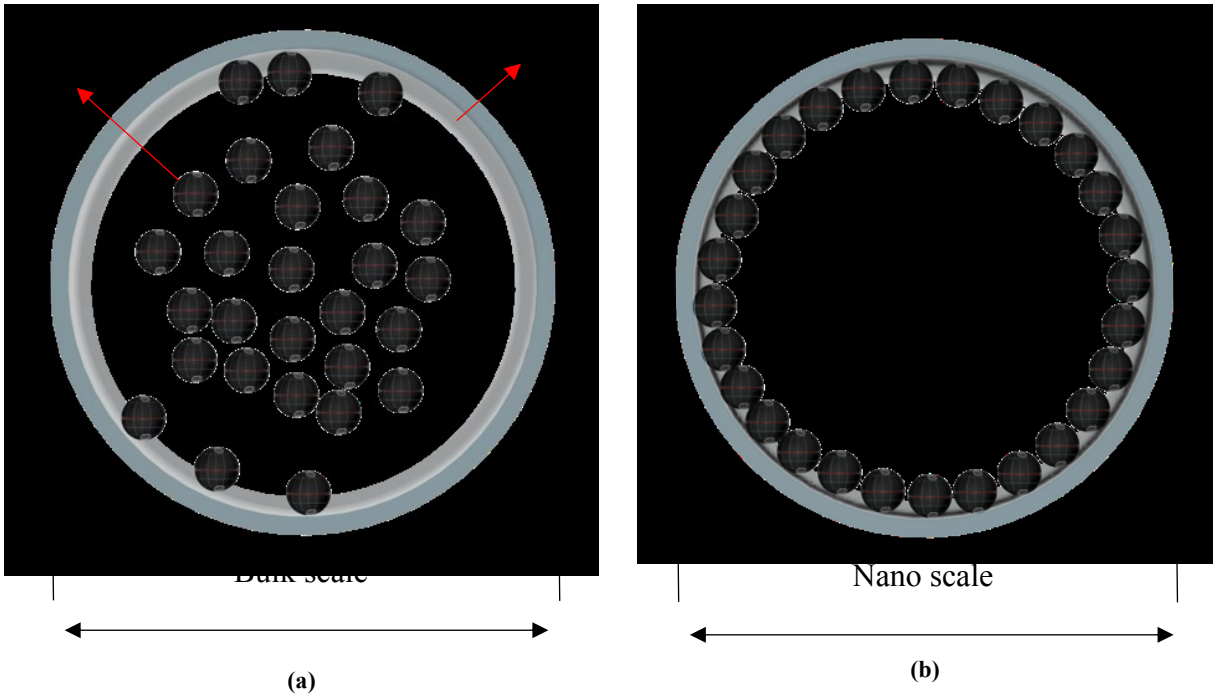

Figure 6-2 – (a) Fluid molecules in a bulk medium with a minimum adsorption effect; (b) molecules of confined fluids in nanopores with adsorption effect.

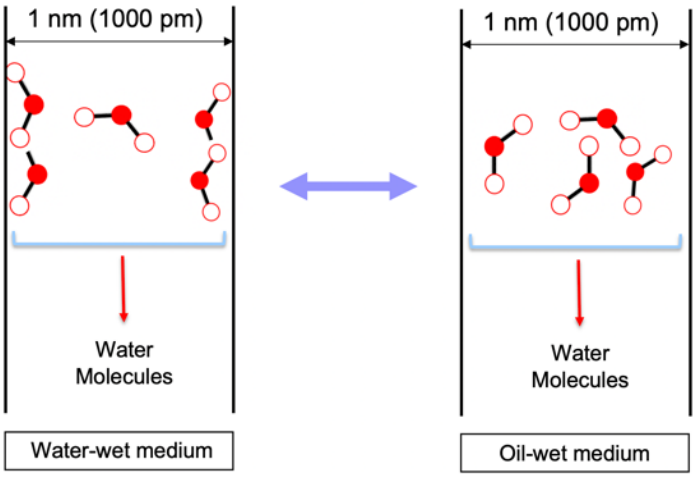

Figure 6-3: Influence of adhesion forces (adsorption) on water molecules in hydrophilic and hydrophobic porous systems.

6.5 Methodology and Experimental Setup

This paper both targeted and focused on the nucleation temperature at which the phase change starts to take place in the rock porous system. The investigation was held with permeable rocks (Berea sandstone and Indiana limestone), featured with high permeabilities (274 and 30 millidarcies), and a low-permeability rock (tight sandstone) with a permeability of 0.1 millidarcies (md). Ensuring a simultaneous and uniform heat transfer into the rocks is critical to prevent inhomogeneous heat distribution along the rock thickness. To do so, a liquid heating system with a slow heating rate was used to increase the overall temperature of rock samples steadily from room temperature (21℃) to the normal boiling point of the hydrocarbon solvents. The selected heating liquid was a polar fluid; hence, it would not mix with the non-polar hydrocarbon solvents, thus forming a solution.

A constant-temperature oven was utilized to heat the liquid bath and, therefore, heat the rock cores gradually. To guarantee a slow heating rate, a viscous heating liquid (glycerol) was used, due to its low thermal conductivity (comparing with water thermal conductivity at 20℃). The phase alteration of solvents was observed visually by a DSRL camera, and the bath temperature was recorded continuously with a contact temperature sensor. **Figure 6-4** illustrates the experimental

setup that was used to examine the nucleation temperature and boiling point of hydrocarbon liquids in various rocks.

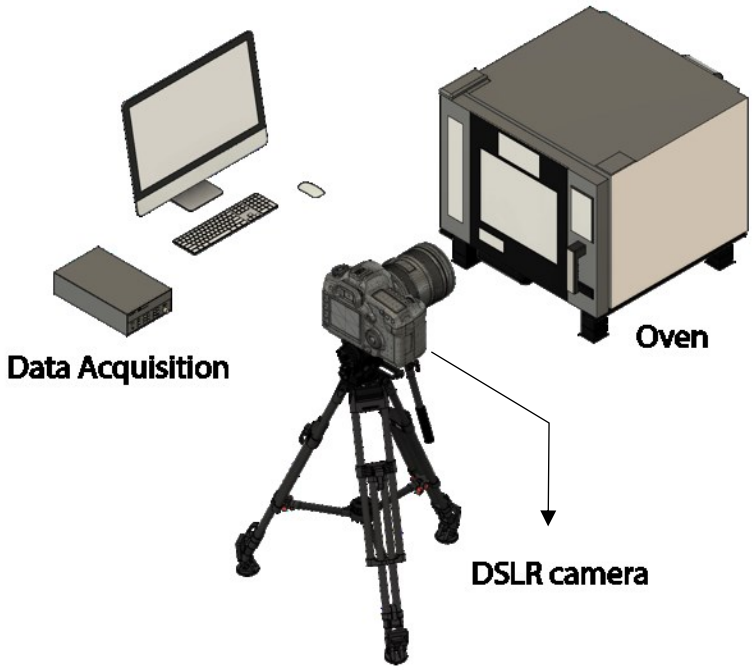

Figure 6-4: Schematics of the experimental system. The liquid bath and rock samples were kept inside the constant-temperature oven.

6.6 Experimental Work

The investigation was initiated by identifying pore size distributions of the rock samples to quantify pore volumes of micro and meso pores in each rock type per sample weight. Such analysis also helped in proving the existence of nanochannels in permeable rocks, like Berea sandstone and Indiana limestone. To inspect the effect of rock wettability on boiling temperatures, the Berea sandstone rocks were chemically treated, with a siliconizing fluid, to change their surface wettability from natural water-wet behaviour to hydrophobic porous media. Contact angle measurements were implemented to quantitatively observe the wettability of outer surfaces before

and after the chemical treatment. We assumed that the outer surface wettability of rocks would generally represent the wettability of inner pores.

6.7 Pore Size Distribution Analysis (PSDA)

In nature, reservoir rocks consist of non-uniform porous media at which rock properties might change from one location to another; the pore size is an example of these inconsistent properties. Formation matrices are usually complicated systems, and the size and shape of pores within the rocks could vary along the same core plug. PSDA analyses the behaviour of solid interaction with gases, such as nitrogen, through gas adsorption and desorption on the rock surface. In our study, the analysis brought two main advantages that other analytical methods (e.g., Winland equation) used to compute average pore sizes could not provide: (1) estimating pore volumes of micro and meso channels, and (2) identifying the median size of pores below 700 nm. **Figure 6-5** shows the pore volume of different pore sizes, extending from 1 to 100 nm, in each rock. Although the vaporization behaviour of solvents was not observed in shale, the rock was included in Figure 5 to compare it with other rocks, thus representing the tightest rock. The pore volume of micro ($\leq$ 2nm) and meso (2 – 50 nm) pores in tight sandstone and shale are relatively higher than what were observed with sandstone and limestone. Nonetheless, based on the analysis, micro/meso pores also exist in permeable rocks with insignificant pore volumes. **Table 6-1** presents median pore sizes and volume percentage of channels smaller than 1000 nm. While the pore volumes of nanopores in sandstone and limestone are considerably low, the existence of extremely confined channels could result in a shift in the vaporization temperature of hydrocarbon solvents. In general, the phase-change behaviour of fluids becomes unusual when medium sizes get smaller than 100 nm, due to the confinement effect (Barsotti et al. 2016). The Thomson equation was also studied with a wide deviation of pore sizes, starting from a minimum pore diameter to the maximum pore size that can possibility exist in the rock. The wide pore size distribution values in Berea sandstone, Indiana limestone, and tight sandstone were brought from Shi et al. (2011), Freire-Gormaly et al. (2015), and Wang et al. (2019).

Table 6-1: Median pore sizes and pore volume percentages in various rock types.

Rock Type	Median Pore Size of channels below 1000 nm (nm)	Volume Percentage of pores smaller than 1000 nm (%)
Berea sandstone	350	4.4
Indiana limestone	470	4.6
Tight sandstone	300	38.2

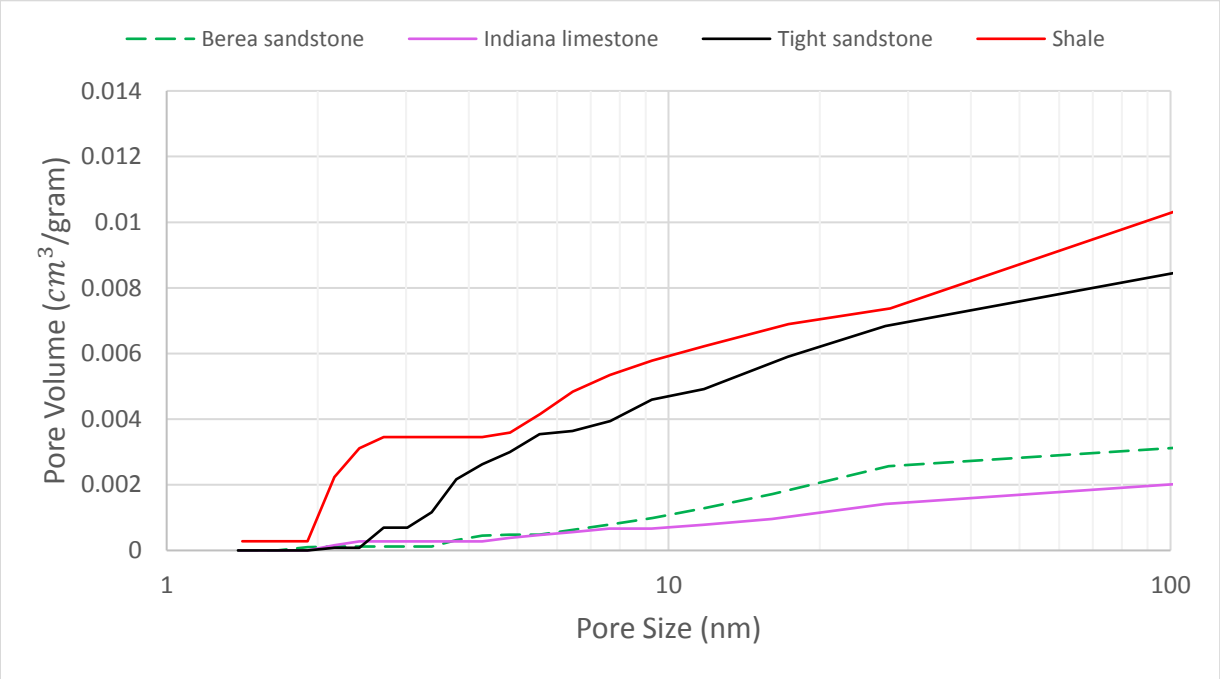

Figure 6-5: Representation of micro and meso pore volumes in various rock types.

6.8 Clay Content and Solvent Adsorption Phenomenon

Clays (e.g., kaolinite) naturally exist in Berea sandstone, and they have significant contributions in liquid adsorption on the surface of the rock. **Figure 6-6** shows a microscopic view of clay particles on the outer surface of Berea sandstone, obtained by the scanning electron microscope

(SEM). Due to the clay existence, adsorption of hydrocarbon liquids takes place in sandstone rocks, despite the water-wet behaviour that sandstone has. One of the goals of the study was to observe the impact of the molecule-surface interaction (adsorption) on the nucleation temperature of hydrocarbons. Heating Berea sandstone rocks to 800°C breaks down the clay structure which causes the clay to lose its typical properties, such as clay swelling and adsorption. Breaking the clay structure insignificantly alters the rock wettability, and it reduces the adsorption capabilities of said clay. Imbibition tests were performed to inspect the change of liquid adsorption in unfired and fired Berea sandstone. **Figure 6-7** illustrates the change of water and heptane cumulative imbibed volumes in unfired and fired core plugs over a timeframe of 6 hours (with water) and 8 hours (with heptane). According to our permeability measurements, heating a Berea sandstone sample to 800 °C caused an increase of rock permeability from 112 to 222 md. Theoretically, higher permeabilities should result in the higher propagation of liquids within the matrix. However, due to the reduction of adsorption in fired samples, the cumulative imbibed volumes of water and heptane decreased noticeably in fired sandstone (with deactivated clays), compared to unfired sandstone, as shown in Figure 7. The behaviour of phase-change was investigated in unfired and fired sandstone in order to observe the alteration of vaporization temperature after reducing the solvent adsorption in sandstone, by firing process.

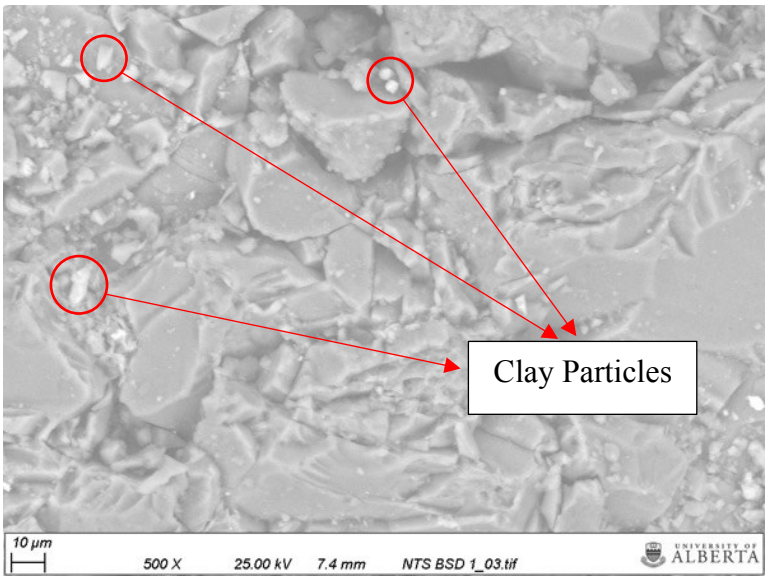

Figure 6-6: Magnified image of clay particles on a scanned sandstone surface.

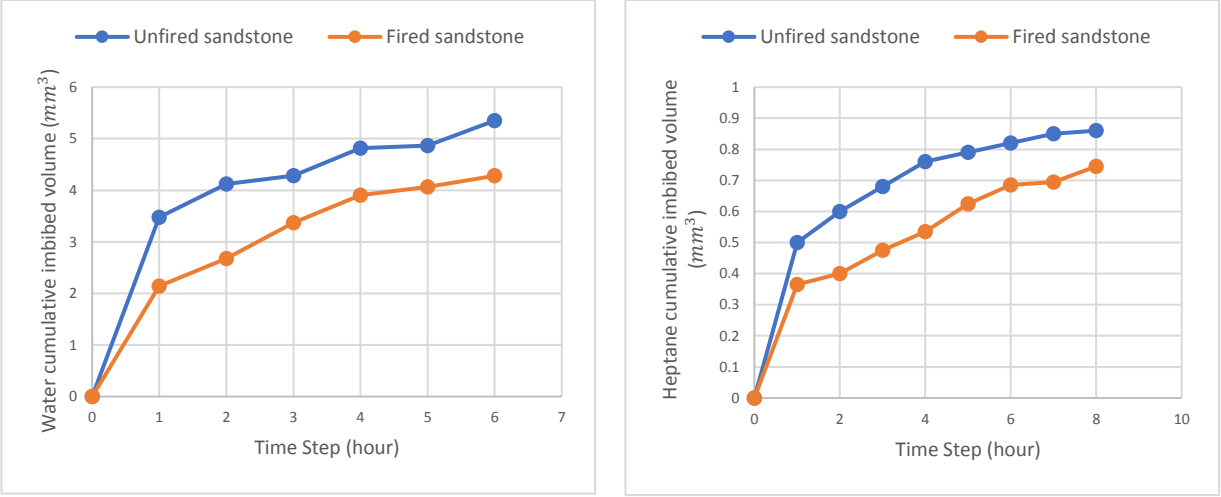

(a) (b)

Figure 6-7 – (a) Change of water cumulative imbibed volume over a period of 6 hours; (b) change of heptane cumulative imbibed volume over a period of 8 hours.

6.9 Wettability Alteration and Contact Angle Measurement

The wettability of the inner pore surface is partially controlled by the adhesion forces (molecule-surface interaction) which influences the phase-change temperature of fluids, especially in confined spaces. To examine such a phenomenon, the vaporization temperature of heptane was inspected in Berea sandstone before and after wettability alteration treatment. Sandstone samples were chemically treated to alter their surface wettability from water-wet to oil-wet.

The wettability of Berea sandstone was chemically altered by forming a monolayer and microscopically thin film on pore walls, using a siliconizing solution (10 wt% dichlorodimethylisilane dissolved in pentane). The film repels water which makes the inner porous media into a strongly hydrophobic system. The rock samples were soaked in the solution for at least 24 hours; thus allowing the wettability alteration to take place within the rocks. Simultaneously, vacuum pressure (12 psi below ambient pressure) was utilized to fully saturate the sandstone rocks with the siliconizing solution. Then, the rocks were completely dried using a furnace to eliminate any trapped fluids within the rock porous systems.

Contact angle measurements were performed to quantify the effect of the siliconizing fluid on sandstone's surface wettability. After the chemical treatment, the rock wettability was successfully changed from hydrophilic to hydrophobic. In all measurements, water was used as a medium, and the contact angle of the heptane droplet was measured on the exterior surface of the rocks. In all cases, the siliconizing fluid has successfully shifted the wettability of Berea sandstone from water-wet to oil-wet. Similarly, the fired samples were treated chemically to change their surface wettability from water-wet to oil-wet. **Figure 6-8a** shows the behavior of a heptane droplet on the sandstone surface with a contact angle of 141.8°, representing a hydrophilic surface. **Figure 6-8b** presents a heptane droplet on a sandstone surface after the wettability treatment with a contact angle of 24.7°, representing a hydrophobic surface. **Figure 6-9** displays the contact angles of the heptane droplet on fired sandstone's surface before and after wettability alteration.

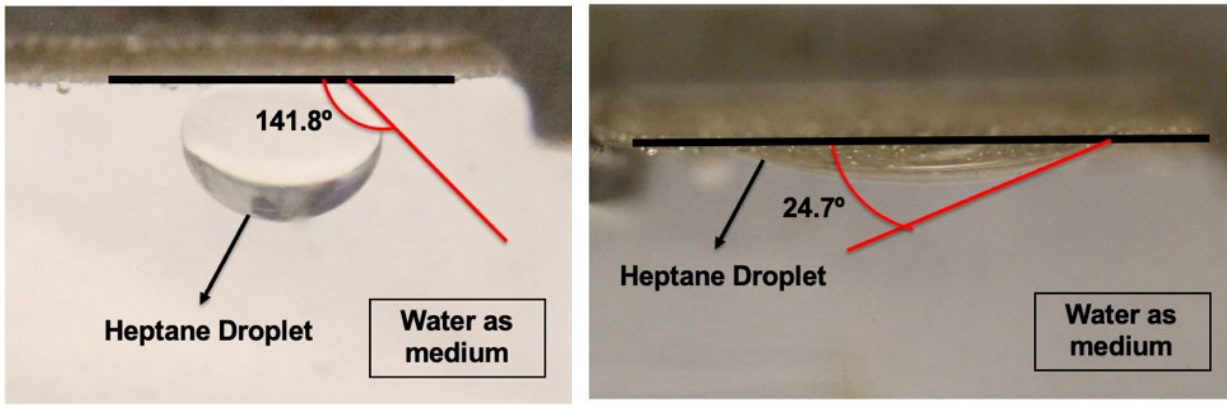

(a) (b)

Figure 6-8 – (a) Contact angle measurement before wettability alteration (water wet); (b) contact angle measurement after wettability alteration (oil wet).

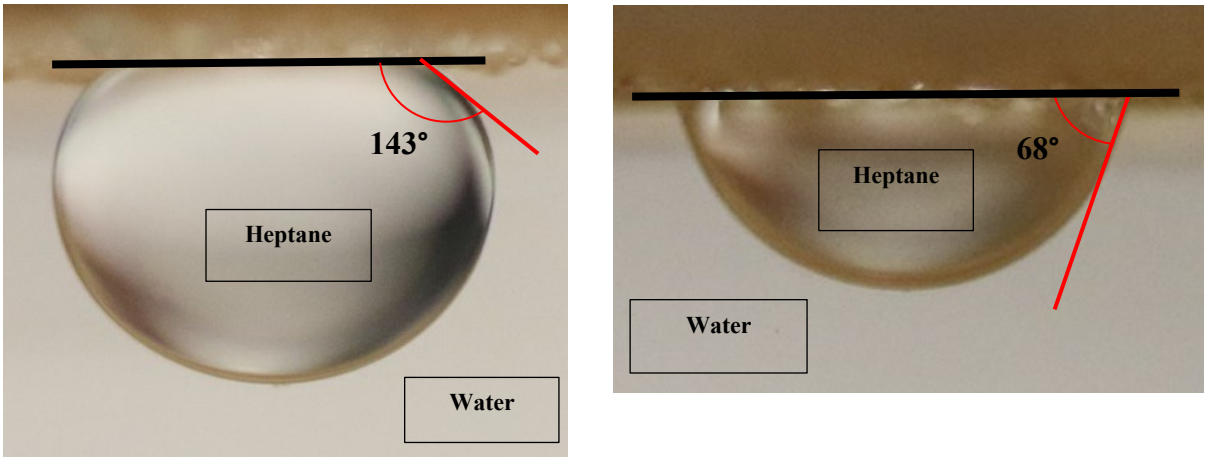

(a) (b)

Figure 6-9 – (a) Contact angle measurement before wettability alteration (water wet); (b) contact angle measurement after wettability alteration (oil wet).

6.10 Adsorption Analysis

Due to the electrical force imbalance, surface solid molecules tend to attract nearby fluid molecules, resulting in a process called fluid adsorption. The adsorption capability defers from one material to another, depending on their surface properties. Theoretically, fluid adsorption affects the movement of the surrounding fluid molecules which can alter its physical properties (e.g., vaporization and condensation); however, such phenomenon has no impact in bulk conditions at which a minor percentage of molecules are attached to the solid surface (Figure 2). It is also well known that hydrocarbon solvents have the capability to be adsorbed by clays, thus affecting the boiling characteristics directly. This may also change the nature of wettability (and pore size as clays make up smaller fonts) as clays exhibit different wettability characteristics from the grains made of quartz.

As the medium gets tighter, the fluid molecule adsorption on the solid surface starts to gain an influence on the phase-change behaviour of the fluid. The results from the imbibition tests were linked with the water/solvent adsorption in Berea sandstone to analyze how clay deactivation would reduce the adsorption. Nonetheless, since imbibition tests are defined as a macro-scale

analysis, several microscopic factors might also affect the change of imbibed volumes of water and heptane over time. Because of that, further investigation was required to better understand the change of liquid adsorption between unfired and fired sandstone. The nitrogen adsorption analysis allowed us to measure the volume adsorbed in the rock pores before and after the firing process, besides wettability alteration, at various relative pressures ($\frac{atmospheric\ pressure\ (P)}{sample\ pressure\ (P_o)}$). **Figure 6-10** shows the variation of nitrogen adsorbed volume in Berea sandstone prior and after firing process/wettability alteration at difference relative pressures (P_o/P) ranging from 0 to 1. Deactivation of clay noticeably reduced the adsorbed volume of nitrogen in sandstone comparing with the unfired sample, as shown in Figure 10a. Additionally, as presented in Figure 10b, changing the rock wettability from water-wet to oil-wet decreases the fluid adsorption.

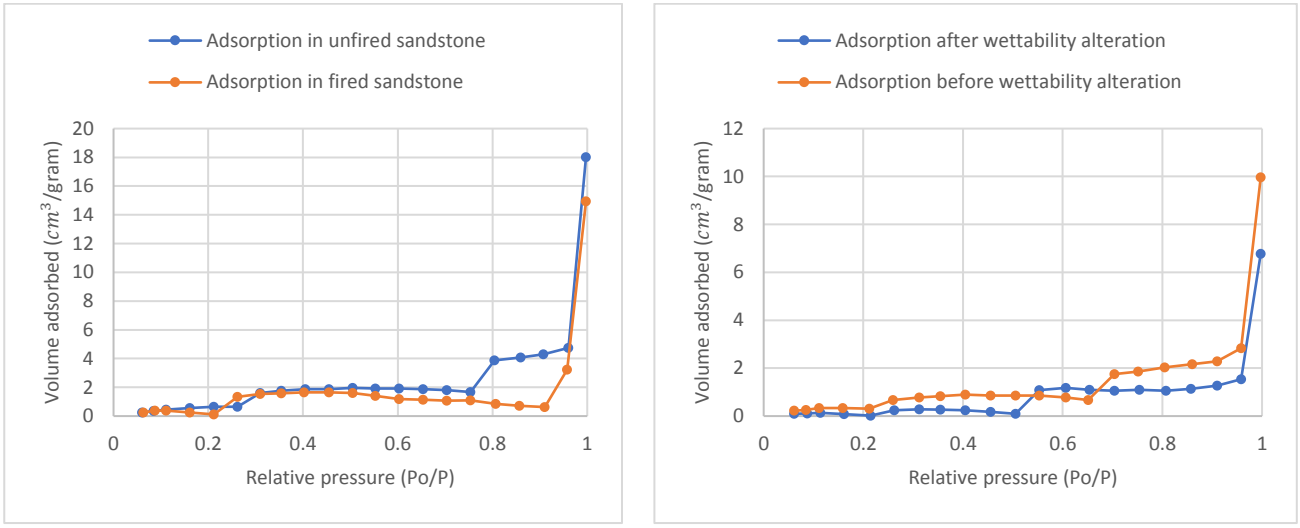

(a) **(b)**

Figure 6-10 – (a) Nitrogen volume adsorbed in unfired and fired sandstone; (b) nitrogen volume adsorbed in sandstone before and after wettability alteration.

6.11 Phase-Change Temperature Measurement

Boiling points of heptane and octane were measured in sandstone, limestone, and tight sandstone under atmospheric pressure (1 atm). During the observation, we focused on two main stages: (a) first bubbles initiation (nucleation stage), and (b) quick and continuous formation of solvent vapor. The second stage was considered as the boiling point, since a major phase alteration begins to take place in the liquid. Note that, to fully avoid any air in the system (rock or solvent in it) which might appear as a bubble during the experiments, the rock samples were saturated with solvent under vacuum. To fully saturate the rocks with the hydrocarbon liquids, they were kept under vacuum pressure (≈ -12 psi) for 24 hours to remove any trapped air. Then, for 48 hours, the rocks were saturated with solvents in vacuumed conditions.

After the saturation stage was complete, the rock sample was immersed in glycerol (**Figure 6-11**), then, kept in the oven to get heated. Starting from room temperature (21℃), each sample was slowly heated until the boiling temperature of the solvent was reached. The temperature of the liquid bath was recorded continuously using the data acquisition system. Simultaneously, images were taken every 15 seconds by a DSLR camera to capture the different stages of phase change. Each experiment was repeated four times (trial 1, 2, 3, and 4) and then average temperatures were considered.

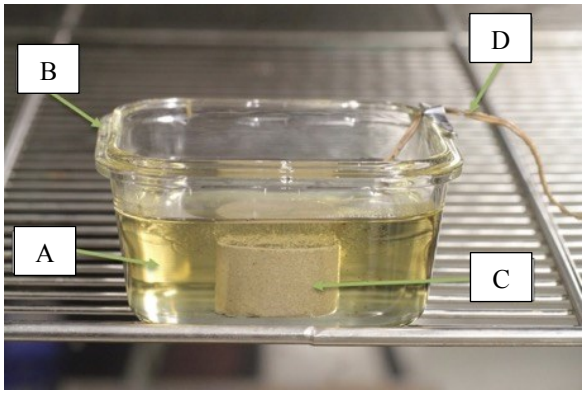

Figure 6-11: Internal experimental system: (A) glycerol, (B) glass container, (C) rock sample, and (D) thermocouple.

6.12 Results and Discussion

In a prior work, boiling points in bulk conditions were measured using bulk models, consisting of silica-glass tubes (Al-Kindi and Babadagli 2020). Measured vaporization temperatures were close to the standard normal boiling points, which we then used as benchmarks for our experimental outcomes. The recorded bulk boiling point of heptane was 96℃, and the normal vaporization temperature of octane was 125℃. **Figure 6-12c** shows the vaporization of heptane in the bulk model (composed of a bundle of capillary tubes of 0.8 mm diameter) at a temperature of 96℃. In the determination of shifted phase-change temperatures, as mentioned previously, two phase-change stages were targeted: initial bubbles formation and fast creation of vapor bubbles. Owing to the presence of micro and meso pores, shifted vaporization temperatures of heptane and octane were observed in Berea sandstone, Indiana limestone, and tight sandstone. For instance, in one of the trails, vapor bubbles began to form at 76℃ (**Figure 6-12a**). A rapid formation of bubbles took place at a temperature of 84℃ (**Figure 6-12b**). **Table 6-2** illustrates the nucleation (stage 1) and boiling (stage 2) temperatures of heptane and octane in different rock types.

Table 6-2: Heptane and octane vaporization temperatures in sandstone, limestone, and tight sandstone.

Rock Type / Solvent	Initiation of vapor – nucleation temperature (℃) (Stage 1)	Rapid creation of bubbles – boiling temperature (℃) (Stage 2)
Berea sandstone / heptane	75	83
Indiana limestone / heptane	68	81
Tight sandstone / heptane	63	79
Berea sandstone / octane	108	114
Indiana limestone / octane	103	112
Tight sandstone / octane	108	112

Altering the rock wettability to oil-wet relatively changed the nucleation temperature of hydrocarbon liquids in the rock. Microscopically, increasing the favorability of the surface towards the liquid strengthens the molecule-surface interactions thus affecting the nucleation nature of confined liquids. The impact of such a phenomenon on vaporization temperatures escalates as the medium sizes get tighter, according to Thomson equation. A set of experiments were done to study the phase change of heptane and octane in sandstone as a water-wet and oil-wet medium. **Table 6-3** shows the nucleation temperatures of heptane and octane in untreated and treated sandstone in comparison to the bulk conditions (the values were validated using the bulk experiments as illustrated in **Figure 6-12c**). Changing the wettability of water-wet porous media caused obvious alteration of heptane and octane nucleation temperatures.

Table 6-3: Heptane and octane vaporization temperatures in Berea sandstone before and after wettability alteration.

Rock type	Boiling temperature (℃) Trial 1	Boiling temperature (℃) Trial 2	Boiling temperature (℃) Trial 3	Boiling temperature (℃) Trial 4	**Average boiling temperature (℃)**	**Boiling temperature at bulk conditions (℃)**
Untreated sandstone (water-wet) - heptane	70	76	71	83	**75**	**96**
Treated sandstone (oil-wet) - heptane	75	85	73	85	**79.5**	**96**
Untreated sandstone (water-wet) - octane	105	109	109	108	**108**	**125**
Treated sandstone (oil-wet) - octane	98	86	88	95	**91.7**	**125**

The investigation also paid closer attention to the nucleation temperature of heptane and octane in fired Berea sandstone in order to examine the influence of solvent adsorption on the phase-change temperature. In Berea sandstone, the liquid adsorption is partly caused by the clays. Heating the rock to 800℃ breaks down the clay structure which reduces the liquid adsorption within the rock

medium. Based on the conducted imbibition tests, the firing process remarkably reduces the water and heptane adsorption in Berea sandstone. **Table 6-4** presents the recorded phase-change temperature of heptane and octane in treated and untreated fired sandstone samples. In the untreated samples, because of the reduction of solvent adsorption, breaking the clay structure reduced the phase-change temperature of heptane and octane by 20% (4.3% in Kelvin unit), comparing with the boiling temperatures in unfired sandstone cores. As observed with unfired sandstone, altering the rock wettability to oil-wet changed the nucleation temperature of heptane and octane in fired sandstone (Table 6-4).

Although all cases presented in **Tables 6-3** and **6-4** followed a consistent trend for the fired and unfired samples, i.e., the boiling temperatures decreased as the clays were deactivated (by firing the sample) reducing the adsorption capacity of the solvents for both heptane and octane, an opposite behavior for the treated samples for the solvents were observed. This can be seen in Table 3 for the unfired sandstone sample (average boiling temperature for heptane increased from 75 to 79.5°C while it decreased from 108°C to 91.7°C for octane). Similarly, the -average- boiling temperature increased from 60°C to 69°C while it decreased from 87°C to 70°C. All these are beyond any experimental measurement or statistical analysis related issues as the experiments have been repeated several times as mentioned earlier and the values are statistically reliable (change in the average values are above standard deviations or so). Therefore, we attempted to search for physical explanations for this observation:

1. In capillary systems, the phase behaviour of confined fluids is affected by two main factors: (1) molecule compaction, and (2) pore-molecule interaction. As the medium gets tighter, the number of molecules per volume decreases. In extended tight channels, the molecules are not fully bonded with other molecules, due to the limited number of molecules, which causes them to lose some of their intermolecular energies. This phenomenon causes the boiling temperature of confined fluids to decline since lower heat energies are needed to induce vaporization. The shift of phase-change behaviour in constrained volumes also alters based on the surface wettability and adsorption. The pore-molecule interactions increase as the molecule adsorption on the solid surface increases. The higher the adsorption is, the higher the heat energy required to break the pore-molecule interactions, thus the particles are able to escape from the liquid phase and solid to the vapour phase.

These observations are in line with the analysis of the data given in **Tables 6-3** and **6-4** regarding the adsorption (see the previous paragraph).

2. The wettability of Berea sandstone was chemically altered using a siliconizing fluid. The chemical forms a monolayer on the inner pore surface to make the porous medium strongly oil wet. The monolayer reduces the size of pores and, therefore, increases the molecule compaction effect on the confined fluid. **Figure 6-13** illustrates schematics of heptane and octane molecules in sandstone pores after wettability alteration. In the case with heptane, it was observed that the heptane boiling temperature increased when the wettability of sandstone was changed to oil wet—due to the increase of pore-molecule interaction. This phenomenon did not occur with octane since it contained larger molecules, compared to heptane, and the increased molecule-compaction effect by the monolayer decreased the boiling temperature of octane—although the pore-molecule interaction was strengthened. It is expected that the boiling temperature of hydrocarbons with a higher carbon number than octane will reduce, even by altering the rock wettability to strongly oil wet.

3. The effect of capillarity on the phase alteration changes based on the molar volume of fluids. For instance, the molar volume of propane is around 20 litres/mol (20,000 millilitres/mol), whereas the molar volume of heptane is 147.5 millilitres/mol. The number of propane molecules in a 100-nm pore is approximately 135 times higher than the number of heptane molecules in the same pore, and the molecule size of propane is smaller than heptane molecules. Therefore, in a 100-nm pore, the effect of molecule compaction on propane is lower than what could be observed with heptane due to the smaller molecules of propane. This leads the propane phase behaviour to be less affected by the capillarity than heptane. The phenomenon was observed in one of our experiments when the vaporization of propane and heptane was studied in Hele-Shaw cells and microfluidic chips (Al-Kindi and Babadagli 2019a). In Hele-Shaw experiments, the boiling point of heptane was reduced by around 20% in a 40-μm medium. Similarly, in a 40-μm capillary tube, the boiling temperature of heptane was 20% lower than the bulk value (Al-Kindi and Babadagli 2019b). However, in the same media, the vaporization of propane did not get affected by

the confinement in the Hele-Shaw cells and micromodels, and the measured vapour pressures were identical to the bulk values.

4. A final evaluation can be made considering the complex nature of the pore network in natural rock systems. In our recent study (Al-Kindi and Babadagli 2021b), we showed that the boiling that starts earlier in smaller pores, which are interconnected to the bigger ones, might cause phase distribution related to the rock texture (or pore network). The "phase distribution-controlled" boiling (or phase behavior) can be seen in wettability altered media as the phases are distributed in a single pore. Then, the whole network is based not only on the texture (pore size characteristics) but also the surface interaction parameters such as wettability and interfacial tension.

The above analyses indicate that more studies are needed to clarify these points. Although substantial (and unignorable) changes in boiling points were observed under different wettability (and adsorption) conditions in this paper, the effects of solvent type (carbon numbers) and composition need more research.

To present the data measured in this study in comparison with the theoretical model (Eq. 4), several figures were prepared. Note that "a pore diameter" is needed to construct these plots. Different options derived from the pore size distribution data given in **Figure 6-5** were used in this analysis. The ultimate goal was to show the degree of the deviation from the classical models (Eq. 4), which is partly caused by the effect of wettability and solvent adsorption (mainly caused by clays). **Figure 6-14** presents the nucleation (stage 1) and boiling (stage 2) temperatures of heptane and octane in sandstone, limestone, and tight sandstone compared with computed boiling points by the Thomson equation, based on the median pore sizes of channels smaller than 1000 nm. Similarly, **Figure 6-15** shows the nucleation and boiling temperature of heptane and octane in the same rock samples, based on their maximum, minimum, and average pore diameters. The pore size values were referred from Shi et al. (2011), Freire-Gormaly et al. (2015), and Wang et al. (2019) who studied the pore size distribution in Berea sandstone, Indiana limestone, and tight sandstone. The main purpose of **Figure 6-15** is to demonstrate the computed boiling temperatures from Thomson equation at different deviation of pore sizes and compare the calculated values with the mea sured

outcomes. **Figure 6-16** illustrates the nucleation temperature of heptane and octane in fired and unfired sandstone before and after wettability alteration.

Table 6-4: Heptane and octane vaporization temperatures in fired Berea sandstone before and after wettability alteration.

Rock type	Boiling temperature (℃) Trial 1	Boiling temperature (℃) Trial 2	Boiling temperature (℃) Trial 3	Boiling temperature (℃) Trial 4	**Average boiling temperature (℃)**	**Boiling temperature at bulk conditions (℃)**
Untreated fired sandstone (water-wet) - heptane	62	57	57	65	**60**	**96**
Treated fired sandstone (oil-wet) - heptane	78	65	65	66	**69**	**96**
Untreated fired sandstone (water-wet) - octane	91	86	85	-	**87**	**125**
Treated fired sandstone (oil-wet) - octane	69	71	71	-	**70**	**125**

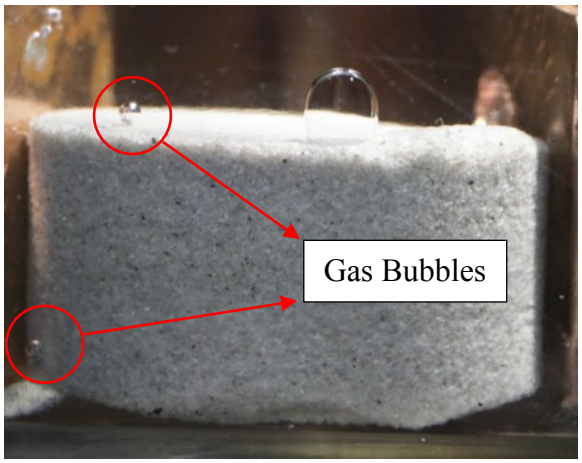

(a)

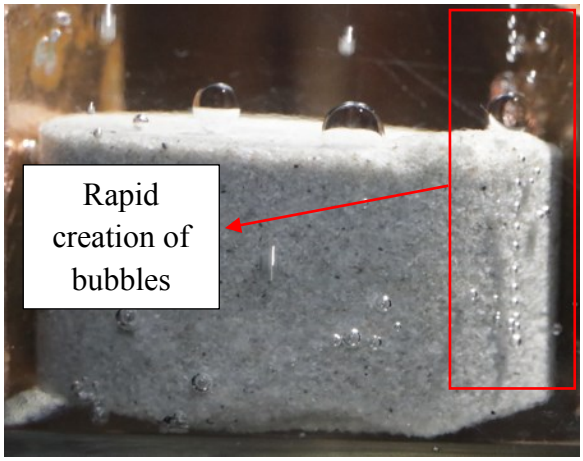

(b)

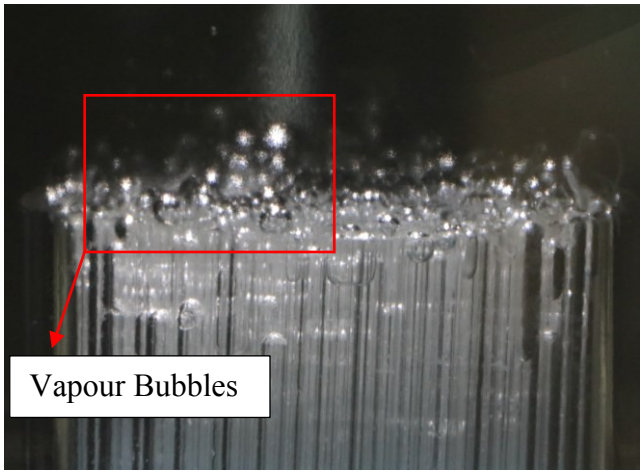

(c)

Figure 6-12 – (a) Initiation of heptane vapor bubbles (stage 1) at 76℃ in sandstone; (b) quick and continuous heptane bubbles creation (stage 2) at 84℃ in sandstone; (c) measuring the boiling of heptane at bulk conditions (96℃). Each capillary tube is in 0.8 diameter.

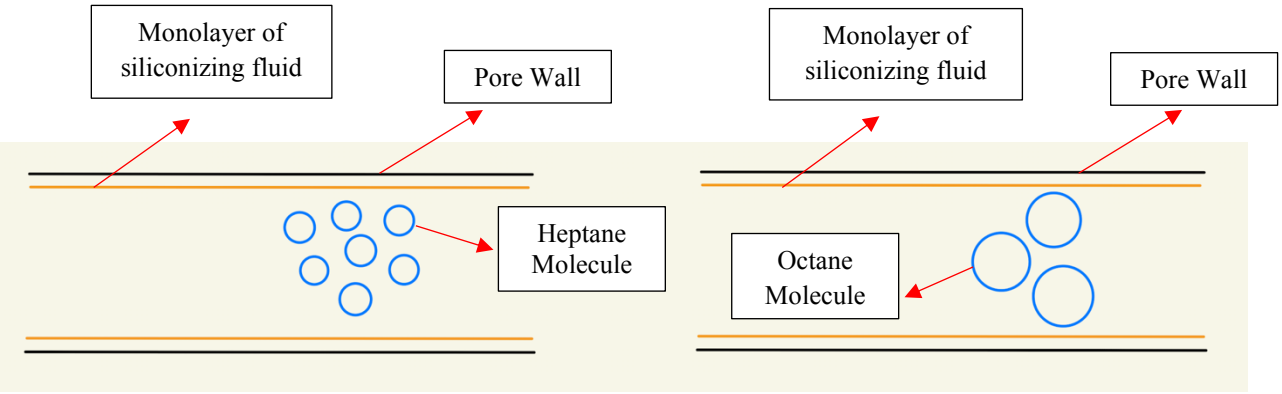

Figure 6-13: Heptane and octane molecules in a nanopore and under the capillary and adsorption effect.

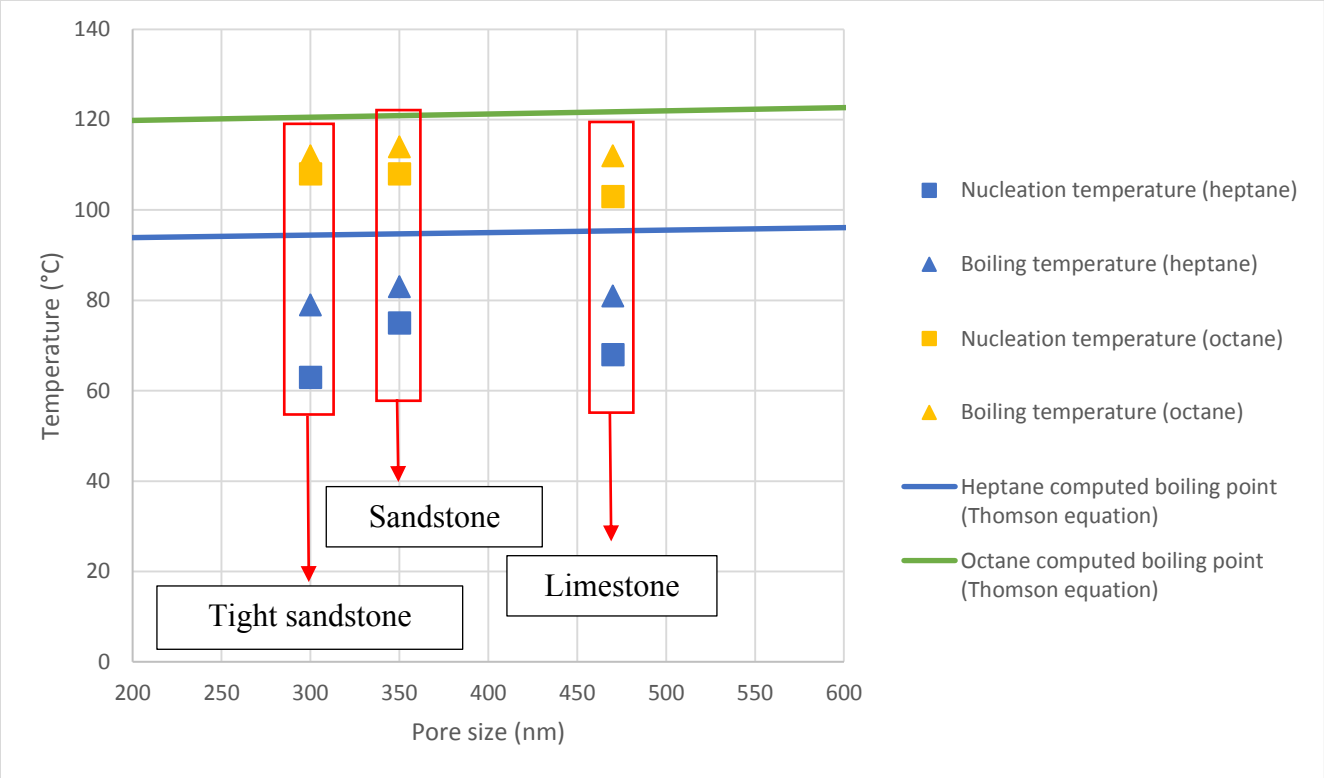

Figure 6-14: Calculated and measured phase-change temperatures of heptane and octane in different rock samples; median pore diameters were considered.

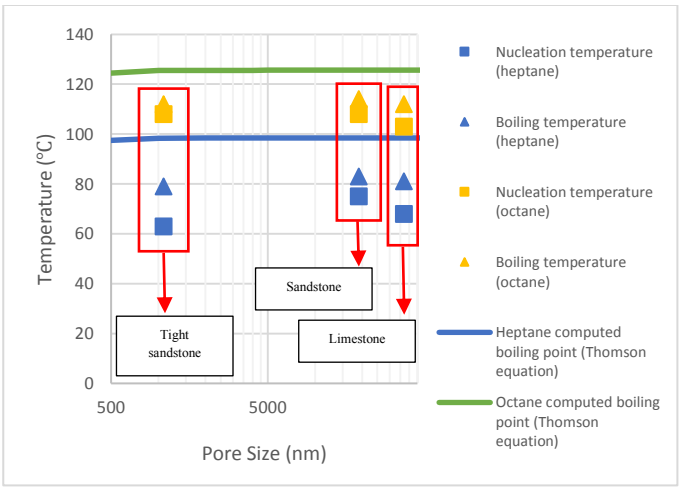

(a)

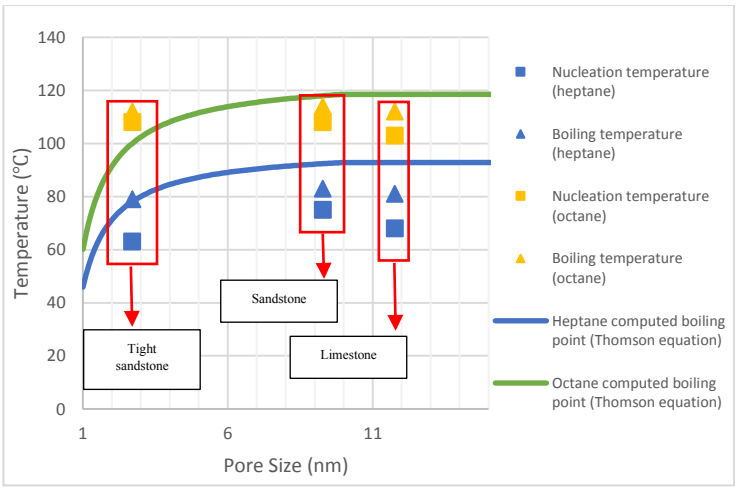

(b)

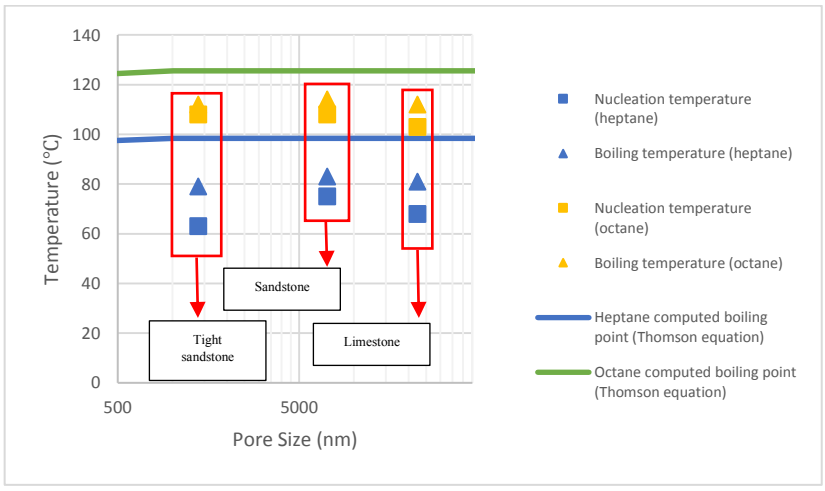

(c)

Figure 6-15 – (a) Computed and measured phase-change temperatures of heptane and octane in different rock samples; maximum pore diameters were considered; (b) computed and measured phase-change temperatures of heptane and octane in different rock samples; minimum pore diameters were considered; (c) computed and measured phase-change temperatures of heptane and octane in different rock samples; average pore diameters were considered.

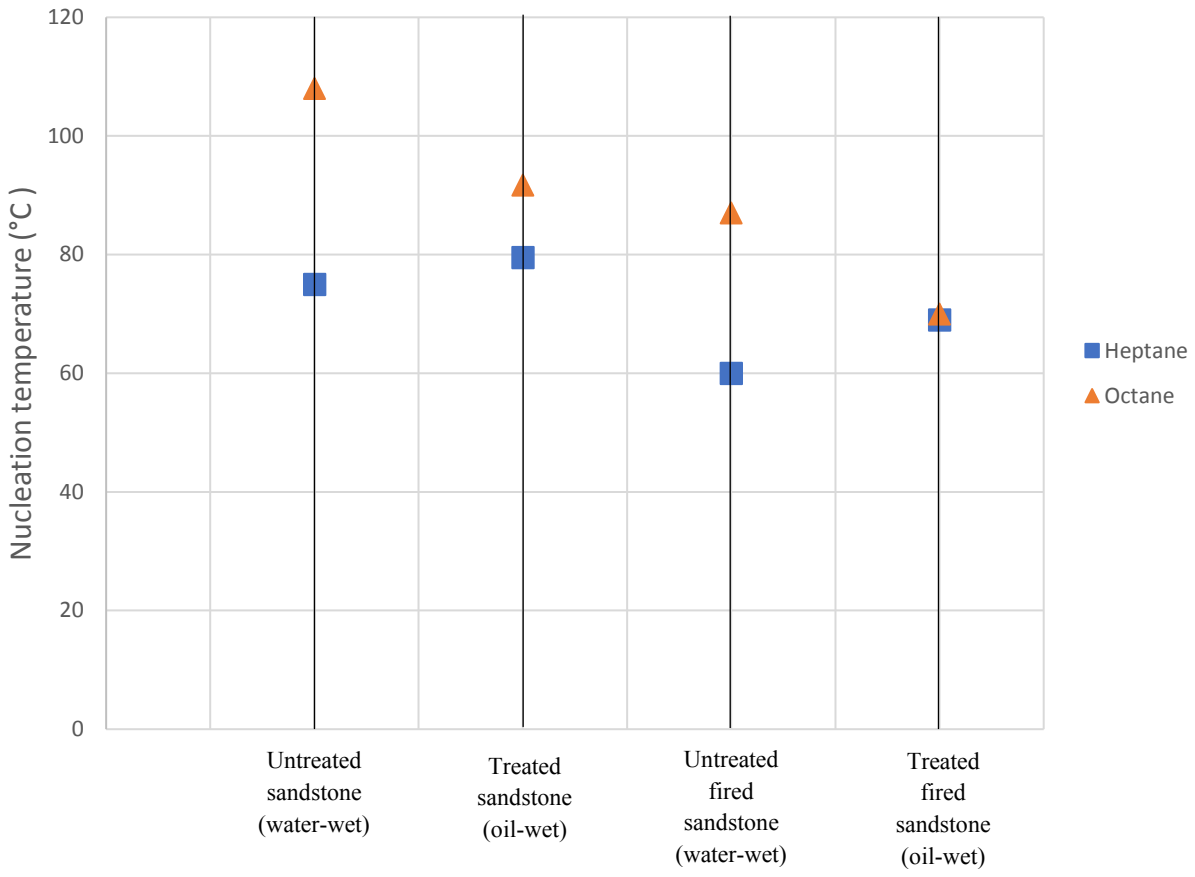

Figure 6-16: Measured phase-change temperatures of heptane and octane in unfired and fired sandstone before and after wettability alteration.

6.13 Conclusions and Remarks

The existence of nanopores in reservoir rocks leads the phase-change temperatures to shift from their bulk values. Despite the low volume percentage (per sample weight) of micropores ($\leq$ 2 nm) and mesopores (2-5 nm) in permeable rocks (e.g., Berea sandstone and Indiana limestone), the minor occurrence of shifted vaporization temperature has considerable impact in reservoir-scale scenarios that could affect the prediction of fluids' dynamics in the porous media.

In this study, boiling points of heptane and octane were measured in the permeable rocks and tight sandstone, then, compared with the computed boiling points, obtained by the Thomson equation. Additionally, the investigation covered the effect of medium wettability and solvent adsorption (caused by clays) on the nucleation temperature of solvents. Based on the pore size distribution

analysis, confined pores (< 1000 nm) occupied around 4.5% of total pore volume in Berea sandstone and Indiana limestone, whereas 38.2% of the tight sandstone pore volume was filled by pores smaller than 100 nm.

Due to the presence of nanopores, shifted boiling points of heptane and octane were observed in sandstone, limestone, and tight sandstone. On average, the boiling temperature of heptane in the rocks was 17% (3.7% in Kelvin unit) lower than its normal boiling point (96℃), meanwhile, on average, octane's boiling temperature was 10% (2.1% in Kelvin unit) lower than its bulk boiling point (125℃). Such shifted vaporizations could have a larger impact on PVT and phase-change modeling in reservoir-scale applications. As shown in Figure 6-13, the average measured boiling temperature of heptane in the rocks was nearly 15% (3.2% in Kelvin unit) lower than the calculated boiling point by the Thomson equation, and the observed boiling temperature of octane was closely 9% (1.9% in Kelvin unit) lower than the computed boiling point.

Altering the wettability of Berea sandstone from its natural water-wet behaviour to oil-wet changed the average nucleation temperature of heptane by 6% (1.3% in Kelvin unit) more than its nucleation temperature (75℃) before wettability alteration. In the case of octane, shifting the rock wettability to oil-wet reduced the phase-change temperature by 15% (0.8% in Kelvin unit), compared to octane's nucleation temperature (108℃) in untreated sandstone. Based on the imbibition and nitrogen adsorption analysis, breaking the clay structure reduced the fluid adsorption in Berea sandstone. Decreasing the solvent adsorption in Berea sandstone significantly lowered the nucleation temperatures, due to the reduced surface-molecule interaction. On average, the nucleation temperatures of heptane and octane in fired sandstone were 20% (4.3% in Kelvin unit) less than what were observed with unfired sandstone and approximately 30% (6.5% in Kelvin unit) lower than their normal boiling points.

As observed with unfired sandstone, wettability alteration had an effect on the nucleation temperature of heptane and octane in fired sandstone. Changing the wettability of fired sandstone to oil-wet changed the average nucleation temperature of heptane by 15% (3.2% in Kelvin unit) more than its nucleation temperature (60℃) before wettability alteration. In case of octane, altering the rock wettability to oil-wet lowered the phase-change temperature by 20% (4.3% in Kelvin unit), comparing with octane's nucleation temperature (87℃) in untreated fired sandstone. Our prior studies (Al-Kindi and Babadagli 2019b, 2020) found that pore size in microfluidic chips

could alter the boiling point of solvents by nearly 20% (4.3% in Kelvin unit) and 10-20% (2.1 - 4.3% in Kelvin unit) in rocks including the extended tight rocks, like shale. In nano porous media (< 1000 nm), Altering the liquid adsorption has a larger impact on nucleation temperatures, comparing with the medium wettability alteration, which makes the molecule-solid interaction more dominant in influencing the phase-change behaviour of fluids than surface wettability.

6.14 Nomenclature

EOR: Enhanced Oil Recovery

TEOR: Thermal Enhanced Oil Recovery

CO2: Carbon dioxide

SEOR: Steam Enhanced Oil Recovery

EOS: Equation-of-State

PVT: Pressure-Volume-Temperature

ΔP: pressure difference

γ: surface tension

$R1$ & $R2$: radii of curvature

θ: contact angle

r: tube or pore radius

V_m: liquid molar volume

r: droplet radius

R: universal gas constant

T: temperature

P_{Bulk}: vapor pressure at flat surface

P_r: vapor pressure at curved interface

T_r: Boiling temperature of confined liquid

T_∞: Bulk boiling temperature

ΔH_{vap}: heat of vaporization

P: pressure

$\bar{V}$: molar volume

md: millidarcies

℃: Degree Celsius

7 Chapter 7: Revisiting Kelvin Equation for Accurate Modeling of Pore Scale Thermodynamics of Different Solvent Gases

A version of this chapter was presented and published as a conference paper at the SPE Western Regional Meeting held in San Jose, California, 23-26 April 2019 (SPE-195319-MS).

7.1 Abstract

Understanding the thermodynamics of fluids in capillary media is essential to achieve a precise modeling of EOR applications such as hybrid (with thermal methods) and sole solvent injection processes. The theoretically derived classical Kelvin equation describes the influence of surface tension, contact angle, pore radius, and temperature on vapour pressures. The deviation of propane vapour and condensation pressures from this equation was determined experimentally by measuring them on capillary/porous media with various sizes and types, namely Hele-Shaw glass cells, silica-glass microfluidic chips, and rock samples. The experimental data were also compared with the vapour pressures obtained for the bulk conditions. The gap thicknesses in Hele-Shaw cells were 0.13 and 0.04 mm whereas the medium size in micromodels was ranging from 142 to 1μm. The results showed that vapour and condensation pressures of propane recorded in the experiments were comparatively close to the bulk vaporization pressure and calculated vapour pressures from the Kelvin equation. Conversely, vapour pressures obtained from rock samples were noticeably lower than bulk vapour pressures.

7.2 Introduction

Using solvents in heavy-oil recovery has become a common thought since injecting said chemicals solely or as co-injectant with steam can improve oil recoveries. Different types of hydrocarbon and non-hydrocarbon solvents were considered previously due to their effective diffusion capabilities into crude oil and bitumen. Nasr et al. (2003) investigated the impact of co-injecting hydrocarbon solvents (propane to heptane range suggesting hexane as the optimal one) with steam in heavy oil and bitumen recovery during steam assisted gravity drainage (SAGD) operations. The research generally focused on improving oil rate, enhancing oil steam ratio, reducing required energy, and dropping water consumption. The selection criteria of solvents was performed based on vaporization and condensation temperatures, and how close they are to the water vaporization and steam condensation temperatures. Léauté and Carey (2007) studied the impact of C5+ condensate on bitumen recovery in cyclic steam stimulation (CSS) process for the Cold Lake field.

The application was inspected in the field as a pilot project through eight wells that were under CSS operation. It was reported that adding 6% volume fraction of diluent into steam during CSS enhanced the well performance and results were above the expectations.

Utilizing hydrocarbon solvents in heavy-oil recovery applications has a significant limitation due to operational cost. Injecting large volumes of solvents could be expensive and uneconomical in many circumstances depending on oil prices. To minimize the overall application cost, Bahlani and Babadagli (2009) introduced the idea of Steam Over Solvent Injection in Fractured Reservoirs (SOS-FR) to retrieve the trapped solvents in the reservoirs thermally by steam or hot-water injection. The process consists of three main stages: (1) injecting steam to condition the oil by reducing its viscosity, (2) injecting solvent to recover remaining oil through chemical diffusion and gravity segregation, and (3) injecting steam or hot water to retrieve the trapped solvents with remaining oil. According to experimental observations and numerical study, trapped solvents could be recovered up to 80-85% with 85-90% of the original oil in place.

The phase-change is controlled not only by pressure and temperature but also capillary and interfacial characteristics as porous media becomes tighter. This phenomenon leads the vapour pressures and boiling points to deviate from the bulk conditions and this process is controlled by the size of the pores and wettability conditions. To model hybrid or sole-solvent injection precisely under non-isobaric and non-isothermal conditions, actual phase-change behaviours of fluids in various porous media should be well understood through experimental and theoretical investigations.

Studying vapour pressure alteration of propane in extended tight rocks, such as shales, was experimentally performed by Zhong et al. (2018) by using nanofluidic chips featured with silicon nanochannels. The chips had various sizes of channels ranging from 20 μm to 8 nm. Condensation of propane within the confined channels was observed under a range of pressure ($\sim 0.6 - 2.3\ MPa$) and temperature ($286.15 - 339.15\ K$). The study also aimed to validate theoretical modelling (Kelvin equation) by comparing calculated results with the experimental outcomes. Vapour pressures, obtained from the Kelvin equation, were closely matching the experimental outcomes even in extended confined channels ($\sim 8\ nm$) making the equation applicable in modelling capillary condensation. Vapour pressure alteration of water in nanochannels was inspected by Tsukahara et al. (2012) using a nanoscale chip. The nanofluidic chip consisted of

microchannels (10 μm deep) and nanoscale channels with a depth range of 90-370 nm. The experiments demonstrated the reduction of water vapour pressure with the decrease of medium size. Additionally, computed vapour pressures from the Kelvin equation were relatively similar to those observed in the experiment; therefore, applicability of the Kelvin equation in predicting vapour pressures within extreme confined media was still valid.

The curvature effect on fluids increases as capillary size becomes tighter due to the change of interfacial properties such as surface tension and pressure difference at the liquid-gas interface. Several investigations were performed to understand the deviation of phase-change behaviour in extreme tight channels featured with nanoscale pore throats (Bao et al. 2017). The majority of these studies were conducted using microfluidic and nanofluidic chips made of silica glass. Per the Kelvin equation, the alteration of vapour pressure in confined pores depends on capillary size, surface tension, and contact angle between the solid surface and liquid. These liquid-solid properties, including molecular absorption of the surface, might change noticeably when the solid material is altered. This paper aims to study the phase-change behaviour of propane in various capillary media starting from Hele-Shaw glass cells to real core samples with different permeabilities, porosities, and pore throat sizes. Moreover, microfluidic chips with uniform and non-uniform properties (grain and pore throat sizes) representing various pore sizes were utilized to obtain a clearer picture of propane phase alteration in porous media using visual support. One of the main targets in this investigation was to inspect the effect of surface properties on propane's vaporization and condensation in confined spaces.

Comparative analysis of the outcomes obtained from glass microfluidic experiments and rock samples provided new insight into the pore scale thermodynamics of the solvents to be used in further computational studies to improve the accuracy of performance prediction.

7.3 Statement of the Problem and Objectives

In heavy-oil recovery applications, injecting solvents with or without steam under variable pressure and temperature could lead to considerable phase alteration. The thermodynamics of injected fluids in porous media play a critical role in controlling the performance of hybrid and cold-solvent injection. Phase alteration during the process could control the distribution of injected

fluids in the reservoir as well as their flow dynamics and eventually, oil recovery. Similarly, solvent retrieval process (SRP) highly depends on solvents thermodynamics in the reservoir. As a result, comprehending the phase-change behaviour of injected fluids is important in choosing the appropriate application conditions (such as pressure and temperature) while maximizing oil recovery and solvent retrieval. In fact, SRP is a critical part of the whole process and has an impact in minimizing the overall operational cost of hybrid (steam-solvent) applications.

The operation becomes more complex and challenging while dealing with heterogeneous reservoirs (fractured carbonates or layered sandstones). Recovering the trapped solvents, in such cases, can be possible by vaporizing them thermally or through pressure depletion process to relocate the trapped solvents from low to high permeability zones. Another common application is unconventional reservoirs where solvents are injected (usually under isothermal conditions) after fracking. The phase change mechanism should be well understood during this process as it directly affects the oil recovery (during injection) and solvent retrieval (during depletion) and the phase behaviour in capillary medium is different from the bulk conditions of which are applied in classical PVT tests and studies.

A similar phenomenon is encountered in oil (heavy-oil, light, oil, and condensate) recovery from unconventional (shales, tight sands) reservoirs in which the most common application suggested is solvent gas (hydrocarbon gases or CO_2). The gases injected (in the form of huff-and-puff) after fracking diffuse into rock matrix and reproduce with oil during the depletion stage. The recovery of oil and solvent retrieval are both controlled by the thermodynamics (mainly the phase change of the solvent and oil). It is well known that the phase change conditions in capillary medium differ from the bulk conditions and this cannot be captured easily using standard PVT analyses.

Per the Young-Laplace equation ($\Delta P = 2\gamma/r$), the curvature radius (r) has an effect on surface tension (γ) when it decreases to microscales or nanoscales (Tsukahara et al., 2012). The Kelvin equation demonstrates the relationship between vapour pressures in capillary and bulk conditions ($P_r = P_\infty \exp\left[\frac{-2\,\sigma\,v^L}{r\,R\,T}\right]$). According to this equation, vapour pressure of fluids becomes lower than those in bulk scenarios when medium sizes are tighter due to the change of surface tension, pressure drop at the interface, and contact angle. As a result, fluids in highly confined spaces tend to have higher viscosities and capillary pressures. This phenomenon is highly critical in modelling

hybrid (with thermal methods) or solvent retrieval applications since the phase-change of injected and originally in place fluids plays an important part in controlling the efficiency of these applications.

The objective of this paper was to experimentally investigate the vapour pressure of propane in different capillary models and compare the outcomes with computed vapour pressures from the Kelvin equation. The vapour and condensation pressures of propane were measured by using Hele-Shaw cells, capillary tubes, and homogenous/heterogeneous micromodels with various pore throat and grain sizes. As a more realistic porous media representation, rock samples such as sandstones, carbonates, and shales were also considered and the vapour pressure of propane was measured in those samples to obtain a wider perspective of how vaporization and condensation of propane occur in various capillary media with dissimilar surface properties and porous structures. Furthermore, the results with rock samples were compared with outcomes obtained from Hele-Shaw and micromodel glass chips.

7.4 Background

Kelvin and Thomson equations are theoretical modelling approaches that describe the influence of curvature radius at vapour-liquid interface on saturation pressures and boiling points. The Kelvin equation can be expressed as

$$P_r = P_\infty \exp\left[\frac{-2\,\sigma\,v^L}{r\,R\,T}\right]$$

where T is temperature, R is universal gas constant, r is droplet (or capillary) radius, v^L is molar volume of the liquid, σ is surface tension, P_∞ is vapor pressure at flat surface, and P_r is vapor pressure at curved interface. When the medium is liquid wet (concave curvature), vapour pressure of the liquid reduces with the reduction of pore size which leads the vapour pressure at confined spaces (P_r) to be lower than the vapour pressure at the flat surface (P_∞). Similarly, liquids in tight (microscale) or extended confined (nanoscale) media sizes tend to have boiling points lower than their normal boiling temperatures at bulk conditions owing to the change of pressure drop at the

gas-liquid interface and surface tension. The Thomson equation defines this phenomenon with the following equation

$$T_r = T_\infty \exp\left[-\frac{2\,\sigma\,v^L}{r\,\Delta H_{vap}}\right]$$

where ΔH_{vap} is heat of vaporization of liquid, v^L is molar volume of liquid, r is droplet (or pore radius), σ is liquid surface tension, T_∞ is temperature at bulk medium, and T_r is temperature at porous medium. In prior works (Al-Kindi and Babadagli, 2018, 2017), boiling temperatures of water, heptane, decane, and naphtha were investigated through visual experiments in tight spaces with various medium sizes and porous structures. The results were then compared with calculated boiling points by the Thomson equation. It was found that boiling points of liquids could be reduced by pore size even if it is 0.1 mm or less unlike the vaporization temperatures computed by the equation. **Figure 7-1** shows boiling points of heptane, obtained from different experiments and the Thomson equation, at various pore sizes. The experiments in previous works were conducted under atmospheric pressure (≈1 atm). The investigation in this paper focused on observing the phase-alteration of propane under atmospheric temperature (≈ 21 °C) at different capillary medium sizes and compares our observations with the Kelvin equation.

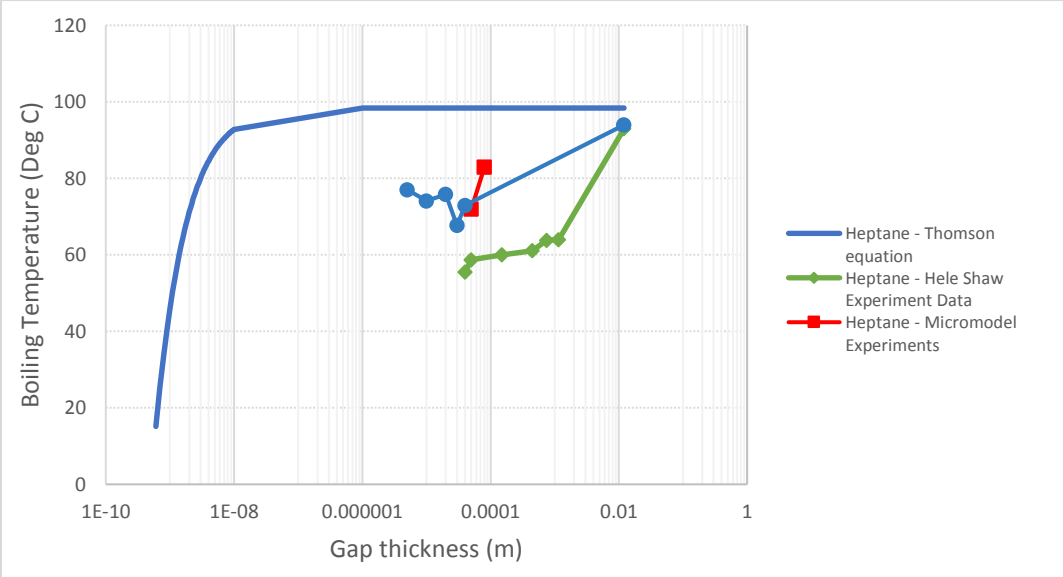

Figure 7-1: Boiling temperature of heptane at different pore sizes (Al-Kindi and Babadagli, 2018).

7.5 Experimental Work

Observations of propane's vaporisation and condensation pressures were performed by using several glass chips and rock samples. The experiments were initiated with Hele-Shaw glass cells of 0.13 and 0.04 mm gap thicknesses. Although the Hele-Shaw cells represent only a simple tight system with smooth and liquid-wet inner surface, they can be useful in providing a clear visualization of bubbles and drops generation of fluids in different pressures which could be difficult to visualize in microfluidic chips. Then, vapour and saturation pressures of propane were inspected in several types of micromodels with uniform and non-uniform properties such as porosity, permeability, porous structure, and pore throat/grain size. To visualize the phase change of propane in more realistic porous media, vapour pressure alteration was examined in sandstone, limestone, and shale rock samples. Using real rock samples provided an advantage of testing the impact of surface characteristics and porous media structure on vapour pressure.

7.5.1 Hele-Shaw Glass Cells

Hele-Shaw cells basically consist of a pair of thin rectangular glass plates with an empty gap in between. The glass cells were made with two main gap thicknesses: (1) 0.04 mm and (2) 0.13 mm. Mainly, the purpose of starting our investigation with glass cells was to get a clear exposure of propane's drops creation in pressure build-up stage and propane's bubbles formation in pressure depletion stage under constant temperature ($\approx 21℃$). In all Hele-Shaw cells, the inner glass surfaces were propane wet during condensation. **Figure 7-2** presents the Hele-Shaw glass cell used in our experiments.

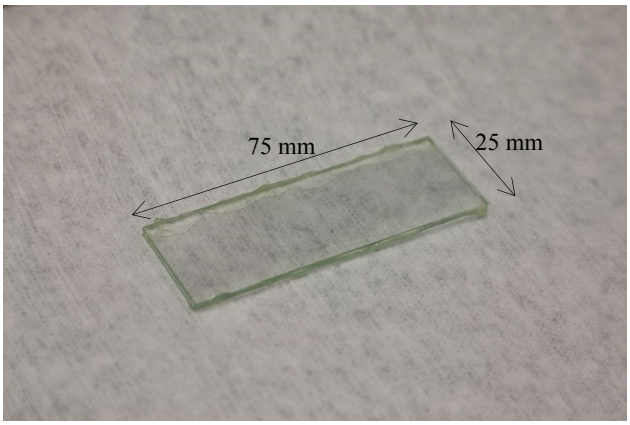

Figure 7-2: Hele-Shaw glass cell (0.13 mm gap thickness).

Experimental setup. The setup consisted of a DSLR camera (Canon 7D), pressure and temperature measurement device (National Instruments), LED light source, thermocouple, pressure transducer, ISCO syringe pump, and pressure windowed cell. **Figure 7-3** illustrates some of the equipment used in experiments with Hele-Shaw cells.

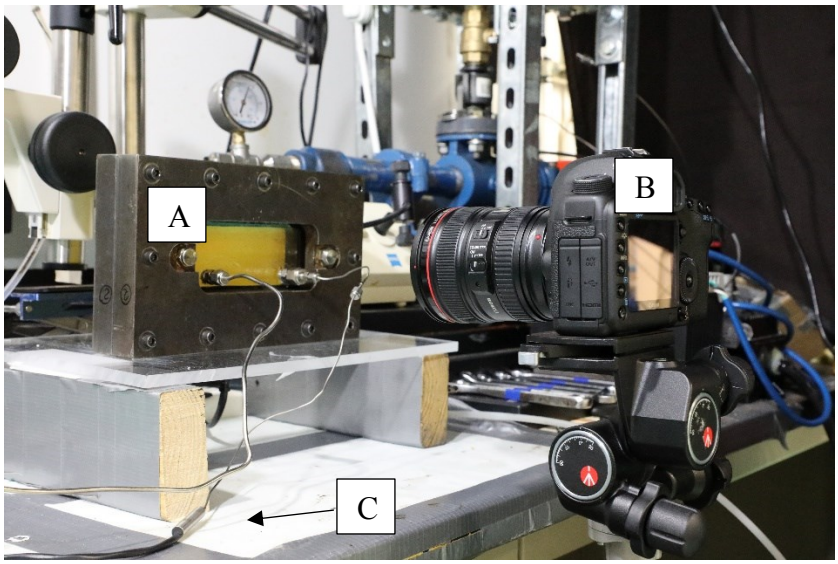

Figure 7-3: Experimental setup: (A) pressure windowed cell, (B) DSLR camera and (C) thermocouple.

Procedure. To pressurize the Hele-Shaw glass models, they were placed in the pressure windowed cell. The pressure cell was featured with plexi-glass windows which allowed a clear visualization through the cell. By using an ISCO syringe pump, the cell was pressurized from a starting pressure ($70\ psi$) to a pressure above the propane vapour pressure in Edmonton (Alberta, Canada) which

was approximately 115 psi in atmospheric temperature. Both the Hele-Shaw glass cell and pressure windowed cell were vacuumed for a period of time to remove the trapped air in the system. We aimed to study both the vaporization and condensation of propane; hence, the pump was programmed to build up the pressure in the cell at a rate of 5-7 psi/min within a duration of 10 min. Likewise, to achieve the propane vaporization and determine the vapour pressure, the pump was set to deplete the pressure at a rate of 5-7 psi/min within the same duration. Meanwhile, a continuous video was taken with the DSLR camera during the process. Additionally, the pressure and temperature in the pressure cell were recorded constantly by the measurement device every two seconds.

Results and discussion. As mentioned previously, Hele-Shaw cells provide a clearer visualization of the nucleation stage unlike microfluidic chips and rocks. Using the glass cells could bring several limitations (flat liquid-solid interface) with it which might not act as a good representation of real reservoir conditions. However, they could be useful in illustrating the phenomena under the simplest conditions. It was expected that the vapour and condensation pressure of propane in the glass cell would be relatively close to bulk pressures since their gap thicknesses were not tight enough to create effective changes in surface tension (γ) and contact angle ($\cos\theta$). During the condensation process, propane went through two main stages: (1) dew point and (2) considerable phase change. In vaporization process, two stages were considered: (1) bubble point and (2) quick formation of bubbles. In the Hele-Shaw cell with 0.04 mm gap thickness, the first propane liquid drops took place at 118.5 psi as shown in **Figure 7-4**. A considerable phase change initiated in the cell at a pressure of 121.2 psi (**Figure 7-5**). In the pressure depletion stage, the first propane bubbles generation took place at 116.6 psi as illustrated in **Figure 7-6**. A quick formation of propane bubbles began in the glass cell at 113.7 psi (**Figure 7-7**). **Figure 7-8** and 7-**9** show the pressures at each stage in 0.04 mm and 0.13 mm gap spaces during pressure build-up and depletion processes.

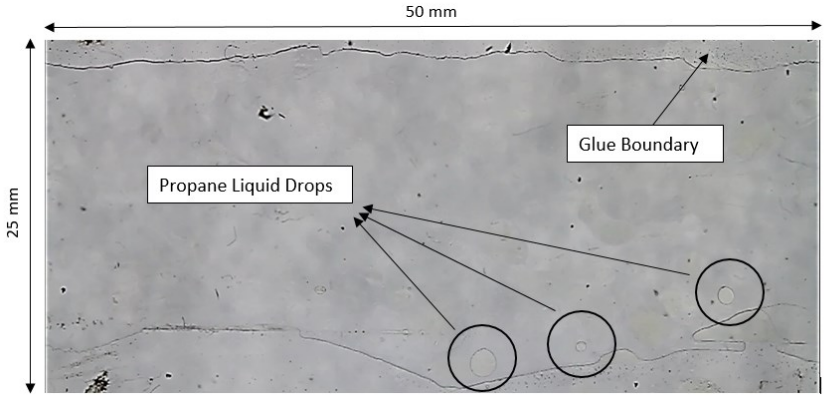

Figure 7-4: Dew point stage at 118.5 psi.

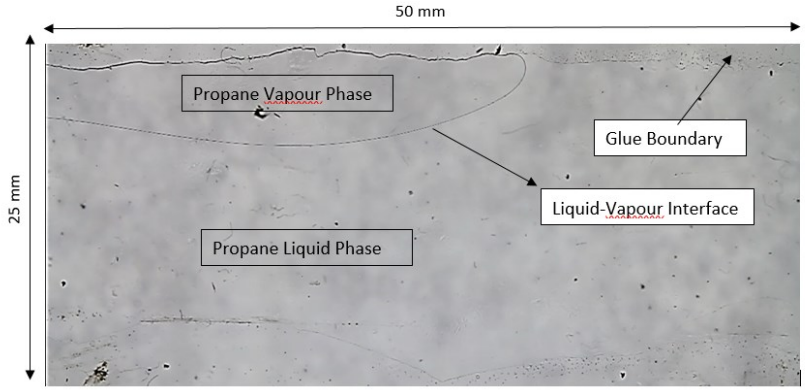

Figure 7-5: Considerable phase change at 121.2 psi.

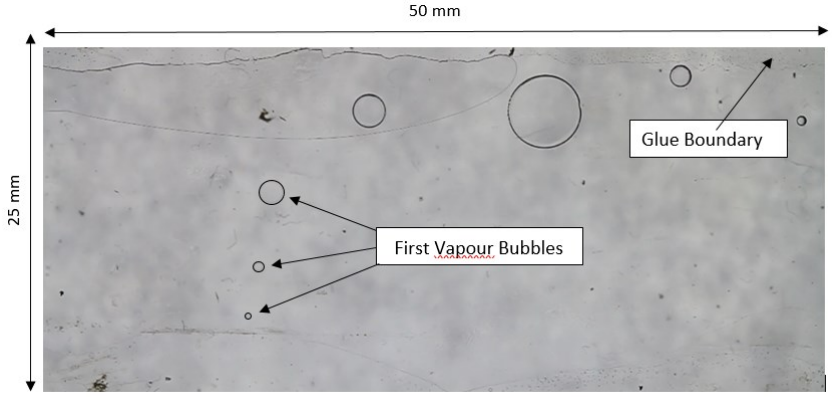

Figure 7-6: Bubble point stage at 116.6 psi.

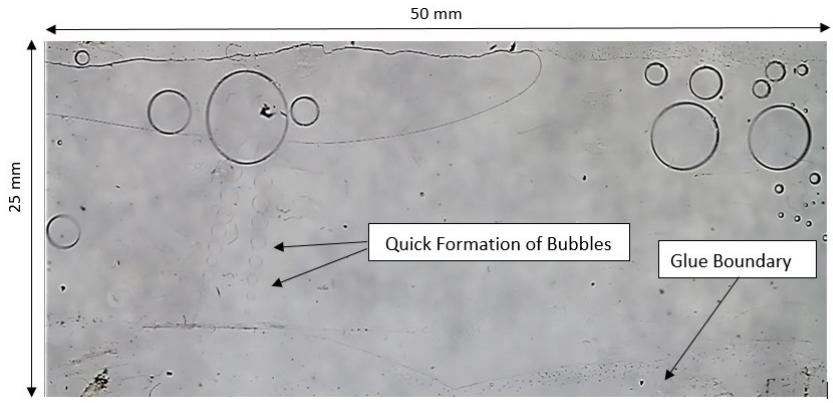

Figure 7-7: Quick formation of bubbles stage at 113.7 psi.

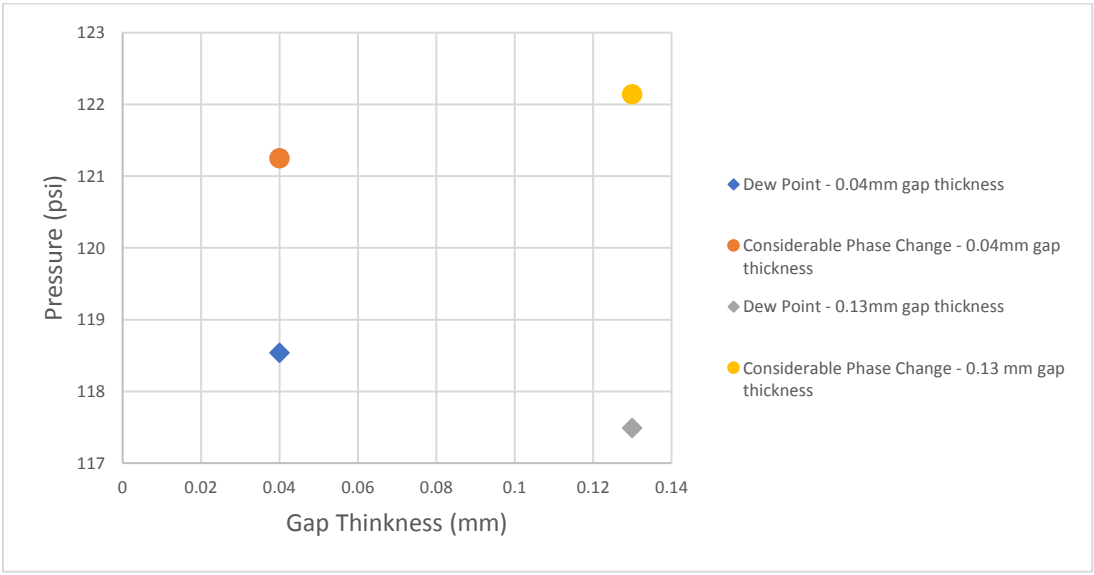

Figure 7-8: Pressure at each stage in 0.04 and 0.13 mm gap thickness during pressure build-up process.

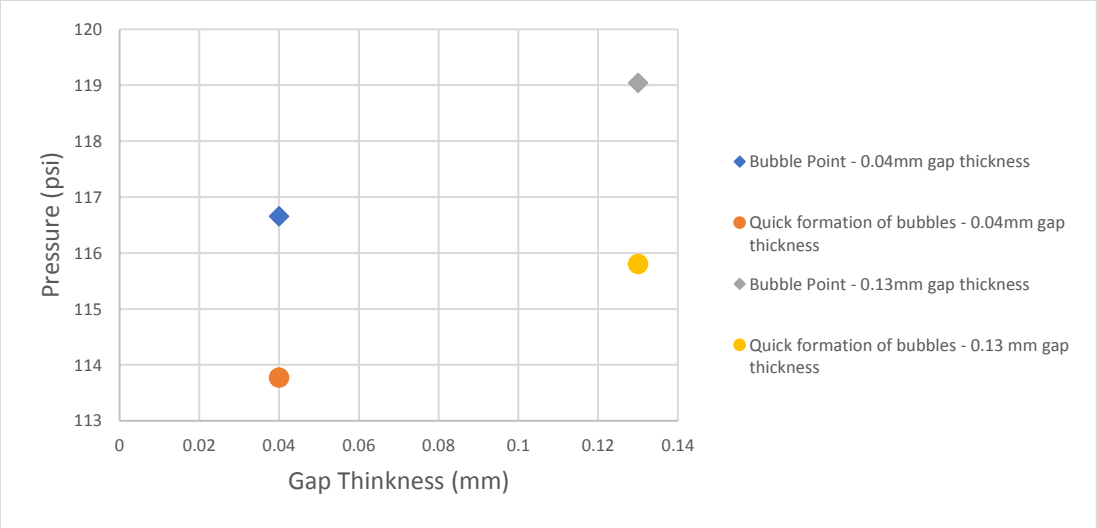

Figure 7-9: Pressure at each stage in 0.04 and 0.13 mm gap thickness during pressure depletion process.

7.5.2 Microfluidic Chips

Compared to Hele-Shaw glass cells, micromodels offer a better representation of porous media in terms of size and shape of the pores. Three categories of microfluidic chips were used: (a) capillary tube model (**Figure 7-10a**), (b) homogenous micro model (**Figure 7-10b**) and (c) heterogeneous micro model (**Fig 7-10c**). Capillary tubes represented straight silica-glass pore throats with various sizes ranging from 40 to 1 μm. Homogenous micromodels were designed with uniform grain and pore throat sizes. In our experiments, two homogeneous models with different properties were utilized: (1) microfluidic model with uniform properties of 0.11 mm pore diameter and 0.01 mm pore throat and (2) model with uniform properties of 0.21 mm pore diameter and 0.01 mm pore throat. Heterogeneous microfluidic chip had a porous structure closer to real rocks with an average pore throat of 142.5 μm.

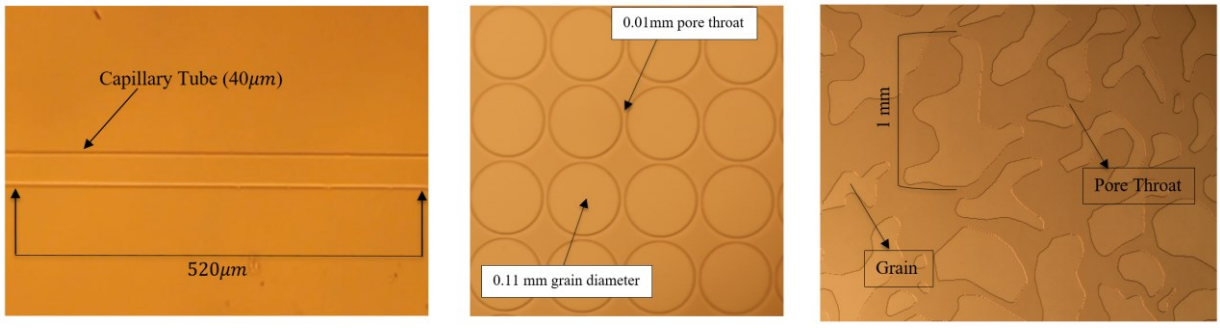

Figure 7-10 - (a): 40 µm capillary tube model; (b): Micromodel with uniform properties (0.11 mm pore diameter and 0.01 mm pore throat); (c): Micromodel with non-uniform properties.

Experimental setup. The setup consisted of a DSLR camera (Canon 7D), Zeiss Stemi 2000C microscope, pressure and temperature measurement device (National Instruments), LED light source, thermocouple, pressure transducer, ISCO syringe pump, and pressure windowed cell.

Procedure. The procedure of pressurizing the micromodels was similar to the Hele-Shaw experiments. The pressure rates in the pressure build-up and depletion process were the same as the rates used in previous experiments with glass cells (5-7 psi/min). The pressure windowed cell and microfluidic chips were vacuumed for one hour to remove the trapped air. All the experiments were performed entirely under atmospheric temperature (~21℃). A continuous recording of pressure and temperature was managed during the build-up and depletion processes.

Results and discussions. The micromodel experiments were initiated with capillary tube models featured with five sizes: (a) 40 μm, (b) 20 μm, (c) 10 μm, (d) 5 μm, and (e) 1 μm. Through capillary tube experiments, it was noticed that liquid propane wets the inner surfaces of the tubes at condensation pressures, which makes these models act as a propane-wet capillary media. In the 40 μm tube, propane started to condense at a pressure of 118.2 psi as shown in **Figure 7-11**. During pressure depletion process, vaporization of propane took place in the tube at 116.1 psi. **Table 7-1** shows the vaporization and condensation pressures of propane in various sizes of capillary tube during the build-up and depletion processes.

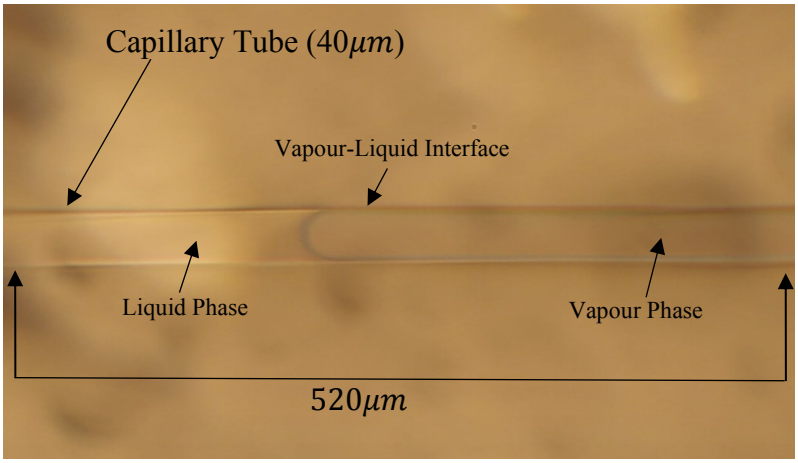

Figure 7-11: Propane condensation in 40 µm capillary tube.

Table 7-1: Vapour and saturation pressures at several capillary tube sizes.

	Vaporization pressure (psi)	Condensation pressure (psi)
40 μm Capillary tube	116.1	118.2
20 μm Capillary tube	113	121.3
10 μm Capillary tube	120.1	116.6
5 μm Capillary tube	116.1	123
1 μm Capillary tube	121.3	121.5

In microfluidic homogenous chips, phase-change pressures were relatively similar to those observed with capillary tube models. In the homogenous model (0.11 mm grain diameter and 0.01 mm pore throat), propane condensation began at 119 psi as illustrated in **Figure 7-12**. At a pressure of 115.3 psi, vapour pressure of propane was achieved in the micromodel. Comparably, propane condensation took place in the heterogonous microfluidic model at 119.1 psi (**Figure 7-13**). **Table 7-2** presents the propane vaporization and condensation pressures in homogenous and heterogonous models.

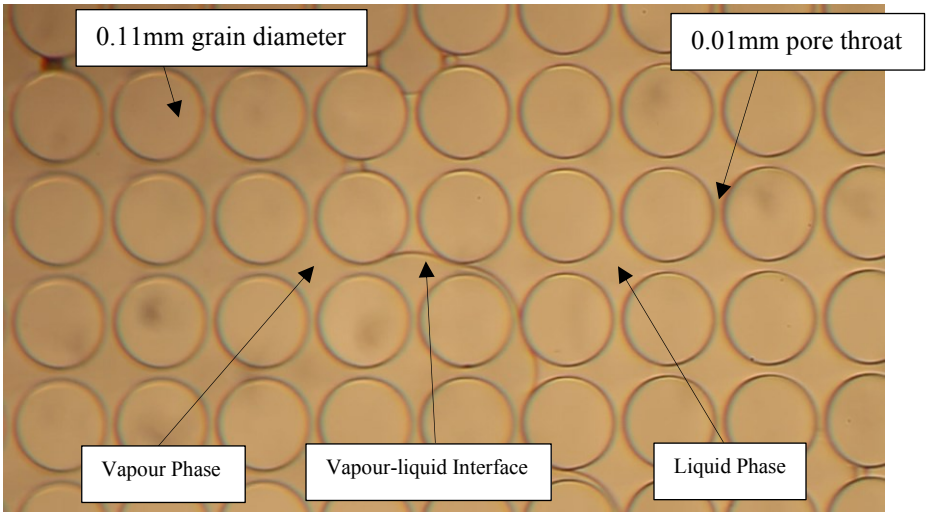

Figure 7-12: Propane condensation in homogenous micromodel (0.11 mm grain diameter and 0.01 mm pore throat).

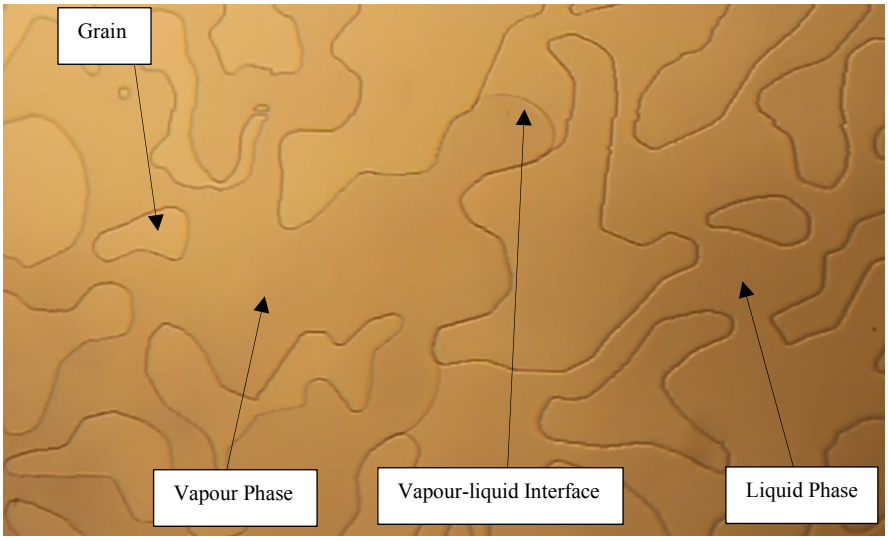

Figure 7-13: Propane condensation in heterogeneous micromodel (average pore throat size of 142.5 µm).

Table 7-2: Vapour and saturation pressures in homogenous and heterogonous microfluidic models.

	Vaporization pressure (psi)	Condensation pressure (psi)
Homogenous model (0.11 mm grain diameter and 0.01 mm pore throat)	115.3	119
Homogenous model (0.21 mm grain diameter and 0.01 mm pore throat)	117	118
Heterogeneous model (average pore throat size of 142.7 μm)	118.8	119.1

7.5.3 Rock Sample Experiments

To observe a more realistic observation of propane phase-change behavior in capillary (porous) media, rock samples with dissimilar properties were used. **Figure 7-14a** to **7-14c** show the sandstone, limestone, and shale samples before the saturation process. **Table 7-3** illustrates permeabilites and average pore throat sizes of the core samples used in the experiments. Due to their different surface properties and pore structures, it was expected that vapour and condensation pressures might alter comparing with those observed in Hele-Shaw cells and microfluidic silica-glass chips.

(a) (b) (c)

Figure 7-14: (a): Limestone core sample; (b): Sandstone core sample; (c): Shale core sample.

Table 7-3: Permeability range of used rock samples.

	Limestone	Sandstone	Shale
Permeability Range (mD)	27 - 33	274	<0.01
Average Pore Throat size (μm)	7.68	22.8	0.052

Experimental Setup. The setup consisted of a DSLR camera (Canon 7D), pressure and temperature measurement device (National Instruments), LED light source, thermocouple, pressure transducer, ISCO syringe pump, and pressure glass vessel. **Figure 7-15** illustrates some of the equipment used in experiments with rock samples.

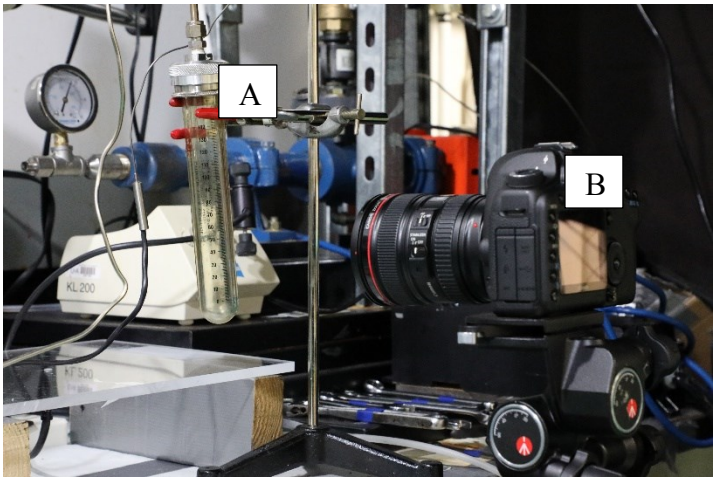

Figure 7-15: Experimental setup: (A) pressure glass vessel and (B) DSLR camera.

Procedure. In rock sample experiments, only a single pressure depletion process was performed for each rock type. To eliminate the trapped air in the rock samples, the whole system was kept under vacuum pressure for one day. After that, the glass pressure vessel, including the core sample, was pressurized with propane until the condensation pressure was achieved. The system was left under pressure ($\sim 125\ psi$) for one day to ensure a maximum saturation of liquid propane in the rock. While performing the experiments, the vessel pressure was depleted with a rate of 5-7

psi/min. Both propane pressure and temperature were recorded continuously during the process every two seconds along with the video which was taken with the DSLR camera.

Results and discussion. Propane in the rocks tended to vaporize at pressures lower than propane's vapour pressure at bulk conditions. For instance, in shale, propane started to change into gas phase at a pressure of 106.6 psi as presented in **Figure 7-16**. Similarly, vapour pressures in sandstone and limestone were 10% lower than those in bulk cases. **Table 7-4** shows the vapour pressure of propane in each rock type used in the experiments.

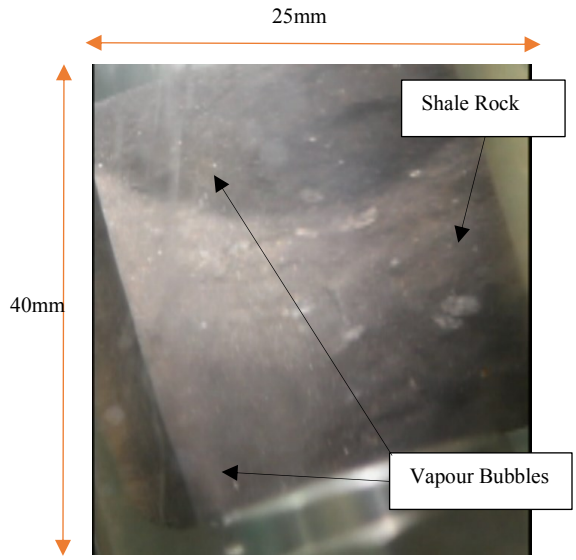

Figure 7-16: Propane vaporization in shale core sample.

Table 7-4: Propane vapour pressure in limestone, sandstone, and shale.

	Limestone	Sandstone	Shale
Vapour Pressure (psi)	104.8	103.2	106.6

7.6 Quantitative analysis

Per the Kelvin equation, vapour pressure could be altered by medium size if it is 100 *nm* or less. The vaporization pressure gets lower as the pore throat gets tighter in size. The bulk vapour and saturation pressures of propane were measured under lab conditions and phase-change, in both pressure build-up and depletion processes, of which took place at approximately 115 psi. In Hele-Shaw and microfluidic experiments, the recorded vapour and condensation pressures were relativity close to the phase-change pressures measured in bulk condition. However, with rock samples, the vapour pressures were noticed to be lower than those measured in bulk cases. **Figure 7-17** and **7-18** show the vapour and condensation pressures of propane measured in Hele-Shaw cells, micromodels, and rock samples.

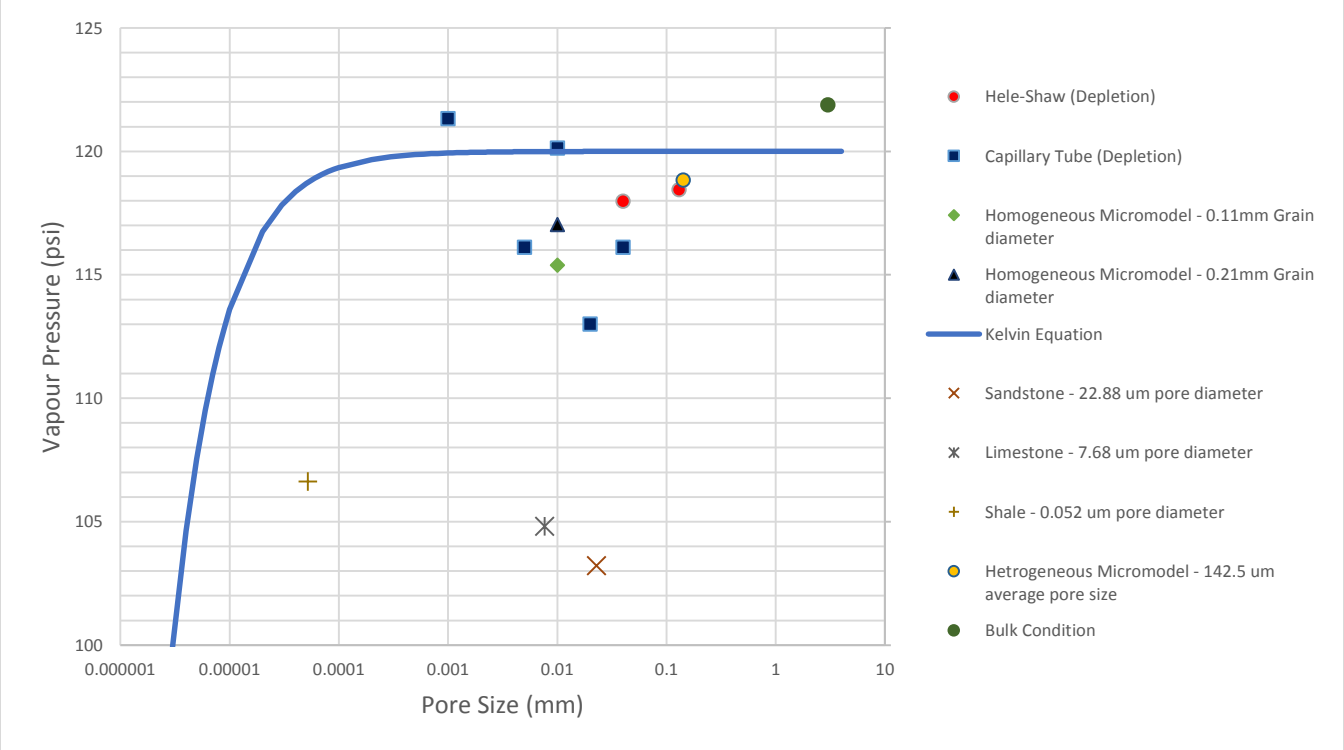

Figure 7-17: Vapour pressures of propane in Hele-Shaw cells, micromodels, and rock samples during the pressure depletion process.

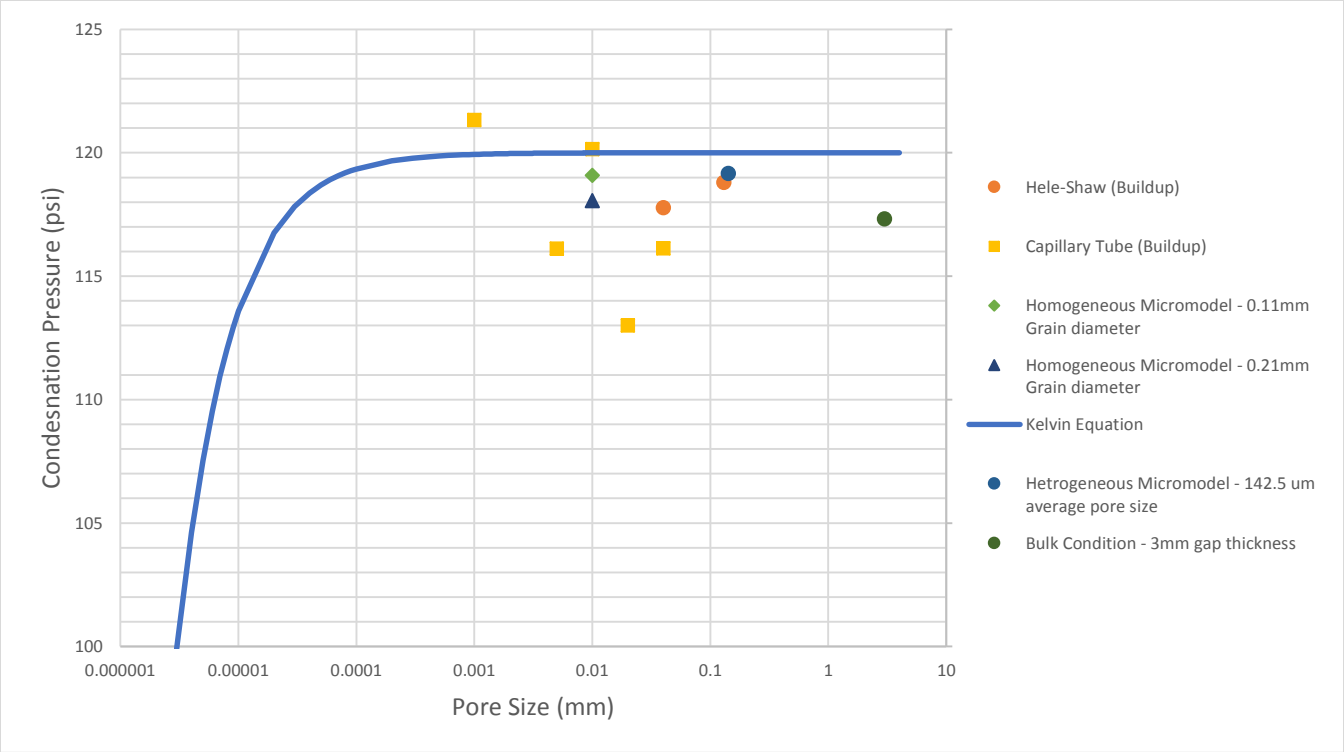

Figure 7-18: Saturation pressures of propane in Hele-Shaw cells, micromodels, and rock samples during the pressure build-up process.

7.7 Conclusions and Remarks

Surface characteristics of the medium including capillary size, surface tension, and curvature of vapour-liquid interface play an important role in controlling the thermodynamics and phase-alteration behaviour of liquids and gases. In order to achieve an accurate modelling of hybrid (with thermal) applications and sole solvent injection processes for oil recovery (and solvent retrieval), it is critical to understand the thermodynamics of the injected fluids (solvents) and originally-existed fluids (heavy-oil, oil, condensate) in capillary medium conditions. The main objective of this paper was to compare our experimental observations with calculated vapour pressures by the Kelvin equation. Condensation and vapour pressures of propane were investigated in capillary/porous media by using Hele-Shaw glass cells, microfluidic silica-glass chips, and rock samples. The vaporization and condensation pressures, measured at bulk condition, were considered as a benchmark and compared with phase-change pressures obtained in the experiments. Vapour and saturation pressures measured with Hele-Shaw cells and microfluidic

chips were comparable with those measured at bulk conditions and computed by the Kelvin equation. Nonetheless, propane vaporized in rock samples at pressures lower than the bulk vapour pressure. The phenomena of phase alteration of propane in rocks can be explained by performing further investigations in the change of interfacial tension and contact angle as well as the effect of rock characteristics (pore structures, clay contents, etc.) on surface absorption.

7.8 Nomenclature

EOR – Enhanced Oil Recovery

SOS-FR - Steam-Over-Solvents in Fractured Reservoir

CSS - Cyclic Steam Stimulation

SRP – Solvent Retrieval Process

v^L: liquid molar volume $[m^3/mol]$

r: droplet radius $[m]$

R: universal gas constant $\left[\frac{J}{K\ mol}\right]$

T: temperature $[K]$

P_∞: vapor pressure at flat surface $[Pa]$

P_r: vapor pressure at curved interface $[Pa]$

T_r: temperature at porous medium $[K]$

T_∞: temperature at bulk medium $[K]$

ΔH_{vap}: heat of vaporization $[J/mol]$

8 Chapter 8: Revisiting Kelvin Equation and Peng-Robinson Equation-of-State for Accurate Modeling of Hydrocarbon Phase Behavior in Nano Capillaries

A version of this chapter was published in Scientific Reports, 2021, **11**(1): 6573.

8.1 Abstract

The thermodynamics of fluids in confined (capillary) media is different from the bulk conditions due to the effects of the surface tension, wettability, and pore radius as described by the classical Kelvin equation. This study provides experimental data showing the deviation of propane vapour pressures in capillary media from the bulk conditions. Comparisons were also made with the vapour pressures calculated by the Peng-Robinson equation-of-state (PR-EOS). While the propane vapour pressures measured using synthetic capillary medium models (Hele-Shaw cells and microfluidic chips) were comparable with those measured at bulk conditions, the measured vapour pressures in the rock samples (sandstone, limestone, tight sandstone, and shale) were 15% (on average) less than those modelled by PR-EOS.

8.2 Introduction

Steam injection is known as one of the traditional methods used to increase heavy-oil recovery by effectively lowering the oil viscosity via raising its temperature. The major drawback of steam injection is the massive energy required to heat the matrix, which usually acts as an energy sink (Al-Bahlani and Babadagli 2011). Such a limitation causes steam-injection applications to be highly expensive projects. This issue has encouraged engineers and researchers to study other alternatives to enhance the mobility of heavy oil in porous matrixes. Using solvents in heavy-oil recovery has become a common thought, since injecting chemicals solely or as co-injectant with steam can improve oil recoveries. Different types of hydrocarbon and non-hydrocarbon solvents were considered previously due to their effective diffusion capabilities into crude oil and bitumen. The diffusion of solvents into the heavy oil results in a reduction of oil viscosity which makes it flow easier within the rock porous media.

Nasr et al. (2003) investigated the impact of co-injecting hydrocarbon solvents (propane to heptane range suggesting hexane as the optimal one) with steam in heavy oil and bitumen recovery during steam assisted gravity drainage (SAGD) operations. The research generally focused on improving oil rate, enhancing the oil steam ratio, reducing required energy, and dropping water consumption. The selection criteria of solvents was performed based on vaporization and condensation temperatures, and how close they were to the water vaporization and steam condensation

temperatures. Léauté and Carey (2007) studied the impact of C5+ condensate on bitumen recovery in the cyclic steam stimulation (CSS) process for the Cold Lake field. The application was inspected in the field as a pilot project through eight wells under CSS operation. It was reported that adding 6% volume fraction of diluent into steam during CSS enhanced the well performance and results were above the researcher expectations.

Utilizing hydrocarbon solvents in heavy-oil recovery applications has a significant limitation due to operational cost. Injecting large volumes of solvents could be expensive and uneconomical in many circumstances, depending on oil prices. To minimize the overall application cost, Al-Bahlani and Babadagli (2009) introduced the idea of Steam-Over-Solvent in Fractured Reservoirs (SOS-FR) to retrieve the trapped solvents in the reservoirs thermally by either steam or hot-water injection. The process consists of three main stages: (1) injecting steam to condition the oil by reducing its viscosity, (2) injecting solvent to recover remaining oil through chemical diffusion and gravity segregation, and (3) injecting steam or hot water to retrieve the trapped solvents with remaining oil. According to experimental observations and numerical studies, trapped solvents could be recovered up to 80-85% with 85-90% of the original oil in place.

In tight matrixes, such as shale and tight sandstone reservoirs, injecting steam could be inefficient in some cases, owing to the great restriction of steam propagation through the reservoir. This restriction leads to considerable volumes of the injected steam condensing in near-wellbore regions because of the ultra-low rock permeabilities. Since the water density is higher than the steam density, the mobility of the hot water through the reservoir is reduced by the tightness of the rocks thus resulting in an enormous heat loss before reaching the bottomhole of the well. Similarly, injecting liquid hydrocarbon solvents into tight reservoirs is a challenging application as the low permeability acts as a barrier against the movement of liquid solvents in the reservoir. Such phenomenon decreases the contact of solvents with the targeted oil; as a result, the reduction of oil viscosity, through solvent diffusion, would take place with only a small volume of the oil in the reservoir.

An alternative option is to inject gas solvents (methane, propane, CO_2), since their low densities and viscosities help in enhancing the propagation of solvents in the matrix. Propane injection has gained substantial attention over the last decade as one of the more efficient EOR applications to recover heavy oil in unconventional reservoirs. Favorable physical properties of propane have

made the usage effective and highly desirable for tight matrixes. According to Nagarajan et al. (2020), one of the significant benefits of injecting propane in the tight Bakken reservoirs was that it contacted greater volumes of oil in the reservoir due to its first-contact miscible pressure (650 psi) at the reservoir temperature. Thus, injecting the gas improved the mobility of larger oil volumes by reducing their viscosities.

The phase-change is controlled not only by pressure and temperature, but also capillary and interfacial characteristics as the porous media becomes tighter. This phenomenon leads the vapour pressures and boiling points to deviate from the bulk conditions and this process is controlled by the size of the pores and wettability conditions. To model hybrid or sole-solvent injection precisely under non-isobaric and non-isothermal conditions, actual phase-change behaviours of fluids in various porous media should be well understood through experimental and theoretical investigations. Studying vapour pressure alteration of propane in extended tight rocks, such as shales, was experimentally performed by Zhong et al. (2018) by using nanofluidic chips featured with silicon nanochannels. The chips had various sizes of channels ranging from 20 μm to 8 nm. Condensation of propane within the confined channels was observed under a range of pressure ($\sim 0.6 - 2.3\, MPa$) and temperature (286.15 - 339.15 K). The study also aimed to validate theoretical modelling (Kelvin equation) by comparing calculated results with the experimental outcomes. Vapour pressures, obtained from the Kelvin equation, were closely matched to the experimental outcomes even in extended confined channels ($\sim 8\, nm$) making the equation applicable in modelling capillary condensation in silica-glass media. Vapour pressure alteration of water in nanochannels was inspected by Tsukahara et al. (2012) using a nanoscale chip. The nanofluidic chip consisted of microchannels (10 μm deep) and nanoscale channels with a depth range of 90-370 nm. The experiments demonstrated the reduction of water vapour pressure with the decrease of medium size. Additionally, computed vapour pressures from the Kelvin equation were relatively similar to those observed in the experiments; therefore, applicability of the Kelvin equation in predicting vapour pressures within extreme confined fused-silica glass media remains valid.

Recent studies show that the accuracy of the Kelvin equation declines in nanopores smaller than 8 nm. Wang et al. (2020) investigated the precision of computed phase-change pressures by the Kelvin equation and equation-of-state-with-capillary-pressure (EOS-P_{cap}) in extended confined

pores. Quantitatively, the study demonstrated that overestimation and underestimation issues were noticed with the Kelvin equation and EOS-P_{cap} when predicting condensation and evaporation pressures of propane in pores below 8 nm, comparing with the density function theory (DFT) predicted outcomes. However, reasonable accuracy of vapour pressure prediction could be achieved with the thermodynamical models when the pore size is above 8 nm.

The curvature effect on fluids increases as capillary size becomes tighter due to the change of interfacial properties, such as surface tension and pressure difference at the liquid-gas interface. When the pore becomes smaller, the pore-fluid interaction begins to display an influence on the phase-alteration nature of confined fluids. In a nanopore, due to the limited number of molecules, a large percentage of molecules are absorbed by the pore wall, and condensation/vaporization behaviours begin to alter from bulk conditions when the medium gets tighter than 100 nm (Cui et al. 2018). Fluids in confined spaces could gain distinctive properties, such as higher viscosity and slower motion of molecules, which could be the reason behind the phenomenon of shifted vapour pressures (Tsukahara et al. 2012). Several investigations were performed to understand the deviation of phase-change behaviour in extreme tight channels featured with nanoscale pore throats (Bao et al. 2017). The majority of these studies were conducted using microfluidic and nanofluidic chips made of silica glass. Per the Kelvin equation, the alteration of vapour pressure in confined pores depends on capillary size, surface tension, and contact angle between the solid surface and liquid. These liquid-solid properties, including molecular absorption of the surface, might change noticeably when the solid material is altered. This paper aims to study the phase-change behaviour of propane in various capillary media starting from Hele-Shaw glass cells to real core samples with different permeabilities, porosities, and pore throat sizes. Moreover, microfluidic chips with uniform and non-uniform properties (grain and pore throat sizes), representing various pore sizes, were utilized to obtain a clearer picture of propane phase alteration in porous media using visual support. One of the main targets in this investigation was to inspect the effect of surface properties on propane's vaporization in confined spaces and compare the experimental outcomes with the computed saturation pressures, computed by the Kelvin equation and Peng-Robinson equation-of-state (EOS). Comparative analysis of the outcomes obtained from glass microfluidic experiments and rock samples provided new insight into the pore scale thermodynamics of the solvents to be used in further computational studies to improve the accuracy of performance prediction.

8.3 Background

The Kelvin equation (Thomson 1872) is a theoretical modelling approach that describes the influence of curvature radius at vapour-liquid interface on saturation pressures. The general Kelvin equation can be expressed as

$$RT \ln\left(\frac{P_v}{P_\infty}\right) = -\frac{2\sigma^{LV} v^L}{r} + v^L(P_v - P_\infty) \quad 1$$

where T is the fluid temperature, R is the universal gas constant, r is the droplet (or capillary) radius, v^L is the molar volume of the liquid, σ^{LV} is the vapour-liquid interfacial tension, P_∞ is the vapour pressure at the flat surface, and P_v is the vapour pressure at the curved interface. The term $(P_v - P_\infty)$ on the right side of Eq. 1 can be neglected owing to its small value comparing to the first term $(-2\sigma^{LV} v^L \backslash r)$ (Berg 2009). Hence, the approximated form of the equation is as follows:

$$RT \ln\left(\frac{P_v}{P_\infty}\right) = -\frac{2\sigma^{LV} v^L}{r} \quad 2$$

When the medium is liquid wet (concave curvature), the vapour pressure of the liquid reduces along with the reduction of pore size thus leading the vapour pressure at confined spaces (P_v) to be lower than the vapour pressure at the flat surface (P_∞) or bulk condition. One of the major limitations of the Kelvin equation is that it is not applicable for computing the shift of vapour pressure of multicomponent fluids in hydrocarbon reservoirs, due to their complexity. In petroleum industries, cubic EOS is commonly used to estimate the phase behaviour of reservoir fluids which helps in forecasting approximated oil recoveries (Fanchi 2020). Peng-Robinson EOS (Peng and Robinson 1976) is considered one of the more common models in reservoir engineering to predict the phase-change behaviour of hydrocarbon mixtures in the reservoir. For a single-component fluid, PR-EOS can be expressed as

$$P = \frac{RT}{V_m - b} - \frac{a\,\alpha}{V_m^2 + 2bV_m - b^2} \qquad 3$$

where R is the universal gas constant, T is the fluid temperature, a and b are constant parameters, α is a temperature dependence function which is related to the reduced temperature and acentric factor, and V_m is the molar volume. Later on, the accuracy of Redlich-Kwong (RK) (Soave 1972) and Peng-Robinson EOS's was improved in predicting phase behaviour of complex hydrocarbon multicomponent mixtures and liquid densities. Le Guennec et al. (2016) developed the improved versions of PR and RK cubic EOS by introducing a consistent α-function which ensures a precise vapour-liquid equilibrium (VLE) calculation with multicomponent fluids and provides accurate extrapolations in areas above critical points. The volume translation was also considered to achieve correct saturated liquid volumes which closely match with the experimental outcomes. Pina-Martinez et al. (2019) proposed an updated version of Soave α-function for PR and RK equation of state. The corrections made in both cubic EOS were constructed based on a wide range of compounds (1721 pure compounds) from various chemical families. Such improvements had impacts on enhancing the reproduction of vapour pressures, calculated by the PR EOS. Considerable enhancements were noticed in systems with heavy molecules.

Peng-Robinson EOS and Redlich-Kwong EOS are widely used cubic EOS models in petroleum applications, owing to their more accurate critical compressibility factors (Z_C) that are closer to experimentally measured values (Fanchi 2020). Though, one of the drawbacks of these cubic EOS models is that they do not consider the confinement effect which causes them to lose some of their accuracies in situations where tight rock media is involved. Reservoir rocks are heterogeneous systems which consist of pores with a varied range of sizes. Generally, extended small channels (< 1000 nm) commonly exist in tight rocks, such as tight sandstone and shale. Thermodynamically, the phase-change behavior of fluids begins to be influenced by the medium sizes when they are smaller than 1000 nm, as stated by the Kelvin equation. Based on our pore scale distribution analysis, micropores ($< 2\,nm$) and mesopores ($2 - 50\,nm$) do exist in permeable rocks with minor pore volumes—which were estimated to be less than 5% of the total pore volume per mass unit. The investigation in this paper focused on observing the phase-alteration of propane under

various temperatures in different rock types and compared the measured vapour pressured with computed phase-change pressures from the Kelvin equation and Peng-Robinson EOS (1976).

8.4 Statement of the Problem and Objectives

In heavy-oil recovery applications, injecting solvents with or without steam under variable pressure and temperature could lead to considerable phase alteration. The thermodynamics of injected fluids in porous media play a critical role in controlling the performance of hybrid and cold-solvent injection. Phase alteration during the process could control the distribution of injected fluids in the reservoir as well as their flow dynamics and eventually, oil recovery. Similarly, solvent retrieval process (SRP) highly depends on solvent thermodynamics in the reservoir. As a result, comprehending the phase-change behaviour of injected fluids is important in choosing the appropriate application conditions (such as pressure and temperature) while maximizing oil recovery and solvent retrieval. SRP is a critical part of the whole process and has an impact in minimizing the overall operational cost of hybrid (steam-solvent) applications. The phase change mechanism should be well understood during this process as it directly affects the oil recovery (during injection) and solvent retrieval (during depletion), and the phase behaviour in capillary medium is different from the bulk conditions of which are applied in classical PVT tests and studies.

A similar phenomenon is encountered in oil (heavy-oil, light, oil, and condensate) recovery from unconventional (shales, tight sands) reservoirs in which the most common application suggested is solvent gas (hydrocarbon gases or CO_2). The gases injected (in the form of huff-and-puff) after fracking diffuse into the rock matrix and reproduce with oil during the depletion stage. The recovery of oil and solvent retrieval are both controlled by the thermodynamics (mainly the phase change of the solvent and oil). It is well-known that the phase change conditions in capillary medium differ from the bulk conditions and this cannot be captured easily using standard PVT analyses. Per the Young-Laplace equation ($\Delta P = 2\gamma/r$), the curvature radius (r) has an effect on surface tension (γ) when it decreases to microscales or nanoscales (Tsukahara et al. 2012). The Kelvin equation demonstrates the relationship between vapour pressures in capillary and bulk conditions ($P_r = P_\infty \exp\left[\frac{-2\,\sigma\,v^L}{r\,R\,T}\right]$). According to this equation, the vapour pressure of fluids becomes lower than those in bulk scenarios when medium sizes are tighter due to the change of

surface tension, pressure drop at the interface, and contact angle. As a result, fluids in highly confined spaces tend to have higher viscosities and capillary pressures.

The objective of this paper was to experimentally investigate the vapour pressure of propane in different capillary models and compare the outcomes with computed vapour pressures from the Kelvin equation and Peng Robinson EOS. The vapour and condensation pressures of propane were measured using Hele-Shaw cells, capillary tubes, and homogenous/heterogeneous micromodels with various pore throat and grain sizes. As a more realistic porous media representation, rock samples such as Berea sandstones, Indiana limestone, tight sandstone, and shale were also considered, and the vapour pressure of propane was measured in those samples to obtain a wider perspective of how the vaporization of propane occurs in various capillary media with dissimilar surface properties and porous structures. Furthermore, the results with rock samples were compared with outcomes obtained from Hele-Shaw and micromodel glass chips, including the computed saturation pressures obtained by the thermodynamical models.

8.5 Experimental Study

Observations of propane's vaporization pressures were performed by using several glass chips and rock samples. The experiments were initiated with Hele-Shaw glass cells of 0.13 and 0.04 mm gap thicknesses. Although the Hele-Shaw cells represent only a simple tight system with smooth and liquid-wet inner surface, they can be useful in providing a clear visualization of bubbles generation of fluids in different pressures that could be difficult to visualize in microfluidic chips. Then, vapour pressures of propane were inspected in several types of micromodels with uniform and non-uniform properties such as porosity, permeability, and pore throat/grain size.

8.5.1 Hele-Shaw Glass Cells

Hele-Shaw cells basically consist of a pair of thin rectangular glass plates with an empty gap in between. The glass cells were made with two main gap thicknesses: (1) 0.04 mm and (2) 0.13 mm. Mainly, the purpose of starting our investigation with glass cells was to get a clear exposure of propane's bubbles formation in pressure depletion stage under constant temperature (≈ 20℃, 293.15 K). In all Hele-Shaw cells, the inner glass surfaces were propane-wet during condensation. **Figure 8-1** presents the Hele-Shaw glass cell used in our experiments. The experimental setup

consisted of a DSLR camera, pressure and temperature measurement device, LED light source, thermocouple, pressure transducer, ISCO syringe pump, and pressure windowed cell. Figure 1 illustrates some of the equipment used in experiments with Hele-Shaw cells.

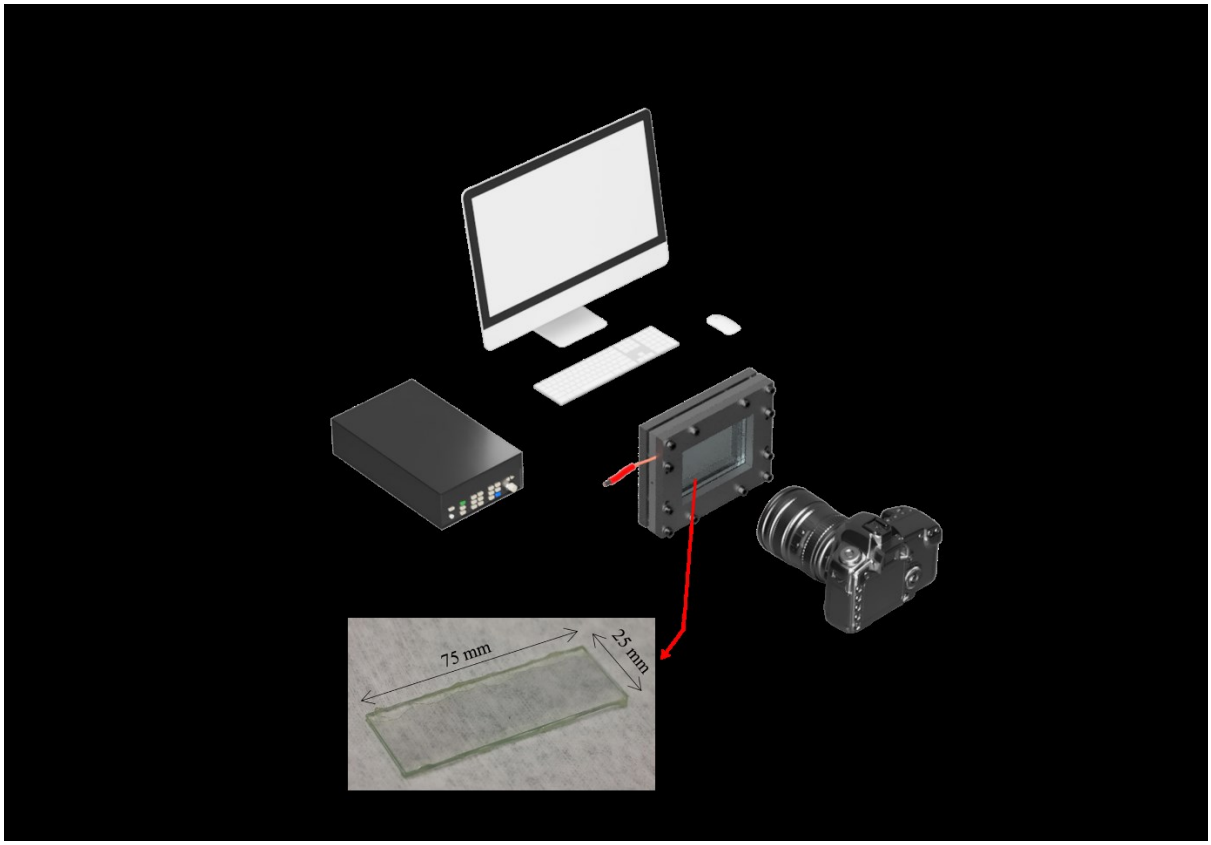

Figure 8-1: Experimental setup used in Hele-Shaw experiments.

Procedure. To pressurize the Hele-Shaw glass models, they were placed in the pressure windowed cell. The pressure cell was featured with plexi-glass windows which allowed clear visualization through the cell. By using an ISCO syringe pump, the cell was pressurized from a starting pressure ($70\ psi$) to 150 psi—which is above the propane vapour pressure (in Edmonton, Alberta, Canada) and is approximately 115 psi in atmospheric temperature ($\approx$ 20℃, 293.15 K). The pressure range was selected based on the pressure limitation of the windowed cell that could withstand a maximum pressure of 160 psi. Both the Hele-Shaw glass cell and pressure windowed cell were vacuumed for a period of time to remove the trapped air in the system. We aimed to study the vaporization and condensation of propane; hence, the pump was programmed to build up and deplete the pressure at a rate of 5-7 psi/min within 10 minutes. Meanwhile, a continuous video was

taken with the DSLR camera during the process. Additionally, the pressure and temperature in the pressure cell were recorded constantly by the measurement device every 2 seconds.

Results and discussion. As mentioned previously, Hele-Shaw cells provide a clearer visualization of the nucleation stage, unlike microfluidic chips and rocks. Using the glass cells could bring several limitations (flat liquid-solid interface) with it which might not act as a good representation of real reservoir conditions. However, they could be useful in illustrating the phenomena under the simplest conditions. It was expected that the vapour and condensation pressure of propane in the glass cell would be relatively close to bulk pressures since their gap thicknesses were not tight enough to create effective changes in surface tension (γ) and contact angle ($\cos\theta$). During the condensation process, propane went through two main stages: (1) dew point and (2) considerable phase change. In the vaporization process, two stages were considered: (1) bubble point and (2) quick formation of bubbles. In the Hele-Shaw cell with 0.04 mm gap thickness, the first propane liquid drops took place at 118.5 psi as shown in **Figure 8-2a**. A considerable phase change initiated in the cell at a pressure of 121.2 psi (**Figure 8-2b**). In the pressure depletion stage, the first propane bubbles generation took place at 116.6 psi as illustrated in **Figure 8-2c**. A quick formation of propane bubbles began in the glass cell at 113.7 psi (**Figure 8-2d**). **Figure 8-3** show the pressures in 0.04 mm and 0.13 mm gap spaces during the build-up and depletion processes.

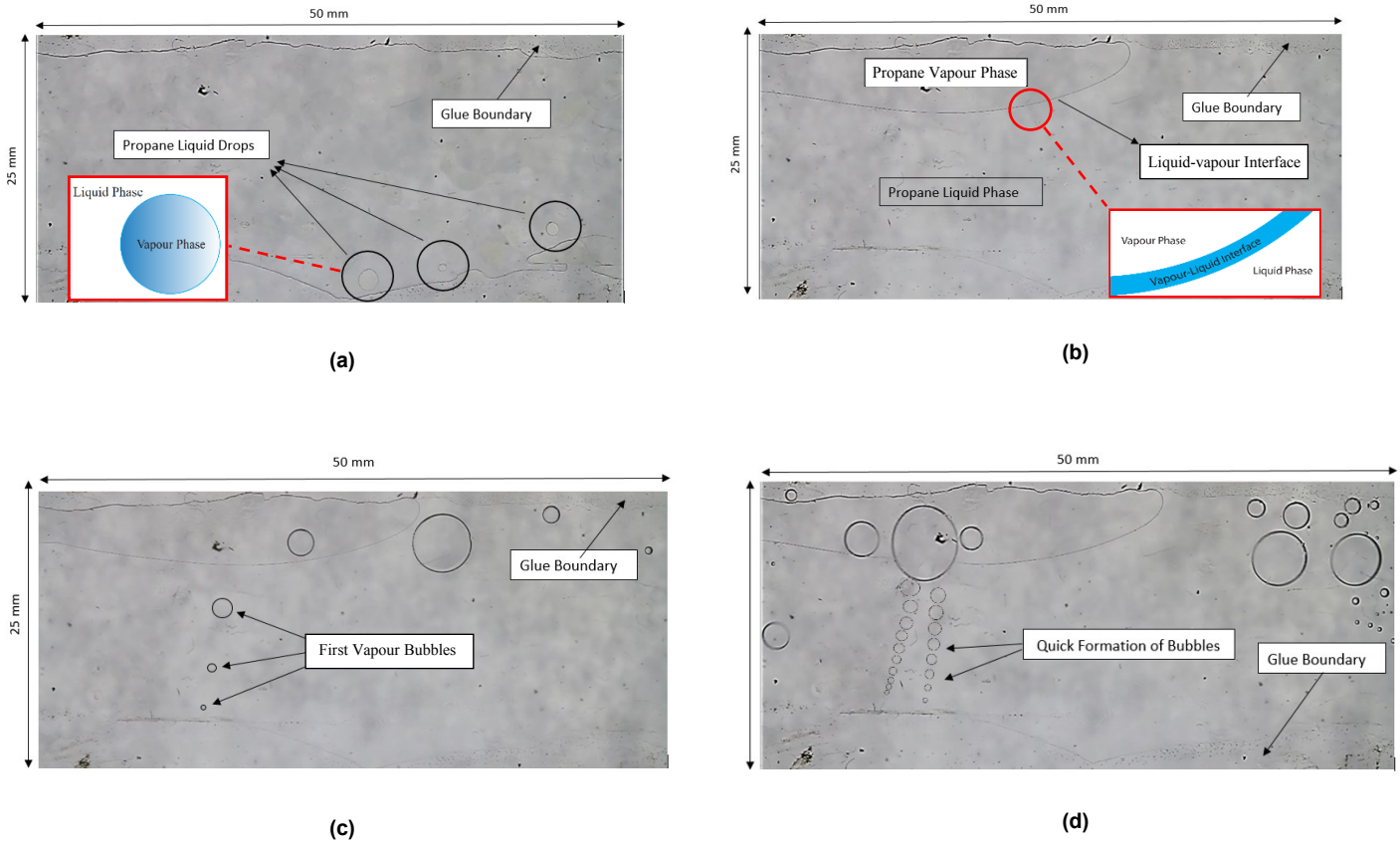

Figure 8-2 – (a) Considerable phase change at 121.2 psi; (b) dew point stage at 118.5 psi; (c) bubble point stage at 116.6 psi; (d) quick formation of bubbles stage at 113.7 psi.

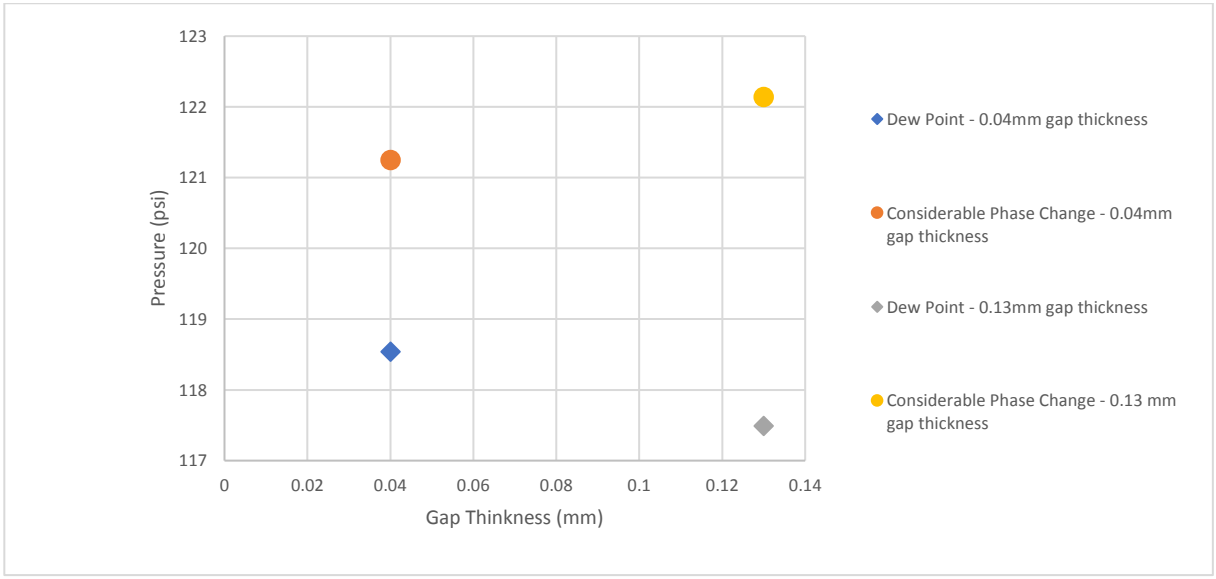

(a)

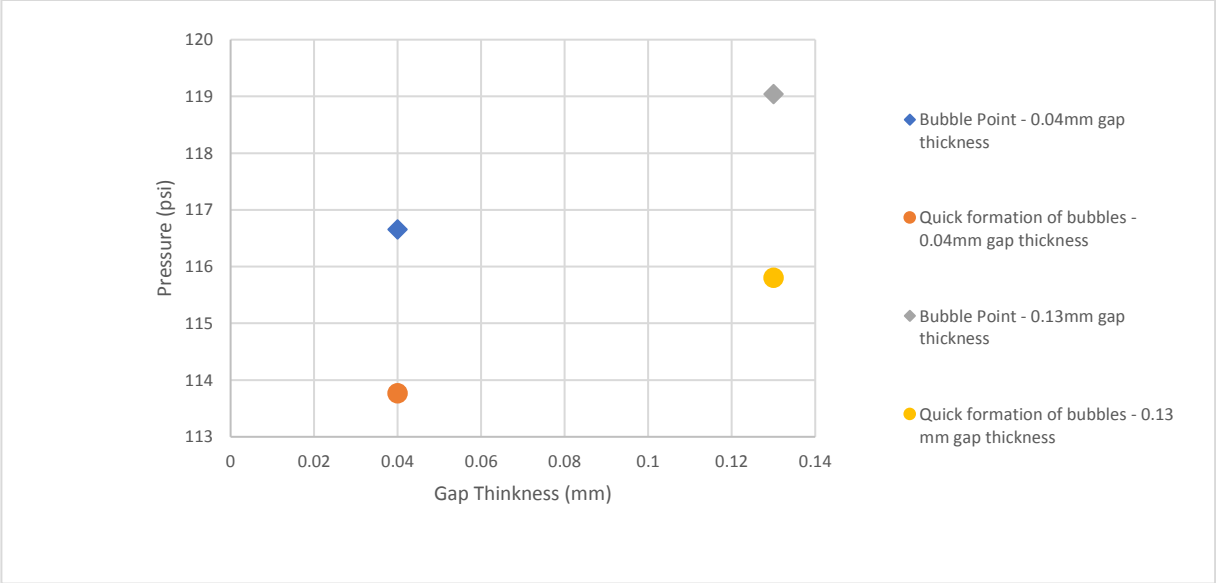

(b)

Figure 8-3 – (a) Pressure at each stage in 0.04 and 0.13 mm gap thickness during pressure build-up process; (b) pressure in 0.04 and 0.13 mm gap thickness during pressure depletion process.

8.5.2 Microfluidic Chips

Compared to Hele-Shaw glass cells, micromodels offer a better representation of porous media in terms of size and shape of the pores. Three categories of microfluidic chips were used: (a) capillary tube model, (b) homogenous micro model, and (c) heterogeneous micro model. Capillary tubes represented straight silica-glass pore throats with various sizes ranging from 40 to 1 micrometer (μm). Homogenous micromodels were designed with uniform grain and pore throat sizes. In our experiments, two homogeneous models with different properties were utilized: (1) a microfluidic model with uniform properties of 0.11 mm pore diameter and 0.01 mm pore throat and (2) a model with uniform properties of 0.21 mm pore diameter and 0.01 mm pore throat. The heterogeneous microfluidic chip had a porous structure closer to real rocks with an average pore throat of 142.5 μm.

Procedure. To pressurize the microfluidic chips, they were placed in the pressure windowed cell, and using an ISCO syringe pump, the cell pressure was increased from 70 psi to 150 psi which is above the propane vapour pressure (115 psi at 20℃, 293.15 K). The pressure range was selected based on the pressure limitation of the windowed cell that could withstand a maximum pressure of 160 psi. The entire system was vacuumed for a period of time to remove the trapped air inside

the windowed cell and silicate glass micromodel. The pump was programmed to build up and deplete the pressure at a rate of 5-7 psi/min within 10 minutes and a continuous video was taken by the DSLR camera during the process. Additionally, the pressure and temperature in the system were recorded constantly by the measurement device every 2 seconds.

Results and discussions. The micromodel experiments were initiated with capillary-tube models featured with five sizes: (a) 40 μm, (b) 20 μm, (c) 10 μm, (d) 5 μm, and (e) 1 μm. Through capillary-tube experiments, it was noticed that liquid propane wets the inner surfaces of the tubes during the condensation stage which makes these models act as propane-wet capillary media. In the 40 μm tube, during the pressure depletion process, vaporization of propane took place in the tube at 116.1 psi, as shown in **Figure 8-4**. **Table 8-1** shows the vapour and condensation pressures of propane in various sizes of capillary tube during the depletion processes. The phase-change pressures were comparable with the pressure values recorded in the bulk conditions because of the size of tubes which had almost no effect on the vaporization and condensation behaviour. Medium (pore) sizes have influences on the phase-alteration behaviour of fluids when they are 100 nm or smaller (Cui et al. 2018).

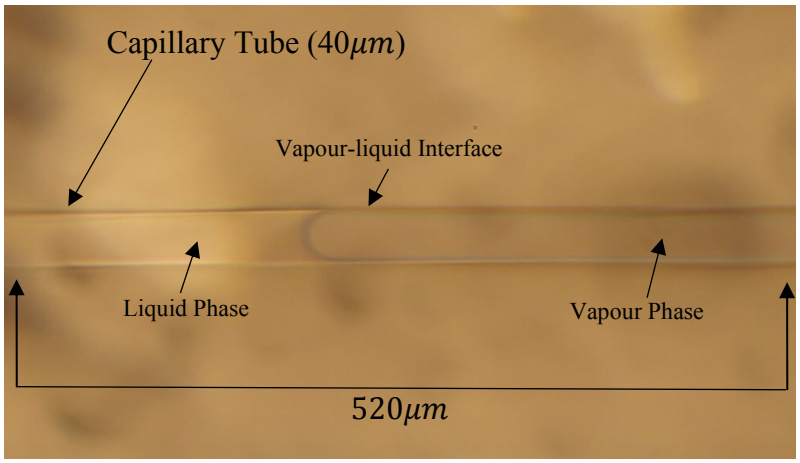

Figure 8-4: Propane vaporization in the 40 µm capillary tube.

Table 8-1: Vapour and condensation pressures of propane in several capillary-tube sizes.

	Vapour pressure (psi)	Condensation pressure (psi)
40 μm Capillary tube	116.1	118.2
20 μm Capillary tube	113	121.3
10 μm Capillary tube	120.1	116.6
5 μm Capillary tube	116.1	123
1 μm Capillary tube	121.3	121.5

In microfluidic homogenous chips, phase-change pressures were relatively similar to those observed with capillary tube models. In the homogenous model (0.11 mm grain diameter and 0.01 mm pore throat), propane vaporization began at 115.3 psi, as illustrated in **Figure 8-5**. Comparably, propane phase change took place in the heterogonous microfluidic model at 118.8 psi (**Figure 8-6**). **Table 8-2** presents the propane vapour and condensation pressures in homogenous and heterogonous models. As observed in the Hele-Shaw experiments, the pore throat sizes in the microfluidic models were not confined enough to alter the vaporization and condensation behaviour. The phase-change pressures of propane in the homogeneous and heterogeneous model were comparable with the bulk values.

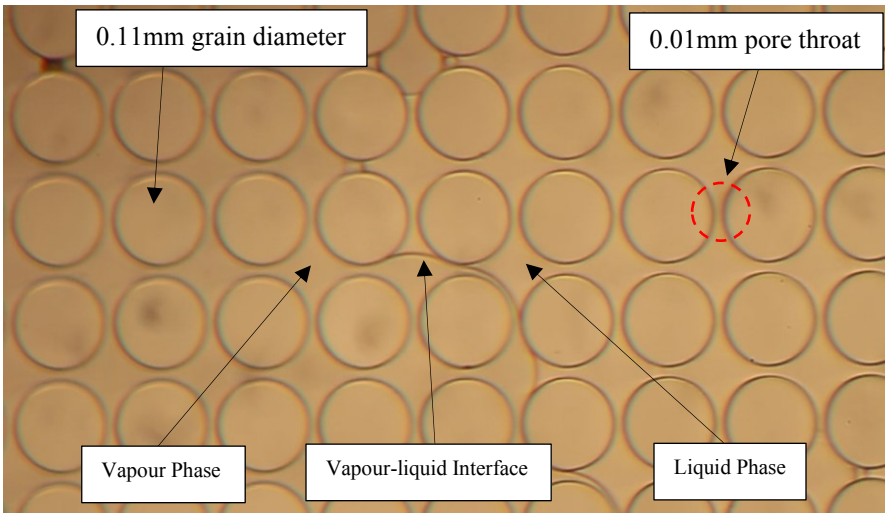

Figure 8-5: Propane vaporization in the homogenous micromodel (0.11 mm grain diameter and 0.01 mm pore throat).

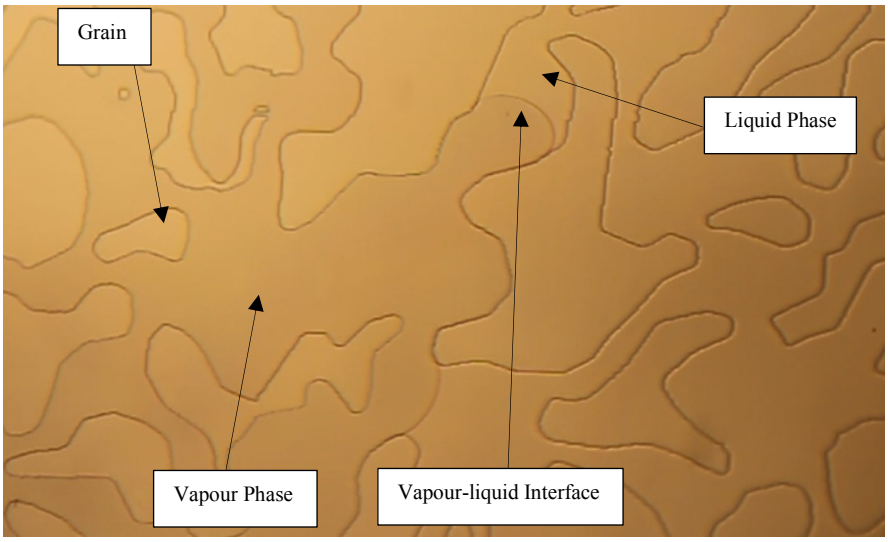

Figure 8-6: Propane vaporization in the heterogeneous micromodel (average pore throat size of 142.5 µm).

Table 8-2: Vapour and condensation pressures in homogenous and heterogonous microfluidic chips.

	Vapour pressure (psi)	Condensation pressure (psi)
Homogenous model (0.11 mm grain diameter and 0.01 mm pore throat)	115.3	119
Homogenous model (0.21 mm grain diameter and 0.01 mm pore throat)	117	118
Heterogeneous model (average pore throat size of 142.7 μm)	118.8	119.1

8.5.3 Rock Porous Media

To visualize the phase change of propane in more realistic porous media, vapour pressure alteration was examined in Berea sandstone, Indiana limestone, tight sandstone, and shale rock samples. Using real rock samples provided an advantage of testing the impact of surface characteristics and porous media structure on the vapour pressure at different surrounding temperatures, ranging from 0℃ (273.15 K) to 40℃ (313.15 K). Due to their different surface properties and pore sizes, it was

expected that the vapour pressure of propane might alter, comparing with those observed in the Hele-Shaw cells and microfluidic silica-glass chips. The average permeability defers from one rock to another, depending on the rock nature. Permeabilities, in some cases, could reflect an approximated insight of the pore sizes that a rock might have. The Winland equation (Kolodzie 1980) is one of the approaches that can be utilized to estimate the average pore size of a rock by knowing its permeability and porosity, and it is commonly used by the petroleum industry (Lucia 2007). The equation, however, computes pore sizes empirically which makes its outcomes highly approximated with a considerable lack of accuracy in certain cases. The pore size distribution analysis assisted us to experimentally measure the actual pore volumes of micro and meso channels in the rock surface. The analysis also allowed us to find the volume percentage of pores tighter than 1000 nm in each rock.

Pore Size Distribution Analysis (PSDA). PSDA was performed by a Brunauer-Emmett-Teller (BET) surface area analyser; the surface area is the available pore area for nitrogen adsorption. The BET surface area, average pore diameter, and total pore volume were evaluated by physisorption of nitrogen in rock porous media. Despite the high permeabilities and porosities that permeable rocks have, inconsiderable pore volumes of nanopores might exist, which, in theory, could alter the phase-change behaviour of fluids located within these tight pores. The investigation evidenced the existence of micro and meso pores in the permeable rocks (sandstone and limestone). **Table 8-3** shows the measured permeability, density, and median pore size of channels below 1000 nm, and volume percentage of pores smaller than 1000 nm in sandstone, limestone, tight sandstone, and shale. The volume percentages were estimated based on the mass unit (gram). **Figure 8-7** shows the deviation of pore volumes of different pore sizes in each rock type. In shale and tight sandstone, the pore volumes of pores, with a size range of 3–10 nm, are higher than what is observed with sandstone and limestone. Also, larger pore volumes in mesopores (2–50 nm) are detected in shale and tight sandstone, compared with sandstone and limestone.

Table 8-3: Average permeability, rock density, and pore volume percentages of various rock types (Al-Kindi and Babadagli 2020).

Rock type	Average permeability (millidarcy)	Density ($kg\ m^{-3}$)	Median pore size of pores smaller than 1000 nm	Volume percentage of pores smaller than 1000 nm (%)
Berea sandstone	274	2129	350	4.4
Indiana limestone	30	2246	470	4.6
Tight sandstone	0.1	2400	300	38.2
Shale	< 0.01	2200	125	94.3

The analysis showed that minor volume percentages (< 5%) of confined pores (< 1000 nm) could be observed in sandstone and limestone despite their high permeabilities. Due to the tight nature, pore volumes of constrained channels in tight sandstone and shale are significantly higher, as presented above in Table 3. Having higher pore volumes of nanopores in tight sandstone and shale would increase the volume of inner fluid that could vaporize at pressures or temperatures different from the bulk conditions. On the other hand, in sandstone and limestone, lower inner fluid volumes would vaporize differently from the bulk values owing to their considerably lower nanopore (< 1000 nm) volumes. Nonetheless, at reservoir scales, the shift of saturation pressure in permeable rocks could be a noticeable impact on the simulated oil recovery or history matching.

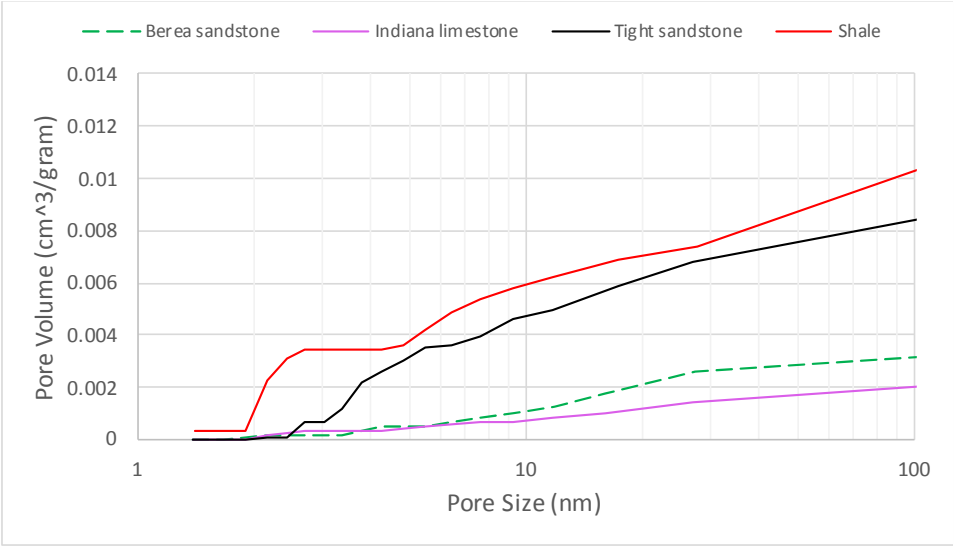

Figure 8-7: Change of pore volumes of various pore diameters, ranging between 1 and 100 nm, based on nitrogen desorption (Al-Kindi and Babadagli 2020).

Experimental Setup. The vapour pressure of propane was studied in various reservoir rocks at different temperatures, including temperatures lower than the ambient temperature (≈ 20℃, 293.15 K). A special borosilicate-glass cell was utilized to pressurize the rock samples above the propane condensation pressure. A cooling liquid bath (**Figure 8-8**) was used to reduce the temperature of rocks and precisely stabilize it throughout the experiment. The liquid bath (water – H2O) temperature was decreased by pumping a liquid coolant through the metal tube at desired temperatures. At freezing temperatures (≤ 0℃), water was freezing at areas around the metal tube. However, due to the naturally slow freezing process, water remained in its liquid form around the glass cell during the experiments. With a constant-temperature oven, the glass cell and rock samples were heated at various temperatures above the ambient temperature (**Figure 8-9**). Using an ISCO syringe pump allowed us to pressurize the system and then deplete the pressure accurately at a specific depletion rate. The temperature inside the glass cell was measured and recorded continually by a measurement device.

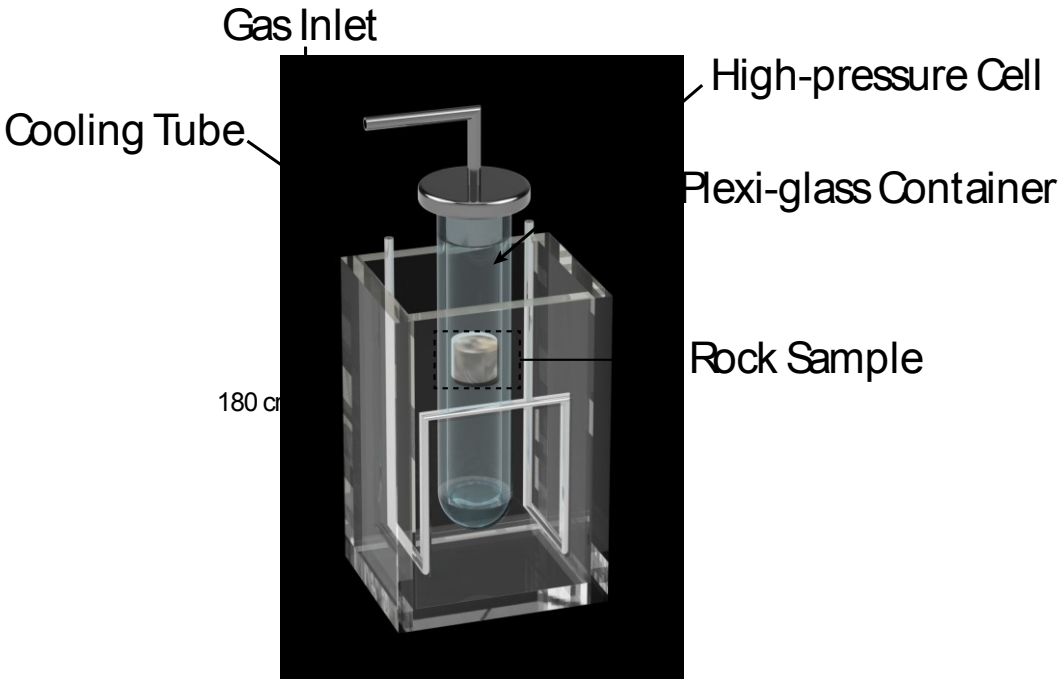

Figure 8-8: Cooling liquid bath used to reduce the rock's temperature below ambient temperature (20℃, 293.15 K). The cooling liquid (water) was placed in the plexi-glass container and cooled gradually by the cooling metal tube.

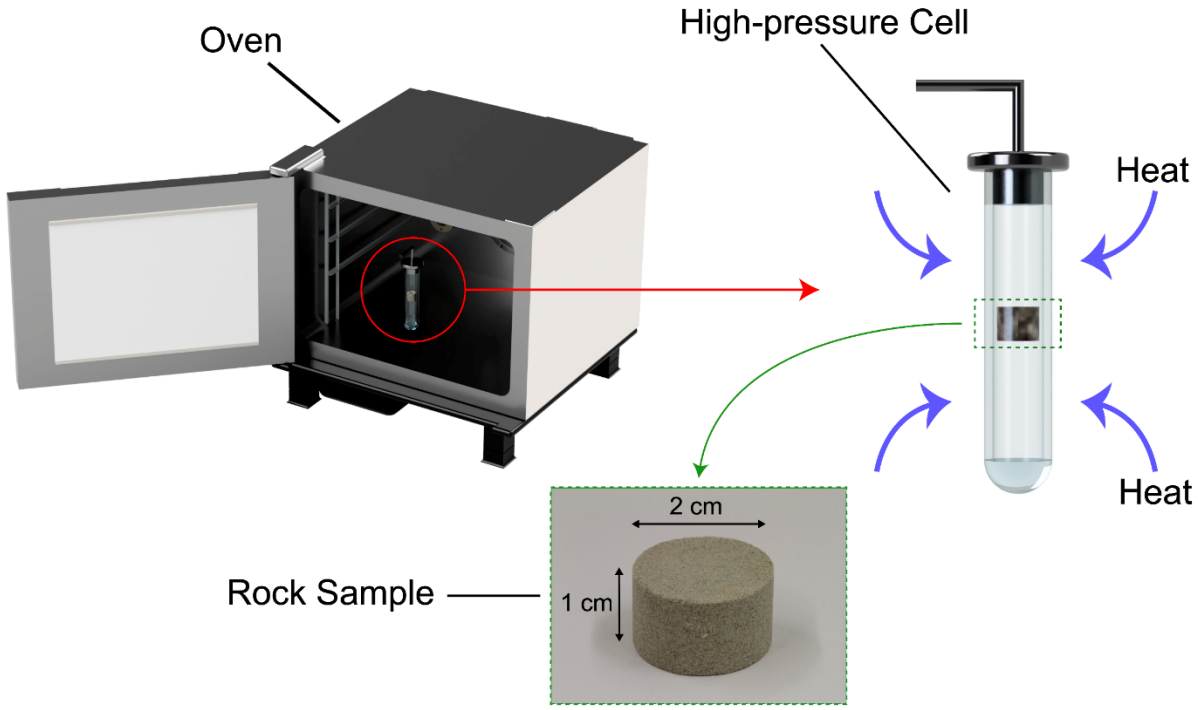

Figure 8-9: Constant-temperature oven utilized to increase the rock's temperature above the ambient temperature. The oven ensured a uniform heat migration to the system and a homogeneous temperature distribution around the rock.

Procedure. Ensuring a high purity of gas within the system was a critical part of our experiments. Including the rock samples, the whole system was vacuumed thoroughly to remove the trapped air and achieve the maximum purity of propane inside the system. After the vacuuming process, the glass cell was pressurized with propane (purity of 99.95%) with the assistance of an ISCO pump. To guarantee a complete condensation, propane was pressurized 20 psi more than its saturation pressure. Generally, the vapour pressure of gases increases as their temperatures rise. The glass cell was limited with a maximum pressure of 220 psi. Therefore, the experiments were restricted with a maximum temperature of 40℃ (313.15 K) since the vapour pressure of propane, at bulk condition and 40℃, is 200 psi. Then, the overall pressure in the system was depleted at a constant rate of 0.6 psi per minute. The vaporization of propane in different rocks was studied at several temperatures which were 0℃ (273.15 K), 10℃ (283.15 K), 20℃ (293.15 K), 30℃ (303.15 K), and 40℃ (313.15 K).

Results and discussion. The investigation of propane phase-change behaviour in various reservoir rocks focused on two main stages of vaporizations: (a) initiation of vapour-phase formation (nucleation), and (b) significant vapour generation. Due to the heterogeneity of pore interconnectivity, the movement of vapour bubbles within the rocks could slightly vary in every experiment; consequently, the temperature at which the bubbles appearing on the rock surface could vaguely change between the trials. Hence, with each rock type, repeatability was the main key to achieve representative outcomes by averaging the measured vapour pressures. Initially, the propane vapour pressure was investigated in bulk conditions using bulk models. The models consist of 0.8 mm silica-glass tubes (**Figure 8-10**); thermodynamically, their diameters should not impact the phase-change behaviour of propane. With the bulk model, the outcomes were relatively similar to the handbook values, as shown in **Figure 8-13** and 8-**14**. In sandstone and limestone, the vapour pressure of propane was noticeably lower than the bulk values, due to the existence of nanopores (< 1000 nm). For instance, **Figure 8-11** presents the two stages of phase change in Berea sandstone at 30℃ (303.15 ^{o}K). The bulk vapour pressure of propane at temperature of 30℃ is 170 psi. In sandstone, the nucleation took place at 159 psi, as shown in Figure 11a. A significant phase alteration was observed at a pressure of 163 psi (Figure 11b).

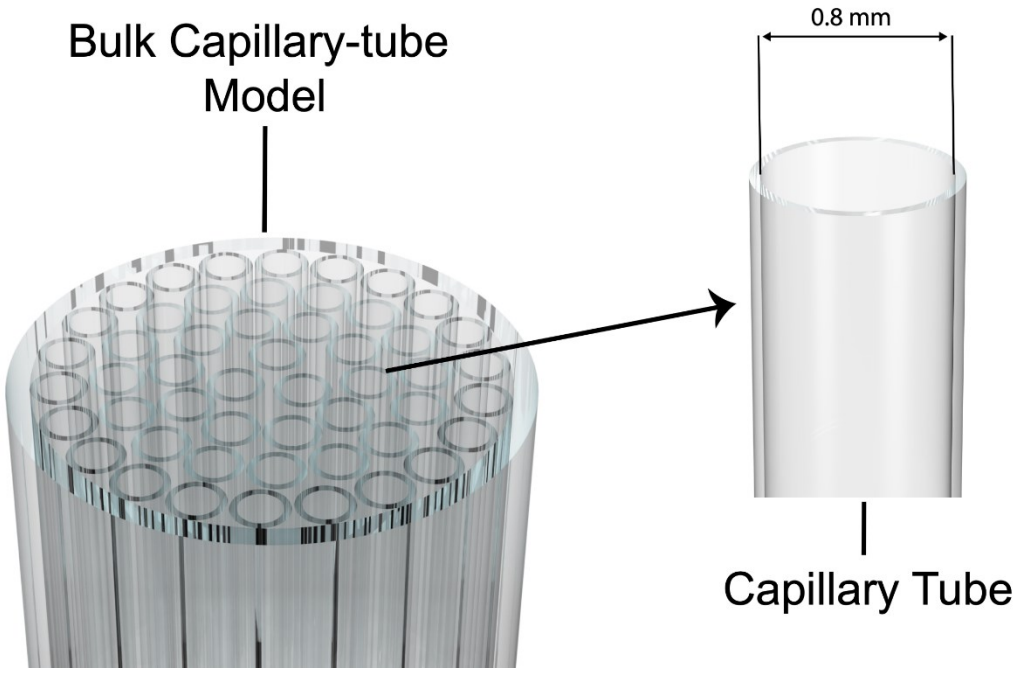

Figure 8-10: Silica-glass bulk model consisting of capillary tubes with constant diameters of 0.8 mm.

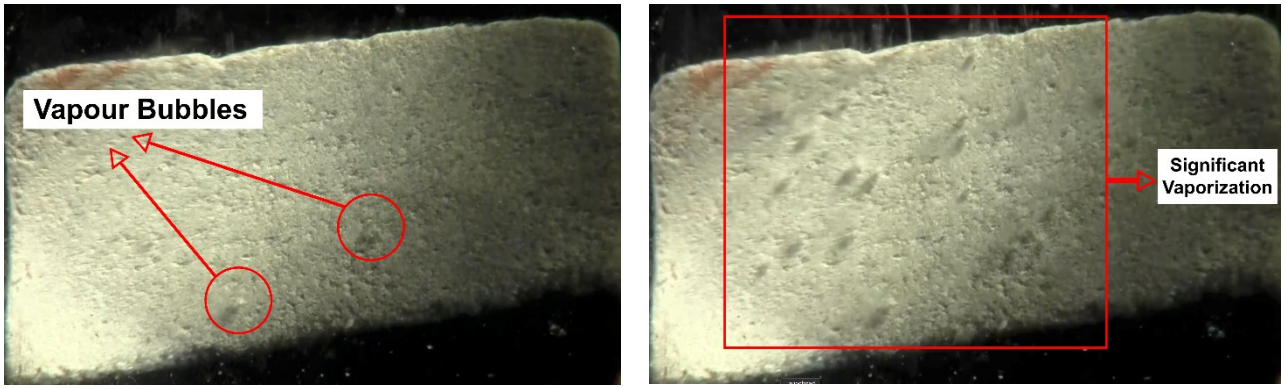

(a) **(b)**

Figure 8-11 – (a) Initiation of vapour-phase (nucleation) in Berea sandstone; (b) significant propane vaporization in Berea sandstone.

8.6 Quantitative Analysis

Per the Kelvin equation, vapour pressure could be altered by medium size if it is 1000 nm or less. The vaporization pressure gets lower as the pore throat gets tighter. In Hele-Shaw and microfluidic experiments, the recorded vapour pressures were relativity close to the phase-change pressures measured in bulk conditions. Due to their inner medium sizes, the existed capillary effects in the silicate glass models were not sufficient to result in shifted vapour or condensation pressures since they were larger than 100 nm. Additionally, the visualized phase change of propane in silica-glass models took place at pressures approximately equal to those computed by the Kelvin equation, based on their medium sizes and temperatures ($\approx 20℃$). Because of the presence of micro (< 2 nm) and meso (2 - 50 nm), the vapour pressures in the rocks were noticed to be lower than those measured in bulk cases. **Figure 8-12** shows the measured condensation pressure in Hele-Shaw and microfluidic experiments, including the computed saturation pressures from the Kelvin equation. Figure 13 presents the vapour pressures that were measured in Hele-Shaw cells, microfluidic chips, and rock samples. Also, it compares the outcomes with the calculated phase-change pressures from the Kelvin equation. The average pore sizes of rocks were the median pore sizes, obtained from the pore size distribution analysis. On average, the vapour pressures in the rocks were 7% less than the bulk and calculated vapour pressures of propane.

The results were also compared with Peng-Robinson EOS which is one of the well-known pressure-volume-temperature (PVT) models in reservoir simulation that is used to predict the phase-change behavior of hydrocarbons. In our case, a phase envelope of the single-component hydrocarbon was generated by PR-EOS and compared with the measured phase-change pressures in the rock samples at various temperatures, ranging from 0℃ (273.15 K) to 40℃ (313.15 K). Since PR-EOS does not consider the capillary effect on its vapour-liquid equilibrium (VLE) calculation, the computed vapour pressures by the cubic EOS were identical to the bulk values and different from those measured in the reservoir rocks. Figure 14 illustrates a comparison between computed vapour pressures from PR-EOS and measured vapour pressures of propane in the bulk condition and reservoir rocks. Shifted vapour pressures were detected in the rocks at different temperatures, owing to the presence of nanopores (≤ 1000 nm). The reduction of phase-alteration

pressures was estimated to be nearly 15% lower than those measured in bulk conditions and calculated phase-alteration pressures from PR-EOS.

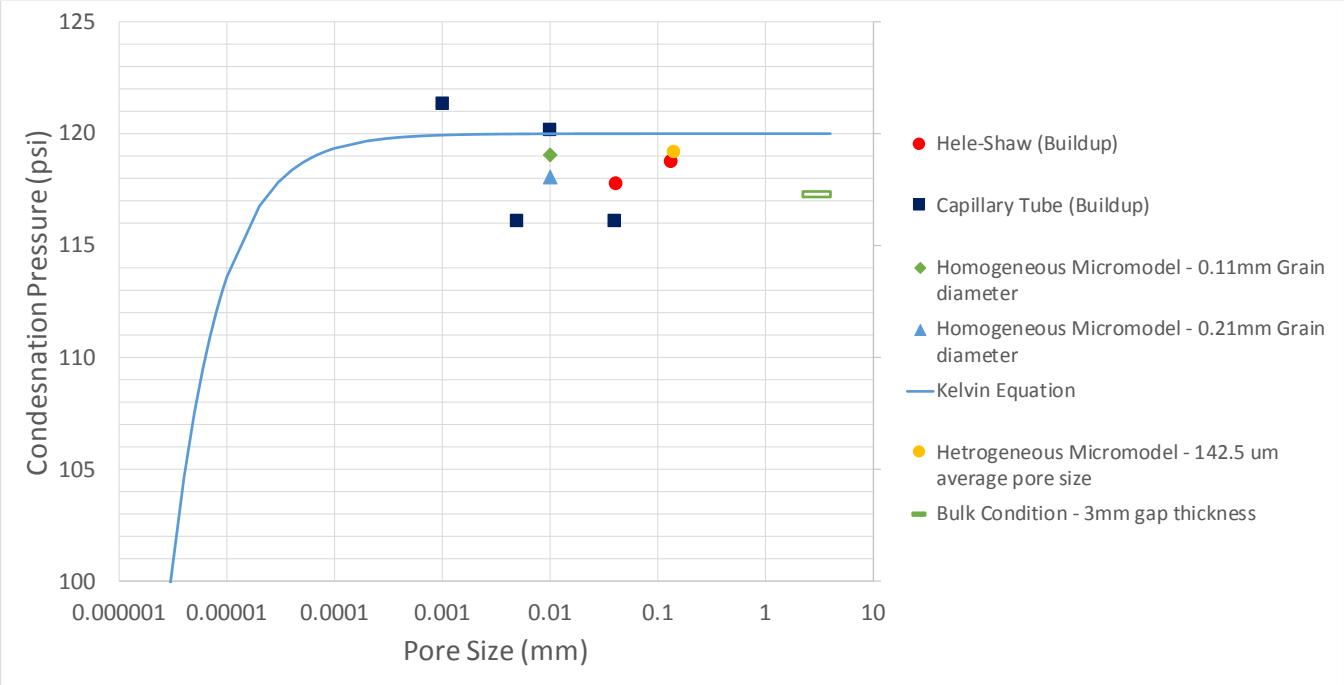

Figure 8-12: —Condensation pressures of propane in Hele-Shaw cells and micromodels during the pressure build-up process. Each point for the bulk condition represents the average of 3 trials, and each point for the Hele-Shaw cell and microfluidic chip represents the average of 2 trials. All the pressure values in this figure were measured at 20℃ (293.15 K).

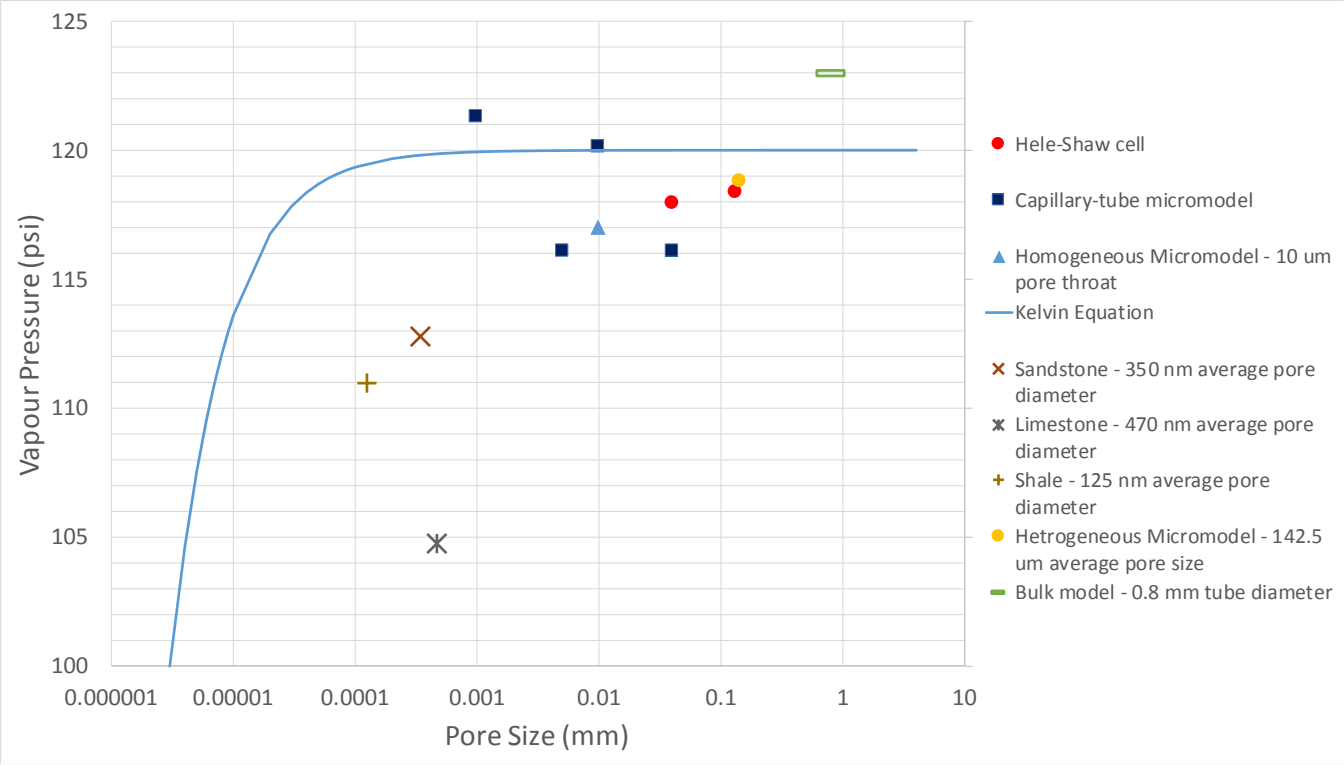

Figure 8-13: Measurement of propane vapour pressure in Hele-Shaw cells, micromodels, and rock samples. Each point for sandstone, limestone, and shale represents the average of 3 experiments (3 trials with 3 core samples from identical reservoir rock blocks). Each point for the bulk condition represents the average of 3 trials, and each point for the Hele-Shaw cell and microfluidic chip represents the average of 2 trials. All the pressure values in this figure were measured at 20℃ (293.15 K).

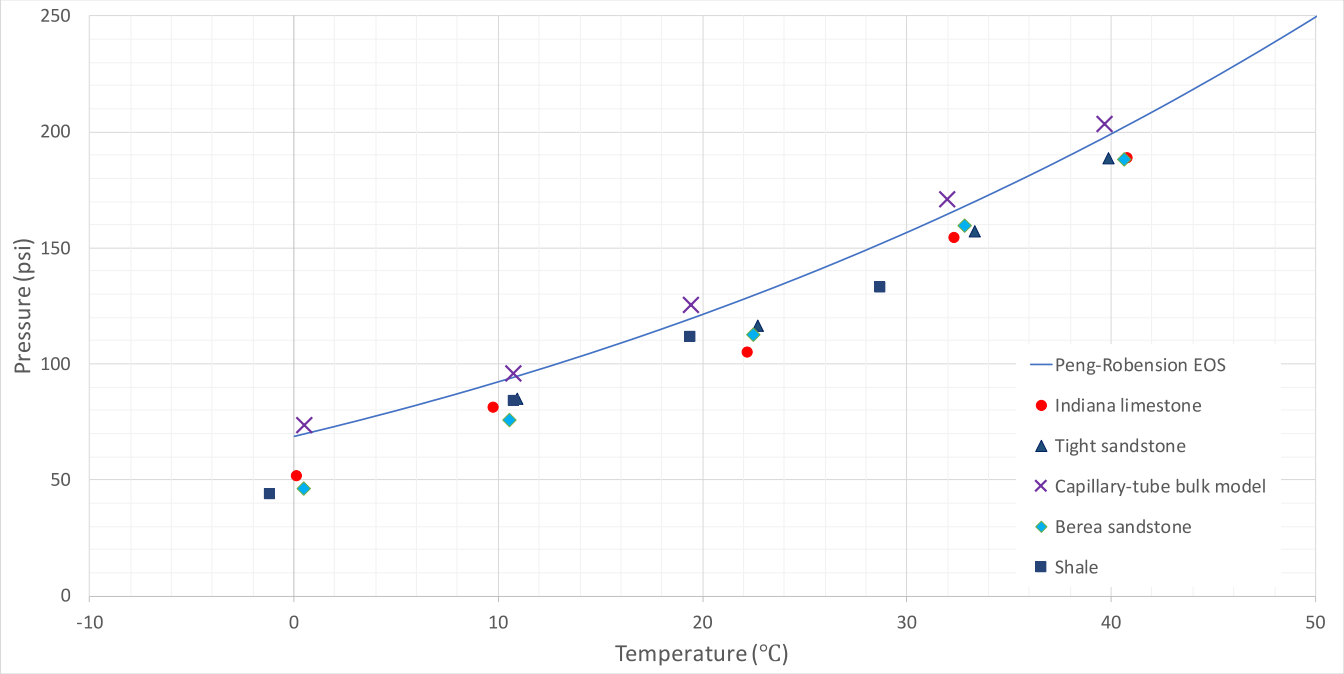

Figure 8-14: Measurement of vapour pressure in Berea sandstone, Indiana limestone, tight sandstone, and shale at various system temperatures. Each point represents the average of 3 experiments (3 trials with 3 core samples from identical reservoir rock blocks). Each point for the bulk condition represents the average of 3 trials.

8.7 Conclusions and Remarks

Surface characteristics of rock porous media, including capillary size, surface tension, and curvature of vapour-liquid interface, play an important role in controlling the thermodynamics and phase-alteration behaviour of liquids and gases. In order to achieve an accurate modelling of hybrid (with thermal) applications and sole solvent injection processes for oil recovery (and solvent retrieval), it is critical to understand the thermodynamics of the injected fluids (solvents) and originally existed fluids (heavy-oil, oil, condensate) in capillary medium conditions. The main objective of this paper was to compare our experimental observations with calculated vapour pressures from the Kelvin equation and Peng-Robinson EOS. Phase-change pressures of propane were investigated in capillary/porous media using Hele-Shaw glass cells, microfluidic silica-glass chips, and reservoir rock samples. The vapour pressures, measured in bulk conditions, were considered as benchmarks.

The propane vapour pressures measured with Hele-Shaw cells and microfluidic chips were comparable with those measured at bulk conditions. Additionally, they were identical with the computed saturation pressures from the Kelvin equation (Figure 8-13). However, propane vaporized in rock samples at pressures lower than the bulk vapour pressure and computed values by 7%. Studying the phase-change pressure of propane at different temperatures allowed us to compare the experimental outcomes with one of sophisticated cubic equations of state (PR-EOS) in reservoir simulation. Due to the confinement effect, the measured vapour pressures in sandstone, limestone, tight sandstone, and shale were 15% (on average) less than those modelled by PR-EOS (Figure 8-14) In reservoir scales, such shifted phase-change pressures could have an impact on the accuracy of reservoir fluid-dynamic simulations and history matching.

8.8 Nomenclature

SAGD: Steam Assisted Gravity Drainage

C5+: pentane and higher carbon number hydrocarbons

EOR: Enhanced Oil Recovery

SOS-FR: Steam-Over-Solvents in Fractured Reservoir

CSS: Cyclic Steam Stimulation

EOS: Equation-of-State

SRP: Solvent Retrieval Process

PVT: Pressure-Volume-Temperature

CO_2: carbon dioxide

PR-EOS: Peng-Robinson equation-of-state

K: Kelvin

v^L: liquid molar volume

r: droplet radius

γ : surface tension

R: universal gas constant

T: temperature

P_∞: vapour pressure at flat surface

P_r: vapour pressure at curved interface

T_r: temperature at porous medium

T_∞: temperature at bulk medium

ΔH_{vap}: heat of vaporization

V_m: molar volume

Z_C: critical compressibility factor

9 Chapter 9: Propagation and Entrapment of Hydrocarbons in Porous Media under Capillarity Controlled Phase Alteration Conditions: A Visual Nanofluidics Analysis

A version of this chapter was submitted to a journal for publication.

9.1 Abstract

The displacement characteristics of gas-liquid systems in capillary media under non-isothermal and non-isobaric conditions are controlled by capillarity as phase alteration (specifically vaporization) starts earlier in smaller (nano) capillaries compared to the larger ones. For an accurate modeling of these types of natural and engineered processes, this thermodynamically dictated displacement process should be well understood. With this aim, the capillarity effect on phase-change and the displacement dynamics of hydrocarbon liquids in homogeneous and heterogenous silicate micro/nanofluidics chips was studied. It was observed that the boiling temperatures of pentane, a pentane-heptane mixture, and a pentane-heptane-octane mixture were 1.6 – 6.9% lower than bulk measurements due to confinement effects, and the early vaporization had a significant influence on the vapour displacement process. In homogeneous (uniform capillary pressure distribution) porous media, the consistency of capillary pressure resulted in a uniform and quicker propagation/displacement of vapour. However, in the media with variable capillary pressure (heterogeneous pore structure), the vapour's flow tended to take place non-uniformly along the system thus leading to a major gas fingering and gas-flow restriction. The presence of other—heavier—components (liquid-phase) in the porous medium developed an excessive barrier against the vapour's flow throughout the pore channels that was specifically caused by the viscous forces of the liquids. Moreover, it was observed that the existence of liquids with high boiling points contribute to slowing the vapour propagation of the lighter components, and the gas displacement becomes slower as the density and viscosity of the liquid-phase components increases.

9.2 Introduction

Phase alteration is a commonly encountered phenomenon in many engineering applications and natural processes in underground reservoir systems or synthetic porous media. These include CO_2 sequestration, conventional and unconventional oil and gas production, geothermal systems, waste deposition, and synthetic porous systems such as filters. Throughout the primary production period of oil or gas, the decline of reservoir pressure leads to the vaporization of hydrocarbons, starting from the lighter components. Likewise, in enhanced oil and gas recovery (EOR) applications,

injecting high-temperature fluids into the reservoir heats the hydrocarbon fluids resulting in the lighter components, such as butane and pentane, to vaporize. Solvent retrieval process is a good example of using the idea of reservoir heating to retrieve considerable volumes of injected solvents in order to reduce the operational cost; in these processes, near wellbore areas are heated with high-temperature fluids to recover injected solvents for EOR by the vaporization process.

In these types of non-isothermal and non-isobaric applications, phase change (typically liquid to gas) takes place resulting in a complex displacement process. Generally, the dynamics of gases in porous media are different from liquids; their movements are influenced by interfacial properties such as wettability, interfacial tension, and pore/rock characteristics. Understanding the dynamics of vapour phase in capillary media with the existence of a liquid phase is critical in obtaining more precise predictions of gas propagation and entrapment behaviour. This is of particular importance in many processes operating under variable temperature and pressure, which are controllable. Obtaining critical pressure and temperature conditions for a given composition of fluids and rock characteristics (wettability, pore texture and size, rock heterogeneity, etc.) to minimize the process cost and maximize the profit is another motivation for understanding gas propagation under variable pressure and temperature conditions.

Small (nano) capillaries have a major impact on the process as boiling occurs quicker (at lower temperatures) compared to larger capillaries (Al-Kindi and Babadagli 2017, 2020). Therefore, capillary size and distribution controls the whole process, meaning further phase change and the displacement and entrapment of the gas and liquid phases. In our prior studies (Al-Kindi and Babadagli 2017, 2018, 2019, 2020), vaporization temperatures of various hydrocarbons were studied using different lab scale capillary models such as Hele-Shaw silica-glass cells, micro/nanofluidics chips, and reservoir rocks (Berea sandstone, Indiana limestone, tight sandstone, and shale). These studies qualitatively and quantitively investigated the phase behavior (boiling temperatures and pressures of hydrocarbon solvents) and showed that phase change occurs more quickly as the medium becomes tighter. Moreover, phase-change temperatures of decane and heptane were noticed to be lower in the reservoir rocks than their normal boiling points, due to the existence of micropores (< 2 nm) and mesopores (2 – 50 nm). The phenomenon of early vaporizations in confined systems leads to an earlier gas phase development in smaller capillaries

which significantly affects the bubble nucleation and displacement process. This paper investigates this process visually using micro/nanofluidics.

9.3 Statement of the Problem and Objectives

Capillarity effect and the physical properties of fluids have an influence on the displacement characteristics (propagation and entrapment) of vapour in the porous media. Comprehending the behaviour of gas dynamics within the rocks is important to predict the ease of vapour flow, as well as the nature of gas displacement while liquid phase exists but is changing in amount due to the non-isothermal and non-isobaric conditions. The phase distribution analysis focused on two main points: (1) capillary effect on nucleation temperatures and the vapour's microscopic displacement in porous media, of which is critical in several applications, such as CO_2 injection, EOR in unconventional reservoirs, and thermal recovery for heavy-oil and geothermal systems; and (2) the effect of liquid density and viscosity on the displacement and distribution of the vapour and liquid phases for single and multicomponent fluids. Based on those two points, the target of this investigation was to understand visually the impact of capillary pressure and liquid density on the dynamics of vapour in silicate glass micro/nanofluidics chips.

9.4 Capillary Effect and Vapour Mobility

Capillary pressure is the pressure difference at the interface between non-miscible fluids, which is governed by surface tension (interfacial tension in cases with immiscible fluids), contact angle, and medium radius:

$$\Delta P = \frac{2\,\gamma\,\cos\theta}{r} \tag{1}$$

where γ is the surface tension, θ is the contact angle, and r is the medium radius. As the vapour starts to form in the porous system due to vaporization caused by increasing temperature or pressure depletion, its flow through the pores is partially affected by the magnitude of the capillary pressure within the pore throats. That means, the higher the capillary pressure is, the harder for the

gas to push the liquid and escape the system. The vapour motion becomes even more restricted when the liquid is favored by the solid medium. **Figure 9-1** shows the flow of gas bubbles through a branched tube filled with a wetting liquid. Owing to the higher capillary pressure in the smaller tube, it is easier for the gas bubble to flow through the larger tube because of its lower capillary pressure. A similar phenomenon occurs in the rock porous media when gas is formed; the vapour tends to escape through larger pores to avoid flowing against higher capillary pressures in the tighter channels.

Another factor that impacts the dynamics of vapour is the liquid density. Fluids in oil reservoirs are complex hydrocarbons, containing a large number of components, ranging from methane (C_1H_4) to C_{50} or higher depending on the reservoir and oil properties. An increase of reservoir temperature or a decrease of pressure causes the lighter components to vaporize before other heaver components. As a result, the movement of the vapour phase of lighter components is impacted by the density and viscous force of the liquid phase in the porous system. **Figure 9-2** illustrates a vapour bubble flowing in a capillary tube saturated with a liquid. The viscous forces (F_v) of the liquid phase govern the flow of the bubble and act against its freedom of motion. In reservoirs with heavy or viscous oil, the movement of gases is restricted by the high viscous forces which drastically affect the flow flexibility of the gas phase within the rocks.

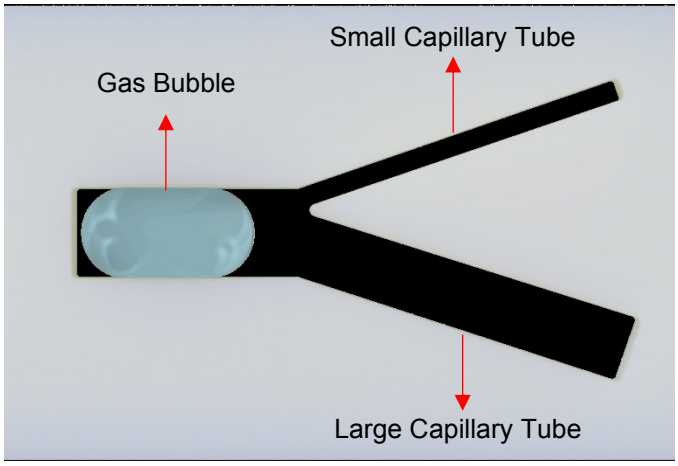

(a)

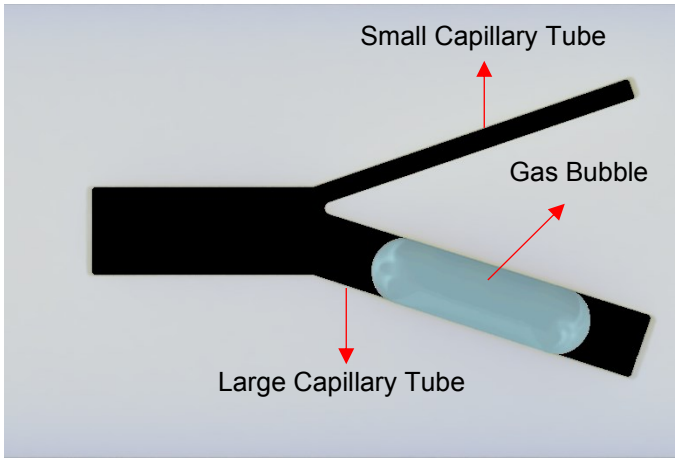

(b)

Figure 9-1 – (a) Initial stage of vapour formation in a branched tube; (b) flow of gas bubble in a larger capillary tube due to the lower capillary pressure.

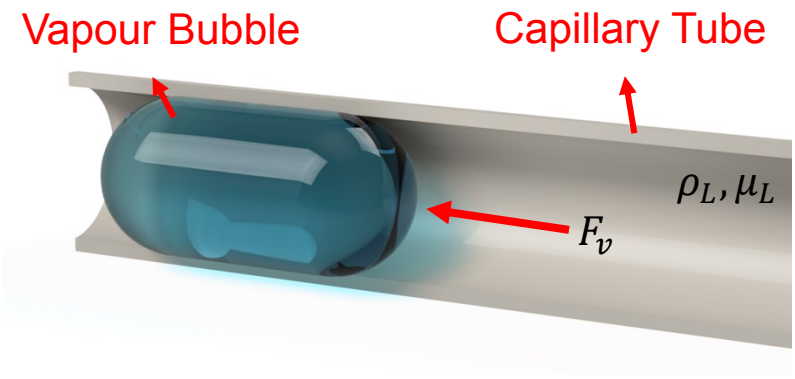

Figure 9-2: Flow of gas bubble through a capillary tube filled with a liquid of certain density (ρ_L) and viscosity (μ_L).

9.5 Micro/Nanofluidics Design

The phase distribution in porous media was investigated visually using silicate glass micro/nanofluidics (to be referred as "micromodel" from this point on) chips with different designs. Initially, the dynamics of gas were studied in a homogeneous micromodel at which the capillary pressure is equally distributed along the chip (**Figure 9-3a**). The uniform glass model represents extended tight rocks, such as shale, which their pore sizes are nearly similar to each other. The variation of pore sizes in shale was investigated by Al-Kindi and Babadagli (2020) and Liu et al. (2019); based on their pore size distribution analysis, shales mostly consist of pores ranging from micropores (< 1 nanometer) to 70 nanometers (nm). Also, most of the nitrogen desorption was detected in pores smaller than 10 nm. Therefore, theoretically, the capillary pressures in shale porous media are expected to be similarly distributed. However, in more permeable rocks (sandstones and limestones), the size or pores can be widely distributed which results in a considerable heterogeneity of capillary pressure in the system. Shi et al. (2011) reported that the pore diameter in Berea sandstone can range—approximately—from 50 to 90,600 nm (≈90 micrometers, μm). In Indiana limestone, the size of pores can vary from 22 up to 100 μm (Freire-Gormaly et al. 2015).

Considering these pore size ranges, heterogeneous (variable pore size) micromodels with non-uniform pore throat sizes ranging from 0.3 to 0.05 mm were also prepared to study vapor dynamics under phase change conditions (**Figure 9-3b**).

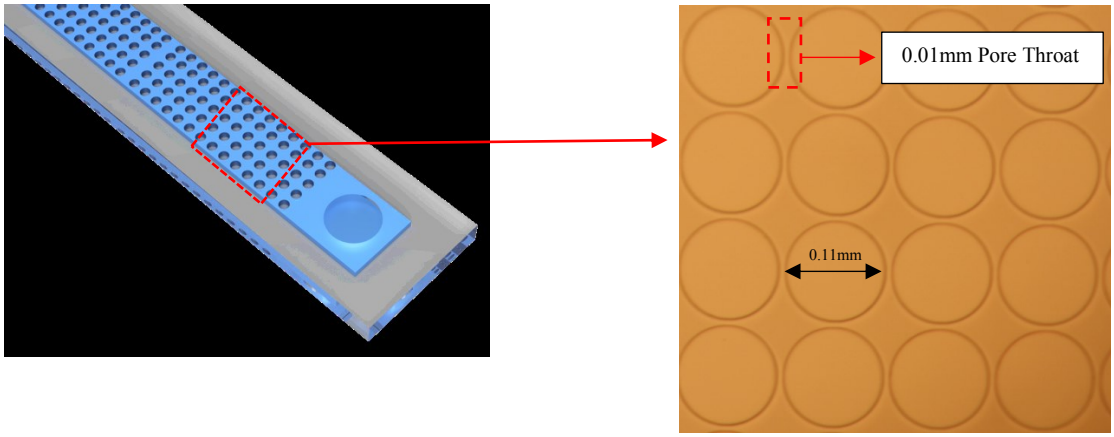

(a)

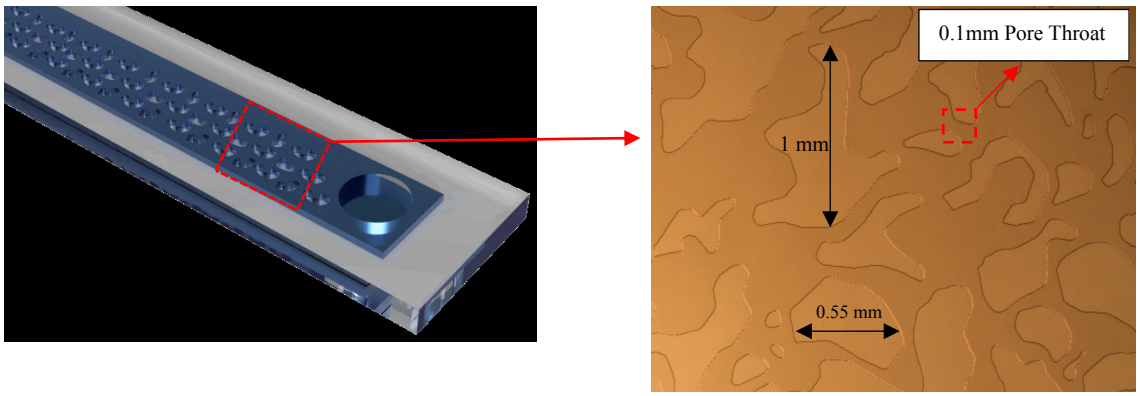

(b)

Figure 9-3: Schematic of (a) homogeneous and (b) heterogeneous micro/nanofluidics chips.

9.6 Experimental Set-up and Procedure

The key purpose of this investigation was to achieve a visual study of a single-component hydrocarbon (pentane) vaporization in a 2-D silicate glass porous media mixed with other hydrocarbons (heptane and octane) with higher boiling temperatures. This set-up mimics different cases encountered in hydrocarbon reservoirs in different ways. For example, a light hydrocarbon can be injected to improve the recovery of a heavier one (solvent injection in heavy-oil reservoirs

or unconventional -light oil- reservoirs). After these applications, the reservoir can be heated to retrieve injected solvent (in the form of gas).

To achieve such analysis, an optical microscope and a high-speed camera were used to capture the formation and motion of the vapour phase within the capillary/porous media. The micromodels were heated using a heating plate which monitors the chip (micromodel) temperature accurately with a precision of 0.2℃. Temperatures on the micromodel surface were sensed by flat thermocouples connected to the acquisition system. One of the issues encountered when heating the micromodel with a heating plate is the non-uniformity of heat transfer along the thickness of the chips. Therefore, the temperature was measured on two points on the top surface of the model (**Figure 9-4**), and average temperatures were considered to represent the inner fluid temperature. **Figure 9-5** shows the setup used to analyze the dynamics of pentane's vapour phase in the silica-glass porous media. The micromodels were vacuumed at 12 psi under atmospheric pressure to saturate them with hydrocarbon solvents and eliminate any trapped air bubbles in the microfluidic porous network.

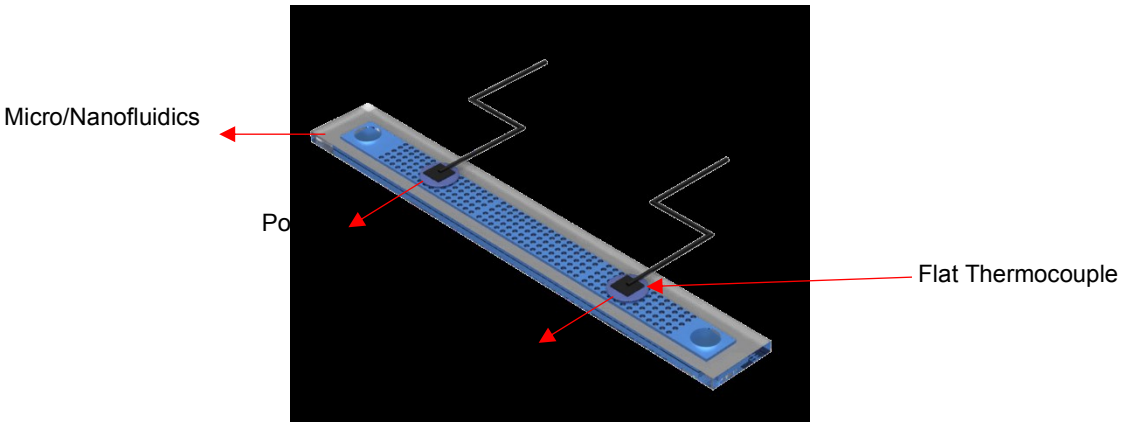

Figure 9-4: Schematic of the experimental setup used to visualize vapour dynamics in micromodels.

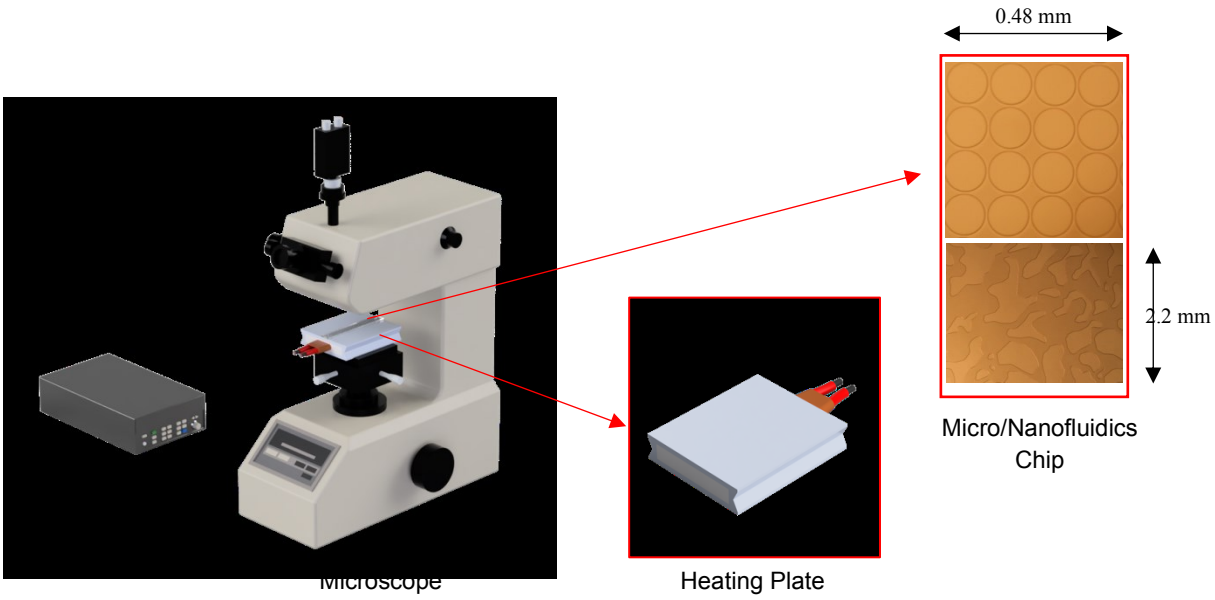

Figure 9-5: Schematic of the experimental setup used to visualize vapour dynamics in micromodels.

9.7 Results and Discussion

The study of vapour dynamics in capillary media was divided into three categories; the first set of experiments focused on the dynamical behavior of pentane's vapour in the porous system as a pure (single) component. The experiments allowed us to clearly comprehend the effect of capillary pressure variation on the vapour flow since the silica-glass media were free of any other hydrocarbon components. Additionally, these initial trials acted as benchmarks for the next sets of experiments. The second group of experiments studied the dynamics of pentane's gas with the existence of another hydrocarbon component (binary component) holding a higher boiling point. The third set of trials inspected the flow of pentane's vapour phase against a binary-component liquid with higher vaporization temperature and density, thus representing a multi component system.

An evaluation was done for two aspects of the process: (1) distribution of the phases in the pores as phase alteration occurs (the statics aspect of the process), and (2) how this distribution affects the progress of the displacement (the dynamic aspect of the process) at larger (sweep efficiency) and smaller (pore scale showing microscopic displacement efficiency) scales. Apparent viscous fingering was caused in the microfluidic porous system owing to two main reasons: (1) variable capillary pressure in the system due to the heterogeneity of the pore structure; (2) presence of

liquid phases in the system which result in non-uniform microscopic displacement of vapour. The cause of viscous fingering could be from both physical phenomena which is the usual scenario in hydrocarbon reservoirs. With pure pentane, which acted as a single-component fluid in the homogeneous micromodel, a nearly steady gas displacement (**Figure 9-6**) was visualized because of the constant capillary pressure along the glass porous media. Such displacement type would be expected to occur in reservoir rocks with narrow pore size distributions, like shale with most of its pores ranging only between micro pores (< 1 nm) and 70 nm.

In the heterogeneous micromodel, the viscous fingering commonly occurred due to the huge variation of capillary pressures (**Figure 9-7**). Having a difference in density or viscosity between two fluids or phases could be the cause of viscous fingering, and this phenomenon commonly occurs in systems where gas movements take place in media filled with liquids. In the micromodels, the fingering effect was captured in both homogeneous and heterogeneous media when a liquid phase was introduced. Although the capillary pressure is constant in the homogeneous model, viscous forces in heptane, for example, restricted the motion of pentane's vapour inconsistently which led the viscous fingering of gas to develop as shown in **Figure 9-8**.

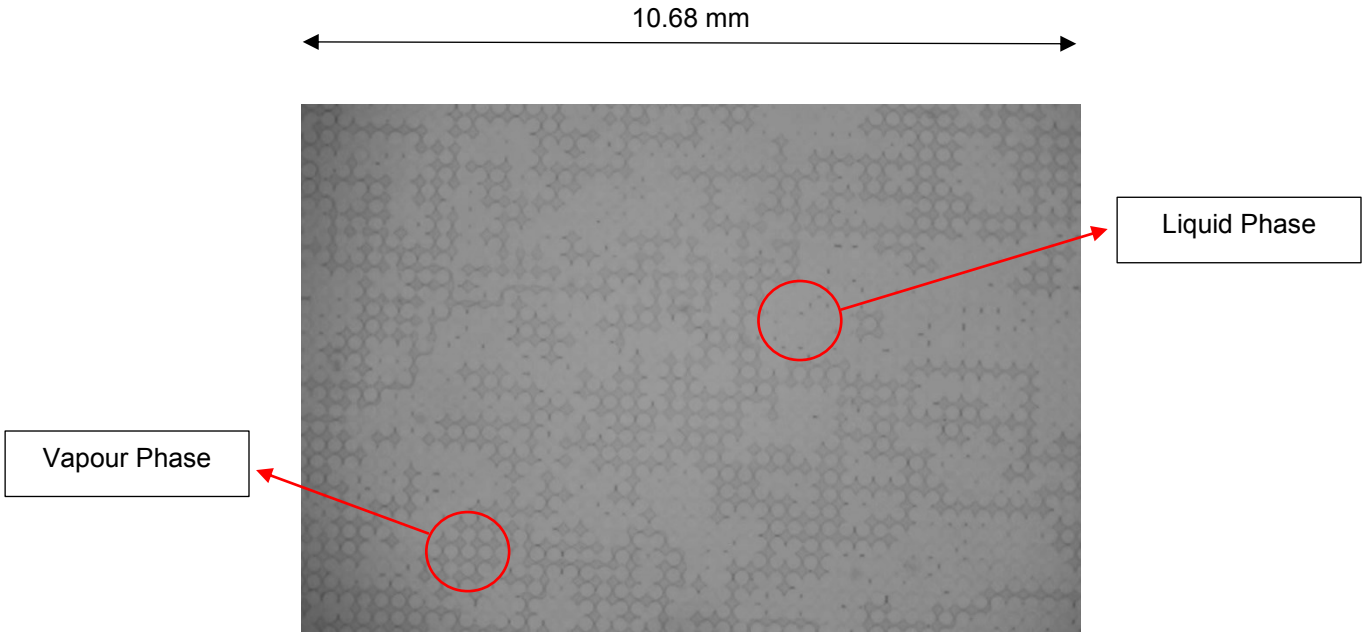

Figure 9-6: Uniform generation of pentane's vapour phase in the homogeneous model at 32°C. The micromodel was pre-saturated with pure pentane, as a single-component liquid. The dark gray areas represent the vapour phase, and the light gray regions represent the liquid phase.

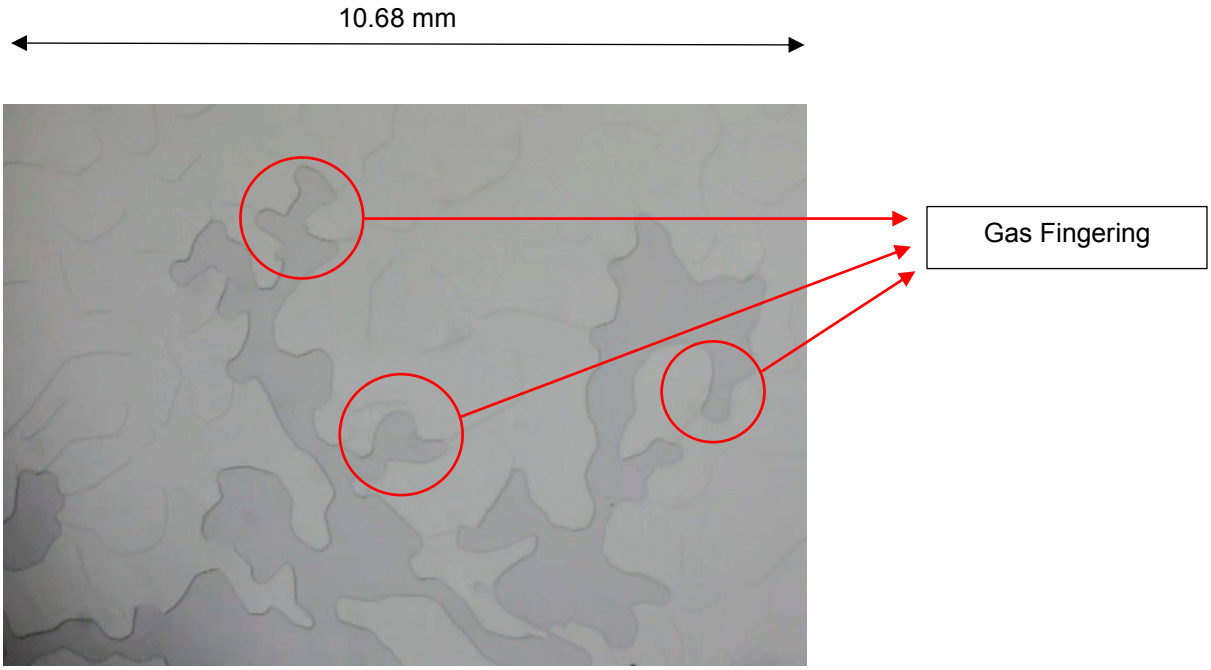

Figure 9-7: Occurrence of gas fingering in the heterogeneous porous medium at 28°C as a form of gas displacement, due to the homogeneity of capillary pressure. The micromodel was pre-saturated with pure pentane, as a single-component liquid. The dark gray areas represent the vapour phase, and the light gray regions represent the liquid phase.

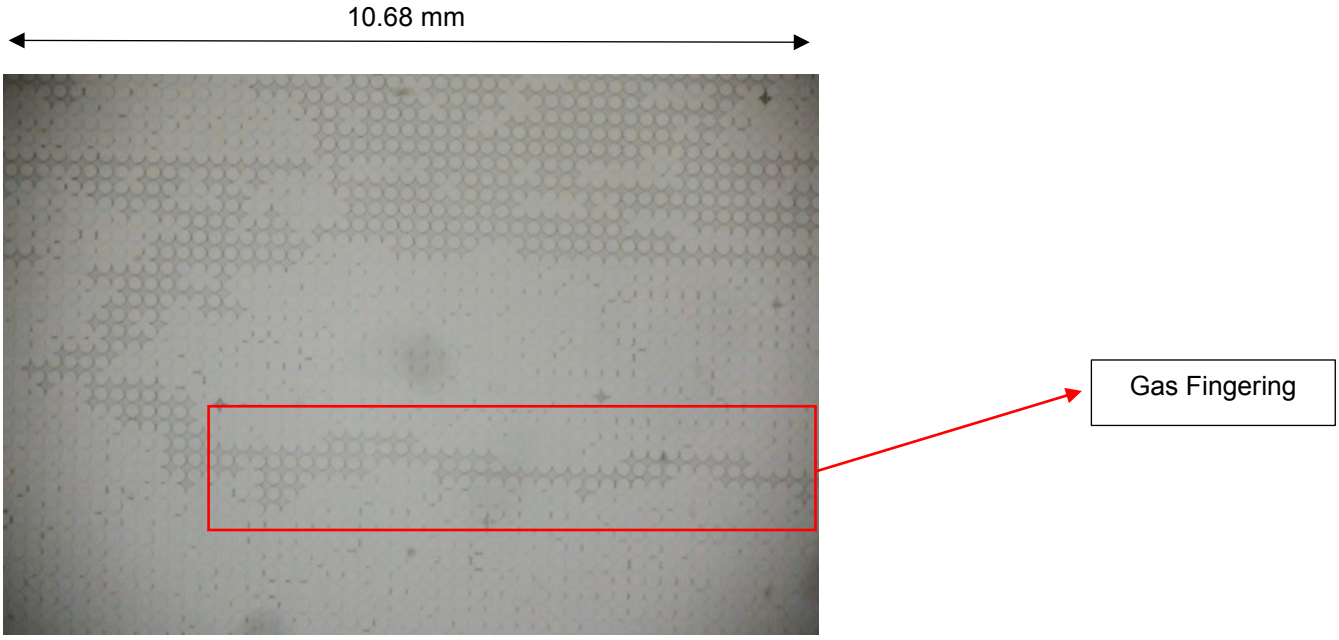

Figure 9-8: Occurrence of gas fingering (pentane vapour phase) in the homogeneous porous medium at 38°C as a form of gas displacement, due to the existence of a liquid phase (heptane) in the system. The micromodel was pre-saturated with a binary liquid mixture (pentane and heptane). The dark gray areas represent the vapour phase, and the light gray regions represent the liquid phase.

Dynamical behaviour of pure pentane (single component). In porous media, capillary pressure characteristically controls the fluid flow which could also impact the phase change, meaning smaller pores (higher capillary pressure) cause quicker phase change (Al-Kindi and Babadagli 2020). Therefore, the capillarity effect controls the uniformity of fluid vaporization in the system if the pore sizes are heterogeneously distributed. **Figure 9-9** presents the vaporization of pentane captured in the homogeneous and heterogeneous models. The capillary pressure in the homogeneous model is equally distributed due to its constant pore throat sizes (**Figure 9-9a**). Consequently, the vaporization of pentane took place nearly uniformly along the porous medium. On the other hand, the pore throat sizes in the heterogeneous micromodel range from 0.3 to 0.05 mm and the deviation of capillary pressures results in a non-uniform vaporization along the model area, as illustrated in **Figure 9-9b**.

In heterogeneous porous systems, the gas phase prioritizes the flow through larger pores due to their lower capillary pressures as also observed in our case. During the gas motion, pentane's vapour flowed mainly through bigger pores to avoid the high capillary pressures in smaller gaps as shown in **Figure 9-10**. This phenomenon could introduce considerable channeling effects in rock types that have widespread pore size distributions, like sandstones and limestones.

Figure 9-11 demonstrates the dynamics of vapour phase and uniformity of vaporization in both micromodels during the 25 seconds period, starting from the time at which the fluid vaporization began. Owing to the fast flow of vapour phase in the model, a high-speed camera was utilized to capture 120 frames of vapour motion every second. Images at the 0 second mark show the initiation of pentane phase change through the pore throats at recorded temperatures. After 10 seconds, in the homogeneous model, around 40% of pentane along the area was vaporized. However, because of the deviation of capillary pressure, only 25% of pentane was vaporized in the heterogeneous model after 10 seconds. The uniform capillary effect in the homogeneous model results in a uniform gas flow. As seen in **Figure 9-11**, after 20 seconds, 70% of the homogeneous model was filled with the vapour phase. Conversely, in the heterogeneous system, the diversity of capillary pressure restricts the vapour to move uniformly which limits its propagation through the porous media during the early stages of vaporization. Another aspect to focus on is the boiling temperature of pentane in both micromodels. The normal boiling point of n-pentane is approximately 35℃ (308.15 K) at ambient conditions in Edmonton, Canada. Because of the effect of capillarity and

pore throat size, pentane tended to vaporize at temperatures lower than its normal boiling point. Specifically, in the homogeneous model, the recorded vaporization temperature was 30℃ (303.15 K) which was 1.6% lower than the normal boiling temperature in Kelvin scale. In the heterogeneous model, the measured vaporization temperature was 27.8℃ (300.95 K) which was 2.3% lower than the bulk boiling temperature in the Kelvin scale.

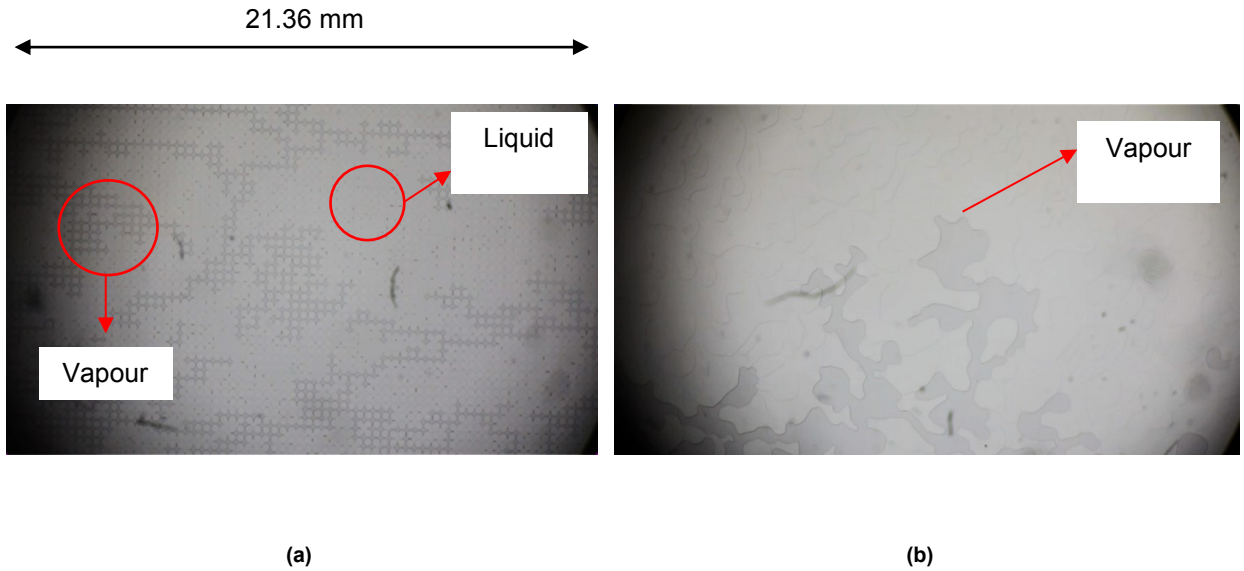

Figure 9-9: (a) Vaporization of pure pentane in a homogeneous model at 31°C; and (b) vaporization of pure pentane in a heterogeneous model at 29°C. Both microfluidic chips were pre-saturated with pure pentane, as a single-component liquid.

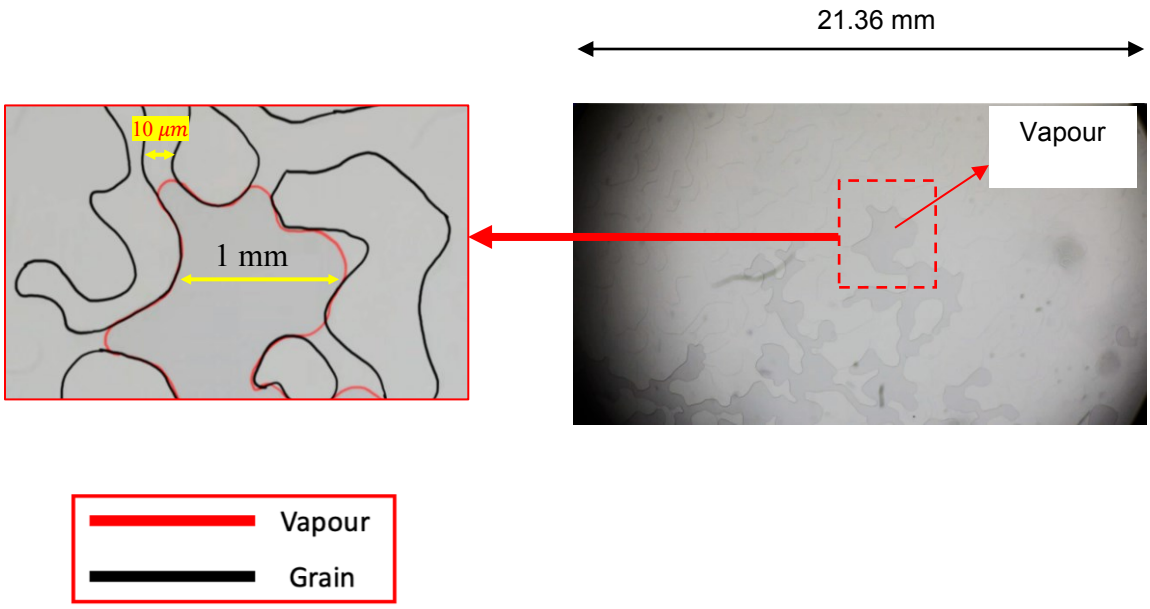

Figure 9-10: Flowing of pentane vapour phase through pore throats in the heterogeneous micromodel.

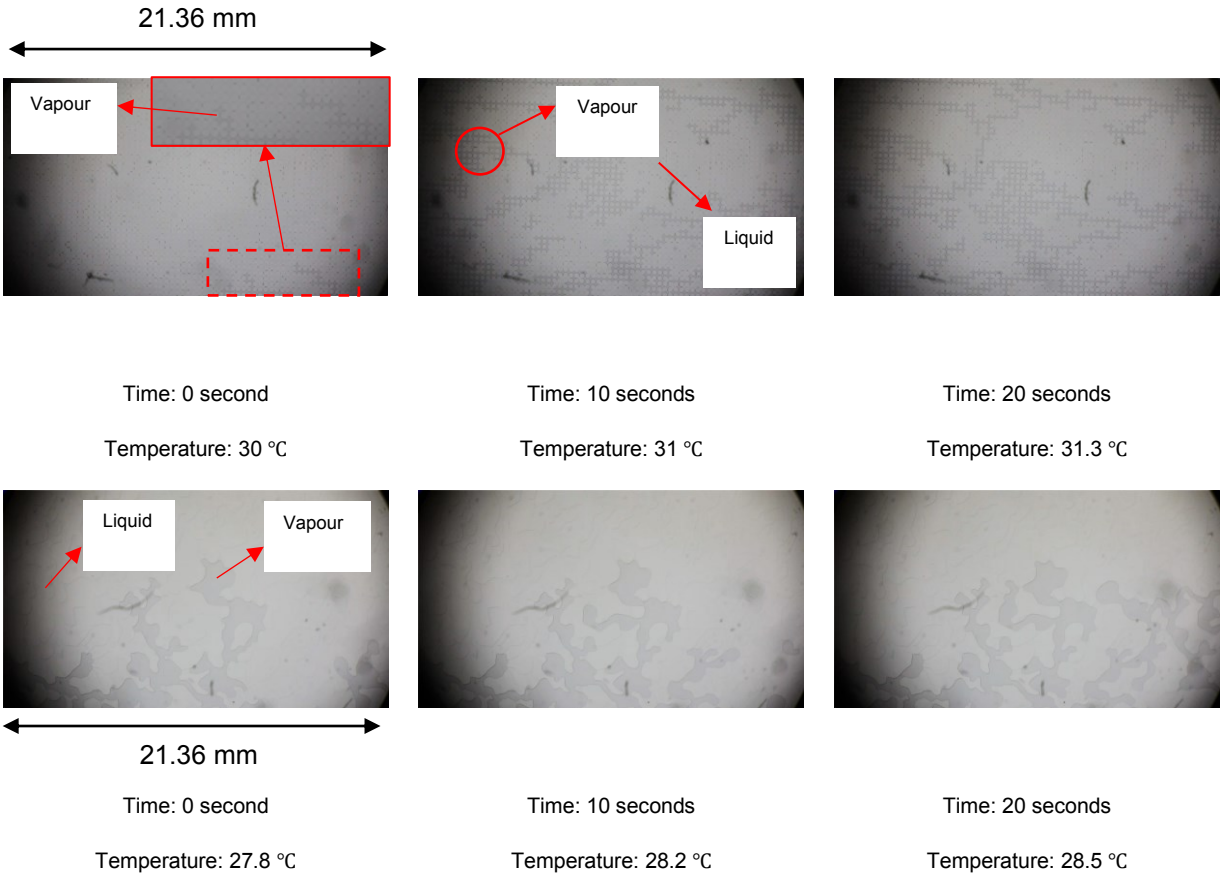

Figure 9-11: Vaporization of pentane in micromodels at different times and temperatures. The microfluidic chips were pre-saturated with pure pentane, as a single-component liquid.

Dynamical behaviour of pentane with heptane (binary component). The existence of another hydrocarbon component could have a significant effect on the vapours' dynamics, especially if the other component has a higher boiling temperature. Having a liquid in the porous medium allows the vapour to flow against the viscous forces of the liquid and capillary pressures caused by the capillarity. Heptane was selected as the second component in the system as it has a higher boiling temperature (97.7℃) than pentane. The bubble point temperature of the binary-component mixture is 35℃.

Despite the uniformity of capillary pressure in the homogeneous model, the movement of the pentane vapour phase at the bubble point temperature was highly restricted by the liquid phase of heptane. **Figure 9-12** shows the vaporization of pentane during the first 20 seconds, starting from the time (0 seconds) at which the mixture vaporization started. Due to the great difference between the vapour density of pentane ($\approx 2.5\ \frac{Kg}{m^3}$) and liquid phase of heptane ($684\ \frac{Kg}{m^3}$), the propagation

of pentane's vapour phase became harder and slower since it had to push a much denser fluid (heptane) in order to travel through the pores. After 20 seconds from the initiation of pentane's vapour, only 10% of the silica-glass porous media was occupied by the gas phase; however, in the case of pure pentane (**Figure 9-11**), 70% of the model was dominated by the vapour after 20 seconds.

The heterogeneity of capillary pressure in the heterogenous micromodel encourages the vapour channeling to take place as the gas phase prioritizes the pores with lower capillary pressures, especially at the early stages of vaporization as illustrated in **Figure 9-10**. **Figure 9-13** presents the vaporization of pentane in the mixture at different periods. Introducing heptane in the system led the vapour phase to propagate slower than the case of pure pentane (**Figure 9-11**) since the gas phase had to overcome the viscous forces of heptane in order to pass through the pore throats. After 20 seconds, 18% of the heterogeneous model was occupied by the vapour phase (**Figure 9-13**); nonetheless, in the case of pure pentane, 35% of the model was filled with pentane's gas (**Figure 9-11**). The early vaporization phenomenon was observed in this case as the previous situation with pure pentane. The bulk bubble point temperature of pentane-heptane mixture is around 54℃ (327.15 K). The recorded boiling temperature in the homogeneous model was 35℃ (308.15 K) and 6.7% lower than the bulk bubble point temperature in the Kelvin scale. In the heterogeneous model, the measured phase-change temperature was 31.4℃ (304.55 K) which was 6.9% less than the bulk value in the Kelvin scale.

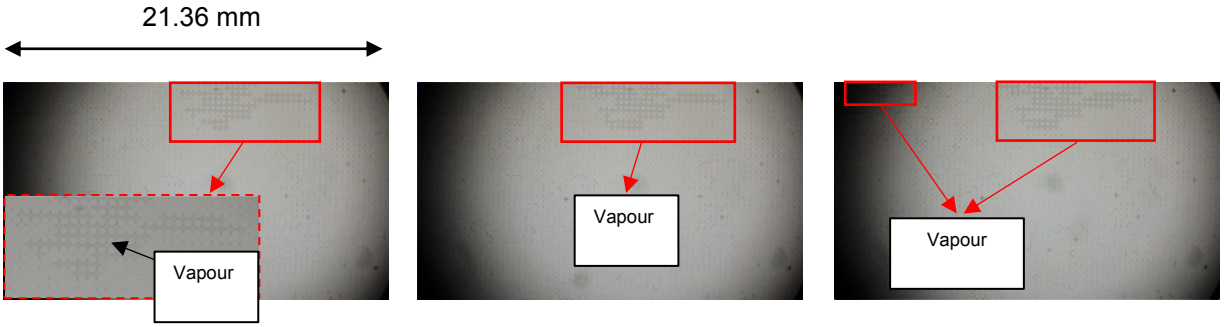

Figure 9-12: Vaporization of pentane in the homogeneous micromodel at different times and temperatures. The microfluidic chip was initially saturated with a binary liquid mixture (pentane and heptane).

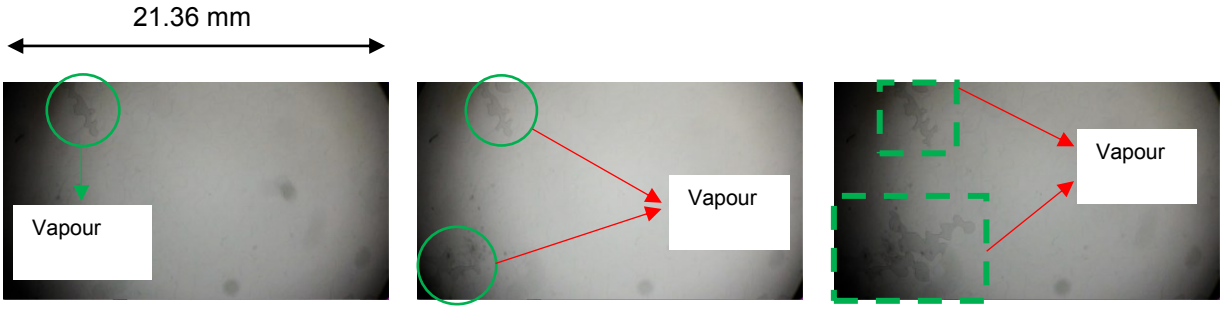

Figure 9-13: Vaporization of pentane in the heterogeneous micromodel at different times and temperatures. The microfluidic chip was initially saturated with a binary liquid mixture (pentane and heptane).

Dynamical behaviour of pentane with heptane-octane mixture (multi-component). In both homogeneous and heterogeneous systems, having denser and higher viscosity liquids would inversely alter the vapour mobility throughout the pore channels. Theoretically, mixing heptane with octane would not result in a drastic increase of density and viscosity since their densities and viscosities are close to each other. **Table 9-1** shows the density and viscosity of heptane and octane at 20℃. Because of the slight increase of the liquid density in the porous system, it was not

expected to observe an obvious change in the dynamics of pentane's vapour. The main target of this trial was to inspect the repeatability of the phenomenon while having an additional hydrocarbon component (octane) at which its density and viscosity were similar to heptane.

Table 9-1: Density of viscosity of heptane and octane at 20°C.

	Heptane (C_7H_{16})	Octane (C_8H_{18})
Density $\left(\frac{Kg}{m^3}\right)$	684	703
Viscosity (mmPa.s)	0.4	0.542

Figure 9-14 shows the vaporization of the mixture (pentane-heptane-octane) in the homogeneous model at different times, starting from the initial stage of phase change at the bubble point temperature (50℃). Similar to the pentane-heptane case, the propagation of gas was limited by the liquid phase of the heptane-octane mixture. After 20 seconds, around 15% of the model was occupied by the gas phase of pentane (**Figure 9-14**), whereas, in the case of pure pentane, 70% of the homogeneous model was dominated by the gas after 20 seconds from the initiation of vapour generation (**Figure** 9-**11**). In the heterogeneous micromodel, after 20 seconds from the beginning of phase change, nearly 20% of the model was occupied by the vapour phase of pentane (**Figure 9-15**). The vaporization of the mixture in both models took place at temperatures lower than the bulk bubble point temperature (65℃, 338.15 K). In the homogeneous micromodel, the initial stage of vaporization was captured at 51.6℃ (324.75 K) which was 3.96% less than the bulk value in Kelvin scale. In the heterogeneous model, the vaporization took place at a temperature (48.5℃, 321.65 K), and it was 4.8% lower than the bulk bubble point temperature.

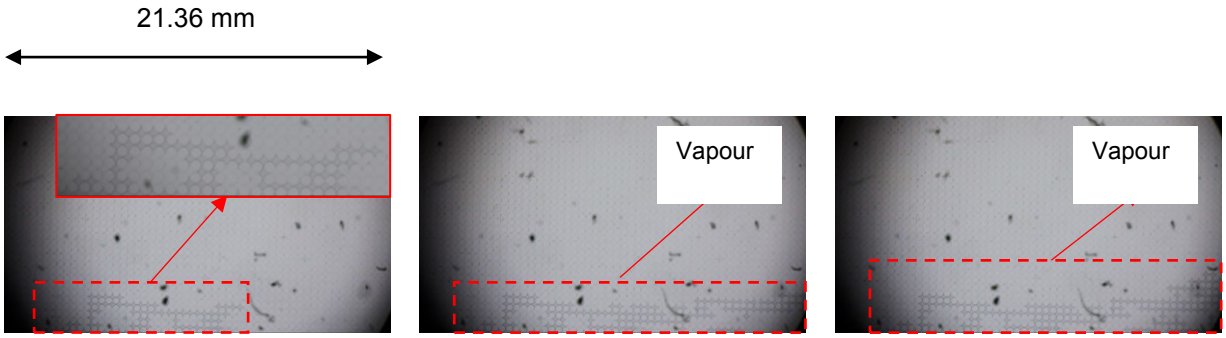

Time: 0 second

Temperature: 51.6 ℃

Time: 10 seconds

Temperature: 52 ℃

Time: 20 seconds

Temperature: 52.4 ℃

Figure 9-14: Vaporization of pentane in the homogeneous micromodel at different times and temperatures. The microfluidic chip was initially saturated with a multicomponent liquid mixture (pentane, heptane, and decane).

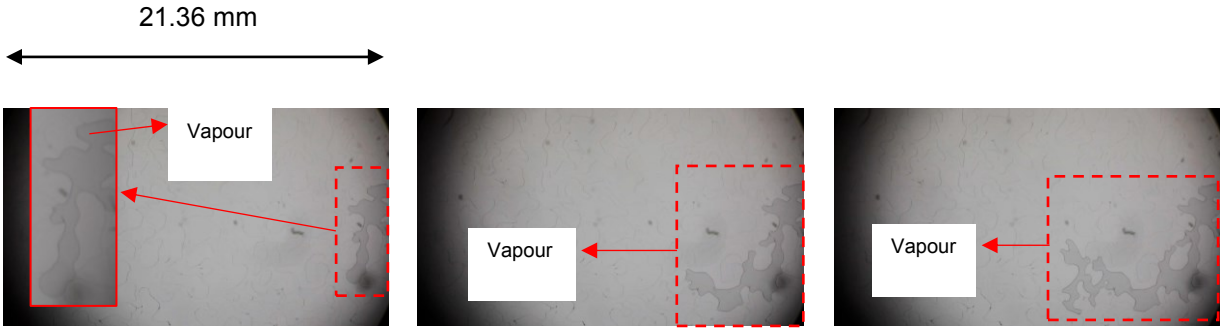

Time: 0 second

Temperature: 48.5℃

Time: 10 seconds

Temperature: 48.8℃

Time: 20 seconds

Temperature: 49.1℃

Figure 9-15: Vaporization of pentane in the heterogeneous micromodel at different times and temperatures. The microfluidic chip was initially saturated with a multicomponent liquid mixture (pentane, heptane, and decane).

9.8 Conclusions and Remarks

In porous media, the capillarity effect has considerable impacts on the dynamics of phase change and the propagation of the vapour phase. Physical phase alteration is a repeatable phenomenon which constantly occurs in reservoirs due to the change of temperature, pressure, or both. Hence, comprehending the dynamical behaviour of gases during the phase change can assist in achieving more accurate predictions in the motion of gases in porous media at different temperatures.

The dynamics of single and multi-component hydrocarbons was studied, and the outcome can be listed as follows:

- Capillary pressures have a considerable impact on the uniformity of vapour's motion along a porous medium. In homogeneous media representing uniformly distributed pores sizes (and thereby capillary pressure), the vaporization takes place uniformly in the system which results in a quicker propagation (displacement) of the gas phase. Such phenomenon can occur in tighter rocks, such as shale, since their pore sizes are limited to a small range of pore size distribution. The deviation of capillary pressure in heterogeneous systems due to non-uniformly distributed pores sizes result in non-uniformity of vapour's flow which leads to a significant gas channeling and restrictions in gas flow.
- Having another -heavier- component (liquid-phase) in a porous system causes a significant restriction of vapour's movement within the pore throats either in homogeneous or heterogeneous media, due to the viscous force in the liquid that acts as a barrier against the gas motion.
- In heterogeneous (variable pore sizes and thereby capillary pressure) porous systems, the existence of liquid phases with high boiling points could slow down the propagation of vapour phase of the lighter components.
- Owing to the capillarity effect in the silicate glass porous media, shifted phase-alteration temperatures of several hydrocarbon solvents were experimentally recorded, and they were 1.6 – 6.9%, in the Kelvin scale, lower than the bulk vaporization temperatures.
- Increasing density and viscosity of liquid-phase components caused by having heavier components in the system results in a slower propagation of the gas phase.

9.9 Nomenclature

C_n: carbon number

H_n: hydrogen number

℃ : degree Celsius

mm: millimeter

μm: micrometer

ρ_L: liquid density

μ_L: liquid viscosity

10 Chapter 10: Conclusions

10.1 Conclusions and Contributions

Specific conclusions obtained through this research are summarized below:

1. The research provided a structured study of phase-change behavior of several hydrocarbons in different capillary media. The analysis was started by measuring boiling points of pure water, heptane, and decane in Hele-Shaw cells with various inner gap thicknesses, ranging from 0.04 to 5 mm. Due to the confinement effect, the recorded boiling temperatures of tested liquids were 10% (in Kelvin scale), on average, lower than their normal boiling points and those computed by the Thomson equation. Also, the results showed that the vaporization behavior of liquids could be altered even when the medium size is larger than 1000 nanometers. Then, boiling temperatures of pure and mixed hydrocarbon liquids were measured in several types of microfluidic chips, providing a better representation of rock porous media. The experimental outcomes showed that the solvent liquids were boiling in the micromodels at temperatures 20% (4.3% in Kelvin unit) lower than their normal boiling temperatures.

2. The investigation was then moved forward by investigating the vaporization of pure heptane and octane, pentane-heptane mixture, and pentane-heptane-octane mixture in several reservoir rocks. The phase-change temperatures of tested solvents in tight rocks (shale and tight sandstone) were 18% (3.8% in Kelvin unit) lower than the bulk values. Also, noticeable reductions of vaporization temperatures were measured in the permeable rocks (sandstone and limestone), due to the existence of micro and meso pores.

3. The next stage of the analysis was measuring the phase-change temperatures of similar hydrocarbons in the rock samples at various pressures and comparing the measured values with bulk measurements and computed values by the Peng-Robinson equation-of-state. The deviation percentages between the recorded and bulk values varied from 4.4% (1.6% in Kelvin unit) to 19.7% (5.2% in Kelvin unit) with pure solvents (heptane and octane) and 1.4% (0.4% in Kelvin unit) to 27.6% (5.3% in Kelvin unit) with the multicomponent

solvents (pentane-heptane mixture and pentane-heptane-octane mixture). Also, the deviation percentages between the recorded and calculated phase-change temperatures were ranging from 4.4 (1.6% in Kelvin unit) to 19.3% (5.1% in Kelvin unit) with pure solvents (heptane and octane). With multicomponent solvents, the deviation percentages were ranging from 2.1 (0.7% in Kelvin unit) to 25.7% (5% in Kelvin unit).

4. Altering the wettability and adsorption of Berea sandstone caused clear shifts of boiling temperatures of heptane and octane. By changing the wettability of sandstone from water-wet to oil-wet, a change of 10.5% (1% in Kelvin scale) of average heptane and octane nucleation temperatures was noticed, comparing with their nucleation temperatures before wettability alteration. Reducing the solvent adsorption in sandstone reduced the vaporization temperatures of heptane and octane by 25% (5.4% in Kelvin scale), comparing to their nucleation temperatures before the firing process.

The vapour pressure of propane (as a hydrocarbon gas) was measured in sandstone, limestone, tight sandstone, and shale under different temperatures; the measured pressures were 7% lower than the bulk vapour pressures and those computed by the Kelvin equation. The study also showed that vapour pressures, computed by the Peng-Robinson equation-of-state, were 15% higher than what were measured experimentally in the rocks. Lastly, the dynamical behavior of single and multi-component hydrocarbon liquids was investigated in homogeneous and heterogeneous nanofluidic models. Capillary pressures in porous media have large influences on the speed of vapour-phase displacement and homogeneity of vapour's motion within the capillary system. Either in homogeneous or heterogeneous media, existence of heaver components in liquid phase drastically limits the flow of vapour phase in the pores.

This research brought a deeper and wider understanding of phase thermodynamics and dynamical behavior in porous systems. It provided a clear analysis of how boiling temperatures and vapour pressures of hydrocarbons change in capillary media by conducting comprehensive experimentations. Also, it offered a series of studies on the effect of rock wettability and adsorption on phase-change behavior.

More specific research/scientific contributions can be listed as follows:

- For the first time in literature, experimental data was provided for the phase change (boiling and condensation), and deviations from the phase behavior at bulk conditions are quantitatively described.
- The effects of capillary (interfacial) characteristics on the process were clarified. The study was not limited to the pore size (and its distribution) effect, but it was extended to identify the effect of wettability, rock type, and mineralogy (mainly clay content).
- A wide range of experimental data is useful to validate the analytical and numerical model studies. Synthetic model results could be useful for validating pore scale computational models while experimental data obtained from rocks could be useful for model validation for practical applications, namely numerical simulators.
- Nano capillary visual studies showed how the displacement processes are impacted by the boiling process controlled by capillarity.
- Above mentioned studies used not only water and single-component hydrocarbons but also binary and ternary combinations of the latter.

In addition to above listed scientific contributions to literature, contributions to industrial applications that could be useful for practitioners were made. At the reservoir scale, deviations in boiling temperatures or vapour pressures from the values obtained at bulk conditions could have a considerable impact on history matching and performance forecasting for oil, gas, and geothermal production, especially in tight reservoirs. In thermal-solvent hybrid applications, this could be highly cost saving as application temperatures and pressures were observed to be considerably lower than previously thought.

It is hoped that this thesis will provide a new insight into the phase behavior in capillary medium, insight that would be critical in developing both new EOR techniques and accurate estimations of their performance.

10.2 Future Work

Several developments can be focused on in to improve the research and widen its contributions. These developments can be listed as the following:

1. Nanofluidic chips with extended tight channels (< 100 nanometers) can be used to study the vaporization and condensation of hydrocarbon and non-hydrocarbon fluids. The analysis will also provide a clear visualization of vapour generation and dynamics in nano-porous media.
2. This research has only studied the phase-change behavior of propane in various porous systems. Other hydrocarbon gas mixtures can be included in the investigation, such as methane-propane mixture and methane-propane-butane mixture.
3. Reservoir fluids are naturally complex hydrocarbons that are mixed with non-hydrocarbon fluids, like nitrogen, water, and CO_2. Therefore, the analysis can be expended by studying more complicated hydrocarbon mixtures (more than three components). It can be started by inspecting the phase-change of kerosene or naphtha in reservoir rocks under various pressures. Then, the experiments can be advanced by using other hydrocarbon mixtures with non-hydrocarbon fluids.
4. The study can be improved by inspecting boiling points of hydrocarbon liquids at pressures higher than 144.7 psi and studying vapour pressures of hydrocarbon gases at temperatures higher than 40℃.
5. Further studies can be done to inspect the accuracy of the Peng-Robinson equation-of-state in modeling the phase behavior of complex hydrocarbons in micro (< 2 nanometers) and meso (2-50 nanometers) pores by using nanofluidic chips.

11 References

Al-Bahlani, A. M. and Babadagli, T. 2008. Heavy-Oil Recovery in Naturally Fractured Reservoirs with Varying Wettability by Steam Solvent Co-Injection. SPE Int. Thermal Oper. and Heavy-Oil Symp., Calgary, Alberta, 20–23 October. SPE-117626-MS. https://doi.org/10.2118/117626-MS.

Al-Bahlani, A. M. and Babadagli, T. 2009. Laboratory and Field Scale Analysis of Steam Over Solvent Injection in Fractured Reservoirs (SOS-FR) for Heavy Oil Recovery. Annual Technical Conference and Exhibition, New Orleans, Louisiana, 4–7 October. SPE-124047-MS. https://doi.org/10.2118/124047-MS.

Al-Bahlani, A. M. M. and Babadagli, T., 2009. Laboratory and Field Scale Analysis of Steam Over Solvent Injection in Fractured Reservoirs (SOS FR) for Heavy Oil Recovery. SPE Annual Technical Conference and Exhibition, New Orleans, Louisiana, 4-7 October. https://doi.org/10.2118/124047-MS.

Al-Bahlani, A.M. and Babadagli, T. 2009. Laboratory and Field Scale Analysis of Steam over Solvent Injection in Fractured Reservoirs (SOS-FR) for Heavy Oil Recovery. Annual Technical Conference and Exhibition, New Orleans, Louisiana, 4–7 October. https://doi.org/10.2118/124047-MS.

Al-Bahlani, A.M. and Babadagli, T. 2009. Laboratory and Field Scale Analysis of Steam Over Solvent Injection in Fractured Reservoirs (SOS FR) for Heavy Oil Recovery. SPE Annu. Tech. Conf. Exhib., New Orleans, Louisiana, 4-7 October. https://doi.org/10.2118/124047-ms.

Al-Bahlani, A.M. and Babadagli, T. 2009. Laboratory and Field Scale Analysis of Steam Over Solvent Injection in Fractured Reservoirs (SOS FR) for Heavy Oil Recovery. SPE Annual Technical Conference and Exhibition, New Orleans, Louisiana, 4-7 October. https://doi.org/10.2118/124047-MS.

Al-Bahlani, A.M. and Babadagli, T. 2011. SOS-FR (Solvent-Over-Steam Injection in Fractured Reservoir) Technique as a New Approach for Heavy-Oil and Bitumen Recovery: An Overview of the Method. Energy and Fuels 25(10): 528-4539. https://doi.org/10.1021/ef200809z.

Al-Bahlani, A.M. and Babadagli, T. 2011. SOS-FR (Solvent-Over-Steam Injection in Fractured Reservoir) Technique as a New Approach for Heavy-Oil and Bitumen Recovery: An Overview of the Method. Energy and Fuels 25: 4528-4539. https://doi.org/10.1021/ef200809z.

Al-Bahlani, A.M. and Babadagli, T. 2011. Steam-over-solvent injection in fractured reservoirs (SOS-FR) technique as a new approach for heavy-oil and bitumen recovery: An overview of the method. Energy and Fuels 25: 4528–4539. https://doi.org/10.1021/ef200809z.

Al-Bahlani, A.M. and Babadagli, T. 2011. Steam-over-Solvent Injection in Fractured Reservoirs (SOS-FR) Technique as a New Approach for Heavy-Oil and Bitumen Recovery: An Overview of the Method. Energy and Fuels 25(10): 4528-4539. https://doi.org/10.1021/ef200809z.

Al-Bahlani, A.M. and Babadagli, T. 2011. Steam-over-solvent injection in fractured reservoirs (SOS-FR) technique as a new approach for heavy-oil and bitumen recovery: An overview of the method. Energy & Fuels 25(10): 4528 - 4539. https://doi.org/10.1021/ef200809z.

Al-Bahlani, A.M.M. and Babadagli, T. 2009. Laboratory and Field Scale Analysis of Steam Over Solvent Injection in Fractured Reservoirs (SOS FR) for Heavy Oil Recovery. SPE Annual Technical Conference and Exhibition, New Orleans, Louisiana, 4-7 October. https://doi.org/10.2118/124047-MS.

Alfi, M., Nasrabadi, H., and Banerjee, D. 2017. Effect of Confinement on Bubble Point Temperature Shift of Hydrocarbon Mixtures: Experimental Investigation Using Nanofluidic Devices. SPE Annual Technical Conference and Exhibition, San Antonio, Texas, 9-11 October. https://doi.org/10.2118/187057-MS.

Alharthy, N.S., Nguyen, T., Teklu, T. et al. 2013. Multiphase compositional modeling in small-scale pores of unconventional shale reservoirs. In SPE Annual Technical Conference and Exhibition in New Orleans, Louisiana, USA, 30 Sep-2 Oct. https://doi.org/10.2118/166306-MS.

Alharthy, N.S., Nguyen, T., Teklu, T. et al. 2013. Multiphase Compositional Modeling in Small-Scale Pores of Unconventional Shale Reservoirs. SPE Annual Technical Conference and Exhibition, New Orleans, Louisiana, 30 Sep–2 Oct. https://doi.org/10.2118/166306-MS.

Ali, S. M. and Abad, B. 1976. Bitumen Recovery from Oil Sands, using Solvents in Conjunction with Steam. J Can Petrol Technol 15(3): 80–90. PETSOC-76-03-11. https://doi.org/10.2118/76-03-11.

Al-Kindi, I and Babadagli, T. 2017. Revisiting Thomson Equation for Accurate Modelling of Pore Scale Thermodynamics of Hydrocarbon Solvents. Annual Technical Conference and Exhibition, San Antonio, Texas, 9–11 October 2017. https://doi.org/10.2118/187384-MS.

Al-Kindi, I. and Babadagli, T. 2017. Revisiting Thomson Equation for Accurate Modeling of Pore Scale Thermodynamics of Hydrocarbon Solvents. SPE Annual Technical Conference and Exhibition, San Antonio, Texas, 9-11 October. https://doi.org/10.2118/187384-MS.

Al-Kindi, I. and Babadagli, T. 2017. Revisiting Thomson Equation for Accurate Modeling of Pore Scale Thermodynamics of Hydrocarbon Solvents. SPE Annual Technical Conference and Exhibition, San Antonio, Texas, 9-11 October. https://doi.org/10.2118/187384-MS.

Al-Kindi, I. and Babadagli, T. 2017. Revisiting Thomson Equation for Accurate Modeling of Pore Scale Thermodynamics of Hydrocarbon Solvents. SPE Annual Technical Conference and Exhibition, San Antonio, Texas, 9-11 October. https://doi.org/10.2118/187384-MS.

Al-Kindi, I. and Babadagli, T. 2018. Thermodynamics of Hydrocarbon Solvents at the Pore Scale During Hybrid Solvent-Thermal Application for Heavy-Oil Recovery. SPE EOR Conference at Oil and Gas West Asia, Muscat, Oman, 26-28 March. https://doi.org/10.2118/190469-MS.

Al-Kindi, I. and Babadagli, T. 2018. Thermodynamics of Hydrocarbon Solvents at the Pore Scale During Hybrid Solvent-Thermal Application for Heavy-Oil Recovery. SPE EOR Conference at Oil and Gas West Asia, Muscat, Oman, 26-28 March. https://doi.org/10.2118/190469-MS.

Al-Kindi, I. and Babadagli, T. 2018. Thermodynamics of Hydrocarbon Solvents at the Pore Scale During Hybrid Solvent-Thermal Application for Heavy-Oil Recovery. SPE EOR Conference at Oil and Gas West Asia , Muscat, Oman, 26-28 March. https://doi.org/10.2118/190469-MS.

Al-Kindi, I. and Babadagli, T. 2018. Thermodynamics of Hydrocarbon Solvents at the Pore Scale During Hybrid Solvent- Thermal Application for Heavy-Oil Recovery. SPE EOR Conference at Oil and Gas West Asia, Muscat, Oman, 26-28 March. https://doi.org/10.2118/190469-MS.

Al-Kindi, I. and Babadagli, T. 2019. Revisiting Thomson Equation for Accurate Modeling of Pore Scale Thermodynamics of Hydrocarbon Solvents. Physics of Fluids 31: 122004-1/16. https://doi.org/10.1063/1.5127754.

Al-Kindi, I. and Babadagli, T. 2019. Revisiting Thomson equation for accurate modeling of pore scale thermodynamics of hydrocarbon solvents. Phys. Fluids 31(12): 122004. https://doi.org/10.1063/1.5127754.

Al-Kindi, I. and Babadagli, T. 2019a. Revisiting Kelvin equation for accurate modeling of pore scale thermodynamics of different solvent gases. SPE West. Reg. Meet., San Jose, California, 23-26 April. https://doi.org/10.2118/195319-ms.

Al-Kindi, I. and Babadagli, T. 2019a. Revisiting Kelvin Equation for Accurate Modeling of Pore Scale Thermodynamics of Different Solvent Gases. SPE Western Regional Meeting, San Jose, California, 23-26 April. https://doi.org/10.2118/195319-MS.

Al-Kindi, I. and Babadagli, T. 2019b. Revisiting Thomson Equation for Accurate Modeling of Pore Scale Thermodynamics of Hydrocarbon Solvents. Physics of Fluids 31(12): 122004. https://doi.org/10.1063/1.5127754.

Al-Kindi, I. and Babadagli, T. 2019b. Revisiting Thomson equation for accurate modeling of pore scale thermodynamics of hydrocarbon solvents. Phys. Fluids 31(12): 122004. https://doi.org/10.1063/1.5127754.

Al-Kindi, I. and Babadagli, T. 2020. Effect of Wettability on Vaporization of Hydrocarbon Solvents in Nano Capillaries. SPE Annual Technical Conference and Exhibition, Denver, Colorado, 5-7 October. https://doi.org/10.2118/201258-MS.

Al-Kindi, I. and Babadagli, T. 2020. Thermodynamics of Liquids in Capillary Medium. Journal of Fluid Mechanics 935:A32.

Al-Kindi, I. and Babadagli, T. 2020. Thermodynamics of liquids in capillary medium. Journal of Fluid Mechanics 905: A32-23. https://doi.org/10.1017/jfm.2020.759.

Al-Kindi, I. and Babadagli, T. 2020. Thermodynamics of liquids in capillary medium. J. Fluid Mech. 905: A32 – 23. https://doi.org/10.1017/jfm.2020.759.

Al-Kindi, I. and Babadagli, T. 2020a. Thermodynamics of liquids in capillary medium. Journal of Fluid Mechanics. 905: A32 – 23. https://doi.org/10.1017/jfm.2020.759.

Al-Kindi, I. and Babadagli, T. 2020b. Effect of wettability on vaporization of hydrocarbon solvents in nano capillaries. In SPE Annual Technical Conference and Exhibition in Denver, Colorado, USA, 5 – 7 October 2020. https://doi.org/10.2118/201258-MS.

Al-Kindi, I. and Babadagli, T. 2021a. Revisiting Kelvin Equation and Peng-Robinson Equation-of-State for Accurate Modeling of Hydrocarbon Phase Behavior in Nano Capillaries. Nature Scientific Reports, 11, article no: 6573 (Mar. 22). https://doi.org/10.1038/s41598-021-86075-8

Al-Kindi, I. and Babadagli, T. 2021a. Revisiting Kelvin Equation and Peng-Robinson Equation-of-State for Accurate Modeling of Hydrocarbon Phase Behavior in Nano Capillaries. Nature Scientific Reports, 11, article no: 6573 (Mar. 22). https://doi.org/10.1038/s41598-021-86075-8

Al-Kindi, I. and Babadagli, T. 2021b. Propagation and Entrapment of Hydrocarbons in Porous Media under Capillarity Controlled Phase Alteration Conditions: A Visual Nanofluidics Analysis. Submitted (in review).

Al-Kindi, I. and Babadagli, T. 2021b. Propagation and Entrapment of Hydrocarbons in Porous Media under Capillarity Controlled Phase Alteration Conditions: A Visual Nanofluidics Analysis. Submitted (in review).

Allen, J. C., Gillespie, R. E., and Burnett, D. B. 1984. Texaco Inc., Superheated Solvent Method for Recovering Viscous Petroleum, United States Patent 4.450.913.

Babadagli, T. 2019. Philosophy of EOR. SPE/IATMI Asia Pacific Oil & Gas Conference and Exhibition, Bali, Indonesia, 29-31 October. https://doi.org/10.2118/196362-MS.

Bao, B., Zandavi, S. H., Li, H. et al. 2017. Bubble nucleation and growth in nanochannels. Phys. Chem. Chem. Phys. 19, 8223–8229. https://doi.org/10.1039/c7cp00550d.

Bao, B., Zandavi, S. H., Li, H., et al. 2017. Bubble nucleation and growth in nanochannels. Phys. Chem. Chem. Phys. 19: 8223–8229. https://doi.org/10.1039/c7cp00550d.

Bao, B., Zandavi, S.H., Li, H. et al. 2017. Bubble nucleation and growth in nanochannels. Phys. Chem. Chem. Phys. 19(12): 8223–8229. https://doi.org/10.1039/c7cp00550d.

Bao, B., Zandavi, S.H., Li, H. et al. 2017. Bubble nucleation and growth in nanochannels. Physical Chemistry Chemical Physics. 19(12): 8223 - 8229. https://doi.org/10.1039/C7CP00550D.

Bao, B., Zandavi, S.H., Li, H. et al. 2017. Bubble nucleation and growth in nanochannels. Phys. Chem. Chem. Phys. 19: 8223–8229. https://doi.org/10.1039/c7cp00550d.

Barsotti, E., Tan, S.P., Saraji, S. et al. 2016. A review on capillary condensation in nanoporous media: Implications for hydrocarbon recovery from tight reservoirs. Fuel 184, 344–361. https://doi.org/10.1016/j.fuel.2016.06.123.

Barsotti, E., Tan, S.P., Saraji, S. et al. 2016. A review on capillary condensation in nanoporous media: Implications for hydrocarbon recovery from tight reservoirs. Fuel. 184: 344 - 361. https://doi.org/10.1016/j.fuel.2016.06.123.

Barsotti. E., Tan, S., Saraji. S. et al. 2016. A review on capillary condensation in nanoporous media: Implications for hydrocarbon recovery from tight reservoirs. Fuel 184: 344-361. https://doi.org/10.1016/j.fuel.2016.06.123.

Berg, J. C. 2009. Fluid interfaces and capillarity, an introduction to interfaces and colloids. World Sci. 936, 23–106. https://doi.org/10.1142/7579.

Berg, J. C. 2010. An Introduction to Interfaces and Colloids, The Bridge to Nanoscience. World Scientific Publishing, Singapore, pp. 26–86.

Berg, J.C. 2009. Fluid Interfaces and Capillarity, An Introduction to Interfaces and Colloids. World Scientific 936: 23–106. https://doi.org/10.1142/7579.

Berg, J.C. 2009. Fluid Interfaces and Capillarity, An Introduction to Interfaces and Colloids. World Scientific 936: 23–106. https://doi.org/10.1142/7579.

Cui, J. and Babadagli, T. 2016. Retrieval of Solvents Injected During Heavy-Oil Recovery from Water- and Oil-Wet Reservoirs: Pore Scale Analysis at Variable Temperature Conditions. SPE Latin America and Caribbean Heavy and Extra Heavy Oil Conference, Lima, Peru, 19–20 October. SPE-181166-MS. https://doi.org/10.2118/181166-MS.

Cui, J. and Babadagli, T. 2017. Retrieval of Solvent Injected during Heavy-Oil Recovery from Water- and Oil-Wet Reservoirs: Pore Scale Analysis at Variable Temperature Conditions. Int. J. of Heat and Mass Trans. 112: 937-849. https://doi.org/10.1016/j.ijheatmasstransfer.2017.05.034.

Cui, J. and Babadagli, T. 2017. Retrieval of Solvent Injected during Heavy-Oil Recovery: Pore Scale Micromodel Experiments at Variable Temperature Conditions. International Journal of Heat and Mass Transfer, 112: 837–849. https://doi.org/10.1016/j.ijheatmasstransfer.2017.05.034.

Cui, J. and Babadagli, T. 2017a. Use of New Generation Chemicals and Nano Materials in Heavy-Oil Recovery: Visual Analysis through Micro Fluidics Experiments. Coll. and Surf. A: Phys. and Eng. Aspects 529: 346-355. https://doi.org/10.1016/j.colsurfa.2017.05.090.

Cui, J. and Babadagli, T. 2017b. Retrieval of Solvent Injected during Heavy-Oil Recovery from Water- and Oil-Wet Reservoirs: Pore Scale Analysis at Variable Temperature Conditions. Int. J. of Heat and Mass Trans., 112: 937–849. https://doi.org/10.1016/j.ijheatmasstransfer.2017.05.034.

Cui, X., Yang, E., Song, K. et al. 2018. Phase equilibrium of hydrocarbons confined in nanopores from a modified Peng-Robinson equation of state. SPE Annual Technical Conference and Exhibition, Dallas, Texas, 24-26 September. https://doi.org/10.2118/191547-MS.

Cui, X., Yang, E., Song, K. et al. 2018. Phase Equilibrium of Hydrocarbons Confined in Nanopores from a Modified Peng-Robinson Equation of State. SPE Annual Technical Conference and Exhibition, Dallas, Texas, 24-26 Sep. https://doi.org/10.2118/191547-MS.

Cui, X., Yang, E., Song, K. et al. 2018. Phase equilibrium of hydrocarbons confined in nanopores from a modified Peng-Robinson equation of state. SPE Annual Technical Conference and Exhibition, Dallas, Texas, 24-26 September. https://doi.org/10.2118/191547-MS.

Das, S. K. and Butler, R. M. 1997. Mechanism of the Vapor Extraction Process for Heavy Oil and Bitumen. J. Pet. Sci. and Eng. 21: 43-59. https://doi.org/10.1016/S0920-4105(98)00002-3.

Fanchi, J.R. 2020. Petroleum Engineering Handbook, Volume V: Reservoir Engineering and Petrophysics. Society of Petroleum Engineering. pp. 1309.

Fanchi, J.R. 2020. Petroleum Engineering Handbook, Volume V: Reservoir Engineering and Petrophysics. Society of Petroleum Engineering. pp. 1309.

Fang, F and Babadagli, T. 2014. Three Dimensional Visualization of Solvent Chamber Growth in Solvent Injection Processes: An Experimental Approach. International Petroleum Technology Conference, Kuala Lumpur, Malaysia, 10–12 December 2014. https://doi.org/10.2523/IPTC-18115-MS.

Fang, F. and Babadagli, T. 2014. Three Dimensional Visualization of Solvent Chamber Growth in Solvent Injection Processes: An Experimental Approach. International Petroleum Technology Conference, Kuala Lumpur, Malaysia, 10-12 December. IPTC-18115-MS. https://doi.org/10.2523/IPTC-18115-MS.

Farouq Ali, S.M. and Abad, B. 1976. Bitumen Recovery from Oil Sands, Using Solvents in Conjunction with Steam. Petrol Technol 15(3): 80-90. https://doi.org/10.2118/76-03-11.

Firoozabadi, A. 1999. Thermodynamics and Applications in Hydrocarbon Energy Production, first edition. United States of America: McGraw-Hill. ISBN: 9780071843256.

Firoozabadi, A. 2016. Thermodynamics and Application in Hydrocarbon Energy Production. McGraw-Hill Education, New York, pp. 88 – 99.

Freire-Gormaly, M., Ellis, J., MacLean, H. et al. 2015. Pore Structure Characterization of Indiana Limestone and Pink Dolomite from Pore Network Reconstructions. Oil & Gas Science and Technology–Revue d'IFP Energies Nouvelles. 3: 33. https://doi.org/10.2516/ogst/2015004.

Freire-Gormaly, M., Ellis, J., MacLean, H., and Bazylak, A. 2015. Pore Structure Characterization of Indiana Limestone and Pink Dolomite from Pore Network Reconstructions. Oil & Gas Science and Technology–Revue d'IFP Energies Nouvelles. 71(3): 33.

Gupta, S., Gittins, S., and Picherack, P. 2004. Insights into Some Key Issues with Solvent Aided Process. J. Can. Petrol. Technol. 51(2): 339–350. PETSOC-04-02-05. https://doi.org/10.2118/04-02-05.

Gupta, S., Gittins, S., and Picherack, P. 2004. Insights into some key issues with Solvent Aided Process. Journal of Canadian Petroleum Technology. 43(02). https://doi.org/10.2118/04-02-05.

Hamada. Y., Koga, K., and Tanaka, H. 2007. Phase equilibria and interfacial tension of fluids confined in narrow pores. Journal of Chemical Physics 127: 084908. https://doi.org/10.1063/1.2759926.

Jin, Z. 2018. Bubble/dew point and hysteresis of hydrocarbons in nanopores from molecular perspective. Fluid Phase Equilibria 458: 177–185. https://doi.org/10.1016/j.fluid.2017.11.022.

Jin, Z. and Firoozabadi, A. 2016. Thermodynamic modeling of phase behavior in shale media. SPE Journal. 21(01): 190 - 207. https://doi.org/10.2118/176015-PA.

Kolodzie, S.J.R. 1980. Analysis of pore throat size and use of the Waxman-Smits equation to determine OOIP in Spindle Field, Colorado. SPE Annual Technical Conference and Exhibition, Dallas, Texas, 21-24 September. https://doi.org/10.2118/9382-MS.

Le Guennec, Y., Privat, R., and Jaubert, J.N. 2016. Development of the translated-consistent tc-PR and tc-RK cubic equations of state for a safe and accurate prediction of volumetric, energetic and saturation properties of pure compounds in the sub-and super-critical domains. Fluid Phase Equilibria 429: 301-312. https://doi.org/10.1016/j.fluid.2016.09.003.

Léauté , R. P., Carey, B. S. 2007. Liquid Addition to Steam for Enhancing Recovery (LASER) of Bitumen with CSS: Results from the First Pilot Cycle. J Can Petrol Technol 46(09). https://doi.org/10.2118/07-09-01.

Léauté, R. P. and Carey, B. S. 2007. Liquid Addition to Steam for Enhancing Recovery (LASER) of bitumen with CSS: Results from the first pilot cycle. J. Can. Pet. Technol. 46(9): 22–30. https://doi.org/10.2118/07-09-01.

Léauté, R.P. and Carey, B.S. 2007. Liquid Addition to Steam for Enhancing Recovery (LASER) of bitumen with CSS: Results from the first pilot cycle. J. Can. Pet. Technol. 46(9): 22–30. https://doi.org/10.2118/07-09-01.

Leyva, H. and Babadagli, T. 2017. High Temperature Solvent Injection for Heavy-Oil Recovery from Oilsands: Determination of Optimal Application Conditions through Genetic Algorithm. SPE Res. Eval. and Eng. 20(2): 372-382. https://doi.org/10.2118/183638-PA.

Leyva, H. and Babadagli, T. 2018. Efficiency of Heavy Oil/Bitumen Recovery from Fractured Carbonates by Hot-Solvent Injection. J. Petr. Sci. and Eng. 165: 752-764. https://doi.org/10.1016/j.petrol.2018.03.004.

Leyva-Gomez, H. and Babadagli, T. 2016. Efficiency of heavy oil/bitumen recovery from fractured carbonates by hot-solvent injection. SPE Heavy Oil Conf. Exhib., Kuwait City, Kuwait, 6-8 December. https://doi.org/10.2118/184095-ms.

Leyva-Gomez, H. and Babadagli, T. 2016. Efficiency of Heavy Oil/Bitumen Recovery from Fractured Carbonates by Hot-Solvent Injection. SPE Heavy Oil Conference and Exhibition, Kuwait City, Kuwait, 6-8 December. https://doi.org/10.2118/184095-MS.

Liu, J., Wang, L., Xi, S. et al. 2017. Adsorption and phase behavior of pure/mixed alkanes in nanoslit graphite pores: an iSAFT application. Langmuir. 33(42): 11189 - 11202. https://doi.org/10.1021/acs.langmuir.7b02055.

Liu, K., Ostadhassan, M., and Cai, J. 2019. Characterizing Pore Size Distributions of Shale. Petrophysical Characterization and Fluids Transport in Unconventional Reservoirs, Elsevier. 3 – 20. https://doi.org/10.1016/B978-0-12-816698-7.00001-2.

Lucia, F.J. 2007. Petrophysical rock properties. Carbonate Reservoir Characterization: An Integrated Approach, pp.1-27.

Lucia, F.J. 2007. Petrophysical rock properties. In Carbonate Reservoir Characterization: An Integrated Approach. pp. 1–27. Springer, Berlin, Heidelberg. https://doi.org/10.1007/978-3-540-72742-2_1.

Luo. S., Lutkenhaus, J., and Nasrabadi, H. 2018. Use of differential scanning calorimetry to study phase behavior of hydrocarbon mixtures in nano-scale porous media. Journal of Petroleum Science and Engineering 163: 731-738. https://doi.org/10.1016/j.petrol.2016.12.019.

Marciales, A. and Babadagli, T. 2016. Pore Scale Visual Investigations on Solvent Retrieval during Oil Recovery at Elevated Temperatures: A Micromodel Study. Chem. Eng. Res. Des. 106: 59–73. https://doi.org/10.1016/j.cherd.2015.12.007.

Marciales, A. and Babadagli, T. 2016. Pore Scale Visual Investigations on Solvent Retrieval during Oil Recovery at Elevated Temperatures: A Micromodel Study. Chem. Eng. Res. Des. 106: 59–73. https://doi.org/10.1016/j.cherd.2015.12.007.

Marciales, A. and Babadagli, T. 2016. Pore scale visual investigations on solvent retrieval during oil recovery at elevated temperatures: A micromodel study. Chem. Eng. Res. Des. 106: 59–73. https://doi.org/10.1016/j.cherd.2015.12.007.

Mohammadzadeh, O., Rezaei, N., and Chatzis, I. 2015. Pore-Scale Performance Evaluation and Mechanistic Studies of the Solvent-Aided SAGD (SA-SAGD) Process Using Visualization Experiments. Transp. Porous Media, 108, 437–480. https://doi.org/10.1007/s11242-015-0484-y.

Mohammed, M. and Babadagli, T. 2013. Efficiency of Solvent Retrieval during Steam-Over-Solvent Injection in Fractured Reservoirs (SOS-FR) Method: Core Scale Experimentation. SPE Heavy Oil Conference, Calgary, Alberta, Canada, 11-13 June. SPE-165528-MS. https://doi.org/10.2118/165528-MS.

Mohammed, M. and Babadagli, T. 2020. New Insights into the Interfacial Phenomena during Miscible Displacement by Hydrocarbon Solvents in Heavy Oil Reservoirs. SPE Improved Oil Recovery Conference, Tulsa, Oklahoma, 29 Aug-2 Sep. https://doi.org/10.2118/200456-MS.

Naderi, K. and Babadagli, T. 2011. Pore-Scale Investigation of Immiscible Displacement Process in Porous Media Under High-Frequency Sound Waves. J. Fluid Mech. 680: 336–360. https://doi.org/10.1017/jfm.2011.166.

Naderi, K. and Babadagli, T. 2014. Use of Carbon Dioxide and Hydrocarbon Solvents during the Method of Steam-Over-Solvent Injection in Fractured Reservoir for Heavy-Oil Recovery from Sandstones and Carbonates. SPE Res. Eval. & Eng. 17(2). SPE 169815-PA. https://doi.org/10.2118/169815-PA.

Naderi, K. and Babadagli, T. 2014. Use of Carbon Dioxide and Hydrocarbon Solvents During the Method of Steam-Over-Solvent Injection in Fractured Reservoirs for Heavy-Oil Recovery from Sandstones and Carbonates. SPE Res. Eval. Eng. 17(2): 286–301. https://doi.org/10.2118/169815-PA.

Naderi, K. and Babadagli, T. 2014a. Experimental Analysis of Heavy Oil Recovery by Alternate Injection of Steam and Solvent (Hydrocarbon/CO2) in Unconsolidated Sand Reservoirs. J Can Petrol Technol 53 (5): 263–274. https://doi.org/10.2118/146738-PA.

Naderi, K. and Babadagli, T. 2014b. Large Scale Applicability of the SOS-FR (Steam-Over-Solvent Injection in Fractured Reservoirs) Method: Optimal Operating Conditions through Numerical Simulation. J. Petr. Sci. and Eng. 122: 497-506. https://doi.org/10.1016/j.petrol.2014.08.011.

Naderi, K. and Babadagli, T. 2014c. Use of Carbon Dioxide and Hydrocarbon Solvents During the Method of Steam-Over-Solvent Injection in Fractured Reservoirs for Heavy-Oil Recovery from Sandstones and Carbonates. SPE Res. Eval and Eng. 17(2): 286–301. https://doi.org/10.2118/169815-PA.

Naderi, K. and Babadagli, T. 2016. Solvent Selection Criteria and Optimal Application Conditions for Heavy-Oil/Bitumen Recovery by Hybrid Thermal and Solvent Methods: A Review and Comparative Analysis. J. of Energy Resources Technology 138, 012904-1/9. https://doi.org/10.1115/1.4031453.

Naderi, K. and Babadagli, T. 2016. Solvent Selection Criteria and Optimal Application Conditions for Heavy-Oil/Bitumen Recovery by Hybrid Thermal and Solvent Methods: A Review and Comparative Analysis. J. of Energy Resources Technology 138, 012904-1/9. https://doi.org/10.1115/1.4031453.

Nagarajan, N.R., Stoll, D., Litvak, M.L. et al. 2020. Successful Field Test of Enhancing Bakken Oil Recovery by Propane Injection: Part I. Field Test Planning, Operations, Surveillance, and Results. Unconventional Resources Technology Conference, 20 July. https://doi.org/10.15530/urtec-2020-2768.

Nagarajan, N.R., Stoll, D., Litvak, M.L. et al. 2020. Successful Field Test of Enhancing Bakken Oil Recovery by Propane Injection: Part I. Field Test Planning, Operations, Surveillance, and Results. Unconventional Resources Technology Conference, 20–22 July 2020. https://doi.org/10.15530/urtec-2020-2768.

Nasr, T. N. and Ayodele, O. R. 2005. Thermal Techniques for the Recovery of Heavy Oil and Bitumen. Presented at SPE International Improved Oil Recovery Conference in Asia Pacific, Kuala Lumpur, Malaysia, 5–6 December. SPE-97488-MS. https://doi.org/10.2118/97488-MS.

Nasr, T. N., Beaulieu, G., Golbeck, H. et al. 2003. Novel Expanding Solvent-SAGD Process "ES-SAGD." J Can Petrol Technol 42(1). https://doi.org/10.2118/03-01-TN.

Nasr, T. N., Beaulieu, G., Golbeck, H. et al. 2003. Novel Expanding Solvent-SAGD Process "ES-SAGD." J. Can. Pet. Technol. 42(1): 13–16. https://doi.org/10.2118/03-01-TN.

Nasr, T.N., Beaulieu, G., Golbeck, H. et al. 2003. Novel Expanding Solvent-SAGD Process "ES-SAGD." J. Can. Pet. Technol. 42(1): 13–16. https://doi.org/10.2118/03-01-TN.

Nasr, T.N., Beaulieu, G., Golbeck, H. et al. 2003. Novel Expanding Solvent-SAGD Process "ES-SAGD." J. Can. Pet. Technol. 42(1): 13–16. https://doi.org/10.2118/03-01-TN.

Nojabaei, B., Johns, R.T., and Chu, L. 2012. Effect of capillary pressure on fluid density and phase behavior in tight rocks and shales. In SPE Annual Technical Conference and Exhibition in San Antonio, Texas, USA, 8 – 10 October 2012. https://doi.org/10.2118/159258-MS.

Pathak, M., Cho, H., and Deo, M. 2017. Experimental and Molecular Modeling Study of Bubble Points of Hydrocarbon Mixtures in Nanoporous Media. Energy and Fuels 31(4): 3427–3435. https://doi.org/10.1021/acs.energyfuels.6b02422.

Pathak, V. and Babadagli, T. 2010. Hot Solvent Injection for Heavy Oil/Bitumen Recovery: An Experimental Investigation. Canadian Unconventional Reservoir and International Petroleum Conference, Calgary, Alberta, 19–21 October. SPE-137440-MS. https://doi.org/10.2118/137440-MS.

Pathak, V. and Babadagli, T. 2010. Hot Solvent Injection for Heavy Oil/Bitumen Recovery: An Experimental Investigation. Canadian Unconventional Reservoir and International Petroleum Conference, Calgary, Alberta, Canada, 19–21 October. https://doi.org/10.2118/137440-MS.

Pathak, V., Babadagli, T. and Edmunds, N.R. 2013. Experimental Investigation of Bitumen Recovery from Fractured Carbonates Using Hot-Solvents. J Can Petrol Technol 52(4): 289–295. https://doi.org/10.2118/159439-PA.

Pathak, V., Babadagli, T., and Edmunds, N. 2012. Mechanics of heavy-oil and bitumen recovery by hot solvent injection. SPE Res. Eval. Eng. 15(2): 182–194. https://doi.org/10.2118/144546-PA.

Pathak, V., Babadagli, T., and Edmunds, N. 2012. Mechanics of Heavy-Oil and Bitumen Recovery by Hot Solvent Injection. SPE Res. Eval. Eng. 15(2): 182-194. SPE-144546-PA. https://doi.org/10.2118/144546-PA.

Pathak, V., Babadagli, T., and Edmunds, N.R. 2011. Heavy Oil and Bitumen Recovery by Hot Solvent Injection. J. Petr. Sci. and Eng. 78(3-4): 637-645. https://doi.org/10.1016/j.petrol.2011.08.002.

Pathak, V., Babadagli, T., and Edmunds, N.R. 2011. Heavy Oil and Bitumen Recovery by Hot Solvent Injection. J. Petr. Sci. and Eng. 78: 637–645. https://doi.org/10.1016/j.petrol.2011.08.002.

Pathak, V., Babadagli, T., and Edmunds, N.R. 2012. Mechanics of Heavy Oil and Bitumen Recovery by Hot Solvent Injection. SPE Res. Eval. and Eng. 15(2): 182–194. https://doi.org/10.2118/144546-PA.

Pathak, V., Babadagli, T., and Edmunds, N.R. 2013. Experimental Investigation of Bitumen Recovery from Fractured Carbonates Using Hot-Solvents. J. of Canadian Petr. Tech. 52(4): 289-295. https://doi.org/10.2118/159439-PA.

Peng, D and Robinson, D. 1976. A New Two-Constant Equation of State. Industrial and Engineering Chemistry Fundamentals. 123: 59 – 64. https://doi.org/10.1021/i160057a011.

Peng, D. and Robinson, D. 1976. A New Two-Constant Equation of State. Industrial and Engineering Chemistry Fundamentals 15(1): 59-64. https://doi.org/10.1021/i160057a011.

Peng, D.Y. and Robinson, D.B. 1976. A new two-constant equation of state. Industrial & Engineering Chemistry Fundamentals 15(1): 59 – 64. https://doi.org/10.1021/i160057a011.

Pina-Martinez, A., Privat, R., Jaubert, J.N. et al. 2019. Updated versions of the generalized Soave α-function suitable for the Redlich-Kwong and Peng-Robinson equations of state. Fluid Phase Equilibria 485: 264-269. https://doi.org/10.1016/j.fluid.2018.12.007.

Redford, D. and McKay, A. 1980. Hydrocarbon-Steam Processes for Recovery of Bitumen from Oil Sands. Presented at the First Joint SPE/DOE Symposium on Enhanced Oil Recovery, Tulsa, Oklahoma, 20–23 April. SPE-8823-MS. https://doi.org/10.2118/8823-MS.

Redlich, O and Kwong, J.N.S. 1949. On the thermodynamics of solutions. V. An equation of state. Fugacities of gaseous solutions. American Chemical Society. 44: 233 – 244. https://doi.org/10.1021/cr60137a013.

Shi, J., Xue, Z., and Durucan, S. 2011. Supercritical CO2 core flooding and imbibition in Berea sandstone – CT imaging and numerical simulation. Energy Procedia. 4: 5001-5008. https://doi.org/10.1016/j.egypro.2011.02.471.

Shi, J., Xue, Z., and Durucan, S. 2011. Supercritical CO2 core flooding and imbibition in Berea sandstone – CT imaging and numerical simulation. Energy Procedia. 4: 5001 – 5008. https://doi.org/10.1016/j.egypro.2011.02.471.

Shu, W. R. and Hartman, K. J. 1988. Effect of Solvent on Steam Recovery of the Heavy Oil. SPE Res. Eng. 3(2): 457–564. SPE-14223-PA. https://doi.org/10.2118/14223-PA.

Soava, G. 1972. Equilibrium constants from a modified Redlich-Kwong equation of state. Chemical Engineering Science. 27: 1197 – 1203. https://doi.org/10.1016/0009-2509(72)80096-4.

Soave, G. 1972. Equilibrium constants from a modified Redlich-Kwong equation of state. Chemical Engineering Science 27(6): 1197-1203. https://doi.org/10.1016/0009-2509(72)80096-4.

Soave, G. 1972. Equilibrium constants from a modified Redlich-Kwong equation of state. Chemical engineering science 27(6): 1197 – 1203. https://doi.org/10.1016/0009-2509(72)80096-4.

Syed, A. H., Mosavat, N., Riordon, J. et al. 2016. A combined method for pore-scale optical and thermal characterization of SAGD. J. Pet. Sci. Eng. 146: 866–873. https://doi.org/10.1016/j.petrol.2016.07.030.

Tai, K. 2005. NanoFab Glass Microfludic Device Fabrication Manual: Complete Process Description and Trouble-Shooting Guide (version 1.0). NanoFab, University of Alberta. https://www.nanofab.ualberta.ca/wp-content/uploads/downloads/2017/02/nanoFAB-Microfluidics-Manual-v-1.0.pdf

Thome, J. R. 2004. Boiling in microchannels: a review of experiment and theory. Int. J. of Heat and Fluid Flow 25(2): 128-139. https://doi.org/10.1016/j.ijheatfluidflow.2003.11.005

Thomson, W. 1871. LX. On the equilibrium of vapour at a curved surface of liquid. The London, Edinburgh, and Dublin Philosophical Magazine and Journal of Science 42(282): 448-452. https://doi.org/10.1080/14786447108640606.

Thomson, W. 1871. LX. On the equilibrium of vapour at a curved surface of liquid. The London, Edinburgh, and Dublin Philosophical Magazine and Journal of Science. 42(282): 448 - 452. https://doi.org/10.1080/14786447108640606.

Thomson, W. 1872. 4. On the Equilibrium of Vapour at a Curved Surface of Liquid. Proc. R. Soc. Edinburgh 7: 63–68. https://doi.org/10.1017/s0370164600041729.

Thomson, W. 1872. 4. On the equilibrium of vapour at a curved surface of liquid. Proceedings of the Royal Society of Edinburgh 7: 63 – 8. https://doi.org/10.1017/S0370164600041729.

Thomson, W. 1872. On the Equilibrium of Vapor at a Curved Surface of Liquid. Proceedings of the Royal Society of Edinburgh 7: 63–68.

Travalloni, L., Castier, M. and Tavares, F.W. 2014. Phase equilibrium of fluids confined in porous media from an extended Peng–Robinson equation of state. Fluid Phase Equilibria. 362: 335 - 341. https://doi.org/10.1016/j.fluid.2013.10.049.

Tro, N. J. 2008. "Chemistry: A molecular approach (2nd Custom ed.)." New Jersey: Person.

Tsukahara, T., Maeda, T., Hibara, A. et al. 2012. Direct measurements of the saturated vapor pressure of water confined in extended nanospaces using capillary evaporation phenomena. RSC Adv. 2: 3184–3186. https://doi.org/10.1039/c2ra01330d.

Tsukahara, T., Maeda, T., Hibara, A. et al. 2012. Direct measurements of the saturated vapor pressure of water confined in extended nanospaces using capillary evaporation phenomena. RSC Adv. 2(8): 3184–3186. https://doi.org/10.1039/c2ra01330d.

Tsukahara, T., Maeda, T., Hibara, A. et al. 2012. Direct measurements of the saturated vapor pressure of water confined in extended nanospaces using capillary evaporation phenomena. RSC Advances 2(8): 3184 - 3186. https://doi.org/10.1039/C2RA01330D.

Tsukahara, T., Maeda, T., Hibara, A. et al. 2012. Direct measurements of the saturated vapor pressure of water confined in extended nanospaces using capillary evaporation phenomena. RSC Adv. 2, 3184–3186. https://doi.org/10.1039/c2ra01330d.

Tsukahara, T., Maeda, T., Hibara, A. et al. 2012. Direct measurements of the saturated vapour pressure of water confined in extended nanospaces using capillary evaporation phenomena. RSC Advances 2(8): 3184–3186. https://doi.org/10.1039/c2ra01330d.

Wang, F., Yang K., You, J., and Lei, X. 2019. Analysis of pore size distribution and fractal dimension in tight sandstone with mercury intrusion porosimetry. Results in Physics. 13: 102283. https://doi.org/10.1016/j.rinp.2019.102283.

Wang, L., Yin, X., Neeves, K. et al. 2016. Effect of Pore-Size Distribution on Phase Transition of Hydrocarbon Mixtures in Nanoporous Media. SPE Journal 21(6): 1981-1995. https://doi.org/10.2118/170894-PA.

Wang, Y., Shardt, N., Lu, C. et al. 2020. Validity of the Kelvin equation and the equation-of-state-with-capillary-pressure model for the phase behavior of a pure component under nanoconfinement. Chemical Engineering Science, 226: 115839. https://doi.org/10.1016/j.ces.2020.115839.

Yortsos, Y.C. and Stubos, A.K. 2001. Phase Change in Porous Media. Current Opinion in Colloid & Interface Science 6(03): 208-216. https://doi.org/10.1016/S1359-0294(01)00085-1.

Zhao, L., Nasr, T. N., Huang, H. et al. 2004. Steam Alternating Solvents Process: Lab Test and Simulation. Presented at the Canadian International Petroleum Conference, Calgary, Alberta, 8-10 June. PETS0C-2004-044. https://doi.org/10.2118/2004-044.

Zhao, L., Nasr, T. N., Huang, H. et al. 2005. Steam Alternating Solvent Process: Lab Test and Simulation. J. Can. Pet. Tech. 44(9): 37-43. PETS0C-05-09-04. https://doi.org/10.2118/05-09-04.

Zhao, L., Nasr, T.N., Huang, H. et al. 2004. Steam Alternating Solvents Process: Lab Test and Simulation. Canadian International Petroleum Conference, Calgary, Alberta, 8–10 June. https://doi.org/10.2118/2004-044.

Zhao, L., Nasr, T.N., Huang, H. et al. 2005. Steam Alternating Solvent Process: Lab Test and Simulation. J Can Petrol Technol 44(9): 37–43. https://doi.org/10.2118/05-09-04.

Zhong, J., Riordon, J., Zandavi, S. H. et al. 2018. Capillary Condensation in 8 nm Deep Channels. J. Phys. Chem. Lett. 9: 497–503. https://doi.org/10.1021/acs.jpclett.7b03003.

Zhong, J., Riordon, J., Zandavi, S. H. et al. 2018. Capillary Condensation in 8 nm Deep Channels. J. Phys. Chem. Lett. 9(3): 497–503. https://doi.org/10.1021/acs.jpclett.7b03003.

Zhong, J., Riordon, J., Zandavi, S.H. et al. 2018. Capillary condensation in 8 nm deep channels. The Journal of Physical Chemistry Letters. 9(3): 497 - 503. https://doi.org/10.1021/acs.jpclett.7b03003.

Zhong, J., Riordon, J., Zandavi, S.H. et al. 2018. Capillary Condensation in 8 nm Deep Channels. J. Phys. Chem. Lett. 9(3): 497–503. https://doi.org/10.1021/acs.jpclett.7b03003.

Zhong, J., Riordon, J., Zandavi, S.H. et al. 2018. Capillary Condensation in 8 nm Deep Channels. J. Phys. Chem. Lett. 9(3): 497–503. https://doi.org/10.1021/acs.jpclett.7b03003.

Zhong, J., Riordon, J., Zandavi, S.H., Xu, Y., Persad, A.H., Mostowfi, F. and Sinton, D. 2018. Capillary condensation in 8 nm deep channels. Phys. Chem. Lett. 9(3): 497–503. https://doi.org/10.1021/acs.jpclett.7b03003.

Zhong, J., Zandavi, S.H., Li, H. et al. 2017. Condensation in One-Dimensional Dead-End Nanochannels. ACS Nano 11(1): 304–313. https://doi.org/10.1021/acsnano.6b05666.